THE INTERACTION OF COBALT, AMINO ACIDS, AND COBALT AMINO ACID COMPLEXES WITH SEDIMENT SURFACES

by

Deborah Lynne Crowther Kay

Dissertation submitted to the Faculty of the

Virginia Polytechnic Institute and State University

in partial fulfillment of the requirements for the degree of

DOCTOR OF PHILOSOPHY

in

Chemistry

APPROVED:

J. G. Dillard, Chairman

H. M. Bell

J. D. Graybeal

J. D. Wightman

L. A. Zelazny

January, 1982

Blacksburg, Virginia

TO MALCOLM

ACKNOWLEDGEMENTS

The author wishes to express her appreciation to her major professor, Dr. John G. Dillard, for his guidance, advice and understanding. She would also like to thank the members of her committee, Drs. Jack D. Graybeal, Harold M. Bell, James P. Wightman, and Lucian A. Zelazny for their support and assistance during this project.

The assistance and patience of workers in the Electronics and Glass Shop in the Department of Chemistry and in the Machine Shop in the Physics Department are appreciated.

The author is especially thankful to her husband, Malcolm Kay, for his encouragement and understanding throughout this endeavor and for typing the initial version of this manuscript. She would also like to thank her parents, brothers, sister and in-laws for their encouragement.

The assistance of Melba Amos and Tammy Henderson for typing this dissertation and the assistance of Pat Cooper for drawing the figures are also appreciated.

Appreciation is extended to the Minerals and Mining Research and Resource Institute and Office of Water Resource Technology for partial support of this work. The author is grateful to the Education Foundation of the Department of Chemistry for granting her a tuition fellowship.

TABLE OF CONTENTS

Page

LIST OF FIGURES

LIST OF TABLES

INTRODUCTION

The interaction of metals with sedimentary materials is important in the areas of soil science (1,2), nuclear waste disposal (3-5), pollution control (6,7), and water treatment (8). Four types of metal-particulate interactions have been documented: 1) adsorption onto clay mineral surfaces, 2) precipitation of the metal as an insoluble hydroxide onto particles, 3) adsorption of the metal onto the precipitated metal hydroxide, and 4) incorporation of the metal into the lattice structure of the particulate matter.(9)

The anomalous behavior of metals in the marine environment with respect to metal concentration in seawater and the amount of metals adsorbed onto suspended particles and sediments have been attributed to organic matter (10-12). Seawater frequently shows an apparent supersaturation with respect to many metals (10). Organic material acts as a chelating agent for metals and can either inhibit or enhance interactions of metal ions with sediments (13,14). Much of the adsorption capacity of marine sediments is attributed to organic material coating the oxide surfaces (15). Conversely, the reactions of organic substrates in seawater are influenced by the metal ions present. Chelation to metal ions in seawater or to metals on the sediment surfaces can enhance the reactivity of organic molecules (10,14).

Amino acids constitute a large percentage of the organic matter found in soils, 12%, (16-18) and in marine sediments, 2.5%, (19-20). In soil systems amino acids represent about 40% of the nitrogen content (17). The interactions of amino acids with soils and sediments is not

only important in metal adsorption, the surface reactions of amino acids with clays are important in studies of the prebiotic beginnings of life (22-24).

Previous studies on metal adsorption (25-28) have been mostly quantitative and gave little information on the nature of the binding of adsorbate to the sediment particle surface. Few studies (29-31) have been conducted on systems comprised of both metals and chelating organic ligands and no known studies have been reported on the adsorption of amino acids or amino acid complexes on manganese dioxide.

The first portion of this dissertation investigates the coinfluence of organic molecules and metal ions on the reaction with sediment surfaces. This was studied by comparing the adsorption of cobalt(II), cobalt(III) amino acid complexes, and amino acids on clay and metal oxide surfaces. Montmorillonite was selected as the clay substrate because of its high cation exchange capacity (32,33). Birnessite (MnO_2) was chosen as the metal oxide because it is one of the forms of manganese dioxide commonly found in manganese nodules (34-37).

The adsorption of cobalt onto montmorillonite and Na^+-birnessite between pH 4 and 10 was studied. X-ray photoelectron spectroscopy (XPS) and microelectrophoresis were used to investigate the adsorption mechanism and to identify the surface species. The possibilities of cation exchange, $CoOH^+$ adsorption, and surface induced precipitation were considered.

Three cobalt amino acid complexes $Co(gly)_3$ (gly = glycinate), $Co(lys)_3^{3+}$ (lys = lysinate), and $Co(asp)_2^-$ (asp = aspartate), were adsorbed onto clay and manganese dioxide as a function of pH. These

three complexes were chosen because they represent neutral, positive, and negative amino acid complexes, respectively. The possibility of hydrolysis and reduction of the adsorbed complex was examined. The amount of complex adsorbed and the bonding of cobalt to the clay and metal oxide surfaces were compared to Co^{2+} adsorption on the substrates.

The adsorption of amino acids onto sodium and cobalt saturated substrates was also investigated. The question addressed was how the metal counterion affected both the adsorption mechanism of the amino acid and the quantity of amino acid adsorbed. Infrared spectroscopy and XPS were used to examine the bonding of the amino acid to the particle surface. The oxidation state and the nature of chemical bonding of cobalt was established by XPS.

The second part of this dissertation pertains to XPS analysis of metals in Pacific manganese nodules. Manganese nodules are known scavengers of transition metals including Co, Ni, Cu, Zn and Fe (38-41). Manganese nodules may someday become an important economic source of these metals (42-45).

Analyses of metals in manganese nodules have centered on the quantification of the trace metals found in the nodules (46-48). However, the selection of extraction processing methods for these metals is limited by knowledge of the chemical environment of the metals in the nodules (49). XPS was used to identify the oxidation state and chemical environment of many of the transition metals found in manganese nodules.

HISTORICAL REVIEW

This literature review is concerned with the interactions of cobalt metal coordination compounds and amino acids with clay and metal oxide surfaces. The review of metal adsorption onto birnessite is discussed separately due to the oxidizing nature of the manganese dioxide surface. Because of the similarity in the surface reactions, some significant works on metal adsorption onto silica, alumina, and other nonoxidizing oxide surfaces are considered in the literature review on metal adsorption onto clays.

A. COBALT ADSORPTION ONTO CLAYS

Surfaces of clays and metal oxides develop a surface charge in an aqueous environment (50-53). Cations or anions adsorb onto these charged sites primarily through coulombic interactions. There are many causes of adsorption other than electrostatic attraction, including: 1) changes in hydration state of the solid or the adsorbate, 2) interactions among the adsorbate molecules or ions themselves, and 3) covalent, van der Waals or hydrogen bonding between the adsorbate and the solid (28). When contributions to the free energy of adsorption from any of these sources are large, adsorption is said to be "specific" and an ion can be adsorbed against electrostatic repulsion (50). Specific adsorption has been found on sediment surfaces (50,51,54).

One of the earliest reports on the mechanism of cobalt adsorption was presented by Banerjee et al. (54). Specific interactions between cobalt and various clays, soils, and peat were investigated. A large portion of the cobalt was nonexchangeable with ammonium acetate but

could be removed with acid. They proposed that the cobalt was initially adsorbed in an exchangeable form and later converted into a more strongly adsorbed species of unknown composition.

Hodgson (55) studied the adsorption of cobalt on montmorillonite in the presence of a large excess of calcium. This was done to eliminate or reduce the amount of nonspecifically adsorbed cobalt. It was found that a rapid period of cobalt adsorption was followed by a period of slower uptake. The adsorption rate change was attributed to two separate reactions. Hodgson (55) suggested that the cobalt taken up during the rapid period was reversibly held and that the cobalt adsorbed during the slow period was nonexchangeable. He concluded that the non-exchangeable cobalt entered the molecular lattice of the mineral. Similar results were found by Tiller and Hodgson (56), who investigated the adsorption of cobalt and zinc on vermiculite, muscovite, biotite, and montmorillonite.

Hodgson and Tiller (57) determined that the adsorption sites for cobalt were primarily on the external basal surfaces of the clay. This conclusion was obtained using three techniques to study the selective bonding of cobalt: 1) polyphosphate ions to block edge sites, 2) collapse of the interlayer spaces with potassium saturation to block internal basal surfaces, and 3) autoradiography to study external basal surfaces.

Spencer and Gieseking (58) postulated that cobalt ions adsorbed on soil clays from a solution of cobaltous chloride consisted of Co^{2+} and the hydroxycobaltous ion, $CoOH^{+}$. This conclusion was based on the observation that a greater amount of cobalt was adsorbed than Ca^{2+} released.

Similar conclusions were reached by Chester (59), who examined the cobalt adsorption isotherm as a function of temperature. The reactivity of cobalt with illite was endothermic. Based on this analysis and suggestions in the literature for the adsorption mechanism (25,60), Chester concluded that cobalt was probably present as Co^{2+}, $CoCl^{+}$, and perhaps $Co(OH)^{+}$.

O'Connor and Kester (25) demonstrated that the copper and cobalt interaction with illite was dependent on pH, ionic strength, and complex forming ligands. The results were interpreted in terms of a model where the trace metals were adsorbed in exchange for surface bound H^{+} ions. It was found that Mg^{2+} interfered with adsorption by competing with trace metals for surface sites. Increases in both the ionic strength and the concentration of complex forming ligands tended to reduce trace metal adsorption.

The possibility that hydrolysis may account for the selective adsorption of heavy metals by clay surfaces was considered by Hodgson et al. (61). This proposition is in contrast to the explanation of specific exchange of the metal with weakly dissociable H^{+}. For a divalent metal, M^{2+}, the two alternative hypotheses can be described as follows:

$$M^{2+} + H_2O \rightarrow MOH^{+} + H^{+} \quad (1)$$

$$MOH^{+} + X^{-} \rightarrow XMOH \quad (2)$$

for hydrolysis, and:

$$M^{2+} + HX \rightarrow MX^{+} + H^{+} \quad (3)$$

for the exchange mechanism, (X represents the adsorbing surface.) The two mechanisms can account for equivalent amounts of H^+ ions released in the adsorption process. The authors (61) studied the adsorption of Co(II) on montmorillonite with and without competing Mg^{2+} ions. Equations were derived showing that θ, the fraction of adsorbing surface covered by Co^{2+}, can be independent of H^+ in the presence of Mg^{2+} if the exchange mechanism predominates. However, for the hydrolysis mechanism θ can still depend on H^+. The hydrolysis mechanism was supported as the major reaction pathway but the possibility that simple exchange may operate concurrently with hydrolysis was not discounted. The point was also made that it is difficult to distinguish whether the influence of pH on the heavy metal adsorption by clays is due to changes in the reacting metal species, alteration of the clay surface, or a combination of both.

Tewari et al. (62) investigated the adsorption of Co(II) on oxide surfaces as a function of Co(II) concentration, solution pH, and temperature. Over a wide range of Co(II) concentrations (10^{-6} to 10^{-3} M), the adsorption of cobalt increased markedly with pH between pH 5.0 and 7.5. Above pH 8 adsorption was marked by precipitation of $Co(OH)_2$. Adsorption was an endothermic process. Hydrolysis of Co(II) was suggested as the adsorption mechanism based on the striking dependence of adsorption on pH and temperature. Results of this study agree with the earlier studies by Chester (59), who also showed that the reaction was endothermic, and by Hodgson et al. (61) who suggested that hydrolysis was the predominant reaction.

Healy et al. (63) studied the adsorption of Co(II) at the silica-water interface as a function of pH, ionic strength, and total Co(II) concentration. At pH less than 6 and concentrations less than 10^{-5} M, the important saturation species were the Co^{2+} ions and adsorption was relatively small under these conditions. For pH values above 6.5 and at concentrations below precipitation of cobalt hydroxide, the authors suggested that Co^{2+} was specifically adsorbed as either of the following forms:

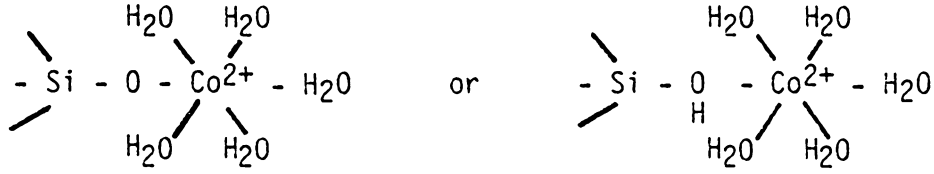

James and Healy (64) further examined the possibility that the first hydrolysis product of Co(II), $CoOH^+$, was the adsorbed species. Their study focused on observations that very little adsorption of hydrolyzable metal ions occurs on oxide surfaces until about one pH unit below the pH of metal hydroxide formation. The amount of Co(II) adsorbed on SiO_2 and TiO_2 was compared to the fraction of $CoOH^+$ in solution at the same concentration and pH, in the absence of oxide. It was found that adsorption of Co(II) could not be related to the amount of $CoOH^+$ or any single hydrolysis product. However, a general qualitative relationship between the pH of abrupt adsorption and the pH of hydrolysis was observed.

Using electrophoretic mobility and streaming potential measurements, James and Healy (65) investigated the adsorption of Co(II), La (III), and Th(IV) on SiO_2 and TiO_2. Three charge reversals (CR) in

order of increasing pH were shown to represent the point of zero charge (PZC) on the SiO_2 substrate (CR1), the pH of metal hydroxide surface nucleation (CR2), and the PZC of the metal hydroxide coating (CR3). CR2 was usually found to appear at a pH below the bulk precipitation pH for oxides with very low available surface area. The possibility that surface $Co(OH)_2$ precipitate is more insoluble than bulk precipitate was discussed. This possibility was dismissed because it would imply that surface and bulk hydroxides were different materials. The surface and bulk hydroxides were shown to be the same by the correspondence of CR3 and the PZC of the "normal" hydroxide. A model was proposed and supported by calculations based on the Born charging equation, to show that the electric field at the interface induces precipitation on the surface at pH values below those of bulk precipitation.

Another study by James and Healy (66) proposed a model for adsorption in the compact part of the double layer in terms of competition between coulombic and chemical energy changes favorable to adsorption and unfavorable to changes in solvation energy. The change in free energy of adsorption, $\Delta G^\circ_{ads_i}$, for a species "i" is the sum of the individual free energy change terms as follows:

$$\Delta G^\circ_{ads_i} = \Delta G^\circ_{coul_i} + \Delta G^\circ_{solv_i} + \Delta G^\circ_{chem_i} \qquad (4)$$

where $\Delta G^\circ_{coul_i}$ is the change in coulombic free energy, $\Delta G^\circ_{solv_i}$ is the change in secondary solvation energy, and $\Delta G^\circ_{chem_i}$ is any specific adsorption energy contribution for the adsorption of an ionic species. In this model, the Born equation was used to assess the free energy

changes for solvation of an ion of charge z. The Born equation for the secondary hydration energy of an ion is:

$$\Delta G^{\circ}_{\substack{\text{secondary}\\ \text{hydration}}} = \frac{-z^2e^2\,N}{8\pi(r_{ion} + 2r_W)\varepsilon_o} \cdot \left[1 - \frac{1}{78.5}\right] \text{joule mole}^{-1} \qquad (5)$$

where z is the ion charge, e is the electronic charge, N is Avogadro's number, and ε_o is the electric permittivity of free space which has a value of 8.85×10^{-12} coulomb $v^{-1}m^{-1}$. The factor (1-1/78.5) is a result of considering secondary hydration when an ion is removed from a vacuum with dielectric, ε_i=1, and placing it in water, with a dielectric ε_f=78.5. The term $(r_{ion} + 2r_W)$, where r_{ion} is the ionic radius and r_W is the water molecule radius, is a result of the assumption that the primary hydration sphere of the ion is unchanged.

James and Healy (66) noted that if the first layer of water molecules on an insulating and low dielectric solid is regarded as electrically saturated and of low dielectric constant, work must be done to remove part of the secondary hydration layer of a cation and to replace it by interfacial water. Because of the quadratic dependence of the secondary hydration energy change on the charge of the ion, it was reasoned that adsorption of highly charged species on low dielectric solids such as silicas and clays was less favorable than adsorption of lower charged species. From the Born equation it was also predicted that a larger ion would have a less negative secondary solvation energy because of the inverse dependence of this energy on the ionic radius. As hydrolysis occurs and the species charge is reduced, the coulombic

energy contributions will become more important and adsorption enhanced. A analytical technique such as XPS can be used to investigate the chemical nature of the adsorbed species.

X-ray photoelectron spectroscopy, (XPS), has been employed by many researchers (67-74) to investigate the adsorption of metal ions on mineral surfaces. Using XPS, the oxidation state and bonding nature of sorbed metals can be analyzed. XPS was used by Tewari and coworkers (71,72) to investigate the chemical environment of Co(II) adsorbed onto TiO_2, ZrO_2, $NiFe_2O_4$, and Al_2O_3. By XPS analysis of Co $2p_{1/2}$ and Co $2p_{3/2}$ satellite features, the energy separation between the Co $2p_{1/2}$ and $2p_{3/2}$ photopeaks, and the binding energies of the Co $2p_{3/2}$ photopeak, they concluded that the surface species for Co(II) adsorbed at pH 8.1 was $Co(OH)_2$.

An XPS investigation of the adsorption of cobalt on a clay surface was conducted by Koppelman and Dillard (73). They analyzed the Co $2p_{3/2}$ and Co $2p_{1/2}$ photopeaks for cobalt adsorbed on chlorite at pH 3 and 7. By comparing the photopeak of the adsorbed cobalt to many cobalt containing reference compounds, it was reasoned that cobalt was adsorbed as Co^{2+} and not as $Co(OH)_2$. XPS was used also to investigate the adsorption between pH 5 and 10 of cobalt on illite (74). The authors concluded that an aqua Co(II) species was adsorbed at pH 6, $Co(OH)_2$ was formed at pH values 7.8 to 10, and a combination of $Co(OH)_2$, Co(II)(aq), or $Co(OH)^+$ could be present in the pH 6.0 to 7.8 range.

B. COBALT ADSORPTION BY MANGANESE DIOXIDE

A comparison of the concentration (weight percent) of cobalt in Pacific marine manganese nodules to that in the surrounding seawater has shown that the concentration in the nodules is approximately 10 million times greater (39). A high percentage of cobalt has also been found in soils containing MnO_2 (52,75). Many model studies involving synthetically prepared and commercially available manganese dioxide have been carried out to investigate the mechanism of cobalt concentration by soil manganese dioxide and manganese nodules.

Specific adsorption of Co(II) onto manganese dioxide referred to as 10Å manganite was reported by Murray and coworkers (76). They found that cobalt was adsorbed at pH values below the iso-electric point, IEP, whereas Li^+, Na^+, and K^+ were not adsorbed. The adsorption of Co^{2+} was compared to that of Cu^{2+} and Ni^{2+}. The observation that Co^{2+} was adsorbed more strongly than Cu^{2+} and Ni^{2+} was attributed to surface oxidation of Co^{2+} to Co^{3+}.

McKenzie (77) studied the adsorption of cobalt, copper, and nickel from solution by a number of synthetic manganese dioxides and compared the quantity of metal adsorbed to the quantity of ions released during the reaction. The initial rapid uptake of all three ions was followed by a period of slow uptake which continued for eight weeks. During the slow phase of the reaction, the uptake of cobalt was greater than that of copper or nickel and cobalt released more manganese into solution. It was suggested that cobalt was able to replace Mn^{3+} in the crystal lattice.

Basak et al. (78) also observed a fast initial reaction followed by a slow reaction during cobalt interaction with manganese dioxide. Based upon crystal field theory and comparison of ionic radii, they concluded that Co^{2+} substituted for Mn^{2+} in the lattice but did not rule out the possibility of Co^{2+} substituting for Mn^{3+}.

Loganathan and Burau (79) proposed that cobalt was able to substitute for both Mn^{2+} and Mn^{3+} in the birnessite lattice. This study was based upon a comparison of the adsorption behavior of Co^{2+}, Zn^{2+}, Ca^{2+} and Na^{+} at pH 4. When Na^{+} or Ca^{2+} was adsorbed by Na^{+}-birnessite, no detectable manganese was found in solution. This implied that sorption involved an exchange in the diffuse layer of the oxide-water interface. When either Co^{2+} or Zn^{2+} was adsorbed, manganese was released into solution. Much more manganese was released in the presence of cobalt than in the presence of zinc. It was inferred that there were three adsorption sites for cobalt, two for zinc, and one for calcium. Calcium could exchange for surface bound H^{+}, zinc exchanged with Mn^{2+}, and Co^{2+} adsorbed at the Mn^{3+} site.

Gray and Malati (80) studied the adsorption of Ni^{2+}, Ca^{2+}, Zn^{2+}, Mn^{2+}, and Co^{2+} on manganese dioxide. The adsorption capacity decreased in the order $Mn^{2+} > Zn^{2+} > Cd^{2+} > Co^{2+} > Ni^{2+}$. With the exception of Co^{2+}, this order is inversely related to that of decreasing hydrated ionic radii, which varies, $Ni^{2+} > Cd^{2+} \cong Zn^{2+} > Co^{2+} > Mn^{2+}$ (80). Since cobalt did not follow the behavior of the other metal ions it was suggested that oxidation to Co(III) occurred, but no mechanism was proposed.

Burns (81) proposed that manganese(IV) oxidizes cobalt(II) and that cobalt(III) substitutes for manganese(IV) in the structure. This hypothesis was based on consideration of the atomic radii of the various manganese and cobalt ions as well as the common crystal structure of MnO_2 and CoOOH.

Direct evidence of the oxidation of Co(II) to Co(III) by manganese dioxide was presented by Murray and Dillard (82) using XPS. No evidence was found for the reduction of the manganese dioxide surface. Molecular oxygen was suggested as the oxidizing agent. The mechanism for the oxidation of cobalt was:

$$Co^{2+}_{(aq)} + O_{2(g)} + 2\ 1/2\ H_2O_{(\ell)} \rightarrow Co(OH)_{3(s)} + 2H^+_{(aq)} \qquad (6)$$

C. ADSORPTION OF METAL COMPLEXES

Little work has been conducted on the adsorption of amino acid complexes on clay surfaces. There are no reports in the literature on the adsorption of cobalt amino acid complexes on manganese dioxide. Most of the discussions on the adsorption of metal coordination compounds report the adsorption of complexes containing nitrogen donor atoms, i.e. ammonia (NH_3) (73,83-87), ethylenediamine ($H_2NCH_2CH_2NH_2$) (84,88-91), diethylenediamine ($H_2N(CH_2CH_2NH)_2H$) (92), 1,10 phenanthroline ($C_{12}H_8N_2$) (93,94), and bipyridyl ($C_{10}H_8N_2$) (93-95). The solid surfaces discussed include clays (73,85,87-95), silica (84,96), and carbon black (83,86).

Bodenheimer et al. (88) were first to report that metal complexes are adsorbed by montmorillonite into the clay interlayers. The cation exchange properties of cobalt complexes were investigated by Knudson and

McAtee (89). $Co(en)_3^{3+}$ readily exchanged for Na^+ on montmorillonite. Each $Co(en)_3^{3+}$ replaced three Na^+ cations. Adsorption was enhanced on those surfaces where exchange had already begun.

Swartzen-Allen and Matijevic (93) compared the exchange of $Co(phen)_3^{3+}$ and $Co(dipy)_3^{3+}$ on Na^+-montmorillonite to exchange on Cs^+-montmorillonite. Electrophoresis measurements showed that both complex ions cause charge reversals at pH 3.5. At saturation coverage, Na^+-montmorillonite adsorbed more than twice as much cobalt chelate as Cs^+-montmorillonite. However, the uptake by Na^+-montmorillonite considerably exceeded the cation exchange capacity of the clay, indicating that mechanisms in addition to ion exchange were responsible for adsorption. In contrast, electrophoretic mobility measurements made by Dalang and Stumm (84) showed that charge reversal did not occur upon adsorption of $Co(NH_3)_6^{3+}$ or $Co(en)_3^{3+}$ on silica particles. These measurements together with the observation that three protons were released for each complex ion adsorbed were cited as evidence that the interaction of $Co(NH_3)_6^{3+}$ and $Co(en)_3^{3+}$ with silica was totally of an electrostatic nature.

The possible catalytic role of oxide surfaces causing hydrolysis of the complexes was first reported by Chaussidon et al. (87). When montmorillonite was saturated with $Co(NH_3)_6^{3+}$ the complex was adsorbed. However, upon evacuating the sample at room temperature or heating the sample in a vacuum the complex decomposes to Co(II) and ammonia is released. This decomposition was surprising in light of the known stability of the complex.

In 1966, Fripiat and Helsen (85) investigated the decomposition of $Co(NH_3)_6^{3+}$ on silica gel, carbon black, and Raney nickel and found that decomposition of the complexes was accelerated under vacuum even at room temperature.

The electronic spectra of $Co(NH_3)_6^{3+}$ and $Co(en)_3^{3+}$ adsorbed on silica gel were measured by Hathaway and Lewis (96). They proposed that the complexes initially exchanged with sodium ions on the surface. Dehydration of the gel at 100°C resulted in the formation of $Co(H_2O)_6^{2+}$ and total loss of ammonia. The mechanism of reduction was postulated to be loss of ammine ligands followed by reduction of Co^{3+} to Co^{2+} by traces of water still present in the silica gel after dehydration.

Berkheiser and Mortland (94) investigated the adsorption of Cu(II) and Fe(III) phenanthroline complexes on the clay mineral hectorite. It was found that van der Waals interactions were responsible for the adsorption of the complexes in excess of the exchange capacity. It was observed by ESR that $Cu(phen)_3^{2+}$ loses a ligand upon adsorption and the corresponding bis complex is formed. However, loss of ligands did not occur for $Fe(phen)_3^{3+}$ upon adsorption. Qualitative tests showed that some Cu^{2+} was reduced to Cu^{+} and Fe^{3+} was reduced to Fe^{2+}. Berkheiser and Mortland (94) reasoned that reduction of the complexes occurred due to destabilization of the oxidized complex through interaction with the silicate surface.

These conclusions made by Berkheiser and Mortland (94) were later refuted by Gillard and Williams (97). They reported that the observed reduction of $Fe(phen)_3^{3+}$ to $Fe(phen)_3^{2+}$ was due to reduction by water

and not to destabilization of the oxidized complex by the silicate surface.

Koppelman and Dillard (73) used XPS to investigate the hydrolysis of $Co(NH_3)_6^{3+}$ on the clay mineral chlorite. This study found that cobalt was reduced to Co(II). Trace iron in the clay was suggested as the reducing agent and the reaction scheme proposed is presented below:

$$Co(NH_3)_6^{3+} + \text{chlorite} \rightarrow \text{chlorite} - Co(NH_3)_6^{3+} \quad (7)$$

$$\text{chlorite} - Co(NH_3)_6^{3+} \rightarrow \text{chlorite} - Co(NH_3)_5H_2O^{3+} + NH_3 \quad (8)$$

$$\text{chlorite} - Co(NH_3)_5H_2O^{3+} \rightarrow \text{chlorite} - Co(H_2O)_6^{3+} + 5NH_3 \quad (9)$$

$$\text{chlorite} - Co(H_2O)_6^{3+} \rightarrow \text{chlorite} - Co(H_2O)_6^{2+} \quad (10)$$

$$NH_3 + H_2O \rightarrow NH_4^+ + OH^- \quad (11)$$

The first study of the adsorption of metal amino acid complexes was carried out by Siegel and Degens (20). They observed the same amount of adsorption for $Zn(gly)^+$ and Zn^{2+}. This was contrary to that expected for coulombic interactions and indicated that other interactions occur such as van der Waals attraction between the glycine ligand and the surface.

Elliot and Huang (31) found that electrostatic forces played a large role in adsorption of Cu(II) in the presence of chelates. The SiO_2 and TiO_2 used in this study had a PZC approximately pH 2 to 3. These oxides showed no affinity for negative Cu(II) aspartate complexes between pH 3 to 10. However, the same complexes showed significantly enhanced adsorption on Al_2O_3, whose PZC is assumed to be pH 9. Adsorption of Cu(II) complexes of NTA (nitrilo-acetate), glycine and aspartic acid was observed at the pH_{PZC} of γ-Al_2O_3. This suggested the presence of

specific chemical interaction. Elliott and Huang (31) stated that the specific interactions involve hydrogen bonding between the ligands and the alumina surface.

Farrah and Pickering (29,30) compared the adsorption of Cu^{2+} and Zn^{2+} on kaolinite with and without glycine. Glycine inhibited precipitation of the metal. The amount of metal adsorbed was reduced in the presence of glycine, however significant adsorption (approximately $1x10^{-4}$ m/g) was observed even in large excesses of glycine. Similar results were obtained for the adsorption of copper on Metapeak soil in the presence of glycine.

Hipps and Mazur (98) used tunneling spectroscopy to study the properties of Ni(II)$(gly)_2$, Co(II)$(gly)_2$, and Co(III)$(gly)_3$ complexes adsorbed onto alumina. The Ni$(gly)_2$ and Co(III)$(gly)_3$ complexes adsorbed. The presence of a well defined Co-N stretching band at 410 cm^{-1} indicated that at least one glycine was coordinated to cobalt. The spectra changed as the pH was reduced from pH 8.6 to 4.0. The frequency of the CN stretching mode at 1053 cm^{-1} decreased by 11 cm^{-1} and its intensity relative to the CH peak decreased dramatically. No explanation for these changes was given. The band corresponding to the Co-N stretching frequency was not observed for Co(II)$(gly)_2$ adsorbed on alumina. However, bands corresponding to glycine were observed. It was concluded that Co(II)$(gly)_2$ merely served as a source of glycine.

D. AMINO ACID ADSORPTION ONTO MINERAL SURFACES

Although amino acids occur in both marine and soil systems, few studies have investigated the interaction of these molecules with clays

and oxide surfaces. The early studies on the adsorption of amino acids centered on the experimental conditions and particular characteristics that enhanced adsorption. Talibudeen (99) investigated the influence of basicity and molecular size on the adsorption of some amino acids and proteins by montmorillonite at pH 2.5. On the basis of the amount of sodium replaced by the organic cations he concluded that basicity was more important than molecular size in determining the extent of adsorption. X-ray analysis of the clay after adsorption revealed that the c-spacing of the interlayers was less than that predicted for the adsorbed amino acids. Contraction of the basal planes was attributed to hydrogen bonding of the amino acids to the surface oxygen atoms of the basal planes.

Greenland et al. (100,101) studied the adsorption of glycine and its di, tri, and tetra peptides on H^+-, Na^+- and Ca^{2+}-montmorillonite. Proton transfer was proposed as the adsorption mechanism between the amino acid, R, and H^+-montmorillonite as follows:

$$\text{Clay} - H_3O^+ + R^+ \rightarrow \text{Clay} - RH^+ + H_2O \qquad (12)$$

Increased adsorption was observed with increased size of the glycine peptide. Greenland et al. (100,101) determined the isotherms for the adsorption of glycine and its di, tri and tetra peptides by montmorillonite and illite saturated with calcium, sodium, and hydrogen ions. Linear ("C"-type) isotherms were obtained for the sodium and calcium clays indicating that the number of energetically equivalent sites at the clay surface did not diminish as adsorption progressed (101). It was suggested that the amino acids and the peptides were

adsorbed as their corresponding zwitterions because very little if any sodium or calcium counterions were displaced from the clay during adsorption.

The general conclusions of Greenland et al. (100,101) were subsequently confirmed by Cloos et al. (102), who examined the cation exchange and proton transfer reactions of glycine, glycylglycine, and β-alanine with montmorillonite. The intercalated amino acid cations were resistant to washing with water but could be desorbed using 0.5M $BaCl_2$.

In contrast to Greenland et al. (100,101), Fripiat (104) observed release of Na^+ and Ca^{2+} from the ion saturated clay upon adsorption of glycine, glycylglycine, and alanine. Fripiat (104) used X-ray diffraction (XRD) to measure the basal spacings of the montmorillonite after adsorption of glycine, glycylglycine, and alanine. The delta value, which is the minimum size of the amino acid or peptide in the interlayer, was calculated by subtracting 9.5Å, the assumed thickness of the aluminosilicate sheet, from the experimentally measured d_{001} spacing. The delta value, Δ, increased with the amount of peptide adsorbed, but even at saturation, delta was 0.7 to 0.9Å less than the minimum molecular dimension of the amino acids or peptides. Fripiat suggested that the amino acid was "keyed" into the octahedral holes of the montmorillonite lattice. Greenland et al. (105) constructed molecular models of the amino acid and the clay surface and showed that it is possible for amino acids to "key" into the octahedral holes of montmorillonite.

Many investigations (106-108) considered the influence of pH upon adsorption of lysine and isoleucine on montmorillonite. The greatest amount of adsorption occurs at pH 2 (the lowest pH studied) and decreases as the pH increases.

Bodenheimer and Heller (109) investigated the influence of sorbed copper on the adsorption of the amino acids glycine, lysine, methionine, and glutamic acid on montmorillonite. Copper enhanced the amount of adsorption except for glutamic acid. Analysis of desorbed copper indicated that glutamic acid desorbed the greatest amount, followed by glycine, methionine, and lysine. It was proposed that desorption of the metal was the first stage of interaction because the interactions of the amino acids occurred over a period of several days rather than the single hour which was observed in a previous study (110) for exchange or complexation of amines on Cu^{2+}-montmorillonite. In fact, glycine tended to extract copper from the clay more readily than the clay adsorbed glycine, but some amino acid was adsorbed. Bodenheimer and Heller (109) suggested that glutamic acid desorbed the greatest amount of copper because aqueous glutamic acid gives rise to an acid solution. Protons in solution can then exchange for copper counterions and a copper-glutamic acid complex can form in the solution, as shown below:

$$\underset{\text{Glutamic Acid}}{\text{HOOC-}\overset{\overset{\text{H}}{|}}{\text{C}}\overset{\overset{\text{NH}_2}{|}}{}\text{-CH}_2\text{CH}_2\text{COOH}} + Cu^{2+}\text{-clay} \longrightarrow \text{Cu(glutamate)} + 2H^{+}\text{-clay} \qquad (13)$$

A series of studies concerning the chemical nature of amino acids on transition metals and alkali metal saturated clays were conducted by Jang and Condrate (111-113). Using infrared spectroscopy, it was shown that at pH 5.6 or lower a monodentate copper-valine complex was formed on H^+ and Cu^{2+}-montmorillonite:

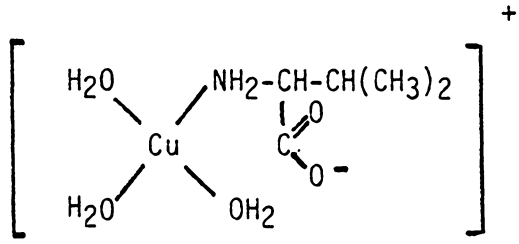

At pH 8.2 the acid group also bonds to the copper and the species has the suggested structure:

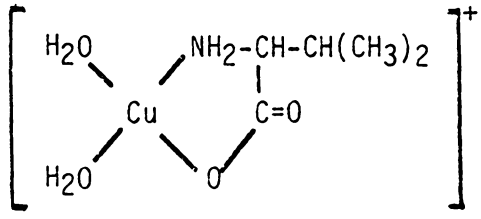

A parallel study (112) with alanine gave similar results. At pH 6.0 a monodentate complex was formed with the copper counterion and a bidentate complex occurred when the pH was greater than 6.0. Below pH 3.0 some alanine cations were adsorbed.

When lysine interacted with montmorillonite saturated with various cations including Co^{2+}, Ni^{2+}, Cu^{2+}, Zn^{2+}, Ca^{2+}, and H^+, lysine coordinated to the transition metals at the natural pH of the clay suspension (112). The predominant species formed was a divalent cation coordinated to two lysine ligands as follows:

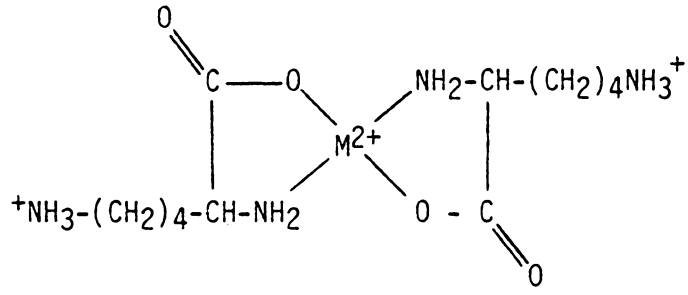

On Ca^{2+}- and H^{+}-montmorillonite the dominant species indicated by infrared spectroscopy was:

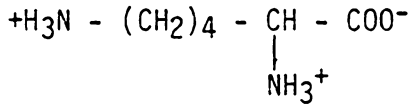

Both amine groups were protonated and the carboxylic acid was in the ionized form.

E. JUSTIFICATION FOR THIS STUDY

The purpose of this research was to study the interaction of metal ions, amino acids, and cobalt amino acid complexes with sediment substrates. Knowledge of these interactions is important in the environment to understand the distribution of metals between the sediment and the water. Much quantitative information has been compiled but little insight into the chemical nature of the surface metal ion has been gained. It has been shown (82) that Co(II) is oxidized to Co(III) on the birnessite surface, and this research investigates the mechanism of oxidation. XPS, particle microelectrophoresis, and other analytical techniques were used to determine the chemical nature of the adsorbed species on birnessite and montmorillonite.

The influence of complexation of metals by amino acid ligands on the bonding of cobalt to the oxide surface and on the chemical nature of the cobalt was investigated. The effect of complex charge on the adsorption mechanism was studied by selecting neutral, positive, and negative amino acid complexes for study. The possibility of surface induced hydrolysis and reduction was considered.

XPS was also used to investigate the interaction of glycine and lysine with montmorillonite and birnessite. Very few studies have used XPS to investigate the adsorption of organic molecules on oxide substrates (114,115). No studies have been reported on the interactions of amino acids with manganese dioxide surfaces.

This research is unique in that it analyzes metal adsorption, ligand adsorption, and metal complex adsorption. By analyzing all three systems it is anticipated that the adsorption of metals in natural solutions, which are composed of both organic and inorganic molecules, may be better understood.

EXPERIMENTAL

A. SUBSTRATES

1. MONTMORILLONITE

The montmorillonite used in this study was STX-1 Texas montmorillonite from Gonzales County, Texas. The clay was obtained from the Source Clay Minerals Repository at the University of Missouri, Columbia, Mo. Montmorillonite is a 2:1 aluminosilicate and has the structure shown in Figure 1 (32). The clay was treated with 30% H_2O_2 to remove organic matter (116), and then sodium or cobalt saturated at pH 6.5 using thirty symmetries of 0.1M NaCl or 0.05M $Co(NO_3)_2$. Excess solute was removed by successive washings of the clay with distilled deionized water until no chloride was detected by 0.1M $AgNO_3$. Nitrate was detected by a spot test (117). The clay was dried under vacuum at room temperature until the pressure was less than 5×10^{-4} torr. This took approximately three days. The N_2 BET (118) and ethylene glycol monoethyl ether (EGME) surface areas (119) and the cation exchange capacities are presented in Table 1. These values agree with those found in the literature (120) which are also given in Table 1. Methods used to determine these properties are described later.

2. SODIUM - BIRNESSITE

Sodium -birnessite was synthesized by first preparing sodium-buserite (121). Two hundred mL of 0.5M $Mn(NO_3)_2$ was placed in a one liter graduated cylinder which was cooled in an ice bath. Oxygen was bubbled through the mixture using a glass frit stick. Two hundred fifty mL of 5.2M NaOH was then added to the cylinder and the reaction was

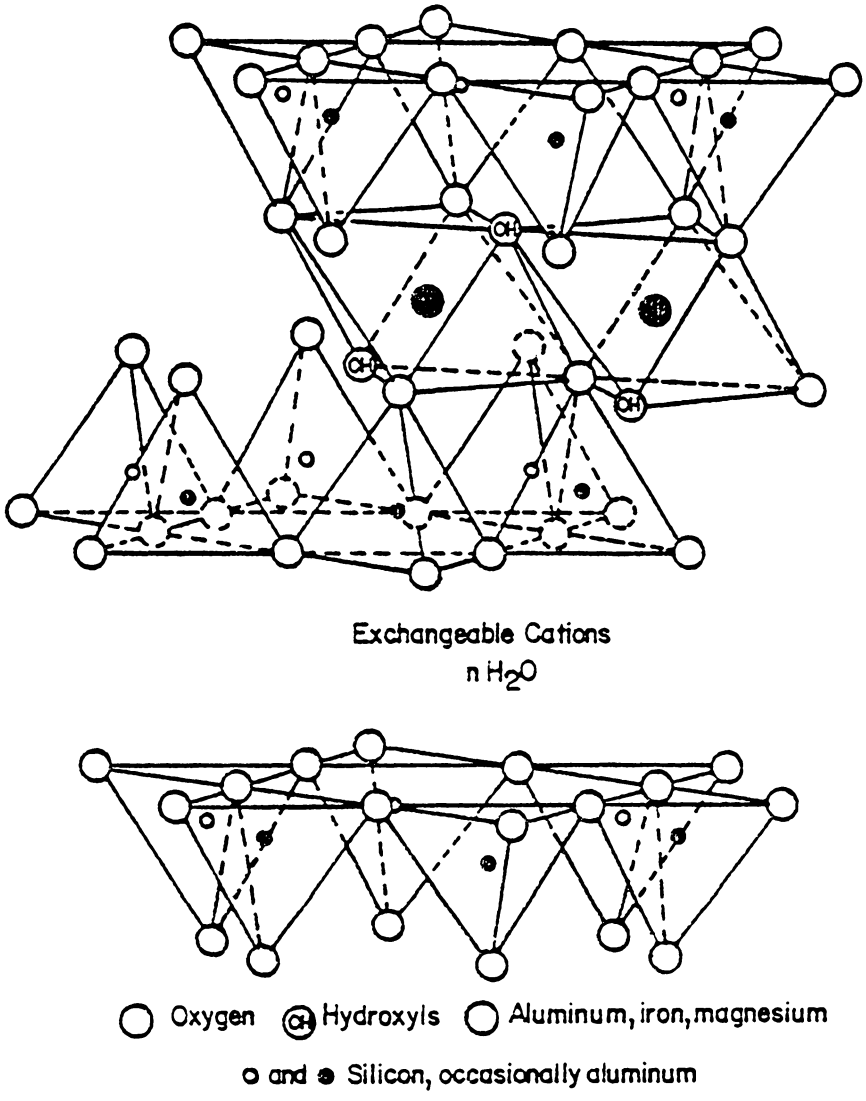

Figure 1. Diagram of Montmorillonite Structure

Table 1

Surface Characteristics of Substrates

	Na^+-Montmorillonite		Na^+-Birnessite	
	Experimental Value	Literature Value	Experimental Value	Literature Value
CEC (meq/100g)	72 ± 2	84.4 (120)	36 ± 2	ND*
N_2BET Surface Area (m^2/g)	104 ± 5	83.79 ± 0.22 (120)	37 ± 2	70 (121) 30-50 (122)
EGME Surface Area (m^2/g)	739 ± 10	750 (120)	ND*	ND*

*ND - Not Determined

allowed to proceed for four hours. The brown-black precipitate was separated by centrifugation and washed repeatedly (approximately 50 times) with distilled deionized water until the suspension had a pH of 7.0. Conversion of Na^+-buserite into Na^+-birnessite was accomplished by drying in air at 120°C for 24 hours.

Much controversy exists in the literature over the nomenclature of the synthetic form of birnessite (37,81,122,123). This confusion can be attributed to the disordered and nonstoichiometric nature of the material formed. Various names have been proposed, including 10Å manganite, todorokite, buserite, 7Å manganite, δ-MnO_2, manganese manganite, and birnessite. The form of birnessite used in this study had only two lines in the x-ray diffraction pattern, at 7.2 and 3.6Å. Burns and Burns (37) suggested that this material be referred to as "synthetic birnessite". The CEC and N_2 BET surface area of this material are presented in Table 1.

B. MANGANESE NODULES

The manganese nodules examined by XPS were provided from two different sources. Dr. Jane Frazer of Scripps Institute of Oceanography LaJolla, CA supplied four nodules and Professor S. E. Calvert of the University of British Columbia, Vancouver, Canada furnished a second set consisting of five nodules. The sample designation and locations where the nodules were found are presented in Table 2 for both sets of nodules.

Table 2

Pacific Manganese Nodules

Frazer Nodules

Sample	South Tow 4FFA	7 Tow 143 D-C	7 Tow 143 D-E	Geosecs 1D
Lat	8.35S	19.5N	19.5N	38.6S
Long	168.5W	168.9W	168.9W	167.9W
Depth(m)	4758	1805	1805	1420

Calvert Nodules

Sample	AMPH	MP43	DWHD16	M2P50	M2P52
Lat	22° 35'S	11° 48'N	16° 29'S	13° 53'S	09° 57'N
Long	150° 48'W	165° 00'W	145° 33'W	150° 35'W	137° 47'W
Depth(m)	807	1620	1270	3700	4930

C. ADSORBATES

1. TRIS(GLYCINATO)COBALT(III)

Tris(glycinato)cobalt(III), $Co(gly)_3$, $C_6H_{12}CoN_3O_6$ was prepared according to the method first described by Ley and Winkler (124). Fresh CoOOH was prepared by oxidizing 100 g $Co(NO_3)_2$ with 100g $NaBO_3 \cdot 4H_2O$. Excess perborate was removed by washing the precipitated CoOOH five times with distilled deionized water. Eighty grams of glycine was added to the fresh CoOOH in three liters of distilled deionized water. The mixture was covered, heated, stirred, and allowed to react at 100°C for eight hours.

$Co(gly)_3$, the purple soluble isomer, was isolated by boiling the three liter solution uncovered until purple crystals appeared. This required reducing the volume to approximately 300 mL. The product was recrystallized from water and dried under vacuum at room temperature until the vacuum was approximately $5x10^{-4}$ torr. CHN analysis was performed by Analytical Services in the Chemistry Department.
Calculated for $C_6H_{12}CoN_3O_6$: C, 25.6; H, 4.0; N, 14.9.
Found: C, 25.5; H, 4.3; N, 15.0.

2. TRIS(L-LYSINATO)COBALT(III) CHLORIDE

Tris(L-lysinato)cobalt(III) chloride, $Co(lys)_3Cl_3$, $C_{18}H_{42}Cl_3CoN_6O_6$ was synthesized according to the method of Ley and Winkler (124). One hundred eighty five grams of L(+)-lysine monohydrochloride was added to freshly prepared CoOOH in three liters of distilled deionized water. The mixture was covered, heated, stirred, and allowed to react at 100°C for eight hours.

The purple solution was then uncovered, boiled down to approximately 300 mL, and cooled. One liter of 95% ethanol was added to induce precipitation of the complex. The product was recrystallized from 95% ethanol. CHN analysis was performed by Analytical Services in the Chemistry Department.

Calculated for $C_{18}H_{42}Cl_3CoN_6O_6$: C, 35.8; H, 7.0; N, 13.9; Cl, 17.6.
Found: C, 35.6; H, 7.3; N, 13.8; Cl, 17.2.

3. HYDROGEN BIS(ASPARTATO)COBALT(III) MONOHYDRATE

Hydrogen bis(aspartato)cobalt(III) monohydrate, $HCo(asp)_2$, $C_8H_{13}CoN_2O_9$, was synthesized according to the method of Ley and Winkler (124). Ninety grams of aspartic acid were added to freshly prepared CoOOH in three liters of distilled deionized water. The mixture was covered, heated, stirred, and allowed to react at 100°C for eight hours.

The purple solution was uncovered and boiled until the volume was 300 mL. After cooling, one liter of 95% ethanol was added to induce precipitation of the complex. The product was recrystallized from 95% ethanol. CHN analysis was performed by the Analytical Services in the Chemistry Department.

Calculated for $C_8H_{13}CoN_2O_9$: C, 28.3; H, 3.85; N, 8.24.
Found: C, 28.5; H, 3.79; N, 8.15.

4. GLYCINE

Glycine (98%) was obtained from Aldrich Chemical Company, Milwaukee, Wisconsin. The glycine was used as received.

5. L(+)-Lysine MONOHYDROCHLORIDE

L(+)-Lysine monohydrochloride (99%) was obtained from Aldrich Chemical Company, Milwaukee, Wisconsin and was used as received.

6. COBALTOUS NITRATE HEXAHYDRATE

The $Co(NO_3)_2 \cdot 6H_2O$ was Baker and Adamson reagent grade, Allied Chemical Division, Morristown, N.J.. This was used as received.

D. REFERENCE COMPOUNDS

The following cobalt-containing compounds were used as standards for XPS and electrophoresis measurements.

1. Cobalt(II) hydroxide $Co(OH)_2$ was obtained from Apache Chemicals, Inc. and was used as received.
2. Cobalt(III) oxyhydroxide (CoOOH) was obtained from Apache Chemicals, Inc. and was used as received.
3. Cobaltous oxide (CoO) - (99.998%) was obtained from Apache Chemicals Inc. It has been reported that CoO is covered with Co_3O_4 (125,126). This was found to be true utilizing XPS. Reduction of Co_3O_4 was accomplished by heating the "as received" CoO in the DuPont electron spectrometer at 400°C for eight hours (125).
4. Cobalt oxide (Co_3O_4) - certified grade Co_3O_4 was obtained from Fisher Scientific Company and was used as received.

E. ADSORPTION EXPERIMENTS

1. ADSORPTION PROCEDURE

The adsorption experiments were conducted by equilibrating 100 mL

of 0.1M adsorbate solution with one gram of clay in polyethylene bottles. The ionic strength was maintained by adding 0.1M $NaClO_4$. The adsorbate solutions were first adjusted to the desired pH before addition to the Na^+- or Co^{2+}-saturated clay. The pH was readjusted four times daily using 0.1M HNO_3 and 0.1M NaOH, and was never allowed to vary by more than ±0.2 pH units of the desired pH. Between pH adjustments, the samples were kept in a 25°C constant temperature bath. After five days the pH of the suspension had stabilized and it was assumed that equilibrium was established. The samples were then centrifuged, and the solid was washed three times with pH 6.5 distilled deionized water and dried in air.

A second set of adsorption experiments was conducted to enable measurement of the sodium released from the sodium saturated substrate surface. The 0.01M adsorbate solutions were first adjusted to the desired pH before addition to the Na^+- or Co^{2+}-saturated substrates. One hundred mL aliquots of solution were added to each one gram clay sample in polyethylene bottles. The pH was readjusted at least four times daily using 0.1M HNO_3 or 0.1M KOH and was never allowed to vary by more than ±0.2 pH units of the desired pH. Between pH adjustments the bottles were stored at 25°C in a constant temperature bath. After five days the pH stabilized, the suspensions were centrifuged, and the supernatant liquid was saved for various quantitative analyses. The solid was washed three times with pH 6.5 distilled deionized water and air dried.

The cobalt amino acid complexes were adsorbed on montmorillonite using $5x10^{-3}$ M, $1x10^{-3}$ M, and $5x10^{-4}$ M adsorbate solutions. The

procedure for these experiments was the same as for the other experiments using 0.01M adsorbate solutions, however $NaClO_4$ was omitted from the solution.

2. ANAEROBIC ADSORPTION EXPERIMENT

The adsorption of Co^{2+} on synthetic birnessite was conducted anaerobically to examine the role of oxygen in the oxidizing reaction. Two grams of birnessite were added to a glass vessel that had been coated with an aqueous dispersion of Teflon (Du Pont Teflon 30) (127). This vessel was designed and used by Koppelman (9). The vessel was sealed with a rubber septum and placed on a vacuum line that was also equipped to pressurize the vessel with argon. The vessel containing the birnessite was evacuated to $1x10^{-5}$ torr and repressurized with argon to 850 torr, for five cycles. These operations were conducted at room temperature. The vessel was then sealed off from the vacuum line by closing the stopcock and placed in a glove bag. The glove bag had two openings: through one opening the glove bag could be pressurized with argon or evacuated. The other opening was sealed around the spout of a vessel containing 0.1M deoxygenated $Co(NO_3)_2$ at pH 6.5. The glove bag was evacuated five times using a water aspirator vacuum and repressurized five times with argon. Five hundred milliliters of the deoxygenated $Co(NO_3)_2$ solution were added through the side arm opening of the vessel and the septum of the vessel was then resealed. The vessel was removed from the glove bag, returned to the vacuum line, and pressurized to 850 torr with argon. The vessel was stored at 25°C in a constant temperature bath for five days. The container was

repressurized once and manually shaken three times daily, but there was no readjustment of pH. The final pH of the adsorbate solution was 6.0. Filtration and washing of the suspension was done under argon in the glove bag. The sample was dried under vacuum.

F. DESORPTION EXPERIMENTS

Desorption experiments were conducted with a known amount (≅0.1 g) of montmorillonite or birnessite that had been equilibrated with the adsorbate solutions. Ten mL of 0.5M $BaCl_2$ (pH 6.5) was added to the solid to desorb the adsorbed ions or molecules from the surface. The solids were equilibrated with the $BaCl_2$ solution for five days at 25°C.

G. DISSOLUTION OF SOLIDS

1. MONTMORILLONITE

To determine the amount of cobalt and cobalt complexes adsorbed on montmorillonite it was necessary to dissolve the solids in concentrated H_2SO_4. A known amount of the clay (±0.2g) was weighed and 10 ml concentrated H_2SO_4 was added. The dissolution was conducted at 100°C for twenty minutes. Although a small portion of the clay did not dissolve, it was established that dissolution of the cobalt containing fraction or desorption of cobalt was complete. This was done by comparing the cobalt analyzed by dissolution of the clay to the cobalt analyzed by the difference between initial and final concentrations of cobalt in the adsorbate solutions.

2. Na^+-BIRNESSITE

For adsorbed cobalt determination, the manganese dioxide was dissolved in HCl. To approximately 0.1g of birnessite was added 10 mL concentrated HCl. Dissolution was conducted at 100°C for ten minutes and total dissolution occurred.

3. MANGANESE NODULES

The manganese nodules provided by Jane Frazer were dissolved in concentrated HCl so that the barium content could be determined. The dissolution procedure was identical to that for Na^+-birnessite.

H. NET Na^+ RELEASE DETERMINATION

The exchange that occurred during adsorption of cobalt on Na^+-montmorillonite was studied by comparing the amount of adsorbate to the amount of surface counterion released. Due to a significant quantity of counterion released into the water in the absence of adsorbate it was felt that a more accurate comparison would be between the amount of adsorbate adsorbed and the net counterion released. The net sodium released was calculated by subtracting the amount of sodium released when the clay was dispersed in water, from the amount of Na^+ released from the surface in the presence of adsorbate. The amount of Na^+ released into the water from Na^+-montmorillonite is presented in Table 3.

Table 3

Sodium Released from Na^+-Montmorillonite

pH	Sodium Released ($\pm 0.2 \times 10^{-4}$ moles/g)
2	7.2×10^{-4}
4	5.2×10^{-4}
6	4.0×10^{-4}
7	3.9×10^{-4}
8	3.9×10^{-4}
10	3.9×10^{-4}
Exchangeable Sodium on Clay Surface (CEC)	7.2×10^{-4}

I. ATOMIC ABSORPTION

Atomic absorption analysis was conducted using a Varian Model AA-175 spectrophotometer. Air was used as the oxidizer and acetylene was the fuel used for all analyses. The preparation of atomic absorption standards is presented below:

1. Cobalt Analysis - Acid Dissolved Montmorillonite

Standards were prepared by dissolving known amounts of $Co(NO_3)_2 \cdot 6H_2O$ in concentrated H_2SO_4.

2. Cobalt Analysis - Acid Dissolved Na^+-Birnessite

Standards were prepared by dissolving known amounts of $Co(NO_3)_2 \cdot 6H_2O$ in concentrated HCl.

3. Barium Analysis - Manganese Nodules

Barium standards were prepared by dissolving $BaCl_2$ in concentrated HCl.

4. Cobalt Analysis - Cobalt Desorbed by 0.5M $BaCl_2$ From Substrates

Cobalt standards were prepared in 0.5M $BaCl_2$ using $Co(NO_3)_2 \cdot 6H_2O$.

5. Cobalt Analysis - Cobalt Determined by Difference

Cobalt standards were prepared in 0.1M $NaClO_4$ using $Co(NO_3)_2 \cdot 6H_2O$.

6. Cobalt Analysis - Cobalt Released From Co^{2+}-Saturated Substrate

Cobalt standards were prepared using $Co(NO_3)_2 \cdot 6H_2O$ in distilled deionized water.

7. Sodium Analysis - Na^+ Released From Na^+-Substrates

Sodium standards were prepared in distilled deionized water using $NaClO_4$.

8. Sodium Analysis - Cation Exchange Experiment

Sodium standards were prepared in 0.1M $BaCl_2$ and in distilled deionized water using $NaClO_4$.

9. Manganese Analysis - Manganese Released From Na^+-Birnessite During Adsorption

Manganese standards were prepared in distilled deionized water using $Mn(NO_3)_2$.

J. NINHYDRIN ANALYSIS

Quantitative measurements of amino acid adsorbed were conducted according to the modified ninhydrin procedure of Troll and Canaan (128). The adsorbed amino acid was desorbed using 0.5M $BaCl_2$. Fripiat et al. (85) have shown that Ba^{2+} exchange totally desorbs amino acids from montmorillonite. One milliliter of the solution containing the desorbed amino acid was added to 1 mL 0.01M KCN in pyridine and 1 mL 80% phenol in ethanol. This mixture was heated for five minutes in a boiling water bath and 0.2 mL of 0.01M ninhydrin in ethanol was then added. This mixture was allowed to react for two minutes in the boiling water bath. After the reaction mixture had cooled, the absorption at 575 nm was measured using a Bausch and Lomb Model 20 Spectrophotometer.

Standards were prepared by adding known amounts of amino acid to 0.5M $BaCl_2$. The detection limit for this method is 2.0×10^{-5} moles

amino acid per gram of clay. The calibration curve for lysine is presented in Figure 2.

K. X-RAY PHOTOELECTRON SPECTROSCOPY (XPS)

Solid samples were analyzed by XPS using a DuPont 650 electron spectrometer. Generally, a magnesium anode ($h\nu$=1254 eV) was used as the x-ray source. For the analysis of cobalt adsorbed on montmorillonite, an aluminum anode ($h\nu$=1486 eV) was used because a portion of the oxygen KVV Auger peak occurs at 780 eV and interferes with the cobalt 2p signal. Background carbon, BE = 284.5 ± 0.1 eV, was used for calibration of the binding energy scale. This value was established using the Au $4f_{7/2}$ photopeak (binding energy = 84.4 eV) as a reference. The analyzer pressure was approximately 3×10^{-7} torr for all measurements.

Samples were prepared by lightly grinding the sample using an agate mortar and pestle. The powders were adhered to a brass probe using double stick tape. A variable temperature probe was also used. Temperatures from -80°C to +400°C could be obtained. For high temperature analysis, samples were prepared by adding a drop of an acetone dispersion of the sample onto the probe and allowing the acetone to evaporate.

Spectra were collected using a Nicolet multichannel analyzer (MCA). This enabled repetitive scanning of the region of interest to improve the signal to noise ratio. Digital data from the MCA were transferred to a Digital Equipment Corporation (DEC) PDP 8/I computer for data storage (on paper tape) or for curve fitting.

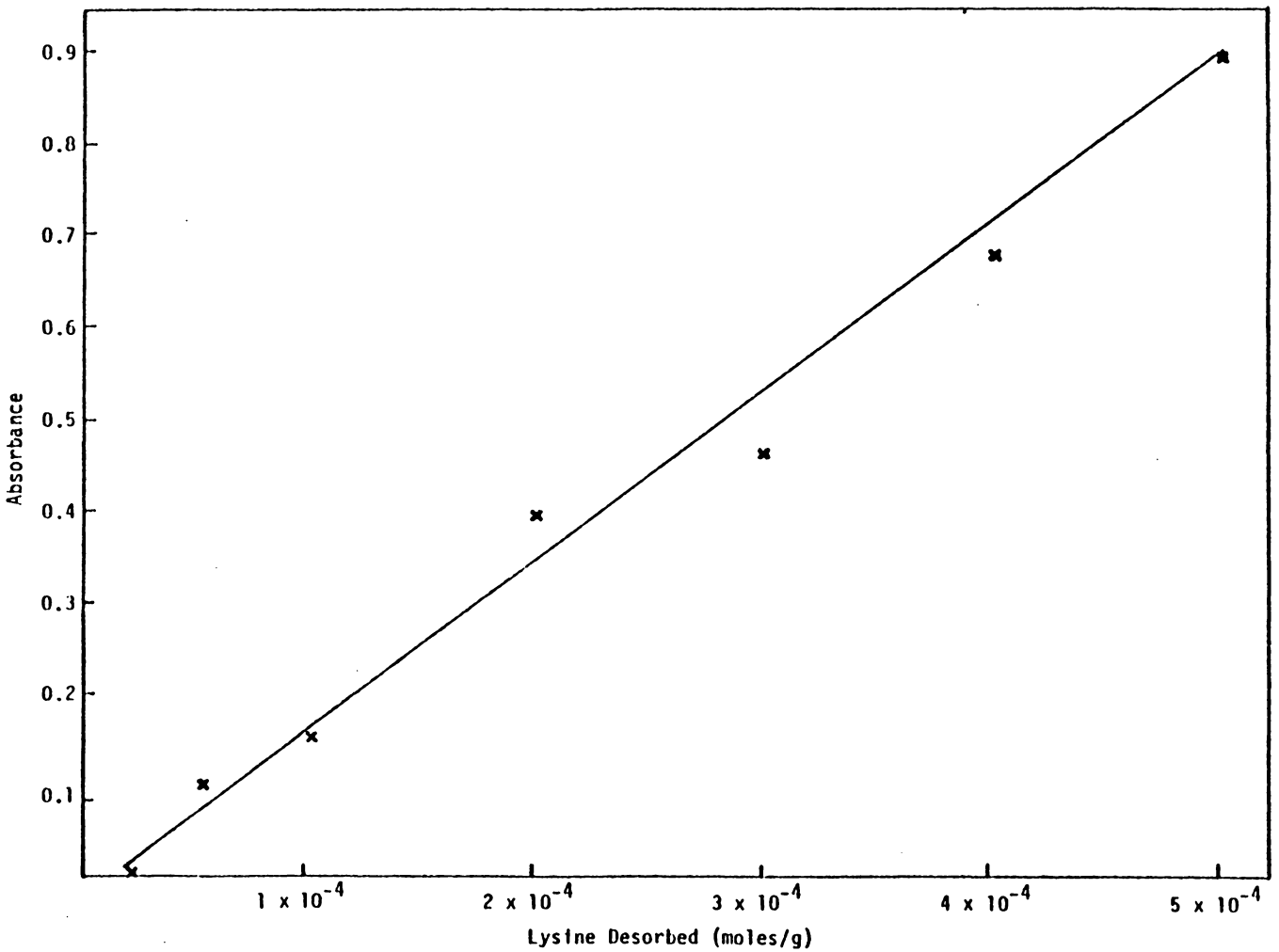

Figure 2. Calibration Curve for Lysine Desorbed from Montmorillonite

The GASCAP IV program (129) was used for curve fitting. Background electron noise was subtracted from the spectra, assuming a linearly increasing baseline. The curve fitting procedure requires input of the number of peaks and the peak intensity, peak position, and peak width at half maximum (PWHM) for each peak suspected of comprising the spectrum. This procedure was used for curve fitting the N 1s spectra of the amino acid complexes adsorbed on montmorillonite and on birnessite. The PWHM used for curve resolving the N 1s multiplets was obtained by curve fitting the N 1s spectrum for L(+)-lysine monohydrochloride. The peak positions and heights of the individual peaks were varied until the computed curve corresponded to the experimental curve.

Integrated peak intensities were obtained by measuring peak areas and correcting for the Scofield photoionization cross sections (130).

The nitrogen to coablt ratio was calculated by measuring integrated peak intensities of the N 1s and Co $2p_{3/2}$ photopeaks. This raw data was then corrected to an atomic ratio using the known N/Co ratio of the pure complex.

L. ELECTROPHORESIS

Electrophoretic mobility measurements of the substrates in various aqueous solutions were conducted using a Rank Brothers Mark II particle microelectrophoresis apparatus with a rectangular flat cell. The effective electrode distance of 7.98 cm was determined by measuring the resistance in 0.01M KCl. The calculation for the effective

electrode distance, L, was:

$$L = RKA \qquad (14)$$

where R is the resistance; K is the electrical conductivity, equal to 1.411×10^{-3} ohm^{-1} cm^{-1} for 0.1M KCl at 25°C; and A is the cross sectional area of the cell. The electrodes were platinized platinum. Applied voltages between 30 and 50 volts were employed but lower voltages were required to reduce outgassing at the electrodes, particularly at pH 2. An applied potential of 10 to 20 V was used in those cases when outgassing at the electrodes occurred.

The electrophoretic mobility measurements were made at the stationary planes of the cell. The stationary planes are the two planes in the cell where the true mobility can be measured and are located at positions 19% of the total distance between the walls (131). At all other positions in the cell there are interferences due to the streaming potentials at the walls of the cell and to the compensating return of liquid which reaches a maximum in the center of the cell (130). These two forces cancel out at the stationary planes.

Suspensions used for electrophoretic mobility measurements had approximately 0.2g substrate per liter of 0.01M adsorbate solution. Higher concentrations of adsorbate could not be used because the higher ionic strength increased the outgassing at the electrodes. The pH of the suspensions was adjusted using 0.1M HNO_3 or 0.1M NaOH. Suspensions were equilibrated for five days before making electrophoresis measurements.

The measurements were made by viewing the movement of the particles in the electric field and timing the movement over a distance of 0.05 mm at 25°C. An average mobility for twenty particles was calculated. Five particles were timed in each direction at both stationary planes.

The error in the electrophoretic mobility measurements is ±0.5 m.u.

M. INFRARED ANALYSIS

Infrared analysis of the amino acids adsorbed on Na^{+}- and Co^{2+}-montmorillonite and $Co(lys)_3^{3+}$ on montmorillonite was carried out using self supporting montmorillonite films. Suspensions were prepared by adding 5 mL of water to approximately 0.2g of clay. Suspensions were placed in an ultrasonic bath for about two minutes. Films were made by casting the suspensions on a polyethylene sheet and allowing the film to air dry.

A Perkin-Elmer 283B infrared spectrophotometer with a computerized data system was used to obtain the spectra. No attempt was made to eliminate water from the system.

N. VISIBLE SPECTROSCOPY

Transmission and diffuse reflectance spectroscopic measurements were made using a Cary 14 spectrophotometer. No dilution of the solutions was necessary for the transmission measurements. Distilled deionized water was used as the reference. Reflectance samples were prepared by applying the powders onto black electrical tape. Magnesium oxide was used as the reference.

O. X-RAY DIFFRACTION

X-ray diffraction measurements for the substrates before and after adsorption were conducted using a Norelco X-ray diffractometer with Ni filtered Cu K_α radiation. The x-ray generator was operated at 40 KV and 20 ma. Scans were acquired at two degrees per minute. The diffractometer was controlled by a Digital Equipment Corporation PDP 11 Computer. Samples were prepared by applying an acetone dispersion of the clay on a quartz slide and then air dried.

P. pH MEASUREMENTS

pH measurements were made using an Orion Research Model 701 digital pH meter. A Sensorex sealed reference combination pH electrode was used. Fisher Standard pH buffers were used for calibration.

Q. CATION EXCHANGE CAPACITY

The cation exchange capacity (CEC) was determined by suspending 0.2g of Na-saturated solid sample in 20 mL 0.5M $BaCl_2$. The sodium released was subsequently measured by atomic absorption spectroscopy.

R. N_2 BET SURFACE AREA

The N_2 BET surface area for the solid substrates was measured in duplicate using a Micromeritics Model 2100-D Surface Area Analyzer. Approximately 0.25g samples were weighed into the sample tubes. The exact amount of substrate in the tube was measured by difference on a Mettler Type B-6 balance to the nearest milligram. The Na^+-birnessite was outgassed for two hours at 100°C under vacuum and montmorillonite

was outgassed under vacuum overnight at 200°C. Isotherms were determined at liquid N_2 temperature.

The adsorption involved pressurizing the manifold with N_2 to approximately 80 torr Hg, and the exact initial pressure, P_1, was recorded. Then the sample valve was opened to equilibrate the known N_2 pressure with the solid substrate. Equilibration was assumed to be the point at which the pressure did not change for 20 seconds. The equilibrated pressure was recorded as P_2. The sample valve was again closed and the manifold was repressurized to a point approximately 20 torr Hg above P_1. The adsorption procedure was repeated until a total of five points were obtained. The initial pressure was increased each time from the preceding P_1 by approximately 20 torr Hg.

A computer program written by Jean Skiles (132) was employed in conjunction with the PDP 8/I computer to calculate surface areas based on the BET equation. The cross sectional area for N_2 was assumed to be 16.2 Å^2/molecule.

S. ETHYLENE GLYCOL MONOETHYL ETHER (EGME) SURFACE AREA DETERMINATION

The adsorption of EGME was used to measure the total surface area (119). A 1.1g sample of montmorillonite was placed in a shallow aluminum weighing pan and dried to a constant weight over P_2O_5 in an evacuated desiccator at room temperature. Approximately 3 mL of reagent grade EGME was added to each dried sample. The slurry was allowed to equilibrate for one hour over a EGME-$CaCl_2$ solvate in a vacuum desiccator. The montmorillonite samples in the aluminum pans were then weighed. The samples were returned to the desiccator and evacuated to

0.25 mm Hg. The samples were reweighed and returned to the desiccator every four hours until the excess EGME was totally removed. This was determined by a constant weight for the samples for the last two weighings. The surface area was calculated from the weight of adsorbed EGME. It was assumed that 2.86×10^{-4} g EGME covered 1 m^2 of surface. Duplicate measurements were made.

Chapter IV - RESULTS AND DISCUSSION

The interactions of cobalt, amino acids, and cobalt amino acid complexes with sediment surfaces were studied on the clay mineral montmorillonite and on the manganese dioxide, birnessite. The adsorption of cobalt, amino acids, and cobalt amino acid complexes on montmorillonite is considered in sections A, B, and C, respectively. The discussions of these same adsorbates on birnessite are presented in section D, E, and F. In the last section, G, the chemical nature of transition metals in manganese nodules is discussed.

A. COBALT ADSORPTION ON MONTMORILLONITE

The study of cobalt adsorption on montmorillonite was conducted to determine the mechanism of adsorption and the chemistry of the adsorbed species. Proposals given in the literature for the adsorption mechanism include: 1) lattice substitution (54-56), 2) cation exchange (54-57), 3) adsorption of $CoOH^+$ (58, 61), and 4) precipitation of $Co(OH)_2$ (93).

Approximately 80% of the affinity of montmorillonite for cations arises from substitution of trivalent aluminum in the lattice for tetravalent silicon in the tetrahedral sheet and ions of lower valence, particularly magnesium for trivalent aluminum in the octahedral sheet (Figure 1) (32). The other 20% of the sites responsible for the cation exchange capacity is due to broken bonds at the edges of the clay lattice (32). Ionization at edge sites is pH

dependent, as shown in the following reactions:

$$Si - OH + H_2O \rightarrow SiO^- + H_3O^+ \quad (15)$$

$$Al - OH + H_2O \rightarrow Al\text{-}O^- + H_3O^+ \quad (16)$$

The important properties of montmorillonite related to adsorption include cation exchange capacity (CEC), surface area, and surface charge. The cation exchange capacity was 72 ± 2.0 meq/100g. The N_2 BET and EGME surface areas were 104 ± 5 and 739 ± 10 m^2/g, respectively. These values agree with those reported in the literature, as presented in Table 1. Montmorillonite has a relatively large ability to adsorb cations by exchanging ions in the interlayers as well as on the outer surface. The electrophoretic mobility was measured to examine the charge on the clay surface. The mobility of Na^+-montmorillonite in 0.01M $NaClO_4$ as a function of pH is shown in Figure 3. Between pH 2 and 10, the mobility is relatively constant and has a value of -5.0 um $sec^{-1}/V\ cm^{-1}$. Cations can be attracted via electrostatic forces to the clay in this pH range because the surface charge is negative.

To aid in understanding the adsorption reaction of cobalt on montmorillonite the hydrolysis properties of cobalt in solution must be considered. Baes and Mesmer (133) summarized the hydrolysis properties of 0.1 m and $1x10^{-5}$m Co^{2+} at 25°C (Figure 4). At both concentrations the principal species in solution up to pH 7.4 is $Co(H_2O)_6^{2+}$. The amount of $CoOH^+$ in solution at pH 8.0 is less than 2% in both 0.1 and $1x10^{-5}$ m Co^{2+}. Some polynuclear species such as $Co_4(OH)_4^{4+}$ form in 0.1 m Co^{2+} at approximately pH 9 but are not present at lower

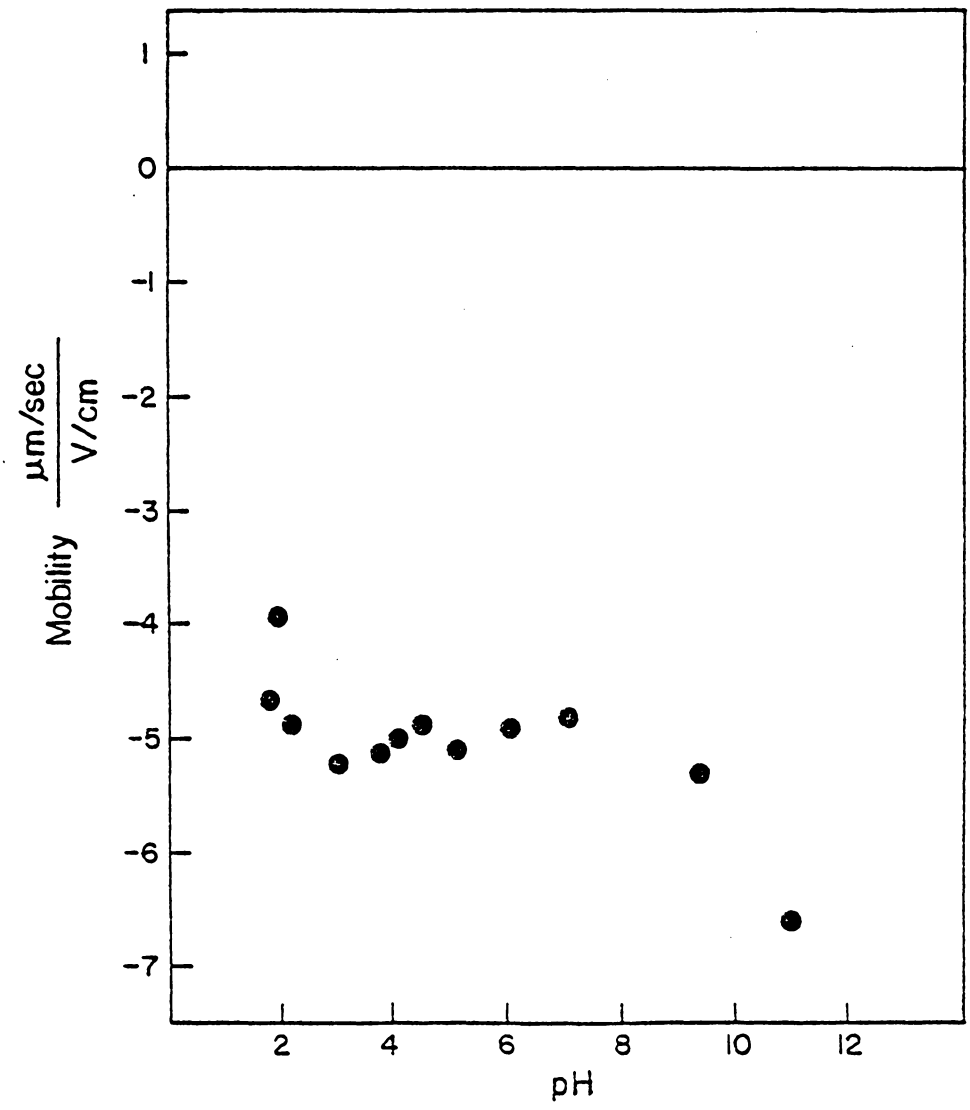

Figure 3. Electrophoretic Mobility of Na^+-Montmorillonite in 0.01 M $NaClO_4$

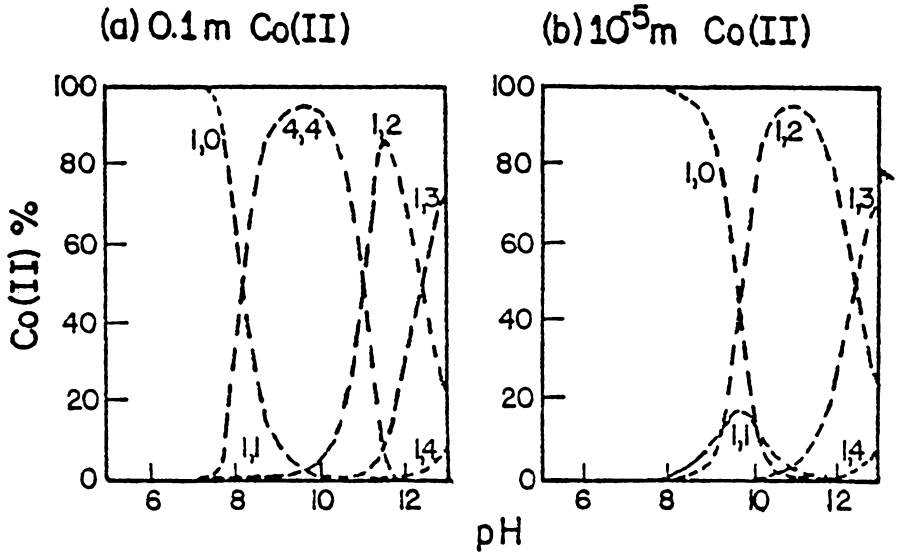

Figure 4. Distribution of Cobalt(II) Hydrolysis Products

concentrations.

The quantity of cobalt adsorbed as a function of pH is shown in Figure 5. The amount of adsorption changes dramatically between pH 7 and 8. Reports in the literature attribute this increase to the adsorption of hydrolyzed Co^{2+} (58,61,93). Hodgson et al. (61) proposed that $CoOH^{+}$ was the species adsorbed, based on consideration of the competitive effect of Mg^{2+} on adsorption. Swartzen-Allen and Matijevic (93) suggested that the surface species above pH 7 was $Co(OH)_2$, based on electrophoretic mobility studies of montmorillonite in $1x10^{-4}$ M Co^{2+}. Sorbed cobalt below pH 7 is due to the adsorption of soluble cobalt species (93). The amount of adsorbed cobalt increases gradually between pH 2 and 7. The lower amount of adsorption at pH 2 is most likely due to competition by both protons and Al^{3+} for adsorption sites on the clay (32,33). The gradual increase in the amount of adsorption up to pH 7 has been attributed to the increasing role of edge sites in Co^{2+} adsorption (28). As the pH increases, the number of negative SiO^{-} edge sites increases as shown in Equation 16 (32,33).

The exchangeable nature of adsorbed cobalt was investigated by three methods. First, the net sodium released into solution from Na^{+}-montmorillonite during adsorption in 0.01M $Co(NO_3)_2$ was measured and compared to the amount of cobalt adsorbed. Secondly, the atomic Na/Si XPS ratio for Na^{+}-montmorillonite treated with cobalt was compared to that for a Na^{+}-montmorillonite sample suspended in water at comparable pH values. The third method was to exchange adsorbed cobalt with 0.1M $BaCl_2$ at pH 6.5 and determine cobalt released.

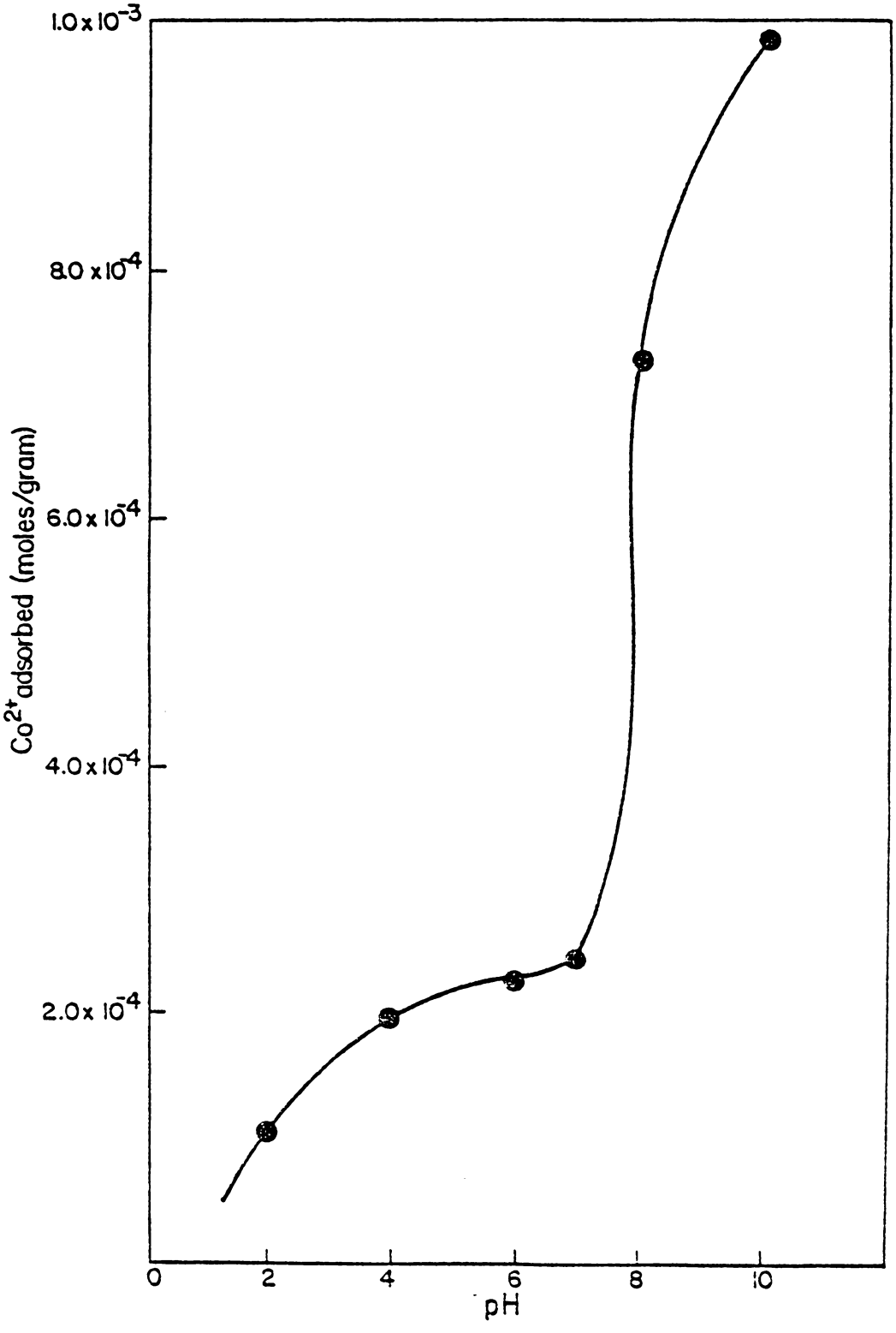

Figure 5. Cobalt Adsorbed on Montmorillonite

The amount of cobalt adsorbed on montmorillonite from a 0.01M solution of $Co(NO_3)_2$ and the net sodium released as a function of pH are presented in Table 4. At pH 2 there is total release of Na^+ from the clay in the presence of both Co^{2+} and water so that the net Na^+ release is zero. The mechanism responsible is exchange of Na^+ by Al^{3+} and H^+ as shown below:

$$Al^{3+} + Na^+\text{-clay} \rightarrow Na^+ + Al^{3+}\text{-clay} \quad (17)$$

$$H^+ + Na^+\text{-clay} \rightarrow Na^+ + H^+\text{-clay} \quad (18)$$

It is not known whether the exchange by aluminum is nonequivalent exchange, as shown above (Equation 17), or equivalent exchange as presented below:

$$Al^{3+} + 3Na^+\text{-clay} \rightarrow 3Na^+ + Al^{3+}\text{-clay} \quad (19)$$

At pH 4, 6, and 7, the ratio of Na^+ released from montmorillonite to the amount of cobalt adsorbed was approximately 1:1. If equivalent exchange occurs $CoOH^+$ could exchange for Na^+ as follows:

$$Co^{2+} + H_2O \rightarrow CoOH^+ + H^+ \quad (20)$$

$$CoOH^+ + Na^+\text{-clay} \rightarrow CoOH^+\text{-clay} + Na^+ \quad (21)$$

A second possible mechanism is nonequivalent exchange between Co^{2+} and surface Na^+ as follows:

$$Co^{2+} + Na^+\text{-clay} \rightarrow Na^+ + Co^{2+}\text{-clay} \quad (22)$$

The higher ratio of adsorbed cobalt to released sodium at pH 8 and 10 is due to cobalt precipitation. At pH 10, Co^{2+} is completely

removed from solution. The net sodium released at pH 8 and 10 is approximately equal to the net sodium released at pH 4 to 7 (Table 4). The observation that there is some additional sodium released at pH 8 and 10 indicates that there is also some cation exchange at these pH values as well as precipitation. This similarity suggests that the same mechanism produces exchangeable cobalt at pH 4 to 10.

The atomic sodium to silicon ratio was measured by XPS for sodium montmorillonite samples prepared in water and in Co^{2+} (aq) (Table 5). At pH 2 no ($<2x10^{-5}$ moles/g) sodium was observed on the clay surface for samples prepared in water or 0.01M Co^{2+}. At all other pH values, the Na/Si ratio for Na^{+}-montmorillonite prepared in 0.01M Co^{2+} was less than that for Na+-montmorillonite prepared in water. This indicates that exchange of Na^{+} by Co^{2+} occurs at pH values 4 to 10 for Na^{+}-montmorillonite in 0.01M Co^{2+}. The Na/Si atomic ratios for samples equilibrated with water and with 0.01M Co^{2+}, presented in Table 5, are in good agreement with the quantitative solution analysis of the net sodium released. This agreement is shown by the linear relationship between the net sodium relased and the difference in the Na/Si ratio for montmorillonite in water minus the Na/Si ratio for the montmorillonite in 0.01M $Co(NO_3)_2$ (Figure 6).

Desorption of the adsorbed cobalt in $BaCl_2$ was carried out to detect the presence of $Co(OH)_2$ or other nonexchangeable cobalt species on the surface. In this experiment it is assumed that $Co(H_2O)_6^{2+}$ and $Co(OH)^{+}$ can be exchanged by $BaCl_2$, whereas $Co(OH)_2$ or other precipitated forms of cobalt cannot be exchanged. The presence of

Table 4

Exchangeable Nature of Cobalt Adsorbed on Montmorillonite

pH	Cobalt Adsorbed ($\pm 0.2 \times 10^{-4}$ moles/g)	Net Na^+ Released ($\pm 0.2 \times 10^{-4}$ moles/g)	Cobalt Desorbed in 0.5M $BaCl_2$ (pH 6.5) ($\pm 0.2 \times 10^{-4}$ moles/g)
2	1.0×10^{-4}	0	1.1×10^{-4}
4	2.0×10^{-4}	1.8×10^{-4}	2.3×10^{-4}
6	2.3×10^{-4}	2.3×10^{-4}	2.5×10^{-4}
7	2.5×10^{-4}	2.5×10^{-4}	2.5×10^{-4}
8	7.3×10^{-4}	2.5×10^{-4}	2.1×10^{-4}
10	9.9×10^{-4}	2.5×10^{-4}	2.1×10^{-4}

Table 5

XPS Atomic Ratio Na/Si on H_2O and Co^{2+} Treated Montmorillonite

pH	Na/Si H_2O/Montmorillonite	Na/Si Co^{2+}/Montmorillonite	$\Delta(Na/Si_{H_2O} - Na/Si_{Co^{2+}})$
2	<0.05	<0.05	0
4	1.0±0.5	0.15±0.03	0.85
6	1.5±0.1	0.28±0.03	1.2
7	2.0±0.1	0.27±0.03	1.7
8	2.0±0.1	0.41±0.03	1.6
10	2.2±0.1	0.84±0.03	1.4

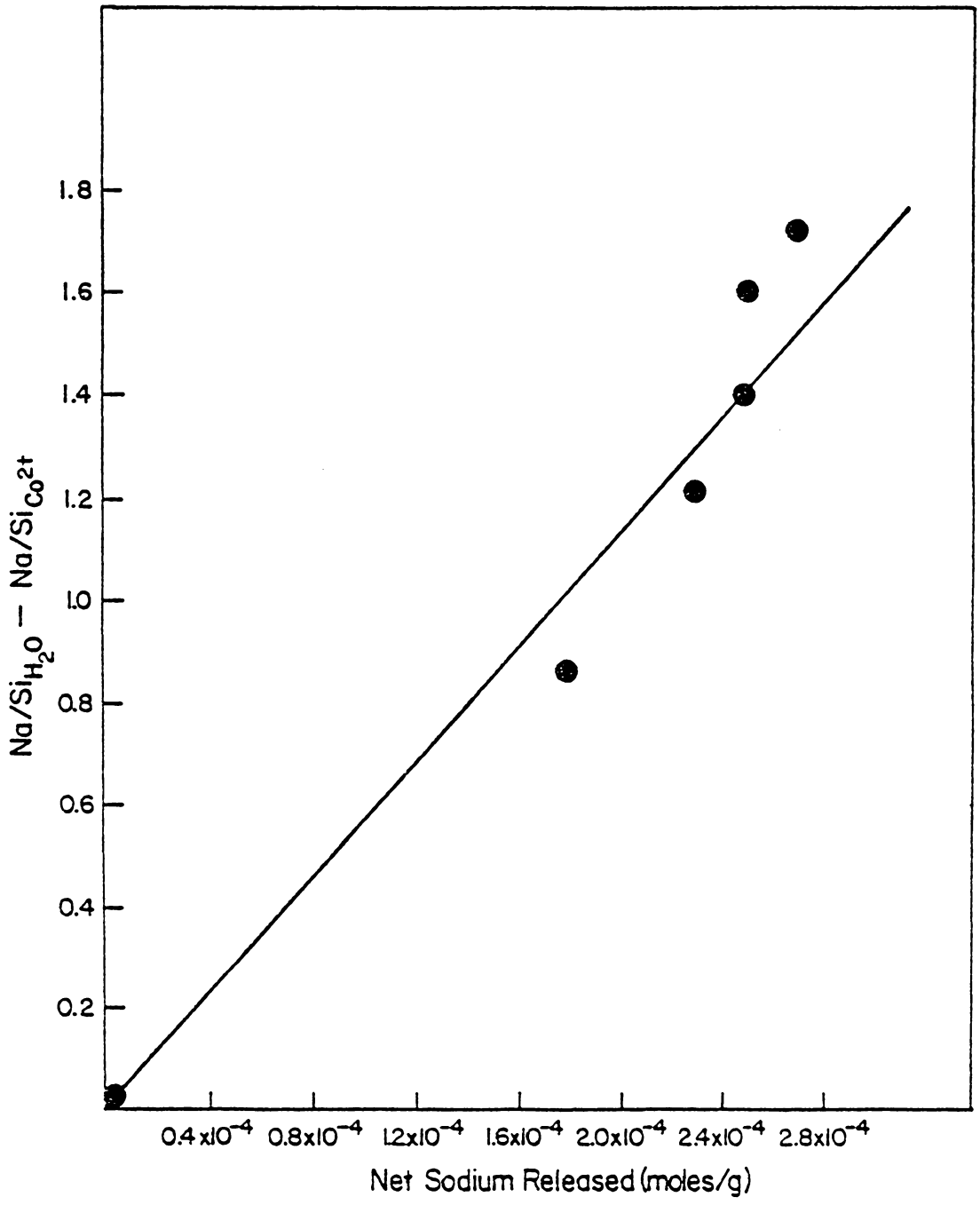

Figure 6. $Na/Si_{H_2O} - Na/Si_{Co^{2+}}$ versus Net Sodium Released

nonexchangeable cobalt can be detected if it is present in quantities greater than 0.2×10^{-4} moles/g clay. The amount of cobalt desorbed in 0.5M $BaCl_2$ and the quantity of cobalt adsorbed are presented in Table 4. Between pH 2 and 7, all of the adsorbed cobalt was exchanged, revealing that $Co(OH)_2$ is not on the surface at pH 7 or below. At pH 8 and 10, a significant amount of cobalt was not exchangeable, which supports the notion that a cobalt precipitate is present. However, not all of the cobalt is due to precipitation because some exchangeable cobalt was also observed.

It might be suspected that the exchangeable cobalt observed in 0.5M $BaCl_2$ is due to dissolution of $Co(OH)_2$. Favorable comparison between net sodium released and cobalt desorbed as well as agreement between cobalt desorbed in $BaCl_2$ at pH 4 and 6 and that at pH 7, 8 and 10 indicate that the observed cobalt is exchangeable. However, this agreement could be fortuitous. Further evidence that the cobalt is exchangeable is provided by the observation that the cobalt released (moles/g) is independent of sample size. If solubilization of $Co(OH)_2$ was responsible for the amount of cobalt dissolved in pH 6.5 $BaCl_2$ the same concentration would be observed in solution no matter what the sample size.

The ratio of desorbable Co^{2+} to net Na^+ released at pH 8 and 10 is approximately 1:1. These results could be explained by exchange of one $CoOH^+$ for one Na^+ ion (Equation 21) or nonequivalent exchange occurs at these pH values (Equation 22). Further analyses by XPS, by XRD, and by electrophoresis were conducted to determine which of these mechanisms is responsible for the observed 1:1 ratio of exchangeable cobalt to

sodium released.

Electrophoretic mobility measurements of montmorillonite in 0.01M Co^{2+} were carried out to investigate the influence of Co^{2+} on the clay surface charge. The mobility of montmorillonite in 0.01M $Co(NO_3)_2$ was compared to the mobility in 0.01M $NaClO_4$. Sodium perchlorate was chosen as a reference medium for the mobility of Na^+-montmorillonite because sodium is the counterion on the clay surface and because there are no reports in the literature for specific adsorption of sodium on montmorillonite. If the mobility remains the same as that observed for Na^+-montmorillonite in $NaClO_4$, it is suggested that cobalt adsorbs by electrostatic forces. The proposed surface interaction is presented below (Representation A):

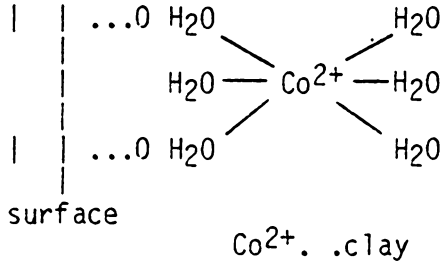

A

A mobility more positive than that of Na^+-montmorillonite would indicate that a +2 cation is specifically held to the surface or the surface has a greater attraction for a +1 species than for Na^+. If specific interactions are observed it is suggested that the adsorbed species is held by forces in addition to electrostatic forces such as hydrogen bonding between oxygen atoms on the clay surface and coordinated water molecules. A representation of this specific

interaction is given below. (Representation B)

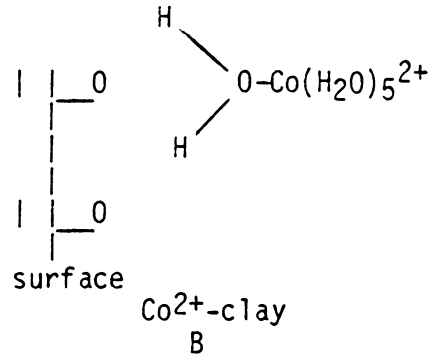

Co^{2+}-clay
B

Specific adsorption of $CoOH^+$ could also account for a more positive mobility. A model for the $CoOH^+$ - surface interaction is given below:

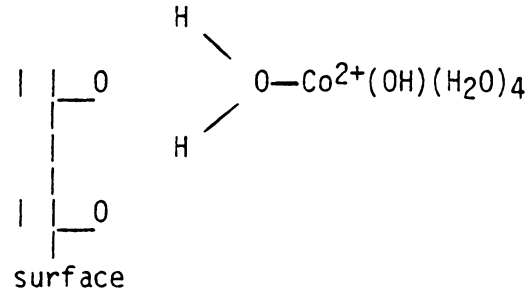

$CoOH^+$-clay
C

James and Healy (65) proposed that $CoOH^+$ has a greater affinity than Co^{2+} to bond to the SiO_2 surface because the solvation energy of the lower charged $CoOH^+$ ion is less than that for Co^{2+}. This would enable $CoOH^+$ to approach closer to the surface which would result in greater coulombic interactions. It is possible that this model can be applied to montmorillonite.

The electrophoretic mobility of montmorillonite in 0.01M $Co(NO_3)_2$ is presented in Figure 7. Between pH 2 and 6, the mobility is more positive than for the clay in 0.01M $NaClO_4$. It is possible that $CoOH^+$

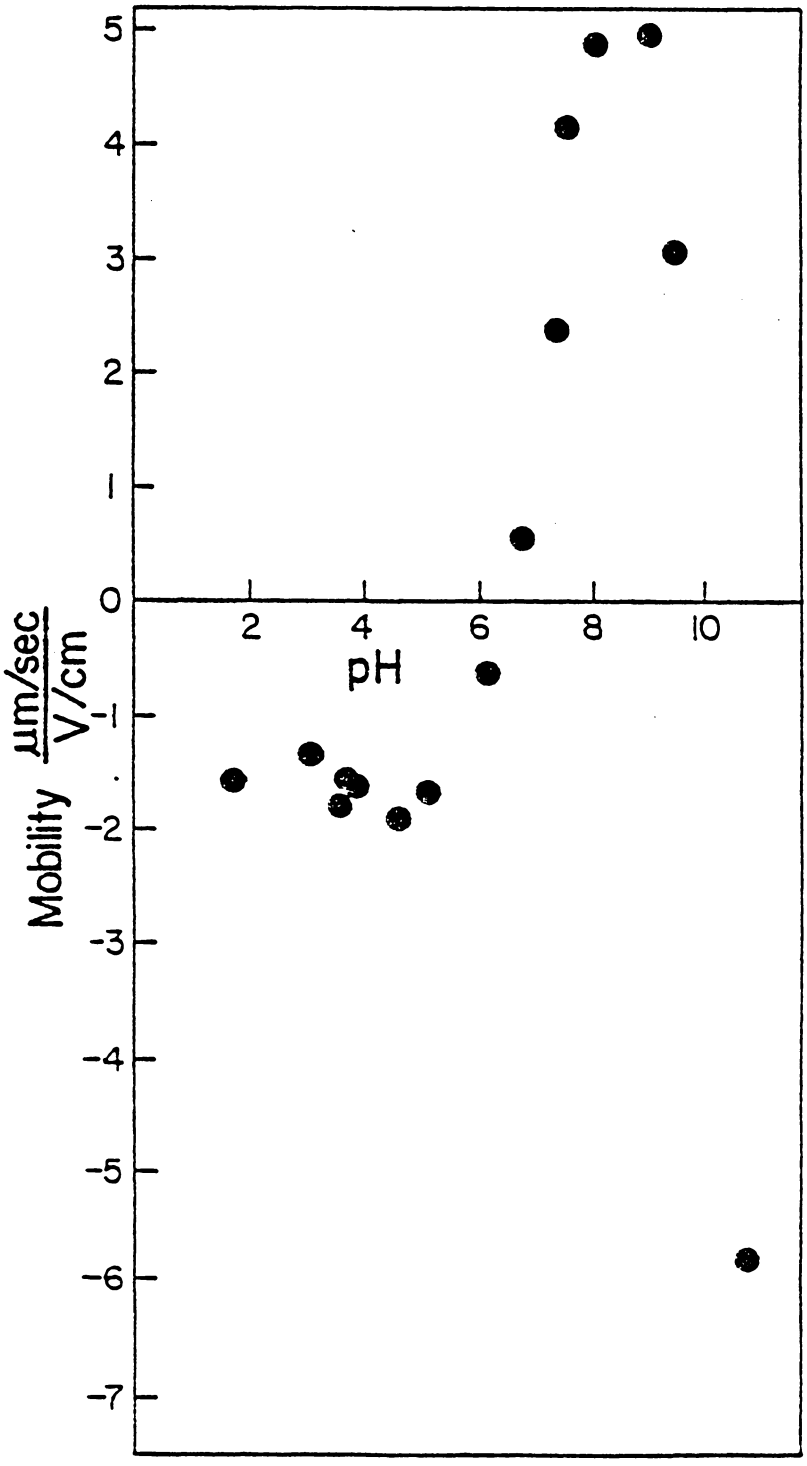

Figure 7. Electrophoretic Mobility of Montmorillonite in 0.01 M $Co(NO_3)_2 \cdot 6H_2O$

is the adsorbed species at pH 2 to 6. However, this is unlikely because this species constitutes less than 1% of the total cobalt in solution. The interaction shown by structure B is also possible because it is consistent with the observation of nonequivalent exchange of Co^{2+} for Na^{+} and would give a more positive mobility. Co(II) is the major species in solution in this pH range and thus is more likely to adsorb than $CoOH^{+}$, unless the clay has a much greater affinity to bond with $CoOH^{+}$.

At pH 7 the charge of montmorillonite in 0.01M $Co(NO_3)_2$ is positive. It is possible that the charge reversal is due to greater amounts of Co^{2+} specifically bound to the surface than that observed at pH 2 to 6, or that some $Co(OH)_2$ is on the clay surface, or both. Although Ba^{2+} exchange indicated that no $Co(OH)_2$ was present on the surface, it is possible that some was present but the quantity ($<0.2 \times 10^{-4}$ mole/g) was too small to detect.

The mobility of montmorillonite in 0.01M Co^{2+} at pH 8 and 10 equals the mobility of $Co(OH)_2$ in 0.01M $NaClO_4$ (Figure 8). The equality of the electrophoresis measurements revealed that $Co(OH)_2$ is precipitated onto the clay surface. The suggestion that $Co(OH)_2$ is the surface species is consistent with Ba^{2+} exchange experiments which demonstrate that the majority of surface cobalt is nonexchangeable. The exchangeable cobalt does not significantly affect the surface charge because the precipitated cobalt coats the montmorillonite particle.

Powder x-ray diffraction patterns for cobalt montmorillonite

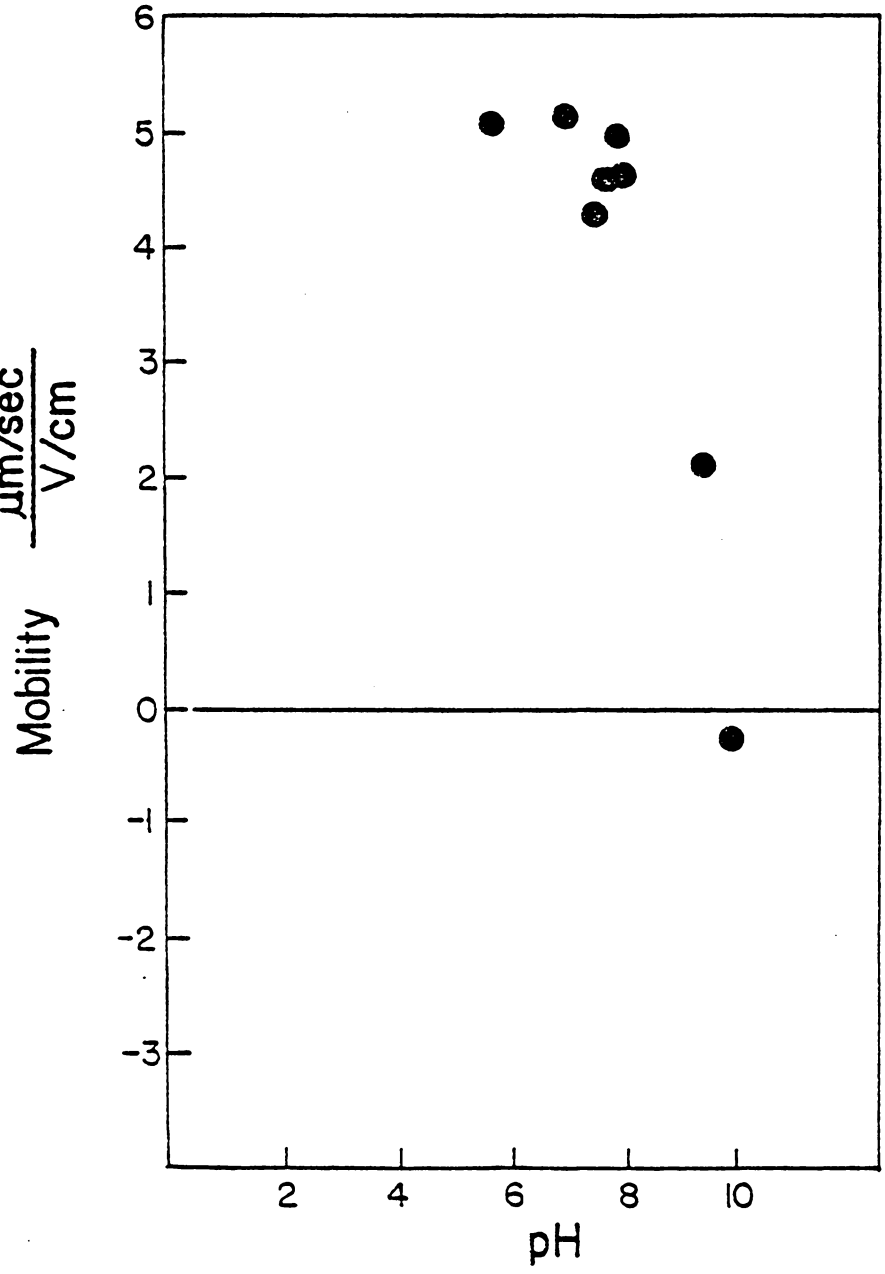

Figure 8. Electrophoretic Mobility of $Co(OH)_2$ in 0.01 M $NaClO_4$

samples prepared at various pH values were measured to obtain information about the interlayer spacing. The d_{001} spacings for cobalt adsorbed on montmorillonite are presented in Table 6. The spacings for Na+-montmorillonite in water, adjusted to the various pH values, are also presented for comparison.

The basal spacing for Co^{2+}-montmorillonite was 16.0Å for samples prepared between pH 4 and 10. The calculated size attributed to adsorbed cobalt in the interlayer, Δ, is 6.5 ± 0.2Å. The diameter for $Co(H_2O)_6^{2+}$, was calculated from the formula $2(r_{Co^{2+}} + 2r_{H_2O})$ (82) using the ionic radius of Co(II), 0.72Å, (134), and the radius of water, 1.38Å (82). The Δ value is less than the calculated diameter for hydrated Co^{2+}. To account for this result, it is suggested that either cobalt loses bound water upon adsorption and bonds to the clay by an innersphere mechanism or the hydrated cobalt is partially "keyed" into octahedral sites in the montmorillonite lattice. It is not possible to distinguish which of these two processes occurs. It is unlikely that cobalt bonds to the basal surfaces by an inner sphere mechanism because the surface oxygen atoms are not ionized and thus are not capable of donating electrons to cobalt.

At pH 10 an XRD peak was observed, with an intensity half that of the 15.8Å peak that corresponded to a basal spacing of 13.2Å. The 13.2 ± 0.2Å basal spacing was measured for Na^+-montmorillonite samples prepared in water at all pH values. This finding for Co^{2+}-montmorillonite at pH 10 shows that some of the basal spacings are due to Na^+ in the clay interlayers and that cobalt(II) is not adsorbed in

Table 6

Basal Spacing for Co^{2+} Adsorbed on Montmorillonite

pH	H_2O/Montmorillonite Å d_{001} ± 0.2Å	Co^{2+}/Montmorillonite Å d_{001} ± 0.2Å	Co^{2+}/Montmorillonite ΔÅ ± 0.2Å
4	13.2	16.0	6.5
6	13.4	16.0	6.5
7	13.4	15.8	6.3
8	13.4	15.8	6.3
10	13.2	15.8, 13.2	6.3, 3.7

the interlayers of all clay particles. It is probable that $Co(OH)_2$ coats the clay so that cobalt(II) cannot adsorb.

X-ray photoelectron spectra for Co^{2+} adsorbed on montmorillonite at pH 4 to 10 were measured to obtain further information on the character of the adsorbed cobalt. The Co $2p_{1/2}$ and Co $2p_{3/2}$ photopeaks were chosen for analysis because the spectroscopic features corresponding to these peaks provide insight into the oxidation state and the chemical environment of adsorbed cobalt. These informative features are the Co $2p_{3/2}$ binding energy, the Co $2p_{1/2}$ - Co $2p_{3/2}$ energy difference, and the nature of shake-up satellites. The binding energies of adsorbed cobalt can be compared to those of reference compounds to infer the chemical environment of the adsorbed species. Atoms with less electron density generally have higher binding energies, but there are exceptions such as for $Co(OH)_2$, which has a higher Co $2p_{3/2}$ binding energy than the Co_2O_3 (71,135). This is due to greater relaxation energy for Co^{3+} compared to Co^{2+} (135,136).

The energy separation or splitting between the Co $2p_{1/2}$ and the Co $2p_{3/2}$ photopeaks is indicative of the oxidation and spin state of cobalt (135). Co(II) high spin has a Co $2p_{1/2}$ - Co $2p_{3/2}$ splitting of 16 eV whereas the Co 2p energy separation for Co(III) low spin is only 15 eV (137). Low spin Co(II) compounds show a splitting of 15.5 eV (137) and can be identified by the presence of shoulders on the Co Co $2p_{1/2}$ and Co $2p_{3/2}$ photopeaks due to multiplet splitting. Although obvious features due to multiplet splitting are not apparent for Co(II) high spin or low spin Co(III), the difference in energy separation of the Co $2p_{1/2}$ - Co $2p_{3/2}$ photopeaks for Co(II) high spin, Co(II) low

spin, and Co(III) low spin are a result of multiplet splitting (137,139,140). Spectra for $Co(NO_3)_2 \cdot 6H_2O$, $Co(OH)_2$, and CoOOH are presented in Figure 9, where it is shown that the energy separation is smallest for Co(III).

The third feature used to assign the spectra of adsorbed cobalt is the satellite structure. Satellite intensity is usually smaller than the main Co $2p_{1/2}$ or Co $2p_{3/2}$ peak and the satellites occur at higher binding energy. In Figure 9, Co(II) has intense satellite features on the high binding energy side of the Co $2p_{3/2}$ and Co $2p_{1/2}$ photopeaks. These shakeup satellites are attributed to charge transfer of an electron from the ligand to the metal 3d orbital when the Co 2p electron is removed by x-ray photoionization (141). The satellite structure is strongly dependent on the nature of the metal ions, the ligand, and the structure of the complex (142). It is known from measurements of spectra of various transition metal halides (143), complexes (143), and metal compounds (137,149) that the satellite intensity increases and the satellite to main peak energy separation decreases with increasing covalency of the metal-ligand bond. The measured Co $2p_{3/2}$ binding energies, the Co $2p_{1/2}$ - Co $2p_{3/2}$ splitting, the satellite to main peak ratio, and the separation of the satellite to main peak for various reference compounds and for cobalt(II) adsorbed on montmorillonite are presented in Table 7. Figure 10 shows how these values were obtained for CoO. The Co 2p photopeaks for cobalt adsorbed on montmorillonite at pH 4, 7, and 10 are presented in Figure 11.

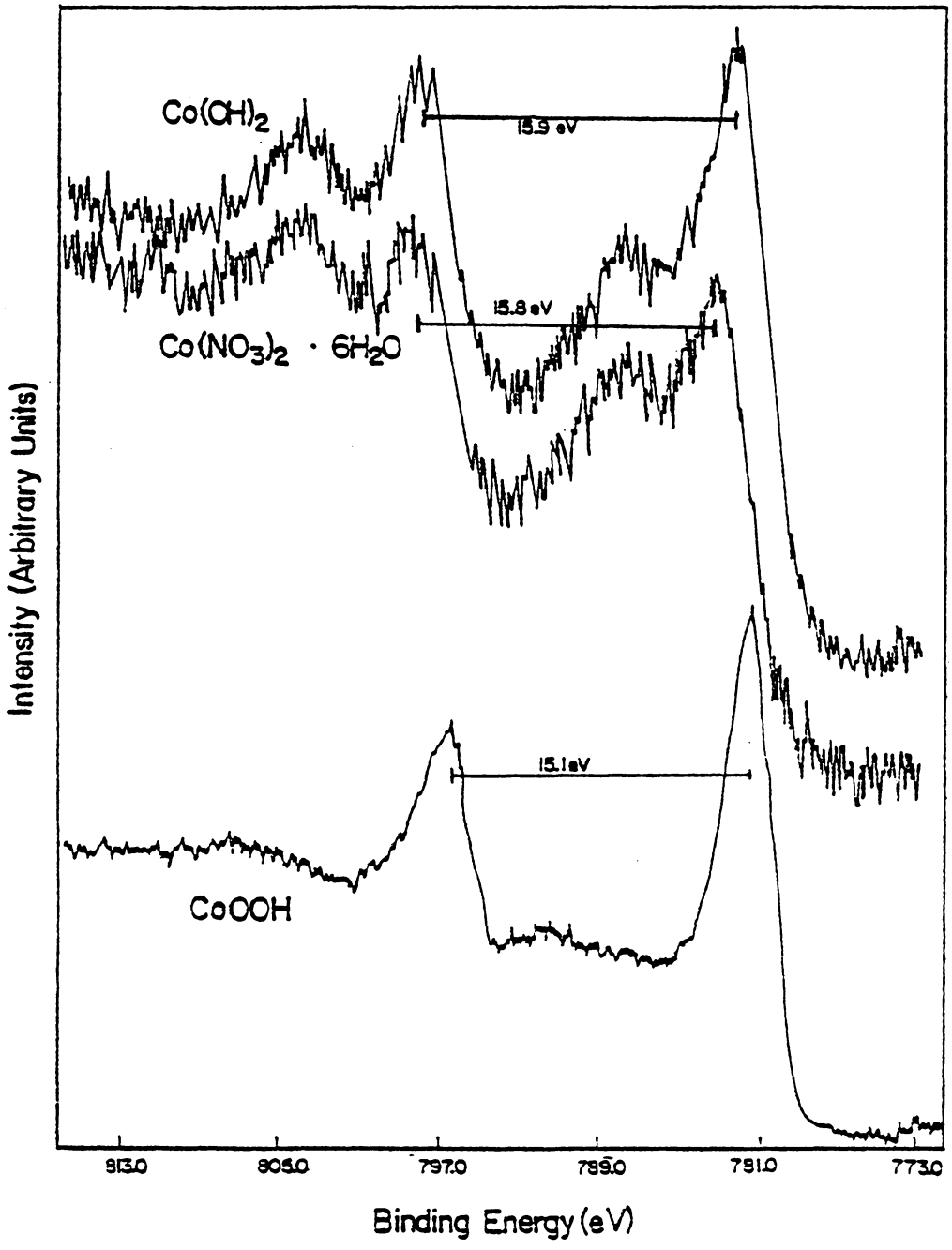

Figure 9. Co 2p Photopeaks $Co(OH)_2$, $Co(NO_3)_2 \cdot 6H_2O$ and CoOOH

Table 7

XPS for Co^{2+} Treated Montmorillonite

Sample	Binding Energy ($Co\ 2p_{3/2}$) (±0.2 eV)	ΔE ($Co\ 2p_{1/2}$ - $Co\ 2p_{3/2}$) (±0.2 eV)	ΔE Sat-Main $Co\ 2p_{3/2}$ (±0.2 eV)	Satellite / Main Peak ($I\ 2p_{3/2}$ / $I\ 2p_{3/2}$)
Co^{2+}/Montmorillonite pH				
4	782.4	15.8	4.2	0.74
6	782.1	15.9	4.5	0.72
7	781.6	15.9	4.8	0.65
8	781.1	15.9	5.5	0.59
10	780.8	15.9	5.5	0.56
$Co(OH)_2$*	780.9	15.9	5.6	0.52
$Co(OH)_2$(143)	781.3	--	5.5	--
$Co(OH)_2$(144)	781.0	15.9	--	--
$Co(OH)_2$(82)	780.9	16.1	--	--
CoO*	780.1	15.9	6.7	0.44
CoO(143)	780.5	--	6.0	--
CoO(145)	780.5	--	--	--
CoO(73)	780.4	16.1	--	--
CoO(147)	780.0	--	6.3	--
Co_3O_4*	779.9	15.4	9.1	0.26

Table 7 (Continued)

XPS for Co^{2+} Treated Montrmoillonite

Sample	Binding Energy (±0.2 eV)	ΔE Co $2p_{1/2}$ - Co $2p_{3/2}$ (±0.2 eV)	ΔE Co $2p_{3/2}$ Sat-Main (±0.2 eV)	I $2p_{3/2}$ Satellite / I $2p_{3/2}$ Main Peak
Co^{2+}/Montmorillonite pH				
Co_3O_4(143)	779.6	--	9.9	--
Co_3O_4(145)	779.5	--	9.0	--
CoOOH*	780.2	15.1	--	--
CoOOH(82)	779.9	15.0	--	--
$Co(NO_3)_2 \cdot 6H_2O$*	782.1	15.8	4.4	0.73
$Co(NO_3)_2 \cdot 6H_2O$(148)	782.1	--	--	--
$Co(NO_3)_2 \cdot 6H_2O$(73)	781.6	15.9	--	--

*This work

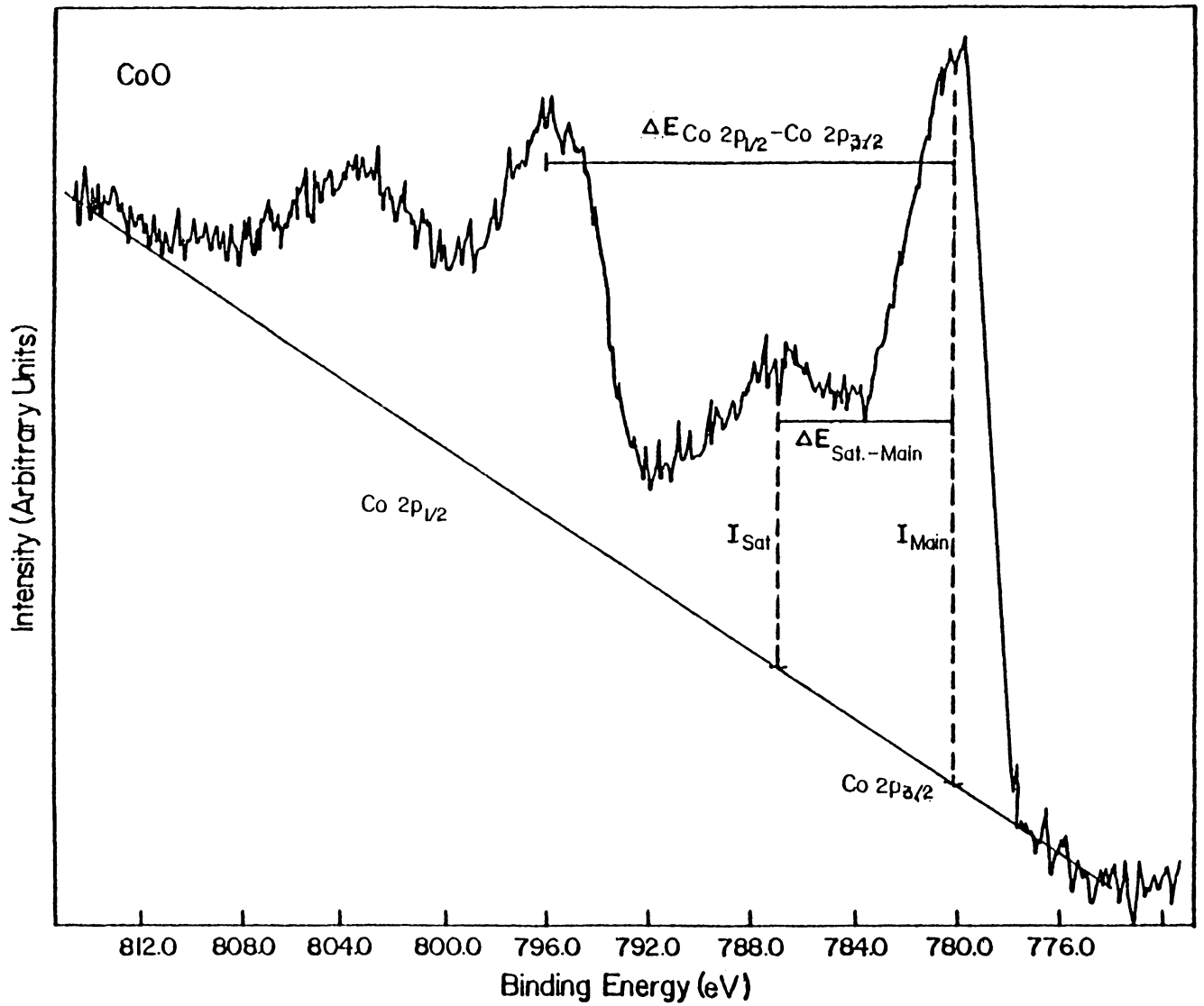

Figure 10. Co 2p Photopeaks for CoO

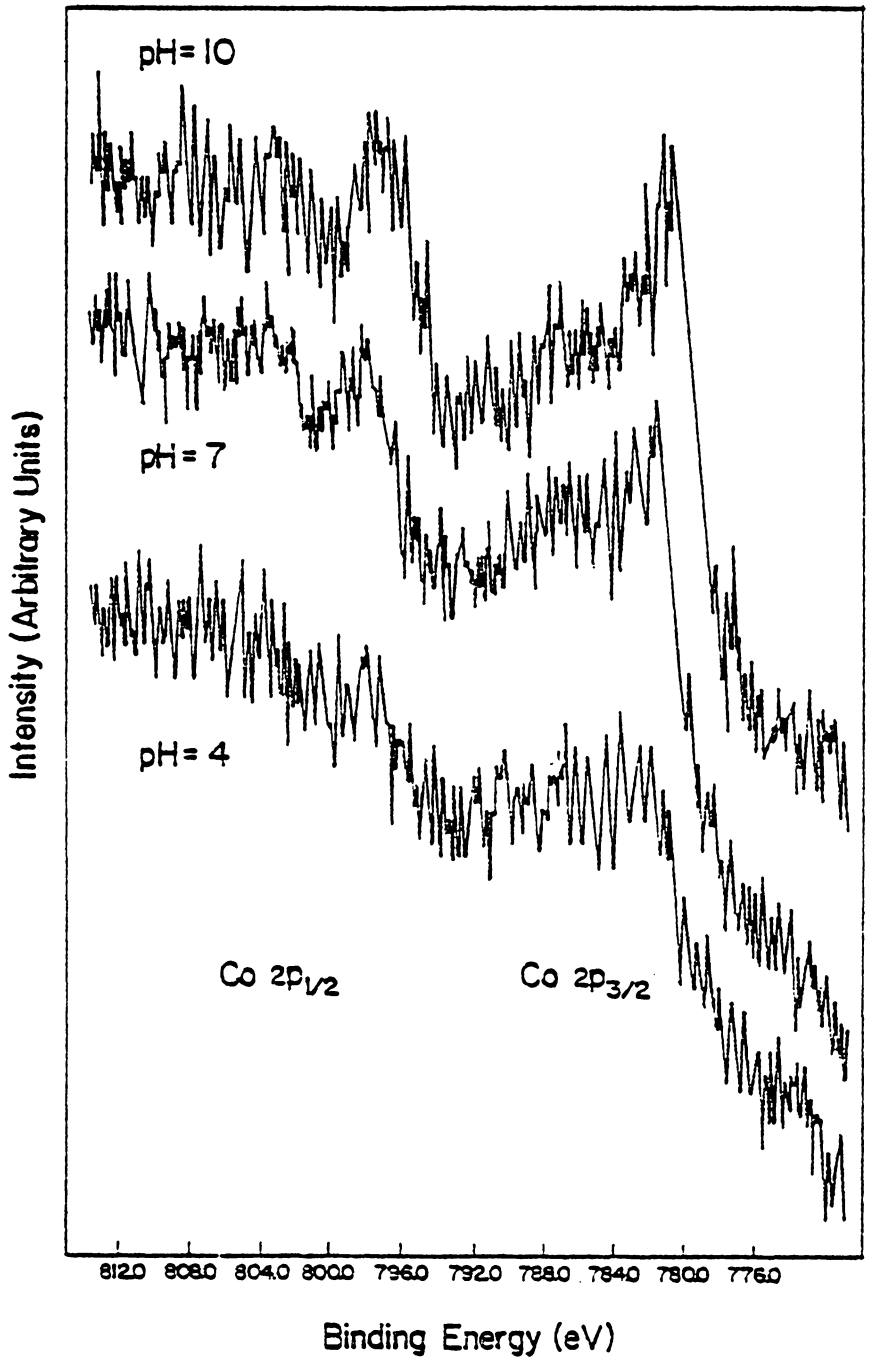

Figure 11. Co 2p Photopeaks for Co^{2+} Treated Montmorillonite (Al Anode)

From the analysis of the XPS data for Co^{2+} on montmorillonite, it may be concluded that the oxidation state of cobalt is Co(II) at all pH values studied. This is confirmed by the Co $2p_{1/2}$ - Co $2p_{3/2}$ energy separation of approximately 16.0 eV and by the presence of satellite features. The binding energy change of 1.6 eV from pH 4 to pH 10 indicates that there is a significant change in the chemical environment around cobalt as the pH changes. The Co $2p_{3/2}$ binding energy for cobalt adsorbed on montmorillonite at pH 4 and 6 compares favorably with the Co $2p_{3/2}$ binding energy for $Co(NO_3)_2 \cdot 6H_2O$. $Co(H_2O)_6^{2+}$ is the major cobalt species in solution at these pH values (132) and therefore it is likely the adsorbed species. However, it is possible that a water is lost upon adsorption and the cobalt bonds to the clay by an innersphere mechanism. The presence of $Co(H_2O)_6^{2+}$ or a cobalt species with similar chemical environment at pH 4 and 6 is also indicated by inspection of the Co $2p_{3/2}$ satellite features. The energy separations between the satellite and main peak, $\Delta E_{sat-main}$, were 4.2 and 4.5 eV at pH 4 and 6, respectively. This agrees with the $\Delta E_{sat-main}$ value of 4.4 eV for $Co(NO_3)_2 \cdot 6H_2O$. The satellite to main peak intensities for cobalt adsorbed at pH 4 and 6, 0.74 and 0.72 respectively, are also similar to that for $Co(NO_3)_2 \cdot 6H_2O$, 0.73. Thus, based on Co $2p_{1/2}$ -Co $2p_{3/2}$ splittings, Co $2p_{3/2}$ binding energies, and satellite features, XPS indicates that $Co(H_2O)_6^{2+}$ is the adsorbed species. XPS cannot determine if Co^{2+} is bound only by electrostaic interactions (model A) or if hydrogen bonding also contributes to the attraction of Co^{2+} to the surface (model B).

At pH 7 the binding energy is intermediate between the values at pH 4 and 6 and at pH 8 and 10. The binding energy of 781.6 eV for the Co $2p_{3/2}$ level at pH 7 is not equal to any of the reference compounds (Table 7). Either cobalt is present as a mixture of Co^{2+} and $Co(OH)_2$ or the chemical environment of the adsorbed species is a hybrid of the bonding enviroment for $Co(H_2O)_6^{2+}$ and $Co(OH)_2$. The $\Delta E_{sat-main}$ is 4.8 eV and the satellite to main peak intensity ratio is 0.67 for Co^{2+} adsorbed on montmorillonite at pH 7. These values fall between the values for $\Delta E_{sat-main}$ and satellite to main peak intensity ratios for $Co(NO_3)_2 \cdot 6H_2O$ (4.4 eV and 0.73, respectively) and $Co(OH)_2$ (5.6 eV and 0.52, respectively). XPS results indicate the presence of a cobalt species that is a hybrid of $Co(H_2O)_6^{2+}$ and $Co(OH)_2$. One candidate for this hybrid species is $Co(OH)^+$, but it is also possible that the surface species is a mixture of $Co(H_2O)_6^{2+}$ and $Co(OH)_2$.

The binding energies of the surface cobalt at pH 8 and 10 are 781.1 and 780.8 eV, respectively. These values compare favorably with the Co $2p_{3/2}$ binding energy for $Co(OH)_2$, 780.9 eV. The satellite to main peak intensity ratios are 0.59 and 0.56 for pH 8 and 10, respectively, and the $\Delta E_{sat-main}$ is 5.5 eV for both pH values. These values are characteristic of $Co(OH)_2$ (I_{sat}/I_{main} = 0.52 and $\Delta E_{sat-main}$ = 5.6 eV). The presence of $Co(OH)_2$ on the clay surface was expected at pH 8 and 10, based on the known hydrolysis behavior of cobalt in solution (132), the XRD results, electrophoresis, and Ba^{2+} desorption data. The XPS results could not be interpreted to indicate the presence of either Co^{2+} or $CoOH^+$ on montmorillonite at pH 8 and 10. It

is reasoned that only $Co(OH)_2$ was detected because it covers the clay surface. XPS is a surface sensitive technique sampling only the top 10 to 20Å of a solid. The Co^{2+} or $CoOH^+$ species would not be easily detected if they are in the clay interlayers compared to $Co(OH)_2$ on the outer surface.

In summary, Co $2p_{3/2}$ binding energies, Co $2p_{1/2}$ -Co $2p_{3/2}$ splitting values, and satellite features revealed that cobalt adsorbed on montmorillonite at pH 4 and 6 is $Co(H_2O)_6^{2+}$. Quantitative measurements of the net sodium released and the amount of exchangeable cobalt at pH 4 and 6 showed that $Co(H_2O)_6^{2+}$ adsorbed by a nonequivalent exchange process. Electrophoretic analysis indicated that Co^{2+} was specifically bound to the surface. However, the nature of the specific bond was not determined but likely models were suggested. XRD showed that $Co(H_2O)_6^{2+}$ was adsorbed in the interlayers and was either "keyed" into the octahedral sites or bound by an innersphere mechanism. These observations are consistent with the following reactions:

$$Co(H_2O)_6^{2+} + Na^+\text{-clay} \rightarrow Na^+ + Co(H_2O)_6^{2+}\text{-clay} \qquad (23)$$

Observations by XPS, electrophoresis, XRD, and quantitative solution analysis of the cobalt species adsorbed on montmorillonite at pH 7 showed that the following reactions are possible:

$$Co(H_2O)_6^{2+} + OH^- \rightarrow Co(H_2O)_5OH^+ + H_2O \qquad (24)$$

$$Co(H_2O)_5OH^+ + Na^+\text{-clay} \rightarrow Co(H_2O)_5OH^+\text{-clay} + Na^+ \qquad (25)$$

XPS indicated that the adsorbed species had a chemical nature inter-

mediate between $Co(H_2O)_6^{2+}$ and $Co(OH)_2$. Electrophoretic mobility revealed that the cobalt was specifically adsorbed by the clay surface, XRD showed that cobalt was adsorbed into the clay interlayers. All this data supports the proposal that the cobalt is held to the clay surface by forces in addition to electrostatic attraction. It is suggested that these additional forces are hydrogen bonding of the coordinated water molecules to the clay surface. Quantitative solution analysis demonstrated that one cobalt species exchanged for Na^+. It is also possible that both Co^{2+} and $Co(OH)_2$ are on the clay surface. Although Ba^{2+} exchanged did not indicate that $Co(OH)_2$ was on the surface, the cobalt hydroxide concentration may have been below the detection limit ($<0.2x10^{-4}$ moles/g) of the analysis.

Cation exchange of cobalt for sodium at pH 8 and 10 was shown by net sodium released, Ba^{2+} exchange, and XPS Na/Si measurements. X-ray diffraction gave further verification of cobalt exchange in the interlayers, but was unable to determine whether $Co(H_2O)_6^{2+}$ or $Co(OH)^+$ was the surface species. Precipitation of $Co(OH)_2$ on montmorillonite at pH 8 and 10 was demonstrated by electrophoresis which indicated that the mobility of the clay in 0.01M Co^{2+} was the same as the mobility of $Co(OH)_2$ in $NaClO_4$. XPS results confirmed that the surface cobalt was the same as $Co(OH)_2$ and quantitative solution analysis showed that precipitation occurred. The reactions for the precipitation mechanism are:

$$Co^{2+} + 2OH^- \rightarrow Co(OH)_{2(s)} \qquad (26)$$

$$Co(OH)_{2(s)} + \text{clay} \rightarrow Co(OH)_{2(s)}/\text{clay} \qquad (27)$$

The following reaction suggesting formation of $Co(OH)_2$ on the clay surface is also possible:

$$Na^+ - clay \rightarrow Co(H_2O)_5^{2+} - clay + Na^+ \quad (28)$$

$$Co(H_2O)_5^{2+}-clay + 2OH^- \rightarrow Co(OH)_2-clay + 6H_2O \quad (29)$$

However, neither electrophoresis nor XPS results gave any indication that this surface $Co(OH)_2$ is significantly different than $Co(OH)_2$ precipitated in the absence of the clay.

Before considering the adsorption of cobalt amino acid complexes, the adsorption of the amino acid ligands on montmorillonite is discussed.

B. ADSORPTION OF AMINO ACIDS ON MONTMORILLONITE

The aim of this study was to investigate the effect of pH and adsorbed metal counterion on the amount of amino acid adsorbed on a clay and on the adsorption mechanism itself. The oxidation state of surface cobalt after interaction of Co^{2+}-montmorillonite with the amino acids was examined.

Due to the presence in the amino acid molecule of both acidic, carboxylate and basic, amino groups, amino acids may exist as cations, zwitterions, or anions depending on the pH of the solution. The chemical structures of the amino acids used in this study, glycine and lysine, are presented in Table 8 along with pK values for the amine and carboxyl groups.

Glycine, the simplest amino acid, and lysine, a basic amino acid, were equilibrated with Na^+- and Co^{2+}-montmorillonite at various pH

Table 8

pH Characteristics of Glycine and Lysine*

Form of Amino acid at pH = 6	pK_a	pK_b
Glycine 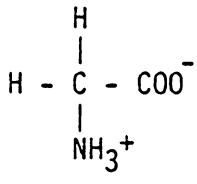	2.34	9.6
Lysine 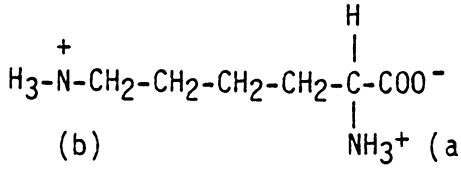	2.18	8.95 (a) 10.5 (b)

*Data from Reference 149

values. Quantitative results of the amount of amino acid adsorbed on Na^+- and Co^{2+}-montmorillonite are presented in Table 9. The results indicate that the greatest amount of glycine is adsorbed on Na^+-montmorillonite at pH 2 and decreases with increasing pH. At pH 2, glycine is a cation in solution and can exchange for surface sodium. The decreased glycine adsorption on montmorillonite with increasing pH is expected because the amount of cationic glycine in solution decreases and the affinity for the negative clay surface decreases. No adsorbed amino acid was detected at pH 8 and 10.

At pH 2, 4, and 6, no significant difference in the amount of glycine on Co^{2+}-montmorillonite compared to Na^+-montmorillonite is observed. However, in contrast to Na^+-montmorillonite, glycine is detected on Co^{2+}-montmorillonite at pH 8 and 10.

The amount of lysine adsorbed on Na^+-montmorillonite is relatively constant between pH 2 and 8. Lysine is cationic at these pH values (149) and can exchange for surface sodium ions. At pH 10, a smaller quantity of lysine adsorbs on the clay because the dominant lysine species at this pH is the zwitterion.

At pH 2, 4, and 6, the quantity of lysine adsorbed on Co^{2+} - montmorillonite is approximately the same as that adsorbed on Na^+ - montmorillonite at the same pH values. The amount of lysine adsorbed on Co^{2+}-montmorillonite at pH 8 and 10 is greater than that on Na^+ - montmorillonite. Increased adsorbed lysine at pH 8 and 10 may be due to coordination of lysine with adsorbed cobalt.

Cobalt released in the adsorbate solution from Co^{2+}-montmorillonite, both in the presence and absence of amino acid, is

Table 9

Amino Acids Adsorbed on Montmorillonite
(moles/g clay)

pH	Glycine /Na^+ Montmorillonite	Glycine/Co^{2+} Montmorillonite	Lysine/Na^+ Montmorillonite	Lysine/Co^{2+} Montmorillonite
2	2.3×10^{-4}	2.4×10^{-4}	2.5×10^{-4}	2.4×10^{-4}
4	1.6×10^{-4}	1.8×10^{-4}	2.5×10^{-4}	2.6×10^{-4}
6	1.1×10^{-4}	1.3×10^{-4}	2.4×10^{-4}	2.7×10^{-4}
8	$<2 \times 10^{-5}$	1.4×10^{-4}	2.3×10^{-4}	3.0×10^{-4}
10	$<2 \times 10^{-5}$	1.6×10^{-4}	1.8×10^{-4}	3.9×10^{-4}

presented in Figure 12. The total amount of cobalt on the Co^{2+}-montmorillonite substrate was $3.0x10^{-4}$ moles/g. When no amino acid was present the amount of Co^{2+} released from Co^{2+}-montmorillonite in water increased with decreasing pH. The increased Co^{2+} release is due to displacement of Co^{2+} by both protons and Al^{3+} at low pH (32,120). Compared to Co^{2+} release into water, a greater amount of cobalt was released from the clay surface in the presence of lysine at all pHs between 2 and 10. This can be accounted for by exchange of the lysine cations for Co^{2+} at pH values 2, 4, and 6. At pH 8 and 10, cobalt hydrolyzes to form $Co(OH)_2$ (132). The cobalt observed in solution at pH 8 and 10 in the presence of lysine most likely arises through coordination of Co^{2+} by the amino acid ligand and subsequent dissociation into solution (21, 30).

At pH 2, the exchange of Co^{2+} by Al^{3+} and H^+ is possible in glycine and water. The cobalt released in the presence of glycine was greater at pH 2 compared to that released in water. Glycine is a cation at pH 2 and can exchange additional cobalt counterions. At pH 4 and 6 glycine is a zwitterion in solution. The amount of cobalt released into the glycine solution was the same as that released into water. This result indicates that glycine exchanges less than $0.2x10^{-5}$ moles of cobalt at these pH values. Glycine is neutral or negative at pH 8 and 10, so exchange for cobalt is unlikely. However, greater release was detected in the glycine solution at pH 8 and 10 compared to pH 2, 4, and 6. The increased cobalt in solution at pH 8 and 10 may be attributed to coordination of the cobalt by glycine in these pH values.

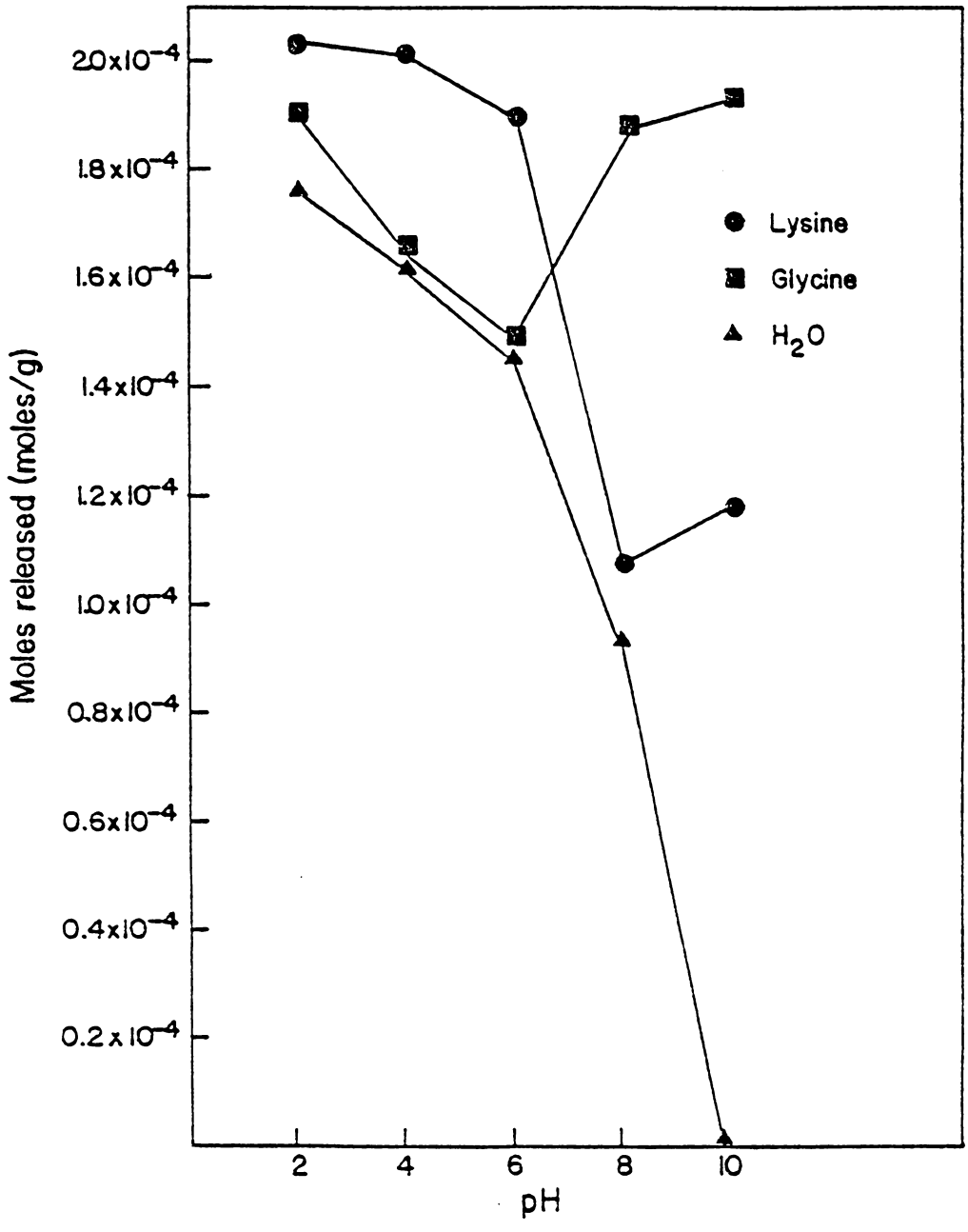

Figure 12. Cobalt Released versus pH

Visible spectra of the adsorbate solutions were measured to determine whether desorbed cobalt was coordinated by the amino acid ligands. The results are presented in Table 10. Bands corresponding to the $^1A_{1g} \rightarrow {}^1T_{1g}$ and $^1A_{1g} \rightarrow {}^1T_{2g}$ transitions for cobalt (III) amino acid complexes were observed in the adsorbate solutions only at pH 8 and 10 for both glycine and lysine. These bands indicate that the cobalt in solution at pH 8 and 10 is Co(III) and is coordinated to the amino acid. Recalling that adsorbed cobalt on montmorillonite is Co^{2+}, the formation of Co(III) complexes must be explained. Cobalt(II) amino acid complexes, $Co(AA)_2$ are oxygen carriers and can be oxidized in solution by the following mechanism (150).

$$\begin{array}{ccc} Co(II) + 2AA & \rightarrow & Co(II)\,(AA)_2 \\ & & \downarrow O_2 \\ & & [(AA)_2CoO_2Co(AA)_2] \\ & & \downarrow \\ Co(III)(AA)_3 & \xleftarrow{AA} & [Co(III)(AA)_2]^+ \end{array} \qquad (30)$$

It is reasonable that Co(III) amino acid complexes in solution are formed by the mechanism following the interaction of amino acids with Co^{2+}-montmorillonite.

Electrophoresis measurements were conducted to glean information concerning the effect of glycine and lysine on the mobility of Na^+ - and Co^{2+}-montmorillonite. The effect of the amino acids was ascertained by comparing the mobility of Na^+-montmorillonite in the amino acids to the mobility of Na^+-montmorillonite in 0.01M $NaClO_4$. For the following interactions, the probable electrokinetic behavior is

Table 10

Transmission Visible Spectroscopy
Amino Acids in the Presence of Co^{2+}-Montmorillonite

Glycine/Co^{2+}-Montmorillonite	Band $^1A_{1g} \rightarrow {}^1T_{1g}$ nm	Intensity Absorbance Units	Band $^1A_{1g} \rightarrow {}^1T_{2g}$ nm	Intensity Absorbance Units
pH				
2	*ND	-	*ND	-
4	*ND	-	*ND	-
6	*ND	-	*ND	-
8	538	0.22	375	0.36
10	532	0.39	375	0.45
0.01M $Co(gly)_3$	539	0.80	374	-
$Co(gly)_3$ (166)	542	†NR	374	-
Lysine/Co^{2+}-Montmorillonite				
pH				
2	*ND	-	*ND	-
4	*ND	-	*ND	-
6	*ND	-	*ND	-
8	522	0.17	368	0.34
10	522	0.22	368	0.36
0.01M $Co(lys)_3^{3+}$	525	.97	372	1.3
$Co(lys)_3^{3+}$ (166)	525	†NR	369	†NR

*ND = Not Detected
†NR = Not Reported

summarized below:

a) equivalent exchange: the mobility remains the same as Na^+-montmorillonite in $NaClO_4$,

b) nonequivalent exchange (a +2 cation exchanges a +1 counterion): the mobility becomes more positive,

c) nonequivalent exchange (a +1 cation exchanges a +2 counterion): the mobility becomes less positive,

d) zwitterion adsorption: the mobility is the same,

e) complexation: the mobility remains the same (bonds to neutral ligand) or decreases (bonds to negative ligand),

f) no reaction: the charge remains the same.

Because more than one possible interaction can give rise to the observed mobility, this data is more useful when combined with other information. Such information includes the species present in solution under the given conditions, and data regarding the adsorption mechanism. Electrophoretic mobility measurements are also useful in understanding the adsorption mechanism because they can provide evidence to eliminate possible suggested reactions.

Comparison of Na^+-montmorillonite mobility in glycine to that in $NaClO_4$ (Figure 13) showed that the mobilities are similar for pHs 2 to 10. Three possible interactions are consistent with these observations: 1) a +1 glycine cation exchanges for surface sodium, 2) the zwitterion is adsorbed and 3) the interaction with glycine is negligible. Between pH 2 to 6, significant amounts of glycine were adsorbed. At pH 2, glycine is cationic in solution and is likely to

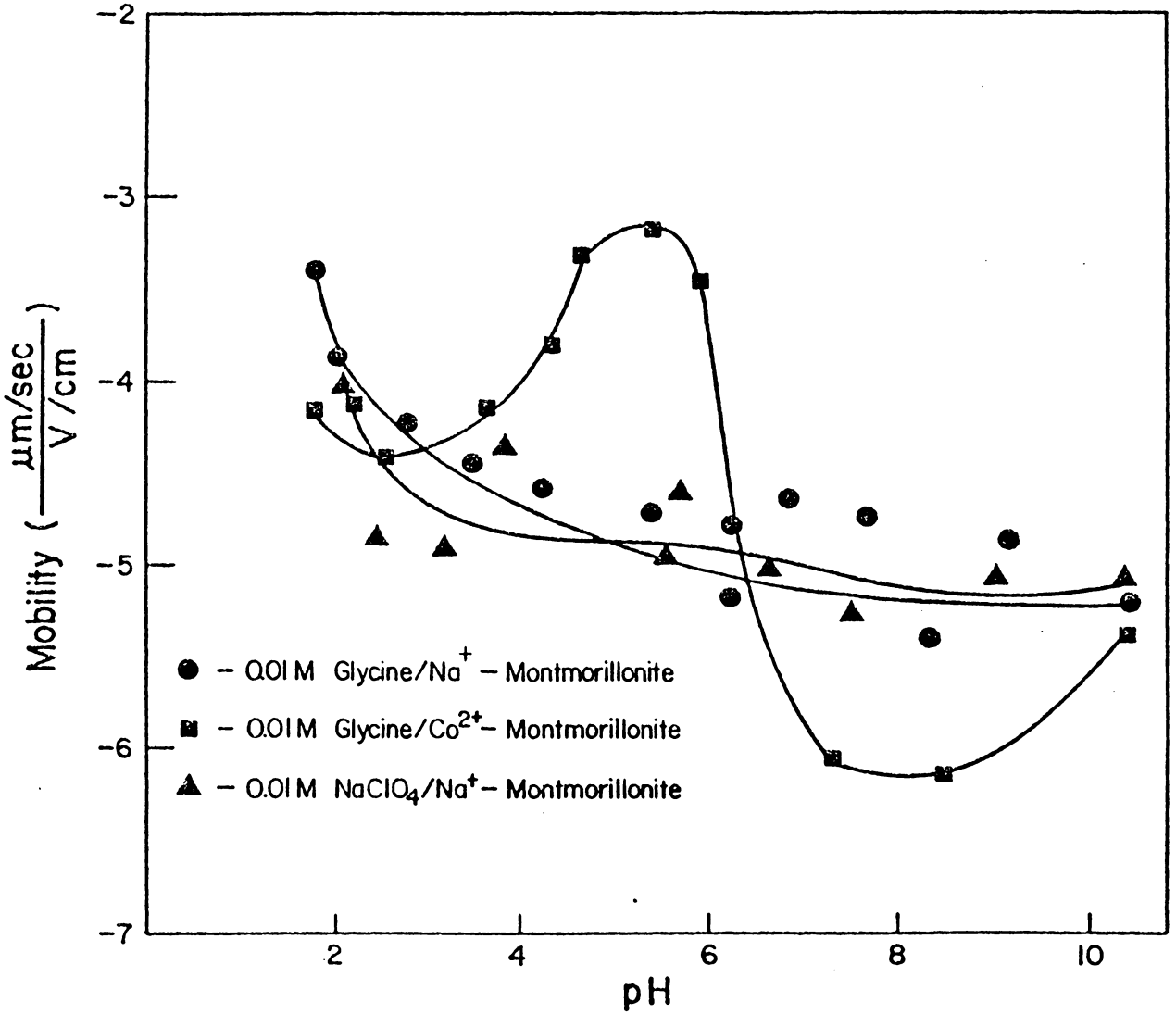

Figure 13. Electrophoretic Mobility of 0.01 M Glycine in M^{n+}-Montmorillonite

exchange. Equivalent exchange of glycine for sodium is indicated because the mobility remains the same. This possible reaction is presented below:

$$\begin{array}{l} \text{COOH} \\ | \\ \text{H-C-NH}_3^+ \\ | \\ \text{H} \end{array} + \text{Na}^+\text{-clay} \rightarrow \text{Na}^+ + \begin{array}{l} \text{COOH} \\ | \\ \text{H-C-NH}_3^+\text{-clay} \\ | \\ \text{H} \end{array} \qquad (31)$$

At pH 4 and 6, glycine is a zwitterion in solution and so it is likely that the zwitterion adsorbs as follows:

$$\begin{array}{l} \text{COO}^- \\ | \\ \text{H-C-NH}_3^+ \\ | \\ \text{H} \end{array} + \text{Na}^+\text{-clay} \rightarrow \begin{array}{l} \text{NH}_3^+ \\ | \\ \text{H-C-COO}^-/\text{Na}^+\text{-clay} \\ | \\ \text{H} \end{array} \qquad (32)$$

However, this does not rule out cation exchange (Equation 31). Identification of the forces bonding the zwitterion to the clay is not established by electrophoresis alone. At pH 8 and 10, significant amounts of glycine did not adsorb, indicating that the interaction of glycine with Na^+-montmorillonite is negligible at these pH values. All the suggested mechanisms are consistent with the observation that the mobility of montmorillonite in glycine is the same as the mobility in $NaClO_4$, between pH 2 and 10.

The mobility of Co^{2+}-montmorillonite in glycine is also presented in Figure 13. At pH 2 the mobility of Co^{2+}-saturated montmorillonite in glycine is more negative than the mobility of cobalt adsorbed on Na^+-montmorillonite in $Co(NO_3)_2$. This difference in mobility signifies that a lower charged species than Co^{2+} is adsorbed on

Co^{+}-montmorillonite. This feature could arise via nonequivalent exchange of Co^{2+} by a glycine cation as shown in Equation 33.

$$\begin{array}{l} \text{COOH} \\ | \\ \text{H-C-NH}_3^{+} \\ | \\ \text{H} \end{array} + \text{Co}^{2+}\text{-clay} \rightarrow \begin{array}{l} \text{COOH} \\ | \\ \text{H-C-NH}_3^{+}\text{-clay} \\ | \\ \text{H} \end{array} + \text{Co}^{2+} \qquad (33)$$

Adsorption of a zwitterion is possible but unlikely because glycine is cationic in solution at this pH. It is also unlikely that cobalt is complexed by glycine because the majority of the surface cobalt is released at pH 2 (Figure 12) and complexation of cobalt is favored by unprotonated amine groups that exist at high pH values.

At pH 4 and 6, the charge on the Co^{2+}-montmorillonite surface in 0.01M glycine was greater than the charge for Na^{+}-montmorillonite in glycine or in $NaClO_4$. Glycine is a neutral zwitterion in solution at these pH values and would not increase the surface charge upon adsorption. The more positive mobility could occur by Co^{2+} adsorption. Electrophoretic mobility measurements for montmorillonite in Co^{2+} showed that the mobility of Co^{2+} on montmorillonite (Figure 7) is more positive than the mobility of Na^{+} on montmorillonite (Figure 13). These observations support adsorption of a zwitterion, as shown in the following reaction:

$$\begin{array}{l} \text{NH}_3^{+} \\ | \\ \text{H-C-COO}^{-} \\ | \\ \text{H} \end{array} + \text{Co}^{2+}\text{-clay} \rightarrow \begin{array}{l} \text{NH}_3^{+} \\ | \\ \text{H-C-COO}^{-}/\text{Co}^{2+}\text{-clay} \\ | \\ \text{H} \end{array} \qquad (34)$$

Between pH 6 and 10, the charge on the Co^{2+}-montmorillonite surface in the presence of glycine is less than that observed for Na^+ - montmorillonite in $NaClO_4$. This is due to the complexation of the surface cobalt by glycine. The interaction is more likely to occur at these higher pH values because the amino acid amine groups are ioinized and can readily donate electrons to cobalt. Nonequivalent exchange could not be responsible for the decrease in charge because glycine is neutral or negative in solution between pH 6 and 10. These observations lead to the following possible reaction:

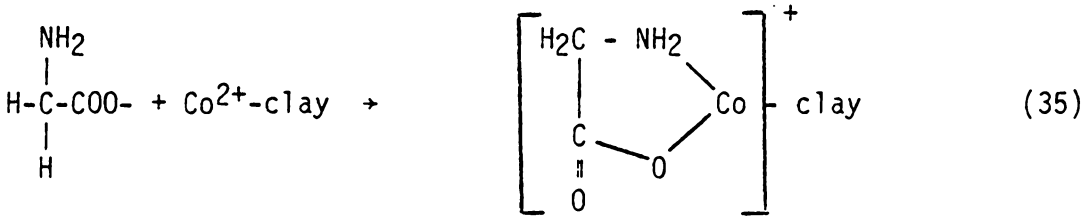

(35)

The electrophoretic mobilities for Na^+-montmorillonite in 0.01M $NaClO_4$ and in 0.01M lysine as a function of pH are presented in Figure 14. The mobility decreases by about 3.5 units between pH 2 and 4. Between pH 6 and 10, the mobility is relatively constant and is the same as for Na^+-montmorillonite in $NaClO_4$.

The more positive mobility for Na^+-montmorillonite in lysine versus $NaClO_4$ at pH 2 indicates that nonequivalent exchange occurs between a +2 lysine cation and the surface counterions. Lysine has a charge of +2 in solution at pH 2, so the following reaction is likely:

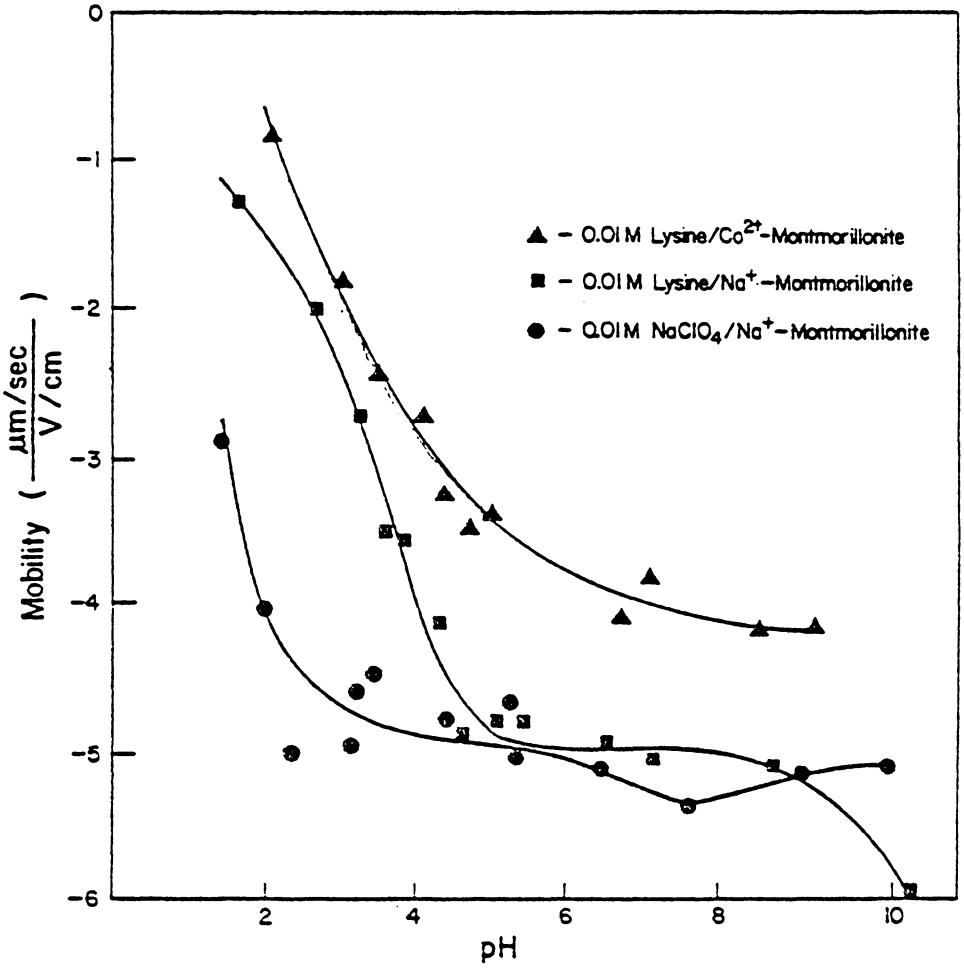

Figure 14. Electrophoretic Mobility of M^{n+}-Montmorillonite in 0.01 M Lysine

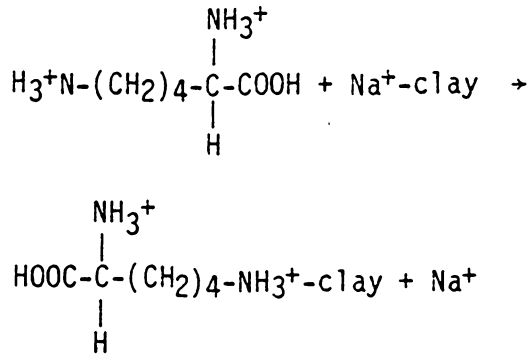

(36)

It is suggested by this reaction that the terminal amine group bonds to the clay surface, but it is also possible for the α-amine group to bond to the surface.

At pH 4 the mobility of Na^+-montmorillonite in lysine, -4.0 mobility units, um/sec/V/cm, (m.u.) was slightly higher than the mobility of Na^+-montmorillonite in $NaClO_4$ at pH 4, -4.9 m.u. This result indicates that some nonequivalent exchange of Na^+ by +2 lysine cations (Equation 36) occurs at this pH, but not as much as was observed at pH 2.

Between pH 6 and 8, the electrophoretic mobility for Na^+-montmorillonite is the same in both lysine and $NaClO_4$. Since lysine exists as a univalent cation in solution at this pH value, it is reasonable that equivalent exchange occurs according to (Equation 37).

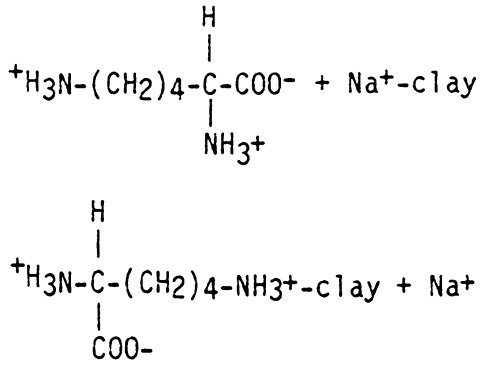

(37)

At pH 10 the mobility of Na^+-montmorillonite in lysine is about the same as that for Na^+-montmorillonite in $NaClO_4$. It is possible for cation exchange to occur (Equation 37) but since the major species in solution is the zwitterion, it is suggested that the zwitterion associates with the clay surface (Equation 38).

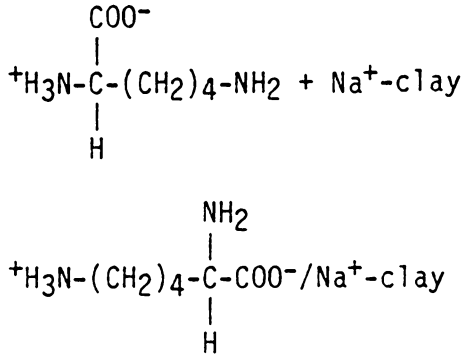

(38)

The electrophoretic mobility of Co^{2+}-montmorillonite in 0.01M lysine is more positive at all pH values than for Na+-montmorillonite in 0.01M lysine or in 0.01M $NaClO_4$ (Figure 14). Quantitative measurements show that approximately the same amount of lysine is adsorbed at pH 2, 4, and 6, onto Co^{2+}- and on Na^+-montmorillonite. The greater mobility can be due to the presence of Co^{2+} on the clay surface in this pH region. Quantitative measurements of Co^{2+} released (Figure 12) show that total release of the 3.0×10^{-4} moles/g of surface cobalt does not occur between pH 2 and 10. Electrophoretic mobility measurements for Co^{2+}-montmorillonite showed that the clay surface has a greater charge than Na^+-montmorillonite at pH 2 to 6 (Figure 7). Complexation of surface cobalt is not considered likely because no additional uptake of lysine onto Co^{2+}-montmorillonite compared to Na^+

-montmorillonite was observed. Thus, exchange of lysine with Co^{2+} on the clay surface is the significant reaction between pH 2 and 6. The possible equivalent exchange reaction at pH 2 is presented below:

$$\begin{array}{l} {}^{+}H_3N\text{-}(CH_2)_4\text{-}\underset{\displaystyle NH_3^{+}}{\overset{\displaystyle H}{\underset{|}{\overset{|}{C}}}}\text{-}COOH + Co^{2+}\text{-clay} \rightarrow \\ \\ \underset{\displaystyle H}{\overset{\displaystyle COOH}{\underset{|}{\overset{|}{{}^{+}H_3N\text{-}C}}}}\text{-}(CH_2)_4\text{-}NH_3^{+}\text{-clay} + Co^{2+} \end{array} \qquad (39)$$

At pH 4 and 6, equivalent exchange of two lysine cations for Co^{2+} is more likely because a lysine cation is the dominant species in solution in this pH range. The possible exchange reaction is presented:

$$\begin{array}{l} 2\ {}^{+}H_3N\text{-}(CH_2)_4\text{-}\underset{\displaystyle H}{\overset{\displaystyle COO^{-}}{\underset{|}{\overset{|}{C}}}}\text{-}NH_3^{+} + Co^{2+}\text{-clay} \rightarrow \\ \\ ({}^{+}H_3N\text{-}(CH_2)_4\ \underset{\displaystyle H}{\overset{\displaystyle COO^{-}}{\underset{|}{\overset{|}{C}}}}\text{-}NH_3^{+})_2\text{-clay} + Co^{2+} \end{array} \qquad (40)$$

At pH 8 and 10, more lysine is adsorbed on Co^{2+}-montmorillonite versus Na^{+}-montmorillonite (Table 7). This additional adsorption is assumed to be due to interaction of the amino acid with the cobalt counterion. Complexation of adsorbed cobalt by lysine to give Co(II) $(lys)_2^{2+}$ or Co(II)lys^{2+} would render a more positive surface compared

to Na^+-montmorillonite. Exchange of Co^{2+} by lysine (Equation 40) or zwitterion adsorption (Equation 41) can also occur as shown below:

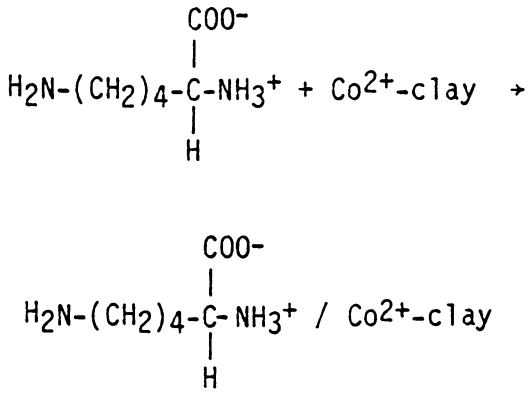

(41)

However, greater uptake of lysine on Co^{2+}-montmorillonite compared to Na^+-montmorillonite supports the following coordination reactions:

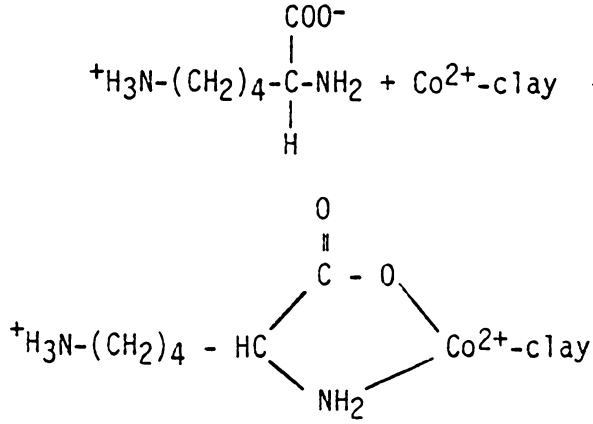

(42)

$$Co(lys)^{2+}\text{-clay} + \text{lysine} \rightarrow Co(lys)_2{}^{2+}\text{-clay} \qquad (43)$$

Powder x-ray diffraction patterns for the clay before and after adsorption were recorded to investigate how interaction with the amino acids affected the interlayer spacing. The measured d_{001} spacing and calculated Δ for lysine, glycine, and water adsorbed on Na^+ - montmorillonite as a function of pH are presented in Table 11. CPK

Table 11

XRD Amino Acids Adsorbed onto Na^+-Montmorillonite

pH	H_2O $d_{001}\pm0.1$Å	Δ ±0.2Å	Glycine $d_{001}\pm0.2$Å	Δ ±0.2Å	Lysine $d_{001}\pm0.2$Å	Δ ±0.2Å
2	16.3	6.8	16.2	6.7	16.3	6.8
4	13.2	3.7	12.8	3.3	14.2	4.7
6	13.4	3.9	12.8	3.3	14.5	5.0
8	13.4	3.9	13.3	3.8	13.4	3.9
10	13.4	3.9	13.2	3.7	13.1	3.6.

Hydration Diameter - $Al(H_2O)_6^{3+*}$ - 6.8Å

*Calculated using equation - $D_{Hydration} = 2\ (r_{Al}^{3+} + 2r_{H_2O})$ (82)

$r_{Al}^{3+} = 0.51$Å (134)

$r_{H_2O} = 1.38$Å (82)

spacefilling molecular models of the amino acids were constructed to determine the minimum molecular dimensions that glycine and lysine could have in the montmorillonite interlayers. The minimum dimension determined for glycine was 4.0Å and for lysine was 4.5Å. Modeling of this sort was previously done by Talibudeen (99) and Greenland et al. (100,101).

At pH 2, aluminum in the clay lattice dissolves and Al^{3+} is formed according to the following reaction:

$$Al_2O_3 + 6H^+ \rightarrow 2Al^{3+} + 6H_2O \qquad (44)$$

The Al^{3+} formed can adsorb in the clay interlayers. XRD analysis indicated that the interlayer spacing for montmorillonite samples prepared in water, glycine, and lysine at pH 2 are significantly higher than the Δ value spacing at higher pH values. Delta values, Δ, of 6.8 ± 0.2Å (Table 11) agree favorably with the suggestion that $Al(H_2O)_6^{3+}$, which has a hydrated radius of 6.8Å (Table 11), is in the interlayers at pH 2.

At pH 4 and 6, the interlayer spacing for glycine adsorbed on Na^+-montmorillonite is 3.3Å, which is significantly smaller than Δ for Na^+-montmorillonite, 3.7 to 3.9Å or the minimum dimension of glycine, 4.0Å. Talibudeen (99) and Greenland et al. (100,101) observed contraction of the interlayers in the presence of glycine.

Possible causes of this contraction include hydrogen bonding and "keying" of amino acids into the octahedral holes of the silicate interlayer (100,101). Glycine is a zwitterion in solution at pH 4 and

6, thus cation exchange with surface sodium is unlikely. Electrophoresis analysis indicates that the surface charge did not vary. If neutral zwitterions adsorb on the clay surface, either by hydrogen bonding or keying, the charge on the montmorillonite surface would not vary. XRD analysis is not able to differentiate between these mechanisms.

At pH 8 and 10, no uptake of glycine is observed. As predicted, XRD showed that the Δ values at these pH values were not significantly different than those for Na^+-montmorillonite in water.

The calculated Δ values for lysine adsorbed onto Na^+-montmorillonite at pH 4 and 6, were 4.7 and 5.0Å, respectively, and were larger than the minimum dimension of the lysine molecule, 4.5Å. This indicates that lysine is not necessarily "keyed" into the octahedral holes in the clay lattice structure at pH 4 and 6. Cation exchange of lysine for Na^+ is possible at these pH values because lysine has a charge of +1. This mechanism would agree with the observed interlayer spacing.

At pH 8 and 10, Δ values 3.9 and 3.6Å respectively, were smaller than the minimum dimension for lysine, 4.5Å. For lysine to be adsorbed at these pH values, lysine must be "keyed" into the octahedral holes. A diagram of lysine "keyed" into the octahedral holes in the clay lattice structure is presented in Figure 15. The protonated α-amine group is probably "keyed" into vacant octahedral holes near sites of isomorphous substitution in the clay lattice. These sites are negatively charged and attract the positively charged protonated amines.

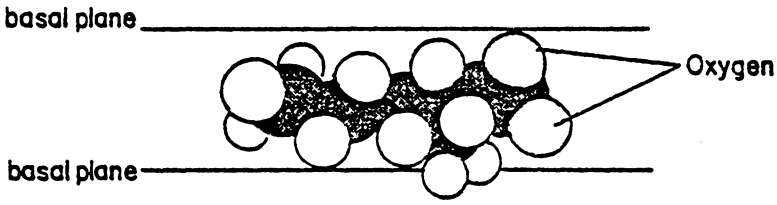

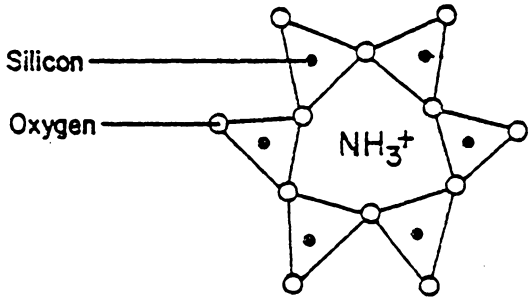

Figure 15. Lysine "Keyed" in Octahedral Holes

XRD analysis of glycine on Co^{2+}-montmorillonite was unable to determine if cation exchange, zwitterion association, or complexation of glycine with the clay surface occurred. This was due to the larger size of $Co(H_2O)_6^{2+}$, 7.0Å, compared to glycine, 4.0Å. Complexation of cobalt would not significantly change the Δ value because of the small size of the glycine ligand. $Co(gly)_3$ has a minimum dimension of 6.2Å. Table 12 presents the d_{001} spacing and Δ values of Co^{2+}-montmorillonite both before and after treatment with glycine and lysine. The Δ values of glycine and lysine at pH 2 were 16.1Å and 16.0Å, respectively. It is not possible to determine if this spacing is due to $Co(H_2O)_6^{2+}$ or $Al(H_2O)_6^{3+}$ in the interlayers because of their similar size.

At pH 4 and 6, lysine on Co^{2+}-montmorillonite gave rise to two XRD diffraction peaks. One peak at 13.8 ± 0.2Å was similar to the d_{001} spacing observed for lysine on Na^{+}-montmorillonite at these pH values. The other peak at 16.0 ± 0.2Å indicated interlayer spacings similar to untreated Co^{2+}-montmorillonite. The peak corresponding to lysine adsorption is probably due to sufficient ion exchange of Co^{2+} so that lysine determines the d_{001} spacing. Figure 12 showed that 2.0×10^{-4} moles and 1.9×10^{-4} moles of cobalt were released at pH 4 and 6, respectively, which is approximately two-thirds of the cobalt on the clay surface (3×10^{-4} moles/g). The second peak at approximately 16.0Å probably corresponds to montmorillonite with some cobalt remaining in the interlayers.

At pH 8 and 10, the interlayer spacings of lysine adsorbed on Co^{2+}

Table 12

XRD Amino Acids Adsorbed on Co^{2+}-Montmorillonite

pH	Glycine/Co^{2+} Montmorillonite d_{001} ±0.2Å	Δ ±0.2Å	Lysine/Co^{2+} Montmorillonite d_{001} ±0.2Å	Δ ±0.2Å
2	16.1	6.6	16.0	6.5
4	15.8	6.3	13.8, 16.0	4.3, 6.5
6	16.1	6.6	14.0, 16.0	4.5, 6.5
8	15.5	6.0	16.1, 16.0	6.6, 6.5
10	15.5	6.0	15.9	6.4

d_{001} - Co^{2+} - montmorillonite (pH - 6.5)	16.0Å
Minimum Dimension Adsorbates Determined by Molecular Models	
glycine	4.0Å
lysine	4.5Å
$Co(gly)_3$	6.4Å
$Co(lys)_3^{3+}$	7.1Å
Hydration Diameter	
$Co(H_2O)_6^{2+}$	7.0Å

- montmorillonite, 16.1 and 15.9Å respectively (Table 12), are not significantly different than for the untreated Co^{2+}-montmorillonite substrate, 16.0Å. However, if one or two lysine ligands did complex cobalt, the basal spacing would not increase if the complex is "keyed" into octahedral sites of the clay or if the carbon chain of lysine lay parallel to the basal clay surface. The minimum size of $Co(lys)_3^{3+}$ was estimated to be 7.1Å, which is not sufficiently different from the hydrated diameter of $Co(H_2O)_6^{2+}$, 7.0Å, to suggest complexation of Co^{2+} by lysine.

The infrared transmission spectra of glycine and lysine adsorbed on Na^+-and Co^{2+}-montmorillonite were measured to further investigate the bonding of the amino acid to the clay and to examine the acid and base character of the adsorbed amino acid. The region between 1800 cm^{-1} and 1300 cm^{-1} was analyzed to obtain ionization information regarding both the carboxylate and the amine groups of the amino acids. Assignments of the various peaks are taken from the literature (111-112, 152-154). The band at approximately 1620 cm^{-1}, corresponding to the asymmetric stretch of COO^-, was not used to analyze the adsorbed amino acid, because of interference from the water deformation band at approximately 1620 cm^{-1}.

Infrared spectra of glycine adsorbed on Na^+- and Co^{2+}-montmorillonite at pH 2 and 4, presented in Table 13, show bands for adsorbed glycine. The spectrum for glycine adsorbed on Na^+-montmorillonite at pH 2 is presented in Figure 16. No bands corresponding to the adsorbed glycine were observed above pH 4.

At pH 2 for glycine on both Na^+- and Co^{2+}-montmorillonite, the

Table 13

Infrared Spectra of Glycine on Montmorillonite

$\nu \pm 0.2$ cm-1

Na^+-Montmorillonite

pH 2 ν(cm-1)	(Intensity)	pH 4 ν(cm-1)	(Intensity)	Assignments
1745	(vs)	--		ν_{as} COOH(unionized
1616	(vs)	1618	(vs)	δH_2O
1503	(vs)	1505	(s)	ν_s $-NH_3^+$
1429	(m)	1417	(vs)	ν_s $-COO^-$

Co^{2+}-Montmorillonite

pH 2 ν(cm-1)	(Intensity)	pH 4 ν(cm-1)	(Intensity)	
1741	(vs)	--	--	ν_{as} COOH(unionized)
1624	(vs)	1618	(vs)	δH_2O
1509	(vs)	1505	(s)	ν_s $-NH_3^+$
1429	(m)	1415	(vs)	ν_s $-COO^-$

s = strong; m = medium; w = weak; vs = very strong

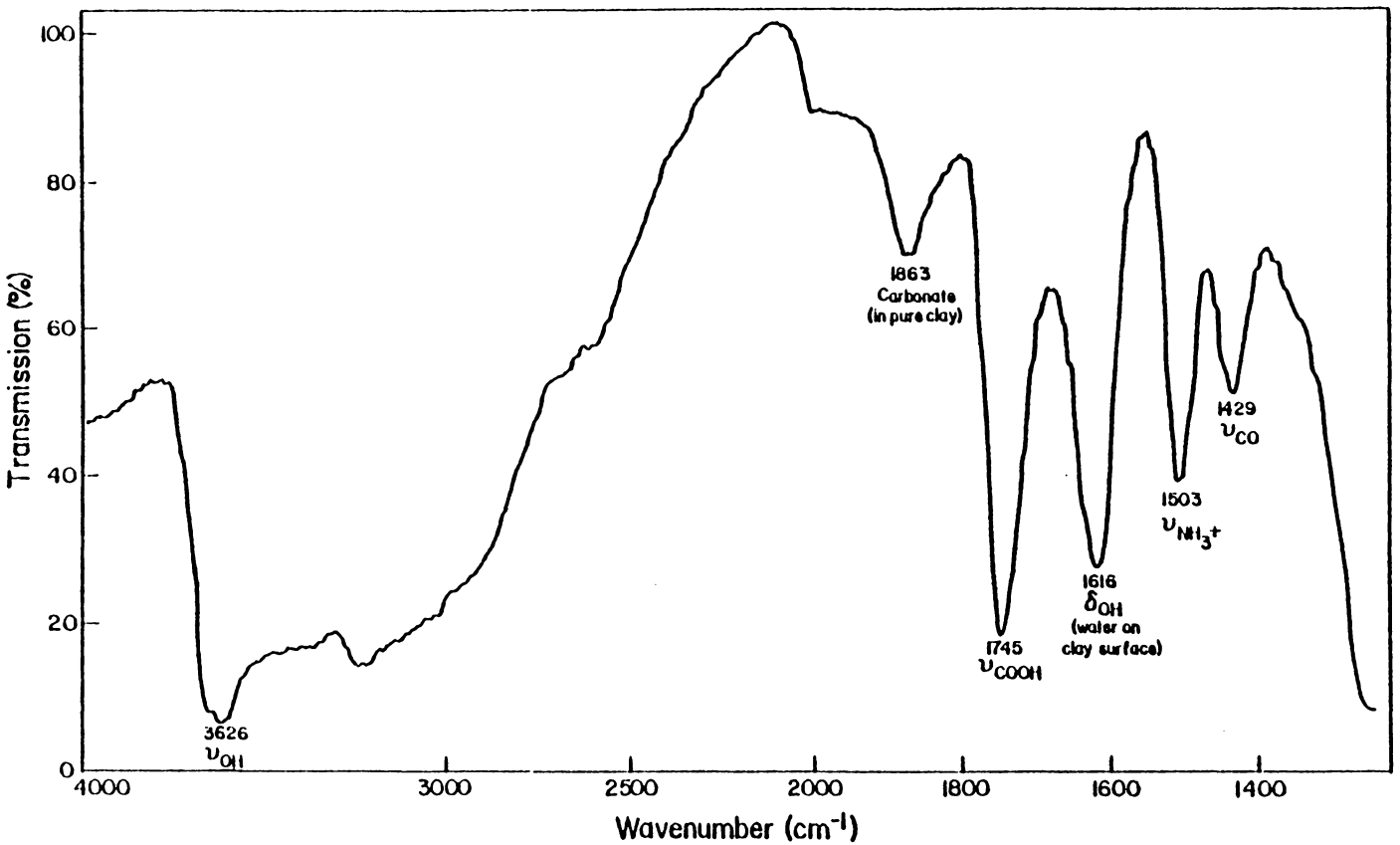

Figure 16. Infrared Spectrum of Glycine Treated Montmorillonite - pH 2

asymmetric stretching band for an unionized carboxylate group, -COOH, was observed at 1745 cm^{-1}. A very intense band for the asymmetric stretch of $-NH_3^+$ was recorded at 1503 cm^{-1} and 1509 cm^{-1} for glycine adsorbed on Na^+- and Co^{2+}-montmorillonite, respecitvely. These bands indicate that cationic glycine is adsorbed onto the clay. An additional peak corresponding to ν_s COO^- was observed at 1429 cm^{-1} which indicates that zwitterionic glycine is also present. Based on the intensity of the band at 1429 cm^{-1} compared to that of 1745 cm^{-1}, it is estimated that one-third of the amino acid is adsorbed as the zwitterion. This was found to be true on both Na^+-and Co^{2+}-montmorillonite.

At pH 4 glycine was adsorbed on both Na^+- and Co^{2+}-montmorillonite. The presence of symmetric stretching bands for both NH_3^+ and COO^- confirm the presence of the zwitterion. No ν_{as} bands corresponding to -COOH were observed, which confirms that the glycine cation is not the adsorbed species at pH 4.

The band frequencies and their assignments for lysine adsorbed on Na^+- and Co^{2+}-montmorillonite at different pH values are presented in Table 14. At pH 2 for lysine on both Na^+- and Co^{2+}-montmorillonite, bands corresponding to the asymmetric stretch for unionized carboxylate groups and the symmetric stretch for $-NH_3^+$ were observed but the ν_s COO^- band was not detected. These results indicate that lysine was adsorbed at pH 2 as $(^+H_3N(CH_2)_4\text{-}CH(NH_3^+)(COOH)$.

At pH 4 bands for ν_{as} -COOH, ν_s $-NH_3^+$ and ν_s COO^- are indicative of both +1 and +2 lysine cations on the lysine treated Na^+- and Co^{2+} - montmorillonite clay surfaces.

Table 14

Infrared Spectra for Lysine on Montmorillonite

$\nu \pm 2\ cm^{-1}$

Na^{+}-Montmorillonite

pH 2 ν (cm^{-1})	(Intensity)	pH 4 ν (cm^{-1})	(Intensity)	pH 6 ν (cm^{-1})	(Intensity)	pH 8 ν (cm^{-1})	(Intensity)	pH 10 ν (cm^{-1})	(Intensity)	Assignments
1719	(s)	1719	(m)	--		--	--	--		ν_{as} -COOH
1614	(vs)	1614	(s)	1618	(vs)	1620	(vs)	1618	(vs)	δ H_2O
1499	(s)	1498	(m)	1495	(s)	1495	(s)	1495	(m)	ν_s $-NH_3^+$
--	--	1389	(m)	1389	(s)	1389	(s)	1389	(m)	ν_s $-COO^-$

Co^{2+}-Montmorillonite

pH 2 ν (cm^{-1})	(Intensity)	pH 4 ν (cm^{-1})	(Intensity)	pH 6 ν (cm^{-1})	(Intensity)	pH 8 ν (cm^{-1})	(Intensity)	pH 10 ν (cm^{-1})	(Intensity)	
1719	(s)	1719	(m)	--	(vs)	--		--	--	ν_{as} -COOH
1620	(vs)	1610	(vs)	1610	(s)	1620	(vs)	1618	(vs)	δ - H_2O
1499	(s)	1498	(ms)	1495	(m)	1501	(m)	1495	(vs)	ν_s $-NH_3^+$
--		1388	(m)	1389		1380	(m)	1376	(m)	ν_s $-COO^-$

vs = very strong; s = strong; ms = medium strong; m = medium; w = weak

No adsorption bands occur near 1720 cm^{-1} for lysine on either Na^{+}- or Co^{2+}-montmorillonite at pH 6 to 10. This indicates the absence of adsorbed species containg the -COOH group. Bands corresponding to the symmetric stretches of both $-NH_3^{+}$ and $-COO^{-}$ were observed. A band at 1389 cm^{-1} corresponds to the symmetric stretch of uncoordinated ionized acid groups (152). This band is present for lysine on Na^{+}-montmorillonite at pH 6 to 10 and lysine on Co^{2+}-montmorillonite at pH 6.

The frequency of the ν_s COO- band is 1380 and 1386 cm-1 at pH 8 and 10, respectively. These frequencies are significantly lower than the values found at pH 4 (1388 cm^{-1}) and 6 (1389 cm^{-1}). The lower frequency observed for ν_s $-COO^{-}$ bands indicates coordination of lysine at higher pHs (152).

The wave number for the COO^{-} symmetric stretch in $Co(lys)_3Cl_3$ is 1378 cm^{-1} which agrees favorably with the value for lysine on Co^{2+}-montmorillonite at pH 8 and 10. The presence of $-NH_2$ on the Co^{2+}-clay surface was deduced by the decrease in the intensity of ν_s NH_3^{+} at pH 8 and 10. Co^{2+}-montmorillonite adsorbed greater amounts of lysine than did Na^{+}-montmorillonite in this pH range (Table 9). The decreased ν_s NH_3^{+} intensity with greater amounts of lysine on the surface indicates that the amine groups are unprotonated ($-NH_2$) and possibly bound to cobalt.

Although infrared analysis was helpful in deducing the chemistry of the acid group on the clay surface, the chemical information about the amine is limited because bands corresponding to the $-NH_2$ group were

not observed. Failure to detect $-NH_2$ bands is due to the presence of water and OH^- bands at approximately 3200 cm^{-1}, where the NH_2 symmetric stretch occurs (111-113). XPS analysis of the clays after interaction with the amino acids was conducted to study the chemical environment of nitrogen and cobalt. However, XPS is not helpful in determining the chemistry of the carboxylate group due to background carbon in the spectrometer and to the large amount of oxygen on the clay.

In Table 15 the XPS data for the pure amino acids and amino acid complexes are summarized. $Co(gly)_3$ has only one type of amine group, which is the α-amine coordinated to the metal. The N 1s binding energy, 399.3 eV, compares favorably with the value observed by Engerholm and Rush (155) 399.1 eV, for coordinated glycine. The N 1s binding energy for glycine and for L(+)-lysine monohydrochloride is 400.6 eV. The higher binding energy observed for these two amino acids compared to $Co(gly)_3$ indicates a more positive chemical environment around the nitrogen. This higher binding energy peak is assigned to protonated amine groups because lysine monohydrochloride is known to have both amine groups protonated and glycine occurs as the zwitterion. The N 1s binding energy for the protonated amine groups compares favorably with the value of 400.3 eV for H-glycine (155).

For $Co(lys)_3Cl_3$ and L(+)-lysine the nitrogen 1s photopeak has a peak width at half maximum (PWHM) of 3.7 eV. This value is significantly greater than the 2.3 ± 0.1 eV PWHM observed for glycine ($-NH_3^+$), L(+)-lysine monohydrochloride ($-NH_3^+$), and $Co(gly)_3$ ($-NH_2$)

Table 15

Amino Acids on M^{n+} - Montmorillonite
XPS Nitrogen 1s Photopeak

pH	N 1s Binding Energy (±0.2 eV)	N/Si (±0.005)	N/N^+
	Glycine/Na^+-Montmorillonite		
2	402.1, 399.5	0.045	1.1±0.1
4	402.0, 399.5	0.021	1.4±0.1
6	401.8, 399.5	0.011	1.4±0.1
8	--	0	0
10	--	0	0
	Glycine/Co^{2+}-Montmorillonite		
2	402.0, 399.5	0.035	1.3±0.1
4	402.0, 399.5	0.026	1.3±0.1
6	402.0, 399.5	0.016	2.3±0.1
8	402.0, 399.5	0.010	1.9±0.1
10	401.8, 399.4	0.017	2.0±0.1
	Lysine/Na^+-Montmorillonite		
2	401.9, 399.5	0.029	0.18±0.01
4	401.9, 399.1	0.054	0.42±0.01
6	401.8, 399.4	0.053	0.42±0.01
8	401.8, 399.5	0.054	0.37±0.01
10	402.0, 399.5	0.042	0.74±0.01

Table 15 (Continued)

pH	N 1s Binding Energy (±0.2 eV)		N/Si (±0.005)	N/N^+
		Lysine/Co^{2+}-Montmorillonite		
2	401.9,	399.4	0.029	0.17±0.01
4	401.8,	399.5	0.048	0.49±0.01
6	401.9,	399.5	0.055	0.53±0.01
8	401.9,	399.4	0.088	0.99±0.05
10	402.2,	399.3	0.126	1.5 ±0.01
Glycine	400.6	--	--	--
L(+)-Lysine	400.6	399.3	--	0.59±0.05
L(+)-Lysine Monohydrochlaride	400.6	--	--	--
$Co(gly)_3$	--	399.3	--	
$Co(lys)_3Cl_3$	400.7	399.3	--	1.0±0.1
H(gly) (155)	400.3	--	--	--
Cu(gly) (155)	--	399.1	--	--

which contain only a single type of nitrogen group. The N 1s photopeaks for $Co(lys)_3^{3+}$ and L(+)-lysine could be resolved into two peaks using the GASCAP IV program (129). The wider XPS photopeaks found for $Co(lys)_3Cl_3$ and L(+)-lysine reveal the presence of more than one chemical form of nitrogen in the samples. The binding energies for the multiplet peaks are equal to the values for protonated and unprotonated amine groups in the other reference compounds. The ratio of unprotonated to protonated amine groups, 1.0 for $Co(lys)_3Cl_3$, is consistent with the bonding in $Co(lys)_3Cl_3$ where the lysine α-amine group is bound to cobalt and the lysine terminal amine group is protonated. L(+)-lysine is a zwitterion with the terminal amine group protonated (155). The N/N^+ ratio observed for L(+)-lysine (0.59) indicates that some of the α-amine groups were also protonated. This could be due to hydration of the amino acid.

Analysis of the N 1s photoelectron peaks for the amino acids indicate that in all cases where adsorbed nitrogen was observed two types of nitrogens were found (Table 15). An unprotonated amine peak was observed that had a binding energy similar to the coordinated amine groups of $Co(gly)_3$. However, the N 1s binding energy at 401.9 eV, is signficiantly greater than the protonated amine groups found in L(+)-lysine monohydrochloride. The higher binding energy peak indicates that protonated amine groups on the clay surface are more acidic than protonated amine groups in the free amino acids. This observation suggests that the negative clay surface removes electron density from the amine group.

Particularly noteworthy is the XPS result that the ratio of the basic amine to acidic amine groups, N/N^+, for glycine at pH 2, 4, and 6 was approximately 1:1. The curve resolved spectrum for the glycine on Na^+-montmorillonite at pH 4 is presented in Figure 17. The presence of the acidic amine group of adsorbed glycine on Na^+-montmorillonite indicates that approximately 50% of the surface glycine is not adsorbed as a cation or as a zwitterion.

Peptide formation between glycine in solution and an already adsorbed glycine molecule would account for the basic amine group found on the clay surface. This reaction is presented below:

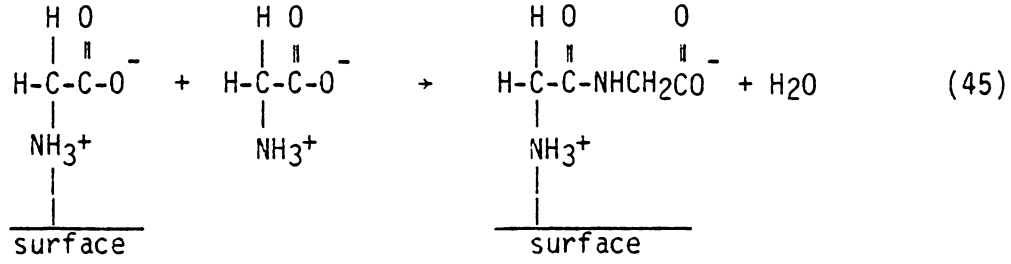

(45)

Greenland et al. (101) reported that the Δ value for glycylglycine on montmorillonite is 3.5Å, which agrees with the Δ values of 3.3Å calculated for glycine on Na^+-montmorillonite at pH 4 and 6. Although the amide stretching band at approximately 1650 cm-1 was not observed by infrared analysis, it may be obscured by the large water band at 1620 cm-1.

A second interaction that could create an unprotonated amine is hydrogen bonding of glycine to the clay surface according to Equation 46. Tailibudeen (99) suggested that this process could account for the decreased Δ values for adsorbed amino acids because shortening of the

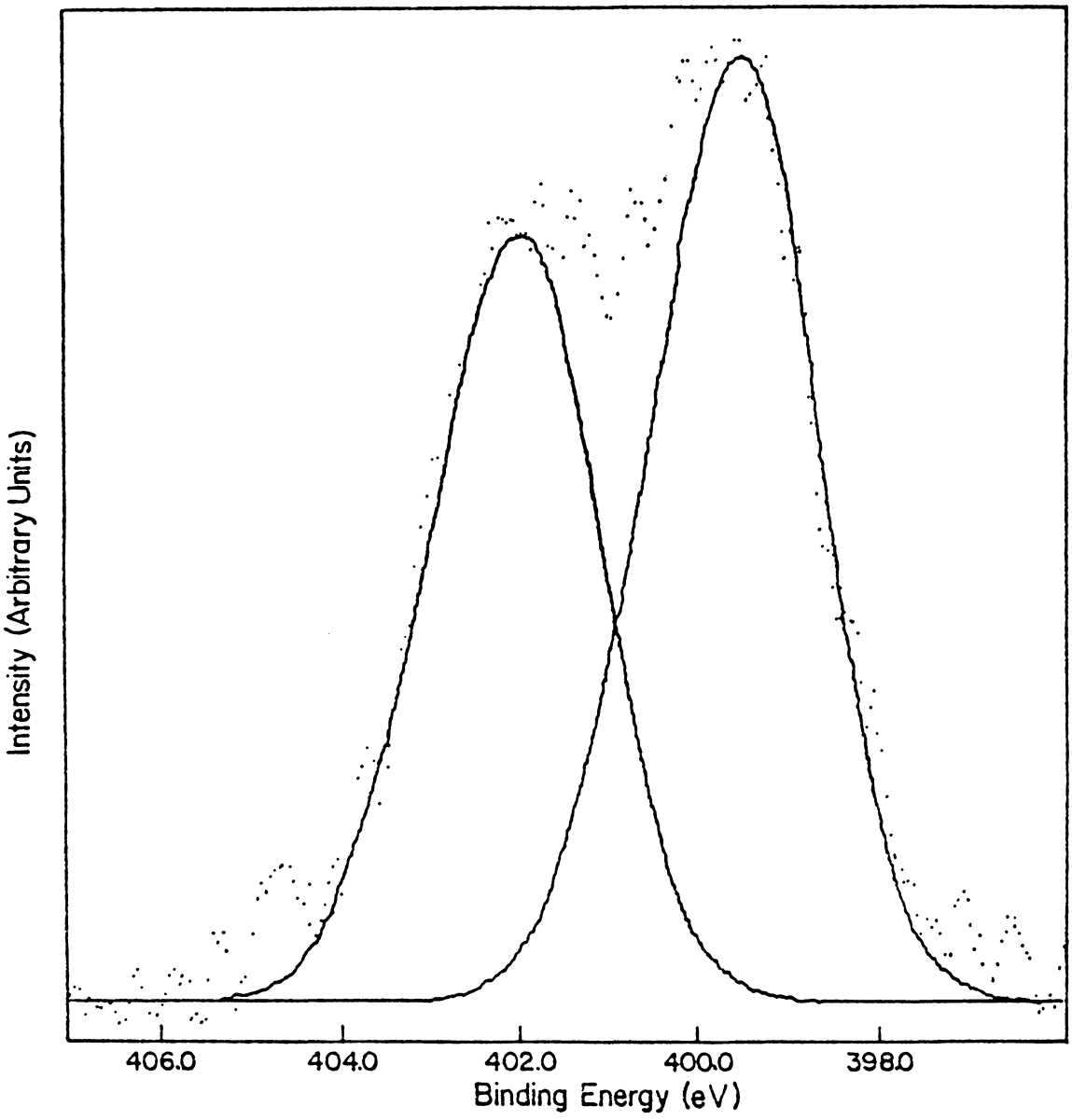

Figure 17. Glycine on Na^{+}-Montmorillonite - pH 4

C-H bonds would occur.

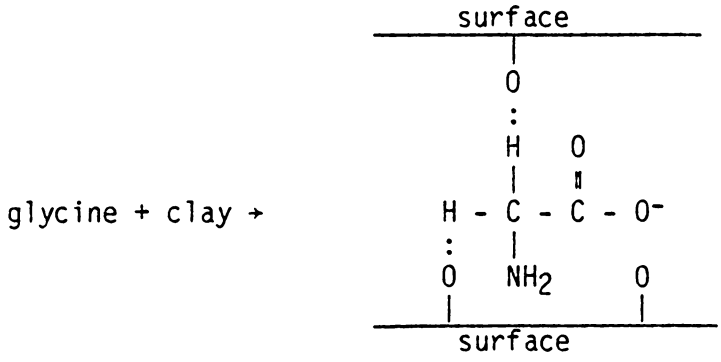

glycine + clay → (46)

Although this mechanism of adsorption is possible, it seems unlikely because it supposes that a negative glycine ion is adsorbed onto a negatively charged clay surface. The electrostatic forces repelling the negatively charged glycine ion would be stronger than the hydrogen bonds holding the amino acid to the clay.

The acidic amine groups found on the clay surface indicate the presence of cationic or zwitterionic glycine. This glycine species can be bound to the clay surface either by exchange of cationic glycine for sodium or by "keying" into the octahedral sites of the clay as a zwitterion. The cation can also be the α-amine group of a peptide held by either of these two mechanisms.

The N/N^+ ratios for lysine adsorbed on montmorillonite increase with increasing pH. This is expected based on the pK_a values of the amine groups. At pH 2 to 8, greater than two-thirds of the amine groups of lysine that sorbed on the surface are protonated. The two amine peaks comprising the N 1s spectrum at pH 4 are presented in Figure 18. Although it is not possible to determine which amine group is bound to the clay surface, the data indicate that the majority of

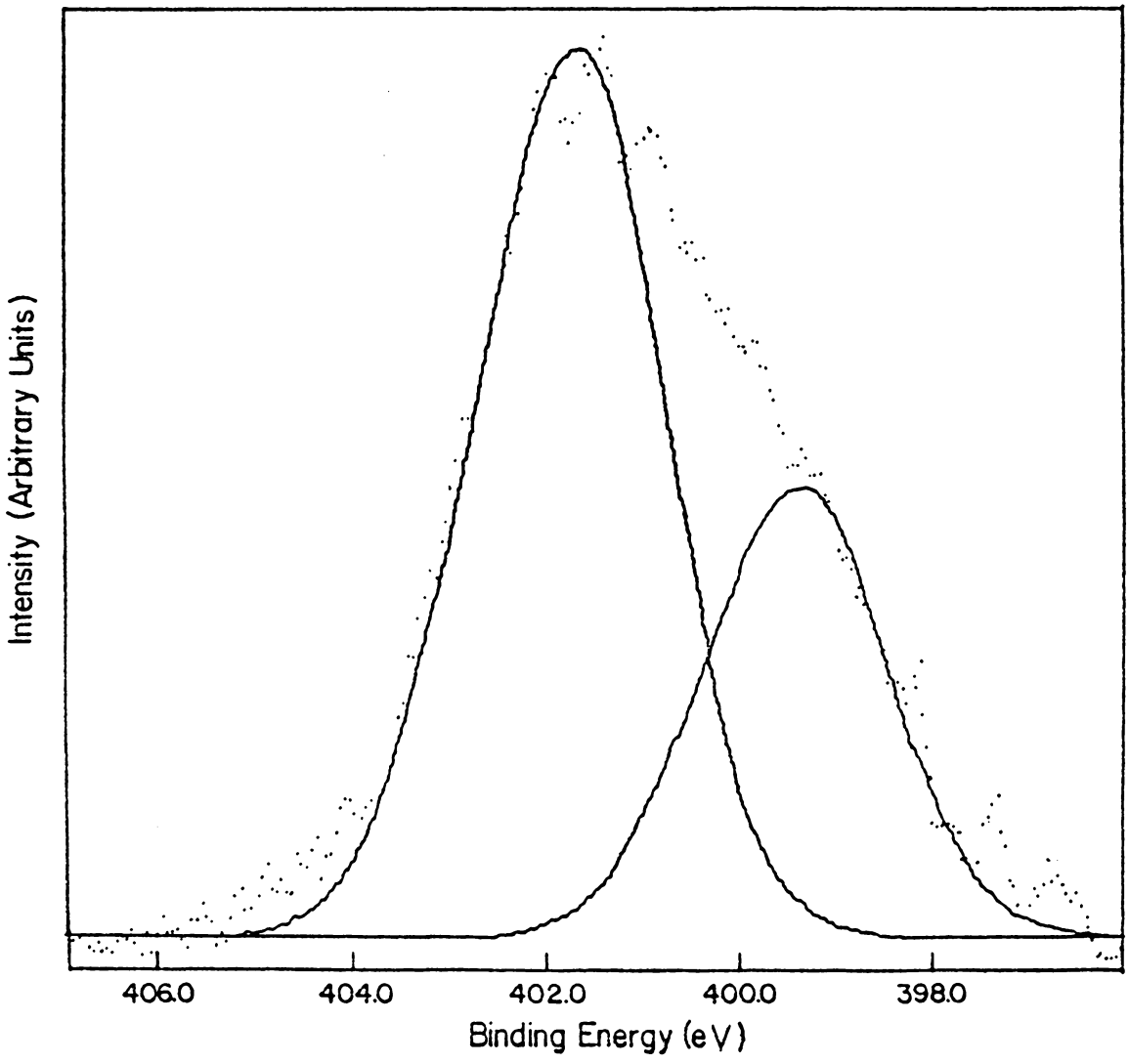

Figure 18. Lysine on Na^{+}-Montmorillonite - pH 4

the lysine molecules have at least one protonated amine group. At pH 2 a very small fraction of the lysine amine groups are basic. Infrared measurements showed that the acid group was not ionized. Thus the surface lysine satisfies two charge sites at this pH. This possibility is also supported by electrophoresis analysis.

The N/N^+ ratio for lysine at pH 2, (0.18) to 6 (0.42) is much less than the N/N^+ ratio for adsorbed glycine (1.1 to 2.3, respectively). The small fraction of unprotonated amine nitrogen found on the clay surface can be due to one or more of the following situations: 1) one of the lysine amine groups is unprotonated and the other bound to the surface, 2) peptide formation, and/or 3) hydrogen bonding.

Hydrogen bonding is probably not the mechanism responsible for unprotonated amines because this would occur more readily for zwitterionic lysine than for anionic glycine. The possible hydrogen bonding mechanism for lysine adsorption in the interlayers is presented below:

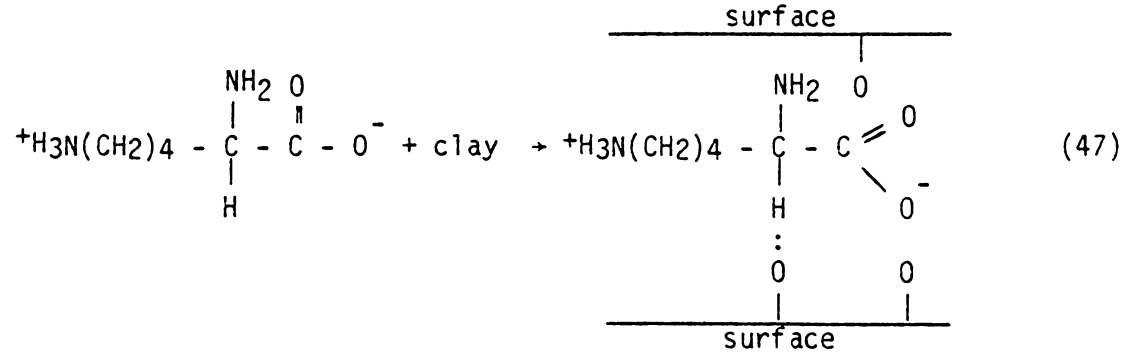

(47)

Previous studies (104, 157-159) have shown evidence for peptide formation on clay surfaces. Peptides are assumed to form during the drying cycle of amino acid treated clays, as shown in Equation 45.

Fripiat and Cloos (104) have detected the formation of glycine peptides by infrared spectroscopy, but a somewhat similar study did not detect peptide formation in lysine (108). Another study comparing glycine and alanine adsorption observed greater amounts of peptide formation for glycine than for the larger amino acid alanine (162). More favorable formation of peptides by glycine versus the larger amino acids indicates that the larger side chain of lysine $^{+}NH_3(CH_2)_4^{-}$ inhibits lysine peptide formation (Equation 48).

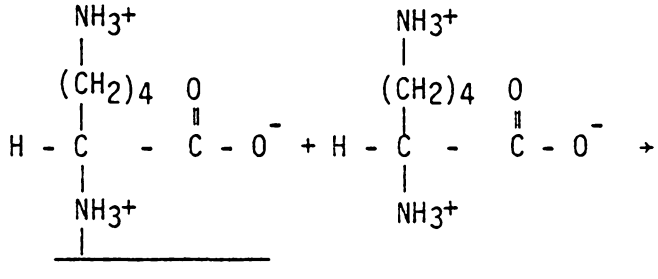

(48)

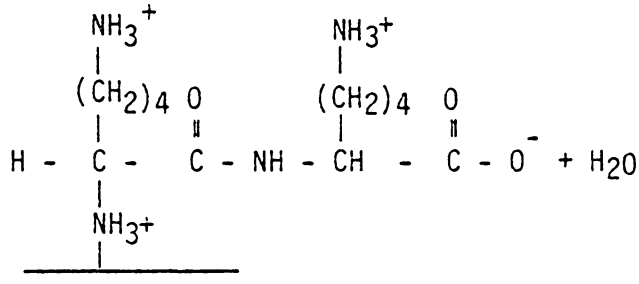

The N/N^{+} ratio for glycine and lysine on Co^{2+}-montmorillonite at pH 2 and 4 was the same as the ratio for these amino acids on Na^{+}-montmorillonite. This similarity indicates that the amino acid adsorbs by an equivalent mechanism onto both Co^{2+}- and Na^{+}-montmorillonite, and that the cobalt does not significantly alter the adsorption mechanism at pH 2 to 4. At pH 6 to 10, the N/N^{+} ratios for the amino

acids on Co^{2+}-montmorillonite were significantly higher than the N/N^{+} ratios for lysine treated Na^{+}-montmorillonite at these same pH values. Based on these results it is proposed that complexation of the amino acid with the surface cobalt occurs. The nitrogen 1s spectra for lysine on Na^{+}- and Co^{2+}-montmorillonite at pH 8 are presented in Figure 19 and 20, respectively. These spectra show that greater amounts of lower binding energy amine nitrogens are present for lysine on Co^{2+}-montmorillonite. At the higher pH values more of the amine groups are unprotonated, which facilitates coordination to the metal.

The Co $2p_{1/2}$ and Co $2p_{3/2}$ photopeaks were measured to investigate the oxidation state and chemical environment of surface cobalt. It has been reported that Co(II) amino acid complexes can react with oxygen to produce Co(III) complexes (Equation 30) (150,160,161). XPS binding energies for the Co $2p_{3/2}$ photopeak and the Co $2p_{1/2}$ -Co $2p_{3/2}$ energy differences are presented in Table 16. Surface cobalt was not observed at pH values where large amounts of cobalt were released from the clay surface. The cobalt binding energy and the cobalt splitting were 782.0 ± 0.1 eV and 15.9 ± 0.1 eV, respectively, for cobalt on the clay surface after interaction with the amino acids. These values do not vary significantly from those observed for the Co^{2+}-montmorillonite substrate. The discussion in the previous section for cobalt adsorbed on montmorillonite indicated that this cobalt was similar to $Co(H_2O)_6^{2+}$. Thus the interaction with the amino acid did not significantly affect the surface cobalt chemical environment.

If $Co(lys)_3^{3+}$ (Co $2p_{3/2}$ BE = 781.0) or $Co(lys)_2^{2+}$ (Co $2p_{3/2}$ BE =

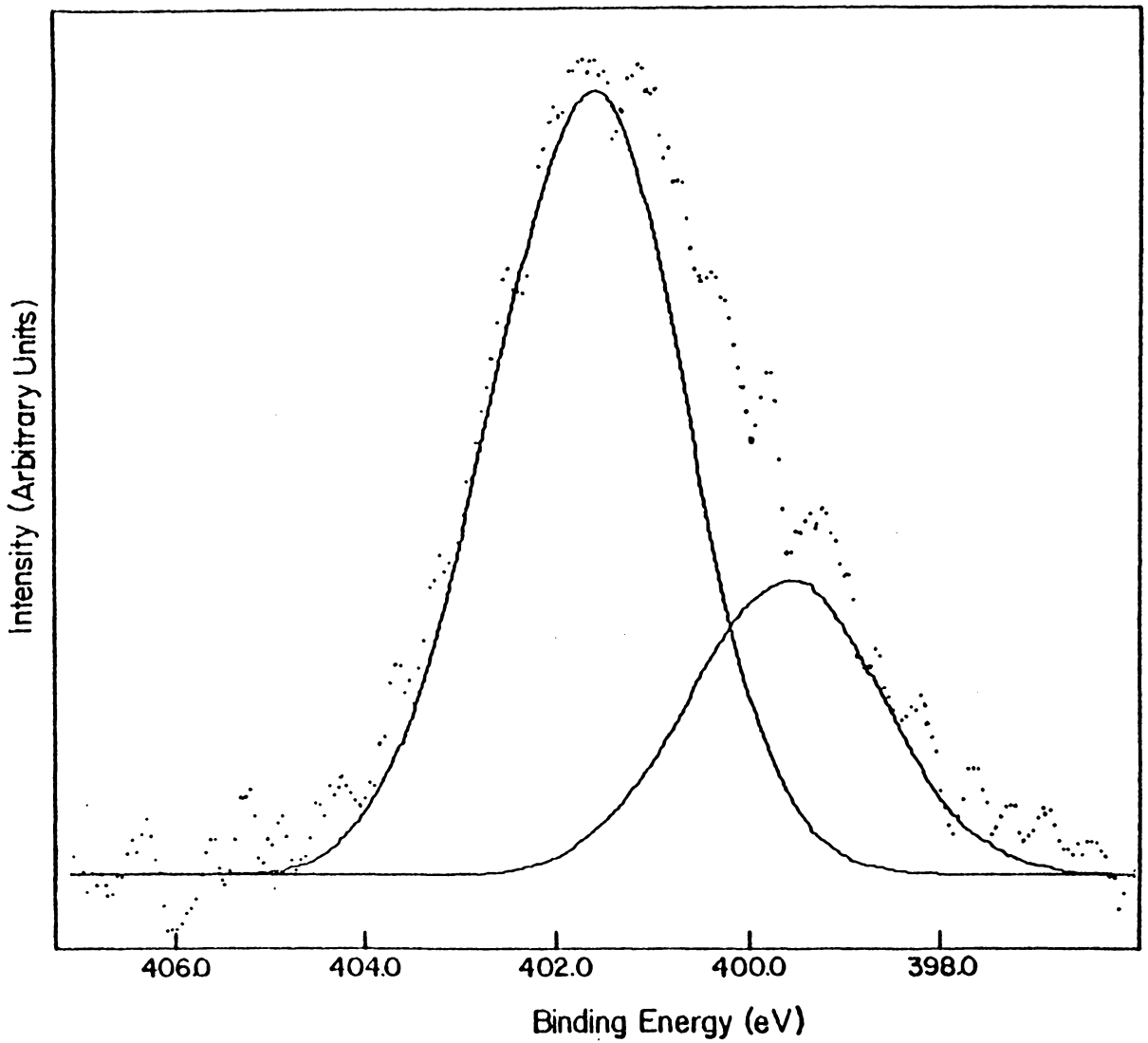

Figure 19. Lysine on Na^{+}-Montmorillonite - pH 8

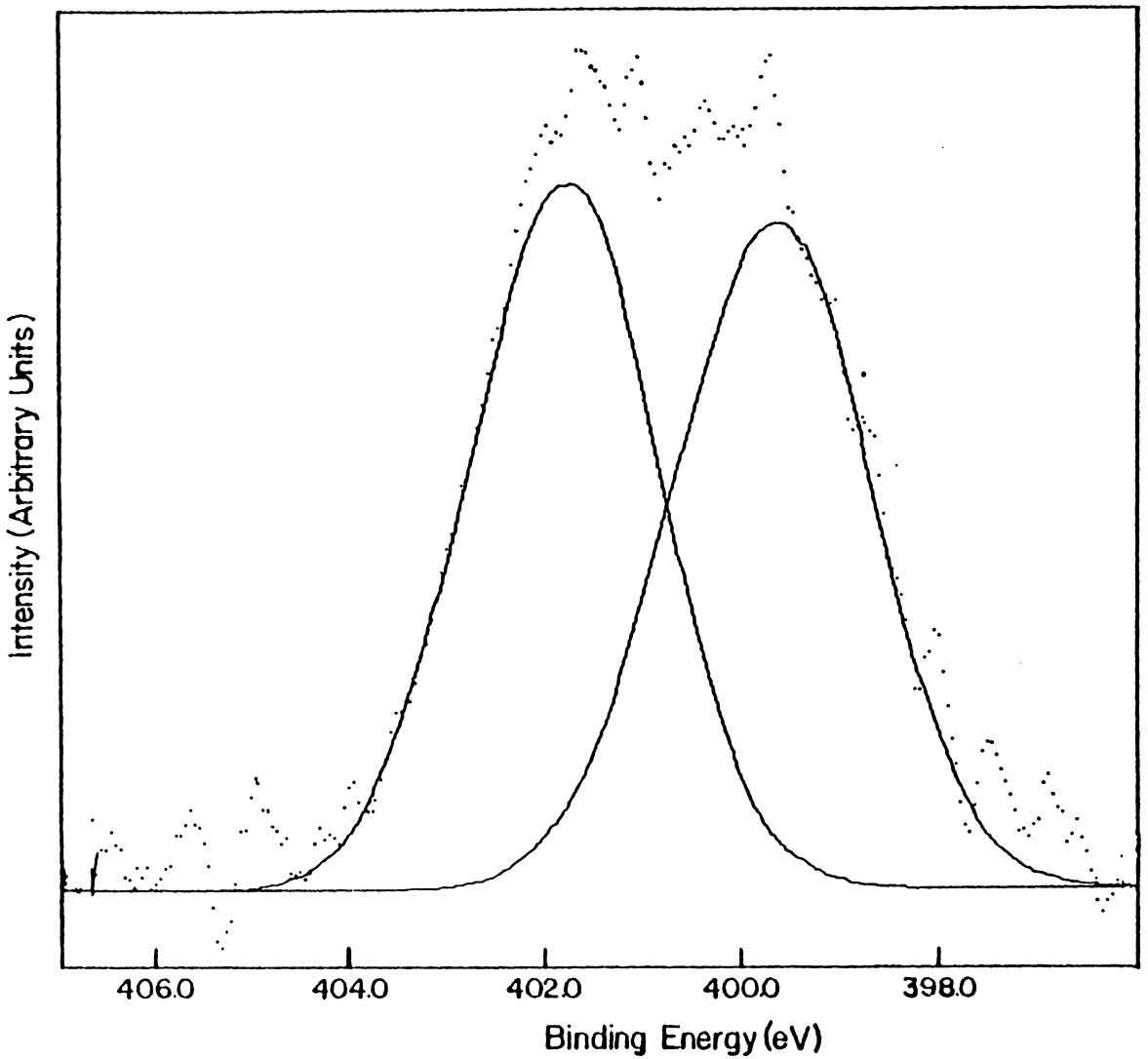

Figure 20. Lysine on Co^{2+}-Montmorillonite - pH 8

Table 16

XPS Amino Acids/Co^{2+}-Montmorillonite
Co $2p_{1/2}$, $2p_{3/2}$

pH	Co $2p_{3/2}$ Binding Energy (±0.2 eV)	ΔE Co $2p_{1/2}$ - Co $2p_{3/2}$ (±0.2 eV)	Co $2p_{3/2}$ Binding Energy (±0.2 eV)	ΔE Co $2p_{1/2}$ - Co $2p_{3/2}$ (±0.2 eV)
2	--	--	--	--
4	--	--	781.9	16.0
6	782.0	15.9	782.0	15.9
8	782.0	15.8	--	--
10	782.1	15.8	--	--

Co^{2+} - Montmorillonite pH = 6	782.0	16.0
$Co(lys)_2^{2+(162)}$	780.4	-
$Co(lys)_3^{3+}$	781.0	15.1
$Co(gly)_3$	781.1	15.1

780.4 (162)) was the species on the montmorillonite surface, it would be expected that the measured Co $2p_{3/2}$ binding energy would be less than that found for untreated Co^{2+}-montmorillonite. However it is possible for $Co(lys)_3^{3+}$ to be formed on the clay surface but only Co(II) detected by XPS, due to greater amounts of uncomplexed cobalt on the surface compared to complexed cobalt. At pH 8 and 10, the additional amount of lysine adsorbed on Co^{2+}-montmorillonite compared to Na^{+}-montmorillonite was 0.7×10^{-4} and 2.1×10^{-4} moles per gram, respectively (Table 9). The amount of cobalt on the surface at these pH values is 1.9×10^{-4} moles/g at pH 8 and 1.8×10^{-4} moles/g at pH 10. Thus if $Co(lys)_3^{3+}$ or $Co(lys)_2^{2+}$ is formed on the surface, approximately 12% to 18% of the cobalt is in this form at pH 8 and approximately 38% to 55% of the cobalt is in this form at pH 10. Although the estimated percentage of complexed cobalt on the surface at pH 10 is higher than the percentage where Co(II) would be detected by XPS and Co(III) by visible spectroscopy, this estimate does show that the majority of the surface cobalt is not complexed to lysine.

In contrast to the XPS results, diffuse reflectance visible spectroscopy did provide evidence for oxidation of the cobalt by lysine at pH values 6 to 10. The reflectance visible spectra observed for the Co^{2+}-clay samples treated with lysine and $Co(lys)_3^{3+}$ are presented in Figure 21. Reflectance bands corresponding to the $^1A_{1g} \rightarrow {}^1T_{1g}$ and $^1A_{1g} \rightarrow {}^1T_{2g}$ transitions of Co(III) were observed at 380 nm and 530 nm for pH values 8 and 10, and at 380 nm and 540 nm for the pH 6 sample. The energies of the $^1A_{1g} \rightarrow {}^1T_{1g}$ and $^1A_{1g} \rightarrow {}^1T_{2g}$ bands are very near the

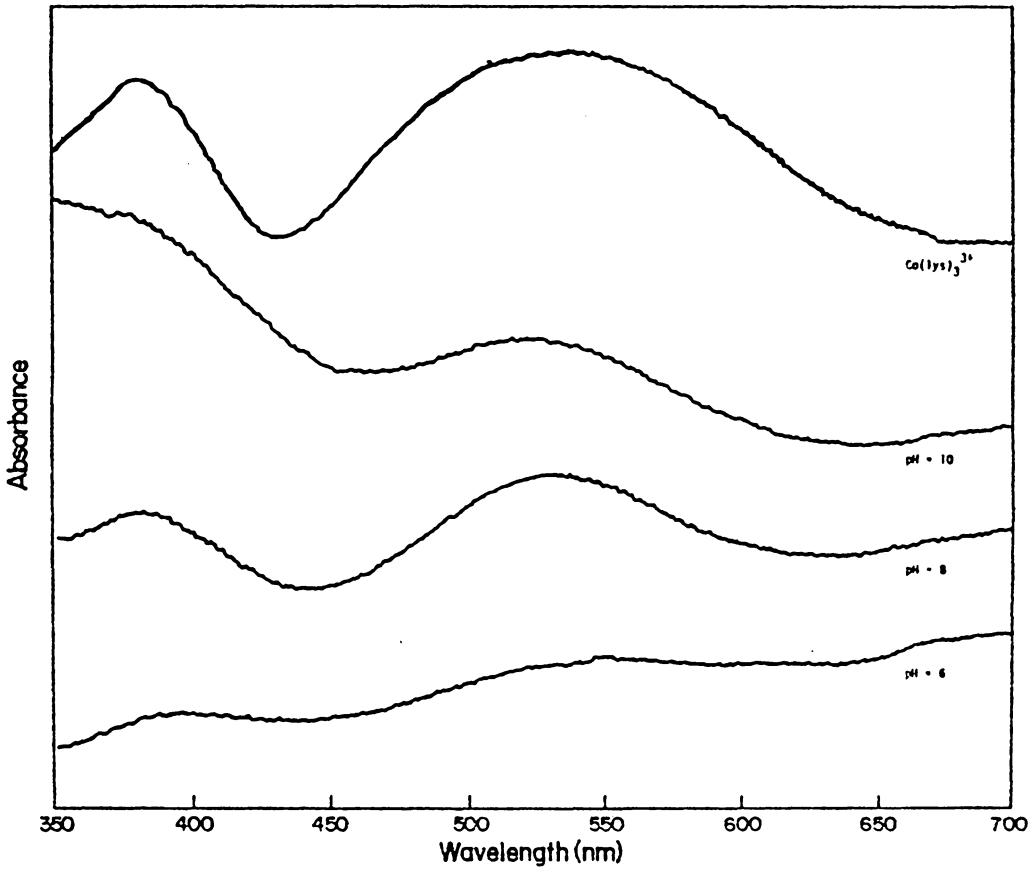

Figure 21. Reflectance Visible Spectra for Lysine on Co^{2+}-Montmorillonite

reflectance bands for $Co(lys)_3^{3+}$, 385 and 540 nm, respectively. A possible mechanism for oxidation of cobalt amino acid complexes is presented in Equation 30.

Diffuse reflectance visible spectroscopy is able to detect Co(III) more readily than Co(II). The molar absorptivity for $Co(H_2O)_6^{2+}$ is 5 (163) for the $^4T_{1g}(F) \rightarrow {}^4T_{1g}(P)$ band at 510 nm whereas that for $Co(lys)_3^{3+}$ is 109 (151) for the band at 525 nm and 178 (151) for the band at 369 nm. Based on these values it is estimated that approximately ten times as much Co(II) compared to Co(III) would have to be present for Co(II) to be detected in the presence of Co(III). However, by XPS it is estimated that Co(III) would only be detected in the presence of Co(II) if Co(III) constitutes approximately 30% or more of the total surface cobalt. Thus, if 10% to 30% of the cobalt is Co(III), XPS would indicate the presence of Co(II) and diffuse reflectance visible spectroscopy would indicate Co(III). It is quite possible that the low concentration of Co(III) on the surface is the cause of the different cobalt oxidation states observed by XPS and visible spectroscopy, because it was estimated that less than 30% of the surface cobalt is $Co(lys)_3^{3+}$. There were no changes in XPS spectral features with time or in sample appearance with XPS x-ray bombardment to indicate that the differences in cobalt oxidation state are due to sample decomposition.

A second possible reason for the different cobalt species observed by XPS and by visible reflectance spectroscopy is the different depths of analysis. XPS is a surface sensitive technique because the number of photoelectrons decreases exponentially with depth. The mean escape

depth of photoelectrons from solid samples is only about 10 to 20Å (146). The cobalt on the outer basal surface is detected more readily than interlayer cobalt because the distance between the surface cobalt and interlayer cobalt is at least 9.5Å, the thickness of the clay sheet. This assumes that the basal planes are perpendicular to the electron ejection path. In contrast, visible light can penetrate the clay interlayers, as shown by visible light being able to pass through clay films approximately 1000Å thick. The clay film thickness was obtained by determining the weight of the clay in the film per square cm (3.0 mg/cm^2) and assuming a density of 2.5 g/cm^3 for montmorillonite (134). It is possible that the density estimate is incorrect due to void spaces in the clay film. However, even if 75% of the clay is void space so that the density would be only 0.68 g/cm^3, the thickness analyzed is 400Å which is deep enough to analyze the interlayers. The different oxidation states for cobalt suggested by XPS and visible spectroscopy can also be due to different forms of cobalt on the surface and in the interlayers of the clay. Co^{2+} can be on the outer surface and Co(III) complexes can be adsorbed in the interlayers.

Either of these two explanations for the discrepancy of the cobalt oxidation state indicated by XPS and visible spectroscopic analysis is possible, but it is not known which or if both explanations are responsible.

In summary, the investigation of glycine and lysine on Co^{2+}- and Na^+-saturated montmorillonite found that the results support several different interactions. The presence or absence of $-NH_3^+$ and -COOH

bands in the infrared spectra and $-NH_3^+$ in the XPS N 1s spectra showed that cation exchange and/or zwitterion adsorption were possible reactions. Unprotonated amine nitrogens on the clay surface revealed that either coordination, peptide formation, of hydrogen bonding occurred. Shifts in the ν_s COO^- band of the infrared spectra showed that coordination of lysine by cobalt occurs for lysine adsorbed on Co^{2+}-montmorillonite at pH 8 and 10. Visible transmission spectroscopy indicated that complexation and oxidation of Co(II) to Co(III) on the lysine treated Co^{2+}-montmorillonite occurred. $Co(gly)_3$ and $Co(lys)_3^{3+}$ were observed in adsorbate solutions at pH 8 and 10 for the amino acid treated Co^{2+}-montmorillonite. It was suggested that coordination by the amino acids inhibited precipitation of $Co(OH)_2$. Because $Co(lys)_2^{2+}$ and $Co(gly)_2$ complexes are known oxygen carriers it was proposed that oxygen was the oxidizing agent, but no anaerobic experiments were conducted to substantiate this proposal.

No changes in the Co $2p_{3/2}$ binding energy, Co $2p_{1/2}$ - Co $2p_{3/2}$ splitting, or satellite features for Co^{2+}-montmorillonite before and after treatment with lysine were observed by XPS. However, it can be concluded from reflectance visible spectroscopic analysis that some complexation and oxidation of Co^{2+}-montmorillonite did occur upon treatment with lysine. There was no indication of Co(III) by either XPS or reflectance visible spectroscopy of Co^{2+}-montmorillonite treated with glycine. This lack of detected Co(III) can be due to cobalt glycine being neutral and thus not held to the clay surface by electrostatic forces.

No evidence was obtained in this study to differentiate between formation of complexes on the clay surface in contrast to complexation of desorbed cobalt in amino acid solutions.

C. COBALT AMINO ACID COMPLEX ADSORPTION ON MONTMORILLONITE

Previous reports have suggested that clays catalyze hydrolysis of cobalt complexes (73,87). The aim of this study was to investigate the effect of cobalt coordination by amino acids on metal adsorption. The role of complex charge and pH upon adsorption was also studied.

$Co(lys)_3^{3+}$, $Co(gly)_3$, and $Co(asp)_2^-$ were adsorbed on sodium montmorillonite. The structures of these three complexes are presented in Figure 22. Coordination to Co(III) by glycine and lysine occurs through the α-amine and α-carboxylate groups. Cobalt bonds to aspartic acid through the α-amine, the α-carboxylate, and the terminal acid group of the amino acid. All three cobalt complexes are relatively inert with respect to hydrolysis (151). To verify the stability of these complexes, 0.01M control solutions were prepared and the pH was adjusted to pH 2, 4, 6, 7, 8, and 10. Transmission visible spectra of the solutions were measured immediately after preparation and five days later and the results for the initial and final solutions are presented in Table 17. No change in the positions or intensities of the $^1A_{1g} \rightarrow {}^1T_{1g}$ or $^1A_{1g} \rightarrow {}^1T_{2g}$ bands measured for 0.01M $Co(gly)_3$ were observed as a function of pH or time over the five day period. $Co(lys)_3^{3+}$ and $Co(asp)_2^-$ showed no changes in the visible spectra at pH 2 to 8. At pH 10 the $Co(lys)_3^{3+}$ and $Co(asp)_2^-$ control solutions had a brown-violet color compared to the striking violet color at the lower pH values.

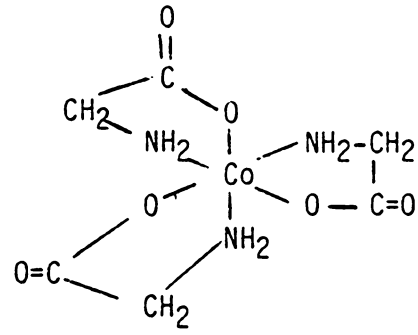

$Co(gly)_3$

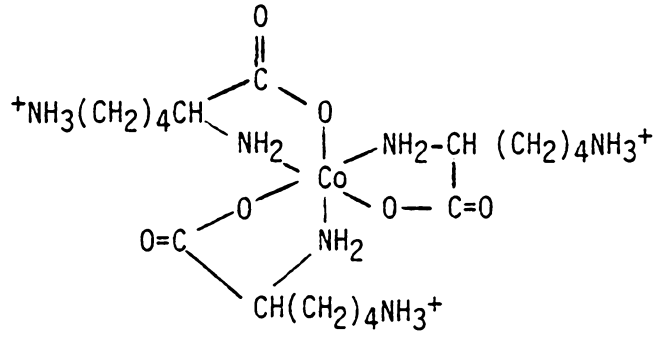

$Co(lys)_3^{3+}$

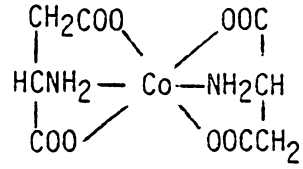

$Co(asp)_2^-$

Fig. 22. Amino Acid Complexes

Table 17

Visible Spectral Data for Cobalt Amino Acid Complex Solutions

	$^1A_{1g} \rightarrow {}^1T_{1g}$		$^1A_{1g} \rightarrow {}^1T_{2g}$	
	Transition		Transition	
0.01 M $Co(gly)_3$	λ (±2 nm)	Intensity Absorbance Units (±0.05)	λ (±2 nm)	Intensity Absorbance Units (±0.05)
Initial Solution	539	(0.80)	374	(1.2)
Solutions 5 days later				
pH				
2	540	(0.76)	375	(1.2)
4	540	(0.79)	374	(1.2)
6	539	(0.80)	373	(1.2)
7	538	(0.80)	374	(1.3)
8	538	(0.79)	372	(1.2)
10	540	(0.80)	375	(1.3)
Literature Value (151)	542	(----)	374	(---)
0.01 M $Co(lys)_3^{3+}$				
Initial Solution	525	(0.97)	372	(1.3)
Solutions 5 days later				
pH				
2	525	(0.95)	372	(1.32)
4	525	(0.99)	373	(1.35)
6	524	(0.95)	372	(1.30)
7	526	(0.97)	372	(1.29)
8	527	(0.97)	373	(1.32)
10	525	(0.97)	---	(>2.0)
Literature Value (151)	525	(----)	369	(----)

Table 17

(Continued)

0.01 M $Co(asp)_2^-$	$^1A_{1g} \rightarrow {}^1T_{1g}$ Transition λ (±2 nm)	Intensity Absorbance Units (±0.05)	$^1A_{1g} \rightarrow {}^1T_{2g}$ Transition λ (±2 nm)	Intensity Absorbance Units (±0.05)
Initial Solution	522	(0.70)	379	(0.44)
Solutions 5 days later				
pH				
2	522	(0.70)	379	(0.44)
4	522	(0.70)	379	(0.44)
6	522	(0.68)	381	(0.43)
7	522	(0.68)	382	(0.44)
8	520	(0.67)	378	(0.43)
10	522	(0.60)	378	(0.62)
Literature Value (150)	520	(----)	380	(----)

Filtration of these solutions revealed a brown precipitate in solutions of $Co(asp)_2^-$ at pH 10 and only a trace of precipitate for $Co(lys)_3^{3+}$. XPS analysis of the precipitates indicated they were $Co(OH)_2$. The Co $2p_{3/2}$ binding energy for each precipitate was 781.0 eV and the Co $2p_{1/2}$-Co $2p_{3/2}$ splitting was 16.0 eV. The XPS Co 2p spectrum for the precipitate from $Co(asp)_2^-$ at pH 10 is presented in Figure 23. The satellite features for the observed spectra are similar in intensity and energy position to those shown for $Co(OH)_2$ in Figure 9.

Although the visible spectral bands for 0.01M $Co(lys)_3^{3+}$ and $Co(asp)_2^-$ at pH 10 are not significantly shifted, the lower wavelength bands appear much more intense than the same bands at the lower pH values. The greater absorbance observed at the lower wavelength is possibly due to the scattering of light by suspended $Co(OH)_2$. The lower wavelength peak would be affected more by this process because the intensity of scattered light is inversely proportional to the fourth power of the wavelength (164).

Atomic absorption was used to measure the amount of cobalt adsorbed onto the clay from solutions of $Co(lys)_3^{3+}$, $Co(gly)_3$, and $Co(asp)_2^-$. The cobalt uptake as a function of complex concentration and at the various pH values is presented in Figures 24, 25, and 26 for $Co(lys)_3^{3+}$, $Co(asp)_2^-$, and $Co(gly)_3$, respectively. Uptake of $Co(lys)_3^{3+}$ increased with increasing concentration and increasing pH. Interactions in addition to electrostatic attraction must account for the increased uptake because the surface charge of Na^+-montmorillonite has a constant negative charge over the pH range studied. If electrostatic forces alone account for the amount of $Co(lys)_3^{3+}$ adsorbed, the amount of

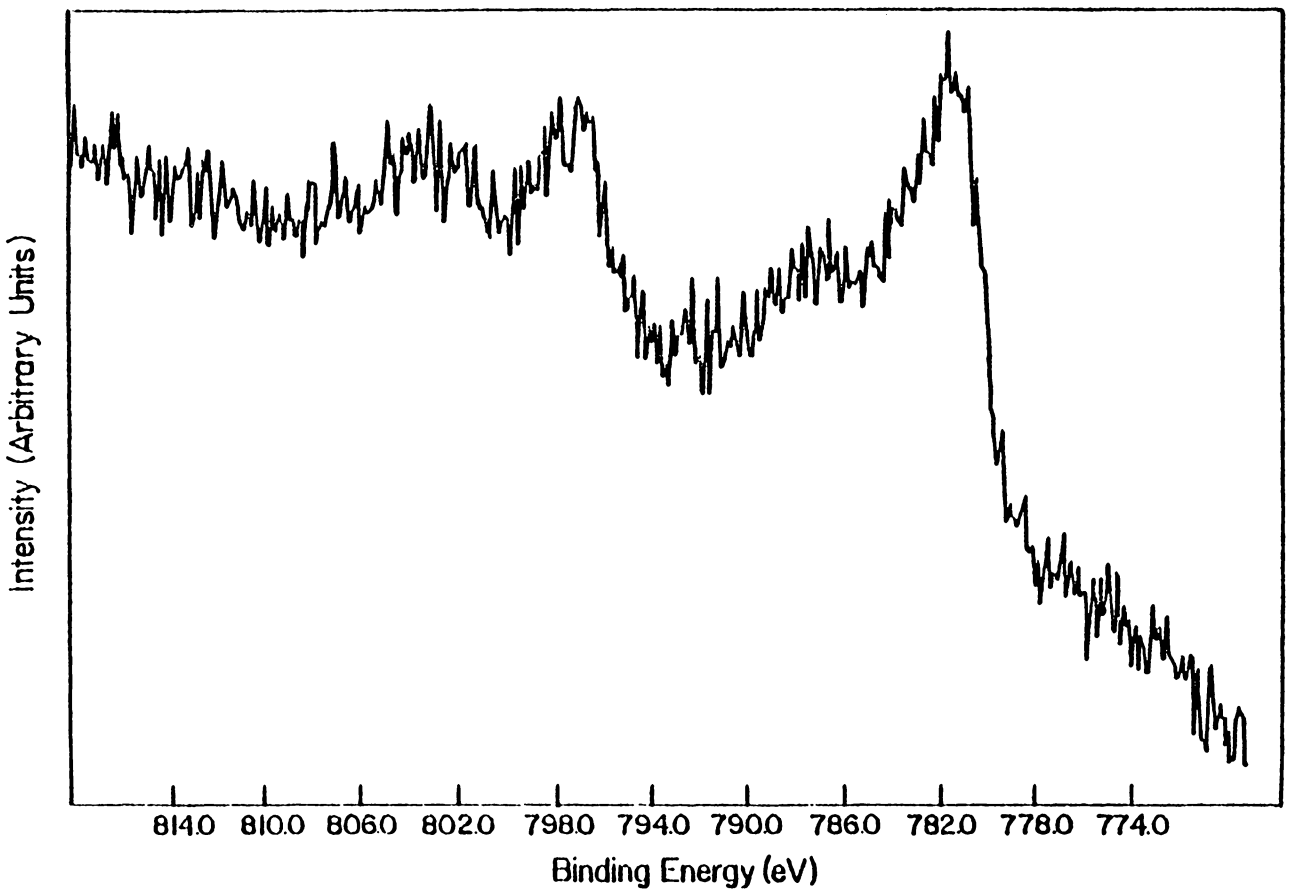

Figure 23. Spectrum for Precipitate - pH 10

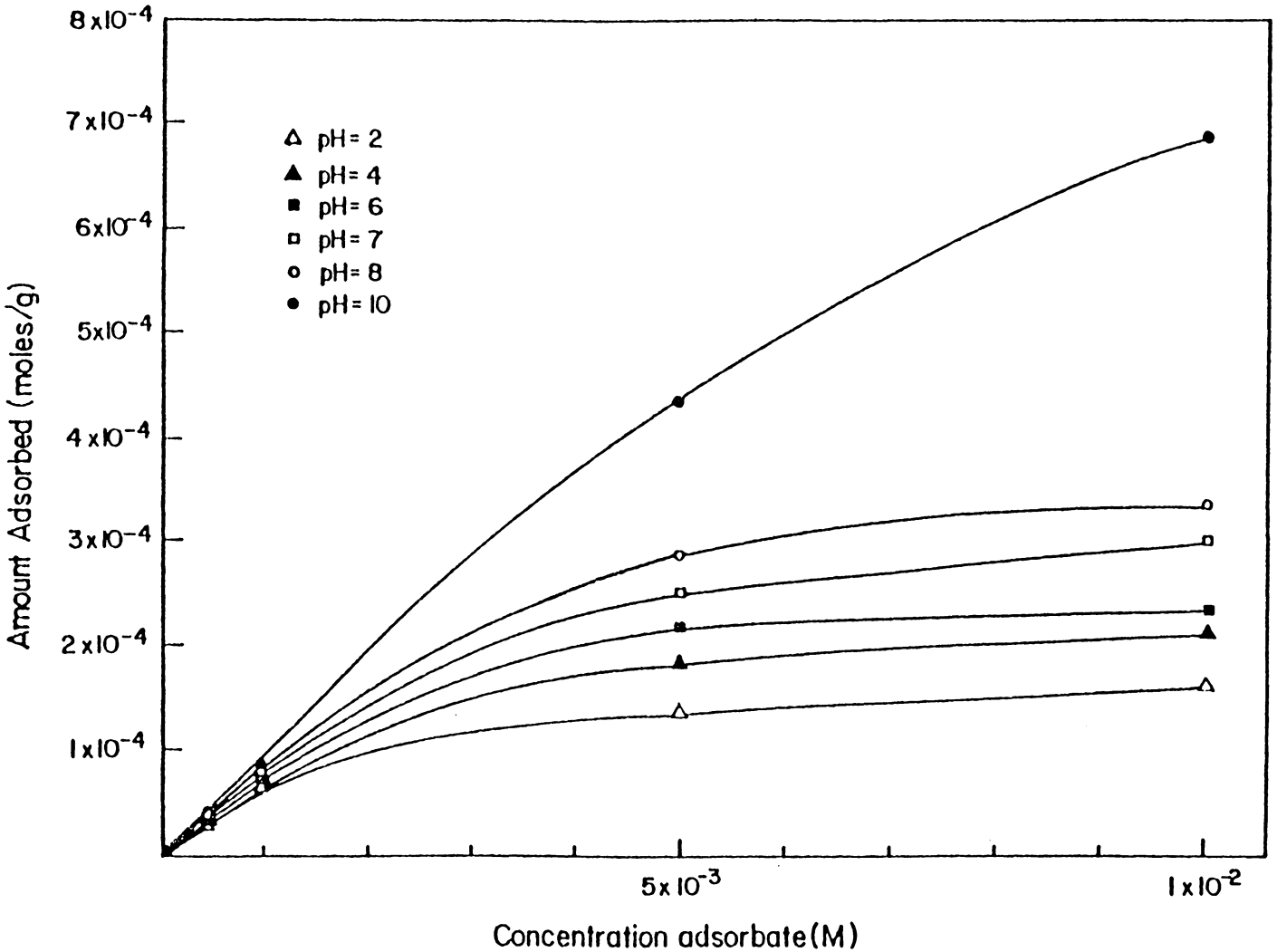

Figure 24. $Co(lys)_3^{3+}$ on Na^+-Montmorillonite

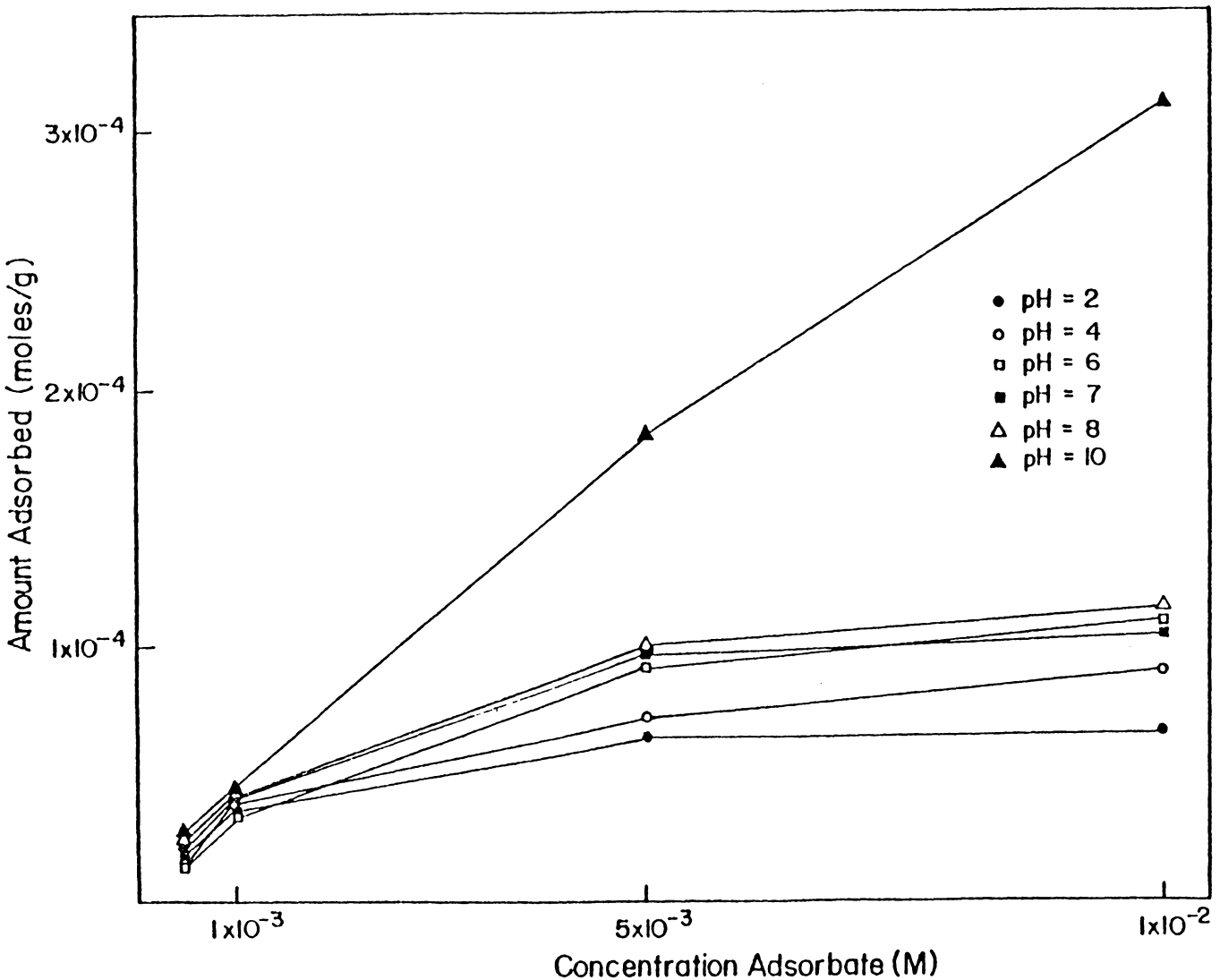

Figure 25. $Co(asp)_2^-$ on Na^+-Montmorillonite

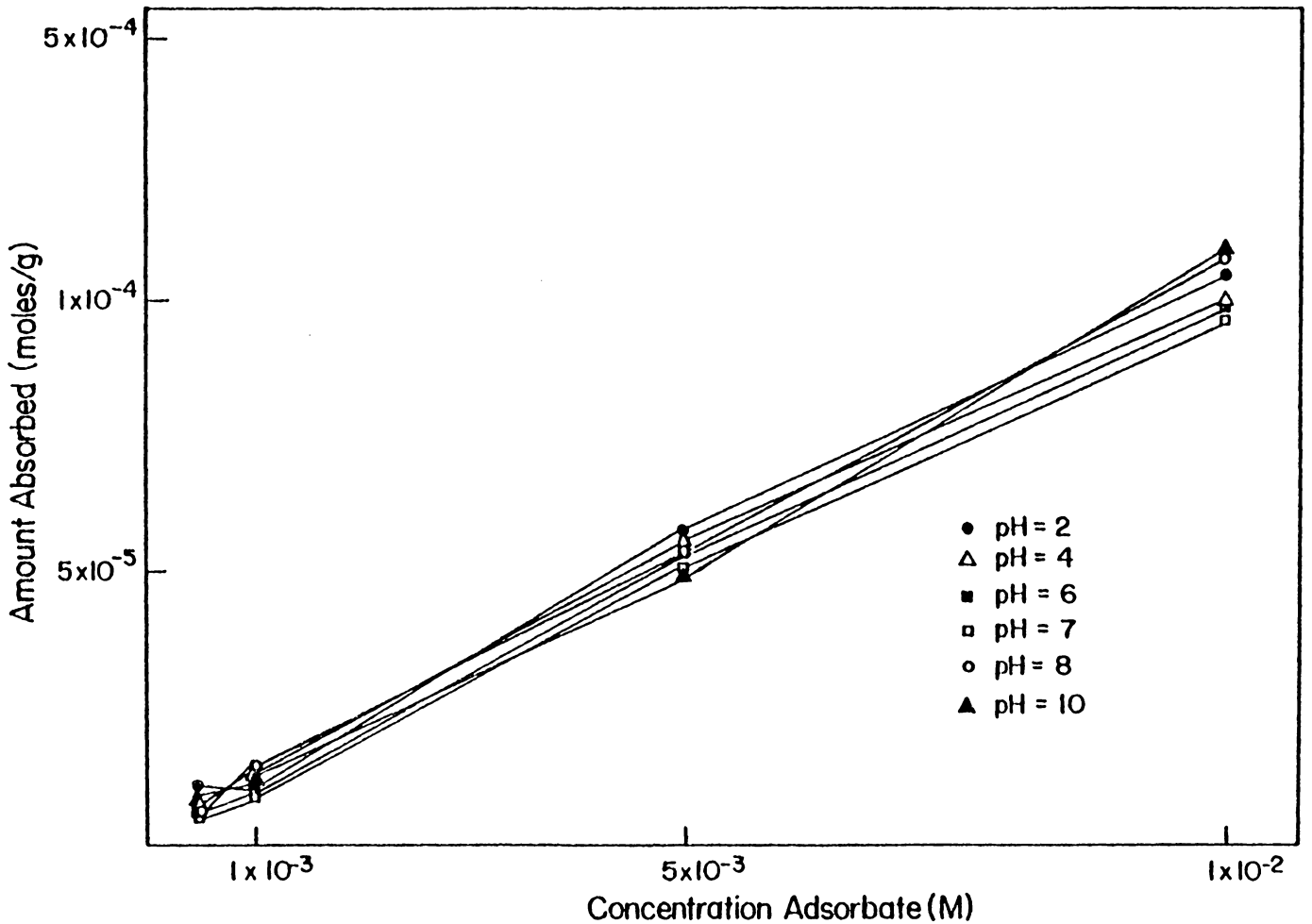

Figure 26. $Co(gly)_3$ on Na^+-Montmorillonite

cobalt adsorbed would either remain constant with pH or decrease with pH because the quantity of acidic lysine terminal amine groups decreases with pH.

Figure 25 shows that the amount of $Co(asp)_2^-$ adsorbed also increases with pH. Electrostatic attraction of the complex to the surface is unlikely because $Co(asp)_2^-$ is a negatively charged complex and montmorillonite has a negative surface charge. Hydrolysis products of $Co(asp)_2^-$, such as $Co(asp)^+$ or $Co(H_2O)_6^{2+}$, could be adsorbed.

In contrast, the adsorption of $Co(gly)_3$ on montmorillonite (Figure 26) shows little pH dependence. Electrostatic forces are not involved because $Co(gly)_3$ is a neutral complex. Interaction with the surface occurs either through forces, such as hydrogen bonding or van der Waals attractions, or through adsorption of a hydrolysis product of $Co(gly)_3$, such as $Co(gly)_2^+$, $Co(gly)^{2+}$, or $Co(H_2O)_6^{2+}$.

The electrophoretic mobility of the clay in 0.01M solutions of the complex was measured to determine the effect of $Co(lys)_3^{3+}$, $Co(asp)_2^-$, and $Co(gly)_3$ on the surface charge of montmorillonite. Swartzen-Allen and Matijevic (93) found that the charge on montmorillonite reverses at pH 3.5 in the presence of $Co(phen)_3^{3+}$ and $Co(bipy)_3^{3+}$, and that specific interactions occur between these complexes and the clay. In contrast, Dalang and Stumm (84) found that $Co(NH_3)_6^{3+}$, $Co(NH_3)_5Cl^{2+}$, and $Co(en)_3^{3+}$ were unable to reverse the surface charge of SiO_2 even in the presence of a large excess of adsorbate.

The electrophoretic mobility of Na^+-montmorillonite in 0.01M $Co(lys)_3^{3+}$, $Co(asp)_2^-$, and $Co(gly)_3$ is presented in Figure 27. The mobility of the clay in 0.01M $NaClO_4$ is also presented. The mobility of

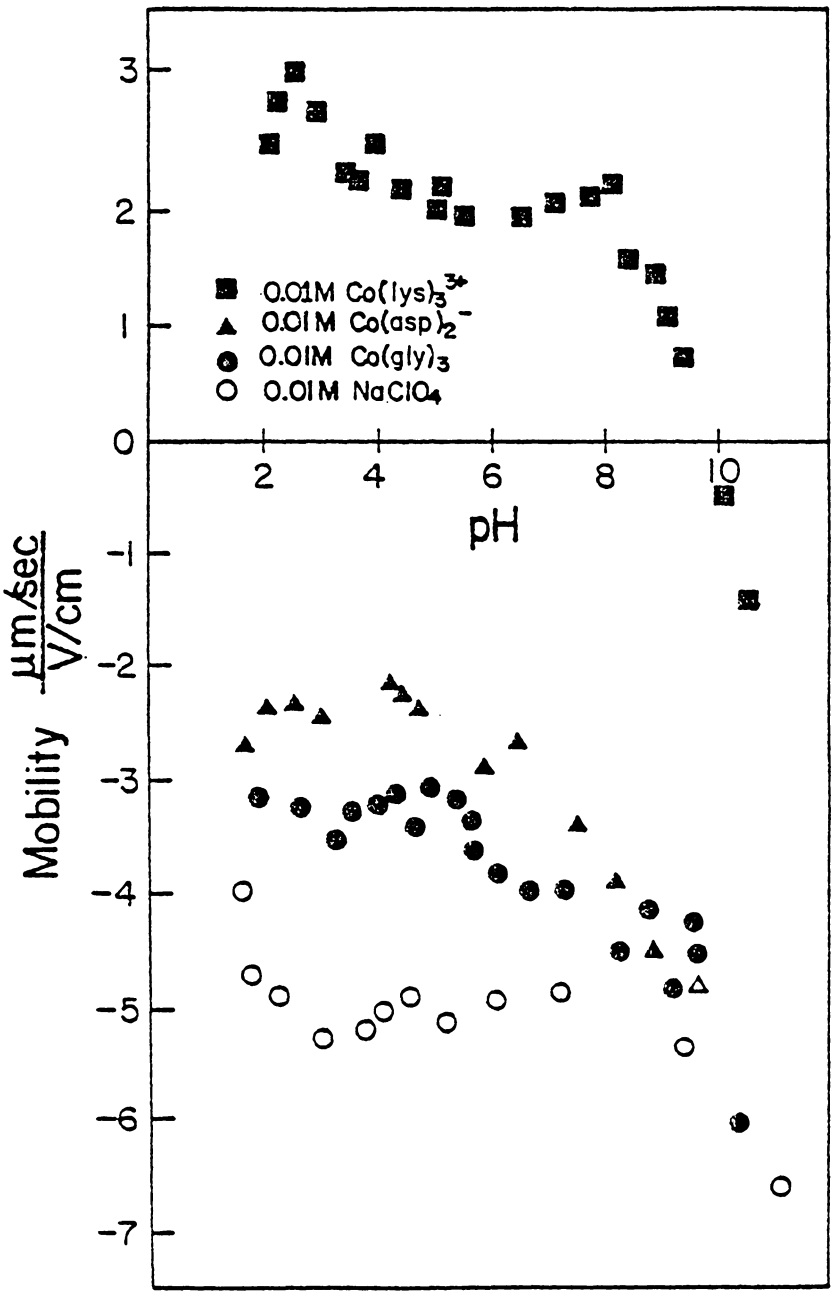

Figure 27. Electrophoretic Mobility of Na^+-Montmorillonite in 0.01 M Cobalt Complex Solutions

montmorillonite in $Co(lys)_3^{3+}$ is reversed in the pH range 2 to 9.5. The mobility of montmorillonite in 0.01M $NaClO_4$ is in the range of -5.0 mobility units (m.u.) while the mobility in 0.01M $Co(lys)_3^{3+}$ falls in the range +3 to +2 m.u. in the pH region 2 to 8. These results indicate that there are strong interactions between the clay and the $Co(lys)_3^{3+}$ complex. One possible interaction that would render the positive surface charge is nonequivalent exchange of $Co(lys)_3^{3+}$ for sodium. This reaction is shown in the following equation:

$$Co(lys)_3^{3+} + Na^+\text{-clay} \rightarrow Co(lys)_3^{3+}\text{-clay} + Na^+ \qquad (49)$$

The nature of the $Co(lys)_3^{3+}$ bond to montmorillonite cannot be determined by electrophoresis. The decreased mobility observed for Na^+-montmorillonite in $Co(lys)_3^{3+}$ with increasing pH indicates that the charge of the adsorbed species also decreases with increasing pH. This suggestion is based on the observations that the charge of Na^+-montmorillonite in $NaClO_4$ is constant between pH 2 and 10 and the amount of cobalt adsorbed increases with pH. The decreasing charge with increasing pH is not due to decreased protonation of terminal amine groups because the pK_a for these amine groups is above 10. It is possible that as the pH increases more hydrolysis products of $Co(lys)_3^{3+}$, which have charges lower than +3, are adsorbed. Possible surface species include $Co(lys)_2OH^{2+}$, $Co(lys)(OH)_2^+$, $CoOH^+$, and Co^{2+}. The isoelectric point (IEP) at pH 9.8±0.3 corresponds to the pH_{IEP} of $Co(OH)_2$, 9.9±0.3. The correspondence agrees with the observation of a $Co(OH)_2$ precipitate at this pH in control solutions.

Electrophoretic mobility studies of montmorillonite in 0.01M $Co(asp)_2^-$ indicate that at pH 2 to 8 a positive species is adsorbed. This hypothesis results from the observation that the mobility is more positive than that measured for montmorillonite in $NaClO_4$. The adsorbed species must be a hydrolysis product because $Co(asp)_2^-$ is a negative species. Possible adsorbed species include $Co(asp)^+$, $CoOH^{2+}$, $Co(OH)^+$, and Co^{2+}. At pH 10 the mobility for montmorillonite in $Co(asp)_2^-$ is the same as that for Na^+-montmorillonite in $NaClO_4$. This behavior can be due to either: 1) a +1 cation such as $CoOH^+$ or $Co(asp)^+$ exchanges for Na^+, 2) $Co(OH)_2$ precipitation on the surface, or 3) little reaction between $Co(asp)_2^-$ and the surface. Based on the observation of a $Co(OH)_2$ precipitate in control solution of $Co(asp)_2^-$ at pH 10, it is considered most likely that the observed mobility is due to $Co(OH)_2$.

The mobility for montmorillonite in $Co(gly)_3$ indicates that the clay has a more positive surface charge in the presence of the complex than in the presence of $NaClO_4$ for the pH range 2 to 7. This more positive mobility indicates that a +2 hydrolysis product of $Co(gly)_3$ is adsorbed. Between pH 8 and 10, the mobility is the same as for the clay in $NaClO_4$. Either little interaction occurs between the clay and the complex or a +1 hydrolysis product of $Co(gly)_3$ such as $Co(gly)^+$ or $CoOH^+$ exchanges for sodium.

Powder x-ray diffraction patterns for the clay before and after adsorption were measured to investigate the size of the species adsorbed in the montmorillonite interlayers and the results are summarized in Table 18. CPK spacefilling molecular models of the amino acid complexes were constructed to calculate the minimum size of the complexes that

Table 18

XRD Cobalt Complexes on Montmorillonite

Complex	pH	d_{001} ±0.2 Å	Δ ±0.2Å
$Co(lys)_3^{3+}$	2	18.6	9.1
	4	18.8	9.3
	6	18.8	9.3
	7	18.9	9.4
	8	18.8	9.3
	10	19.0	9.5
$Co(gly)_3$	2	16.1	6.6
	4	15.8	6.3
	6	13.2	3.7
	7	13.0	3.5
	8	13.0	3.5
	10	13.0	3.5
$Co(asp)_2^-$	2	15.5	6.3
	4	16.1	6.5
	6	14.7	5.2
	7	13.4	3.9
	8	13.0	3.5
	10	13.0	3.5
Na^+-montmorillonite		12.3	2.8

Size of Complexes from Molecular Models (±0.2Å)

$Co(lys)_3^{3+}$	7.1
$Co(II)(lys)^{2+}$ or $Co(III)(lys)^{3+}$	5.2
$Co(gly)_3^3$	6.2
$Co(II)(gly)^+$ or $Co(III)(gly)^{+2}$	4.5
$Co(asp)_2^-$	6.7
$Co(II)(asp)_2$ or $Co(III)asp^-$	4.7

Minimum Size Calculated from XRD

$Co(OH)_2$ (165)	1.6

Minimum Size - Hydrated Diameter

$Co(H_2O)_6^{2+}$ (82)	7.0

that could occupy the interlayer positions. These were compared to the observed d_{001} spacings to ascertain if the interlayer spacing was large enough to contain the unhydrolyzed complex. The d_{001} spacing for $Co(lys)_3^{3+}$ adsorbed on montmorillonite shows a basal spacing of 18.6Å to 19.0Å between pH 2 and 10. Because these basal spacings were measured at a low diffraction angle, the experimental error of ±0.2Å indicates that no significant change in the basal spacing occurs as a function of pH. Delta values, calculated from the measured d_{001} spacings, indicate that the size of the adsorbed species is between 9.1Å and 9.5Å. It is physically possible for $Co(lys)_3^{3+}$ to adsorb into the interlayers because the calculated Δ values are larger than the minimum size of $Co(lys)_3^{3+}$ determined from the models.

The interlayer spacings for $Co(gly)_3$ treated montmorillonite vary with pH. At pH 2 and 4, the interlayer spacing is 16.1Å (Δ = 6.6Å) and 15.8Å (Δ = 6.3Å), respectively. The delta values are larger than 6.2Å, the minimum dimension of $Co(gly)_3$, which indicates that it is possible for $Co(gly)_3$ to adsorb intact into the interlayers. At pH 6, 7, 8, and 10, the delta values are 3.7, 3.5, 3.5, and 3.5, respectively. The adsorbed species at these pH values must be a species smaller than $Co(gly)_3$ such as a hydrolysis product of $Co(gly)_3$. $Co(gly)^{2+}$ and $Co(gly)^{+}$ have minimum dimensions of 4.5Å, but Greenland et al. (100) showed that the basal spacings can decrease up to 1.2Å due to "keying" into octahedral sites in the clay lattice. Thus, it is possible that these hydrolysis products are "keyed" into the interlayers.

$Co(asp)_2^{-}$ adsorbed on montmorillonite also showed changes in the basal spacing as a function of pH. The measured basal spacing decreases

with increasing pH. However, at all pH values the basal spacing was too small to accommodate the $Co(asp)_2^-$ ion. Thus, a smaller cobalt containing species such as $Co(OH)_2$, $Co(H_2O)_6^{2+}$, or $Co(asp)^+$ must be adsorbed.

Infrared spectra were obtained for all three complexes adsorbed on the clay but bands due to complex adsorption were detected only for $Co(lys)_3^{3+}$. Absence of $Co(gly)_3$ and $Co(asp)_2^-$ bands was due either to lack of adsorption or to adsorption in quantities below the detection limit of the infrared analysis ($<1.2 \times 10^{-4}$ moles/g). The IR spectral data for $Co(lys)_3^{3+}$ on montmorillonite are presented in Table 19. Assignments of the various peaks are taken from the literature (111-113, 152-154). The spectra for $Co(lys)_3^{3+}$ on montmorillonite at pH 4 and for Na^+-montmorillonite from 4000 to 1250 cm^{-1} are presented in Figure 28.

The infrared spectral data provide evidence that the lysine ligands remain bound to the cobalt upon adsorption. The COO^- symmetric stretch observed at 1380 cm^{-1} agrees favorably with the value, 1382 cm^{-1}, given by Jang (113) for the acid group bound to cobalt. IR bands characteristic of unionized acid groups were not found for montmorillonite samples prepared in $Co(lys)_3^{3+}$ at any of the pH values studied. The $-NH_2$ symmetric stretching bands were observed at 3240 to 3259 cm^{-1} at pH 2 to 10 for $Co(lys)_3^{3+}$ adsorbed on the clay. This band was identified earlier as $-NH_2$ bound to cobalt (113). Bands for the $-NH_3^+$ symmetric stretch were measured at 1500 to 1520 cm^{-1}. The intensity of the ν_s-NH_3^+ symmetric bands decreases with increasing pH, indicating that at the higher pH values the percentage of unprotaned terminal amine groups

Table 19

Infrared Spectra $Co(lys)_3^{3+}/Na^+$-Montmorillonite

pH=2 (cm^{-1})	pH=4 (cm^{-1})	pH=6 (cm^{-1})	pH=7 (cm^{-1})	pH=8 (cm^{-1})	pH=10 (cm^{-1})	Assignments
3255(vw)	3255(w)	3252(w)	3250(w)	3250(w)	3252(vw)	ν_s - NH_2
2930(w)	2932(w)	2934(w)	2932(w)	2932(w)	----	ν_s - CH_2
1618(vs)	1626(vs)	1618(vs)	1623(vs)	1620(vs)	1622(vs)	ν_{as} - COO^-
1497(m)	1501(m)	1517(m)	1501(m)	1520(w)	----	ν_s - NH_3
1380(m)	1380(m)	1377(m)	1378(m)	1380(m)	1379(vw)	ν_{as} - COO^-

w = weak; m = medium; s = strong, vs = very strong; vw = very weak

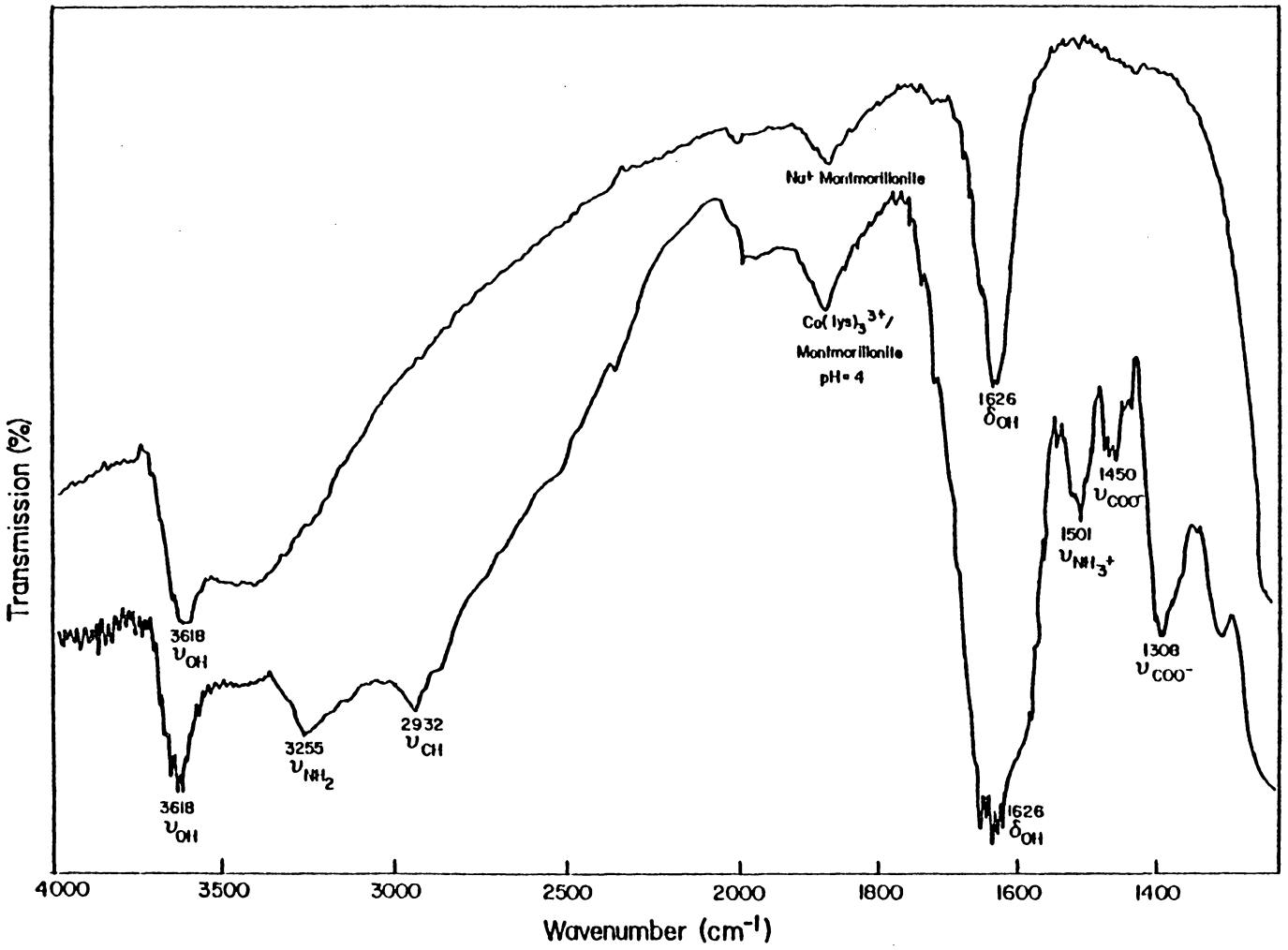

Figure 28. Infrared Spectra of $Co(lys)_3^{3+}$-Treated Montmorillonite - pH 4

increases for adsorbed $Co(lys)_3^{3+}$. Bands corresponding to the adsorbed complex were also observed at pH 10.

XRD measurements show that the interlayer spacing was large enough for $Co(lys)_3^{3+}$ to be present. Electrophoresis indicated that $Co(OH)_2$ was on the clay surface at pH 10. It is possible that both $Co(OH)_2$ and $Co(lys)_3^{3+}$ are present. $Co(OH)_2$ can be precipitated on the outer surface and the complex adsorbed in the interlayers. $Co(H_2O)_6^{2+}$ and $Co(OH)_2$ exhibit Co-O stretching bands in the 900 to 1000 cm^{-1} range but these bands cannot be detected by infrared spectroscopy for the cobalt complex treated montmorillonite samples because of interference by Al-O and Si-O vibrational bands.

XPS analysis of the amino acid complexes on montmorillonite was conducted to glean information about the chemical environment of the adsorbed amine group and the oxidation state of cobalt. Nitrogen/cobalt atomic ratios were calculated to provide information on the ratio of amino acid ligands to cobalt. The N/Co ratios indicate the maximum number of ligands which can be bound to surface cobalt atoms, but the ratio does not necessarily indicate that all of these ligands are chelated to the metal. The N/Co atomic ratio was obtained by measuring the integrated peak intensities for the N 1s and Co $2p_{3/2}$ photopeaks. For example, a value of six for $Co(lys)_3^{3+}$ would indicate that three lysine ligands were on the surface to each cobalt atom.

The ratio of unprotonated (BE = 399.8 ± 0.2 eV) to protonated amines (BE = 402.0 ± 0.2 eV), N/N^+, was obtained by curve resolution of the N 1s photopeak. A N/N^+ ratio of less than one on the montmorillonite surface prepared in $Co(lys)_3^{3+}$ reveals that some of the lysine

is not bound to cobalt. If the amino acid ligands are bound to cobalt for adsorbed $Co(gly)_3$ and $Co(asp)_2^-$ only unprotonated amines will be observed. The presence of protonated amines on montmorillonite treated with these complexes indicates that the ligands are not bound to cobalt.

The N 1s binding energies, N/N^+ and N/Co ratios for the cobalt amino acid complexes on montmorillonite are reported in Table 20. The XPS spectra indicated that the complexes on montmorillonite were different than the original complexes. The N/Co ratio was less than that for the pure complexes. The N/Co ratio for $Co(lys)_3^{3+}$ on montmorillonite showed that less than one lysine ligand was present for each surface cobalt between pH 4 and 10. The N/Co ratio decreases with increasing pH. The N/N^+ ratio increases with increasing pH as expected based on the acid-base behavior of the lysine terminal amine group. An N/N^+ ratio of greater than one indicates that is possible for all the lysine ligands to be bound to cobalt.

Similar results for the N/Co ratio were obtained for $Co(gly)_3$ and $Co(asp)_2^-$ on montmorillonite. The N/Co ratio indicated, on the average, less than one glycine or aspartic acid ligand per cobalt on the surface at all pH values studied. The N/N^+ ratio was 1.7 at pH 4 and increased to 2.7 at pH 10 for $Co(asp)_2^-$ on montmorillonite. A similar increase was observed for $Co(gly)_3$ on montmorillonite (1.8 at pH 4 to 2.8 at pH 10). These results indicate that some ligand was dissociated from the metal. The decrease in protonated amines with increasing pH suggests that a greater percentage of the ligands found on the surface are bound to cobalt at higher pH values.

Table 20

Co(Amino Acid)/Montmorillonite
Nitrogen 1s Photopeaks

pH	N 1s Binding Energy (±0.2 eV)	N/N^+ (±0.1)	N/Co
	$Co(lys)_3^{3+}$/Montmorillonite		
4	402.0, 399.8	0.9	1.9 ± 0.2
6	402.0, 399.8	0.9	1.0 ± 0.2
7	402.1, 399.8	1.1	1.1 ± 0.2
8	401.9, 399.8	2.0	1.0 ± 0.2
10	401.9, 399.8	1.8	0.025 ± 0.005
$Co(lys)_3^{3+}$	400.7, 399.3		6.0
	$Co(asp)_2^-$/Montmorillonite		
4	401.9, 399.9	1.7	0.60±0.05
6	401.9, 399.9	1.7	0.54±0.05
7	402.0, 399.8	2.5	0.53±0.05
8	402.0, 399.8	2.7	0.30±0.05
10	----- 399.9	only basic amine observed	0.26±0.05
$Co(asp)_2^-$	----- 399.3		2.0
	$Co(gly)_3$/Montmorillonite		
4	402.2, 399.9	1.8	0.93±0.05
6	402.1, 400.0	1.9	0.61±0.05
7	403.0, 399.9	2.0	0.53±0.05
8	401.9, 399.8	2.2	0.50±0.05
10	402.0, 399.8	2.8	0.38±0.05
$Co(gly)_3$	----- 399.3		3.0

The Co $2p_{3/2}$ binding energies, and Co $2p_{1/2}$ - Co $2p_{3/2}$ splittings for cobalt amino acid complex treated montmorillonite are reported in Table 21. The Co $2p_{1/2}$ - Co $2p_{3/2}$ splitting and Co $2p_{3/2}$ binding energy indicate that $Co(lys)_3^{3+}$ is not the only adsorbed species on the montmorillonite surface at pH 4 and 6. The Co $2p_{1/2}$ - Co $2p_{3/2}$ energy differences for $Co(lys)_3^{3+}$ treated montmorillonite at pH 4 and 6, 15.3 and 15.4 eV respectively, are intermediate between the splitting that would be observed for Co(III), 15.0 eV, and the splitting that would be observed for Co(II), 16.0 eV. The spectrum for $Co(lys)_3^{3+}$ at pH 6 is presented in Figure 29, where shake-up satellites confirm the presence of Co(II). The binding energies 781.7 eV and 781.6 eV at pH 4 and 6, respectively, are intermediate between the value expected for Co^{2+} on the clay surface, 782.4 eV, and the value for $Co(lys)_3^{3+}$, 781.0 eV. It is possible that the observed binding energy and intermediate Co $2p_{1/2}$ - Co $2p_{3/2}$ splitting value is due to a mixture of Co^{2+} and $Co(lys)_3^{3+}$. Although curve resolution of the spectra would confirm if the observed spectra are composites of these two species, curve resolution is not feasible because of the low intensity of the cobalt signal at pH 4 and 6.

The Co $2p_{1/2}$ - Co $2p_{3/2}$ splitting of approximately 16 eV is indicative of Co(II) at pH 7, 8, and 10. The Co 2p XPS spectra at pH 7 and 10 are presented in Figure 29. The Co $2p_{3/2}$ binding energy at pH 7 and 8, 781.6 eV, is less than that measured for $Co(H_2O)_6^{2+}$, 782.4 eV, on the clay surface. The possible surface species that would have the reported binding energy include $Co(lys)^{2+}$ and or $CoOH^+$. These species are suggested because the N/Co ratio indicated that less than one lysine

Table 21

Complexes/Na^+-Montmorillonite
Co 2p Photopeaks

pH	Co $2p_{3/2}$ Binding Energy (±0.2 eV)	ΔE Co $2p_{1/2}$-$2p_{3/2}$ (±0.2 eV)
	$Co(lys)_3^{3+}$/Montmorillonite	
4	781.7	15.3
6	781.6	15.4
7	781.6	15.8
8	781.6	15.8
10	780.8	15.9
$Co(lys)_3^{3+}$	781.0	15.1
	$Co(gly)_3$/Montmorillonite	
4	782.2	15.9
6	782.2	15.9
7	782.0	15.9
8	782.0	15.9
10	781.9	15.9
$Co(gly)_3$	781.1	15.1
	$Co(asp)_2^-$/Montmorillonite	
4	782.2	15.9
6	782.2	16.0
7	782.2	15.9
8	781.1	16.0
10	781.1	15.9
$Co(asp)_2^-$	781.1	15.1

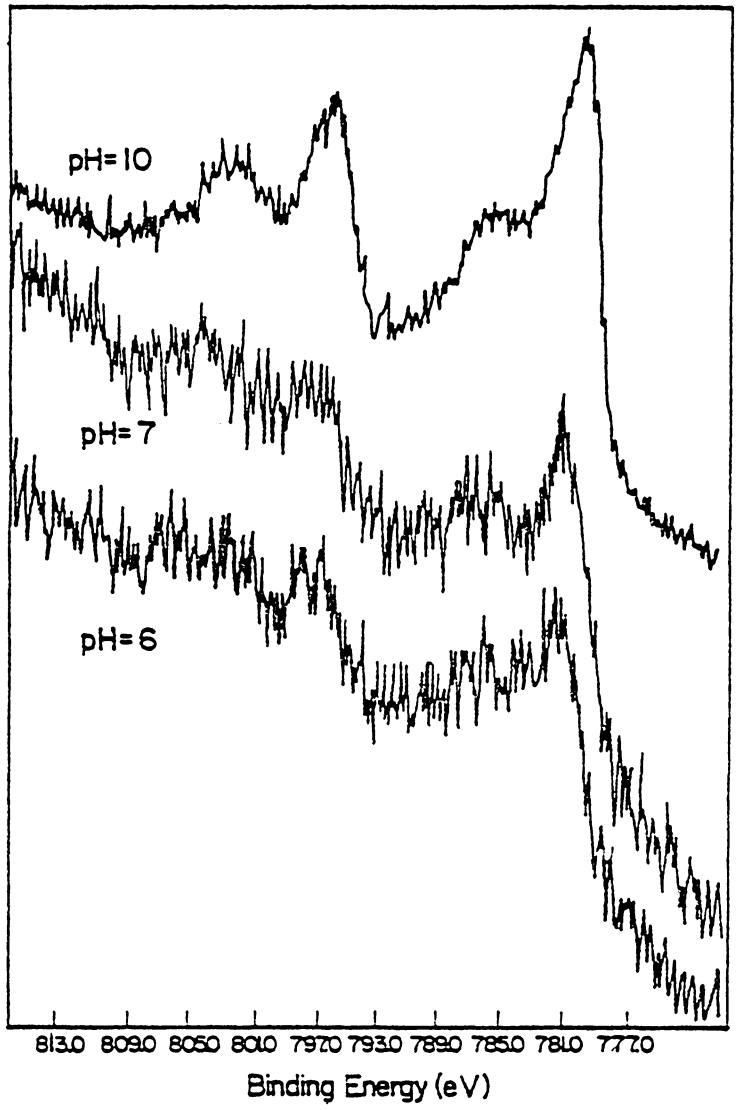

Figure 29. Co 2p Photopeaks - $Co(lys)_3^{3+}$-Treated Montmorillonite

ligand was on the surface for each cobalt. $Co(lys)^{2+}$ and $CoOH^{+}$ would be expected to have a lower binding energy than Co^{2+} because of the greater electron density around the cobalt due to coordination to the amino acid strong donor ligands.

The species adsorbed at pH 10 in the presence of $Co(lys)_3^{3+}$ is $Co(OH)_2$. The N/Co atomic ratio was 0.025, which shows that less than 2% of the surface cobalt can be bound to a lysine ligand. The Co $2p_{3/2}$ binding energy, 780.8 eV, and the Co $2p_{1/2}$ - Co $2p_{3/2}$ splitting, 15.9 eV, for $Co(lys)_3^{3+}$-treated montmorillonite at pH 10 compare favorably with the corresponding values for $Co(OH)_2$, 780.9 eV and 15.9 eV. The cobalt observed is probably the result of hydrolysis of the complex and precipitation of $Co(OH)_2$.

The XPS results for $Co(lys)_3^{3+}$-montmorillonite appear to contradict observations by XRD and infrared spectroscopy. X-ray diffraction results were interpreted to indicate that a cobalt complex is contained in the interlayers and transmission infrared analysis indicate that $Co(lys)_3^{3+}$ is present. It is possible that this apparent contradiction arises due to different sampling characteristics. XPS is a surface technique that is sensitive to the top 10Å to 20Å of the sample (152). XPS is most sensitive to the external surface of the clay because its sensitivity decreases exponentially with depth. Electrophoresis is sensitive to the charge on the "outer surface" of a particle (130). Although the exact definition of the "outer surface" is not known, it is considered to be the top monolayer of the particle and includes adsorbed species which are located within their hydration diameter of the particle surface (130). Electrophoretic mobilities also

indicated the presence of $Co(OH)_2$ on the surface at pH 10.

The cobalt XPS results are consistent with the presence of Co(II) adsorption of $Co(gly)_3$ and $Co(asp)_2^-$ on montmorillonite at all pH values studied. Cation exchange is not possible between these complexes and the clay because the two complexes are not positively charged. At pH 4, 6, and 7 for $Co(asp)_2^-$ and $Co(gly)_3$ and at pH 8 and 10 for $Co(gly)_3$, the binding energy values, 782.0 ± 0.2 eV, are equal to the values for surface cobalt $Co(H_2O)_6^{2+}$, 782.2 ± 0.2 eV. The equivalence in binding energies suggests that the surface species is an aqua cobalt species and that hydrolysis of the complexes occurred. The assertion that $Co(OH)_2$ is not the surface species at pH 8 and 10 for $Co(gly)_3$ adsorption indicates that precipitation is not the adsorption mechanism and that $Co(gly)_3$ is hydrolyzed and reduced on the surface. The XPS Co 2p spectra for $Co(gly)_3$ and $Co(asp)_2^-$ at pH 8 are presented in Figure 30. The XPS spectra for $Co(gly)_3$ and $Co(asp)_2^-$ at pH 10 are similar to the spectra recorded at pH 8. At pH 8 and 10, the presence of $Co(OH)_2$ on montmorillonite equilibrated with $Co(asp)_2^-$ is supported by the near equality of the Co $2p_{3/2}$ binding energies with the binding of $Co(OH)_2$. No precipitate was observed for $Co(asp)_2^-$ control solutions at pH 8, which indicates that formation of $Co(OH)_2$ is induced on the surface. The large amount of $Co(OH)_2$ at pH 10 is probably due to precipitation from solution following hydrolysis of the complex.

Diffuse reflectance visible spectroscopy was used as a second method of detecting the surface cobalt oxidation state. Spectra could be recorded only for adsorbed $Co(lys)_3^{3+}$ and are presented in Figure 31. Also shown is the spectrum for the cobalt(III) lysine complex. The

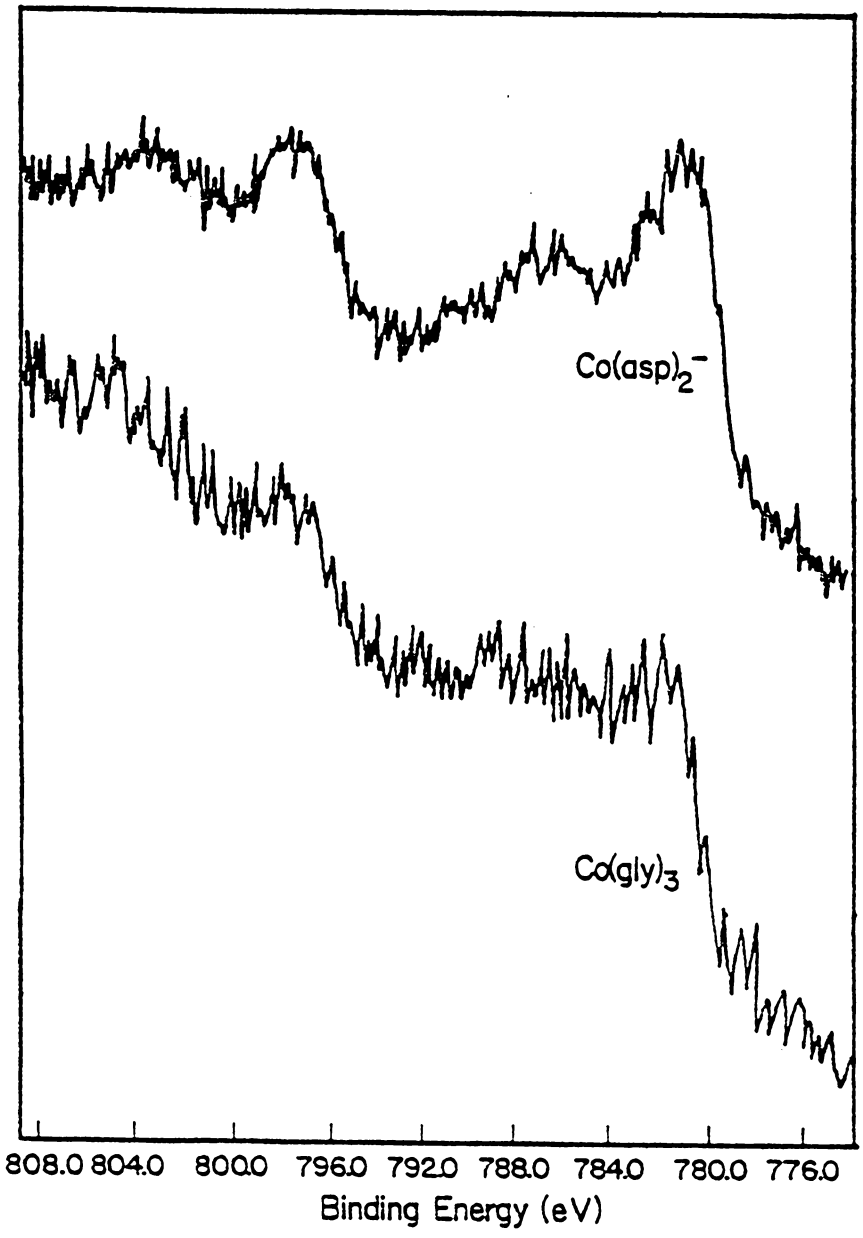

Figure 30. Co 2p Photopeaks for $Co(gly)_3$ and $Co(asp)_2^-$ - pH 8

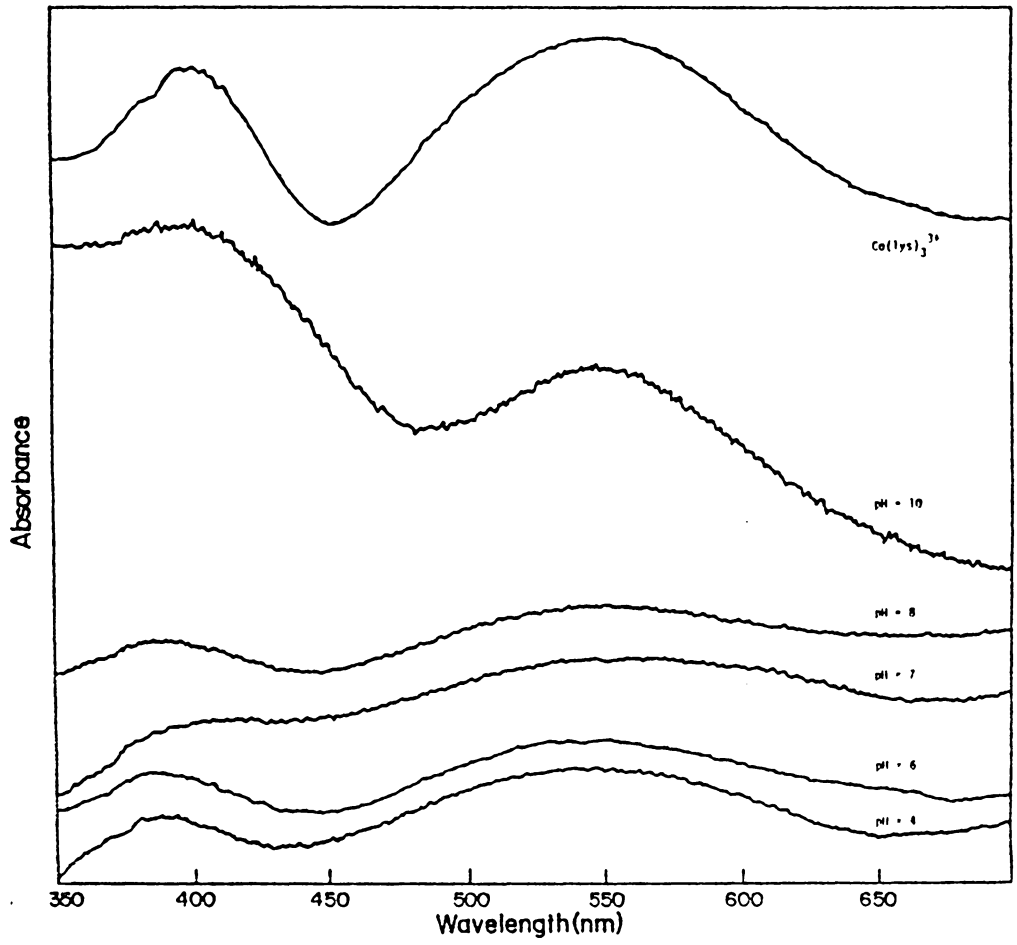

Figure 31. Diffuse Reflectance Visible Spectra-
$Co(lys)_3^{3+}$ Treated Montmorillonite

recorded spectra are indicative of the $^1A_{1g} \rightarrow {}^1T_{1g}$ and $^1A_{1g} \rightarrow {}^1T_{1g}$ transition of $Co(lys)_3^{3+}$. Equivalence of the spectra indicate that no hydrolysis or reduction has occurred on the clay surface. These measurements show that some of the complex adsorbs by an exchange mechanism, but do not rule out the presence of Co(II). Co(II) is not readily detected by visible spectroscopy in the presence of $Co(lys)_3^{3+}$ because the Co(II) molar absorptivity is about twenty times less than that for Co(III) (150,163).

The observation of Co(III) on the clay surface by visible spectroscopy and of Co(III) and Co(II) by XPS raises the question of possible sample decomposition in the XPS spectrometer during analysis. The $Co(lys)_3^{3+}$-montmorillonite sample at pH 6 was selected to test for decomposition of Co(III) to Co(II) in the XPS spectrometer. This sample was selected because of its intense purple color indicative of $Co(lys)_3^{3+}$. The reflectance visible spectra for $Co(lys)_3^{3+}$ treated montmorillonite at pH 6, both before and after irradiation by x-rays overnight in the spectrometer, are presented in Figure 32. No changes in band position or appearance of the samples were observed. The reflectance visible results confirm that the integrity of the $Co(lys)_3^{3+}$ treated montmorillonite sample is maintained during XPS analysis. A comparison of XPS and visible reflectance spectroscopy indicate that the principal discrepancy occurs as a result of different surface sensitivities of the two techniques. To further examine the possibility of hydrolysis, an additional analytical method for determining the N/Co ratio was employed.

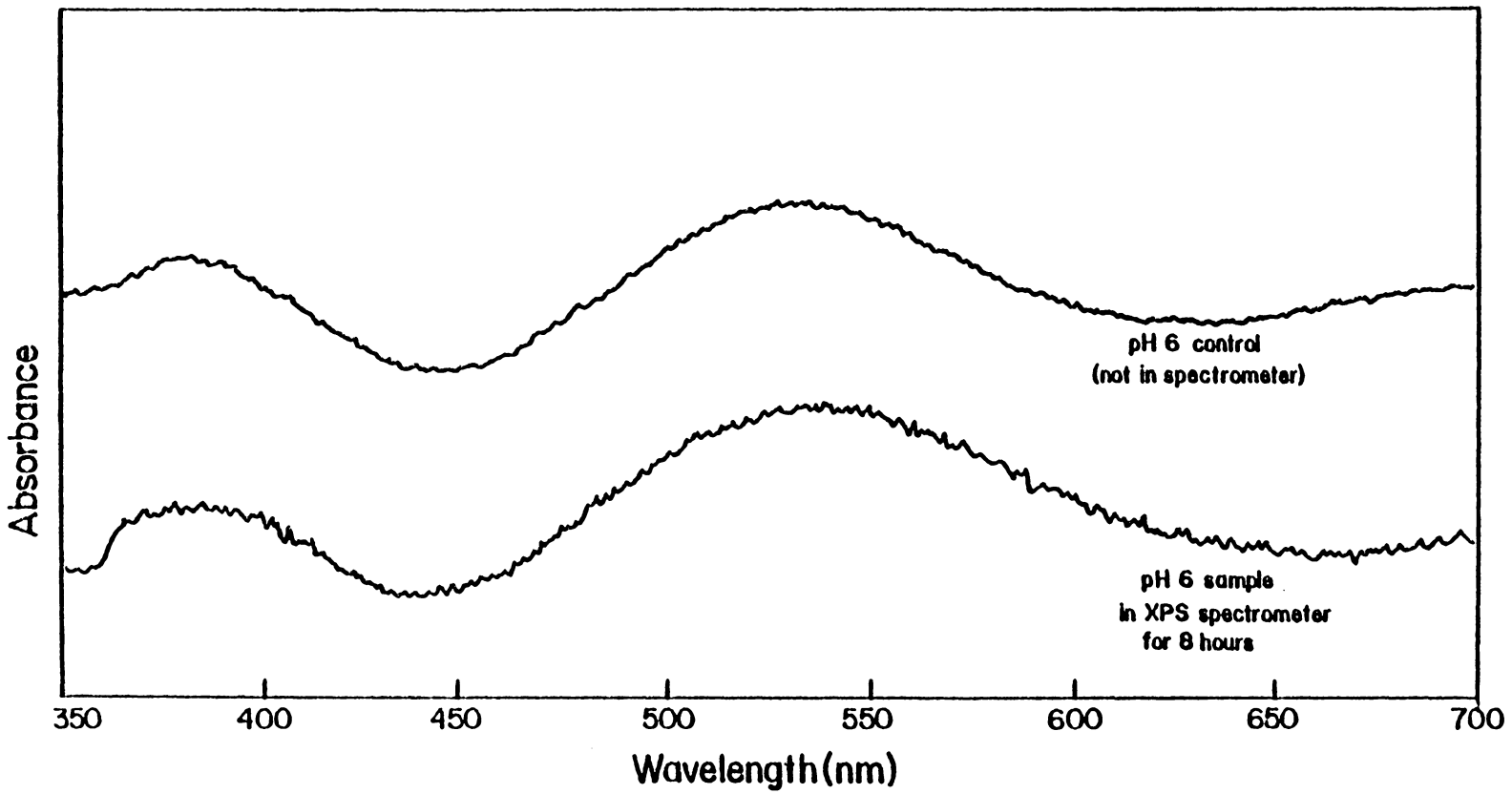

Figure 32. Diffuse Reflectance Visible Spectra - $Co(lys)_3^{3+}$-Treated Montmorillonite at pH 6, Before and After XPS Analysis

The second method of determining the N/Co ratio involved atomic absorption analysis of cobalt after acid dissolution of the clay and ninhydrin determination of amino acid desorbed by Ba^{2+} exchange. The determination of the N/Co ratio assumes total displacement of all amino acid and cobalt containing compounds. XPS was unable to detect surface nitrogen after Ba^{2+} exchange, indicating less than $2x10^{-5}$ moles of amino acid were present per gram of clay after exchange. Total desorption of cobalt in concentrated H_2SO_4 was indicated by favorable comparison of the cobalt in the $Co(lys)_3^{3+}$ sample determined by difference of the cobalt concentration in adsorbate solutions before and after equilibrium with the clay and by acid dissolution of the clay sample. The N/Co ratio could not be determined for the $Co(gly)_3$ or $Co(asp)_2^-$ samples because the amount of amino acid was below the ninhydrin detection limit ($<2x10^{-5}$ moles/g). The N/Co ratios determined by bulk quantitative analysis of the $Co(lys)_3^{3+}$-montmorillonite samples and by XPS are presented in Table 22. The analytical N/Co ratios are all less than 6, supporting the notion that at all pH values hydrolysis of the adsorbed compounds occurred. The larger N/Co ratio observed by bulk analysis suggests that greater amounts of ligand are contained in the interlayers than on the clay surface.

In summary, the interaction of amino acid complexes with montmorillonite depends on the charge of the complex and on the pH of the solution. Much more adsorption was observed for the positive $Co(lys)_3^{3+}$ complex that can be electrostatically attracted to the surface, compared to $Co(gly)_3$ and $Co(asp)_2^-$. Adsorption of $Co(lys)_3^{3+}$ was inferred by IR, electrophoresis, reflectance visible spectroscopy,

Table 22

$Co(lys)_3^{3+}$/Montmorillonite

pH	N/Co(Bulk)	N/Co (XPS)
4	3.0 ± 0.3	1.9 ± 0.2
6	2.8 ± 0.3	1.0 ± 0.2
7	2.2 ± 0.3	1.1 ± 0.2
8	2.4 ± 0.3	1.0 ± 0.2
10	0.4 ± 0.05	0.025 ± 0.005

and XRD. Reversal of the electrophoretic mobility shows that nonequivalent exchange occurred, as presented below:

$$Co(lys)_3^{3+} + Na^+\text{-montmorillonite} \rightarrow Co(lys)_3^{3+}\text{-montmorillonite} + Na^+ \quad (50)$$

Infrared spectroscopy indicated that the ligand was coordinated to the cobalt. XRD showed that the Na^+-montmorillonite interlayer spacing increased upon treatment with $Co(lys)_3^{3+}$ and that the spacing was large enough to accommodate the unhydrolyzed complex. The most convincing evidence for adsorption of unhydrolyzed $Co(lys)_3^{3+}$ was obtained by reflectance visible spectroscopy. This analysis revealed $^1A_{1g} \rightarrow {}^1T_{1g}$ and $^1A_{1g} \rightarrow {}^1T_{2g}$ bands similar to those for the pure $Co(lys)_3^{3+}$ complex. Other interactions of $Co(lys)_3^{3+}$ with the clay surface, such as hydrolysis, were revealed by XPS and analytical measurements. XPS showed reduction of Co(III) to Co(II).

Evidence was obtained from XPS, electrophoresis, and XRD to support the suggestion that hydrolysis of $Co(asp)_2^-$ and $Co(gly)_3$ occurs upon adsorption. XRD analysis indicated that the clay interlayer spacing was too small to accommodate $Co(gly)_3$ and $Co(asp)_2^-$ but was able to incorporate hydrolysis products of these complexes above pH 6. A more positive mobility for montmorillonite in the presence of these complexes compared to $NaClO_4$ was noted from electrophoresis data. This indicates that positively charged hydrolysis products are adsorbed and not the neutral or negative complexes.

Mechanisms consistent with these observations are presented below (Equations 51 to 55). In contrast to previous studies on complex

adsorption on clays, which suggested that iron may be the reducing agent, the mechanism proposed here suggests that water is the reducing agent. The selection of H_2O as the reducing agent is based on the fact that Texas montmorillonite contains less than 0.15% FeO (120), 2.1×10^{-5} moles Fe(II)/g clay. This is not enough Fe(II) to reduce the 5×10^{-5} to 7×10^{-4} moles cobalt/g clay on the surface. Reduction by water has been observed previously on non-iron containing substrates such as silica (84,95) and carbon black (83,86).

The proposed mechanism suggests that reduction occurs after hydrolysis because this reaction is much more thermodynamically favored than reduction of the complex (179). A possible reaction scheme for the hydrolysis of $Co(lys)_3^{3+}$ on the clay surface is presented as follows:

$$Co(lys)_3^{3+} + \text{clay} \rightarrow Co(lys)_3^{3+}\text{-clay} \quad (51)$$

$$Co(lys)_3^{3+}\text{-clay} \rightarrow \text{lysine} + Co(lys)_2(H_2O)_2^{3+}\text{-clay} \quad (52)$$

$$Co(lys)_2(H_2O)_2^{3+}\text{-clay} \rightarrow \text{lysine} + Co(lys)(H_2O)_4^{3+}\text{-clay} \quad (53)$$

$$Co(lys)(H_2O)_4^{3+}\text{-clay} \rightarrow \text{lysine} + Co(H_2O)_6^{3+}\text{-clay} \quad (54)$$

$$Co(H_2O)_6^{3+}\text{-clay} + 1/2\ H_2O \rightarrow Co(H_2O)_6^{2+}\text{-clay} + 1/4\ O_2 + H^+ \quad (55)$$

The amount of water molecules bound to cobalt is unknown, however possible numbers are given in the above mechanism.

At pH 10 for $Co(asp)_2^-$ and $Co(lys)_3^{3+}$, precipitates were observed in solution in the absence of the clay. Thus, it is suggested that at this pH, these complexes hydrolyze and are reduced in solution. A possible mechanism for base hydrolysis of $Co(asp)_2^-$ is shown in Equations 56 to 59. The example given is for $Co(asp)_2^-$, but it is assumed that the reaction for $Co(lys)_3^{3+}$ is similar.

$$Co(asp)_2^- + OH^- + 2H_2O \rightarrow Co(asp)(OH)(H_2O)_2 + \text{aspartic acid} \quad (56)$$

$$Co(asp)(OH)(H_2O)_2 + 3H_2O \rightarrow Co(OH)(H_2O)_5^{2+} + \text{aspartic acid} \quad (57)$$

$$Co(OH)(H_2O)_5^{2+} + 1/2\ H_2O \rightarrow Co(H_2O)_6^{2+} + 1/4\ O_2 \quad (58)$$

$$Co(II) + 2OH^- \rightarrow Co(OH)_2 \quad (59)$$

D. COBALT ADSORPTION ON BIRNESSITE

In the next three sections D, E, and F of this study, the interactions of cobalt, amino acids, and cobalt amino acid complexes with birnessite are discussed. The adsorption experiments were carried out under the same experimental conditions used to investigate the chemical interactions with montmorillonite. Birnessite is one of the forms of manganese dioxide found in both soil (75-77) and marine manganese nodules.

Mechanisms proposed for cobalt adsorption include Co(III) substitution for Mn(IV) (35), Mn(III) (76,79), and/or Mn(II)(80) and oxidation of cobalt by the manganese surface (76) or dissolved oxygen. The role of the manganese surface and dissolved oxygen in the reaction with cobalt, and the chemical environment of the adsorbed cobalt were investigated.

Cobalt (II) was adsorbed on Na^+-birnessite at pH 4, 6, 7, 8, and 10 under aerobic conditions and at pH 6.5 under both aerobic and anaerobic conditions. The amount of cobalt adsorbed as a function of pH is presented in Table 23. The quantity of manganese released into solution upon adsorption of cobalt is also included. The amount of cobalt adsorbed was compared to the amount of manganese released to determine if cobalt exchanged for manganese. The quantity of manganese

Table 23

Cobalt Adsorbed and Manganese Released from Birnessite

pH	Cobalt Adsorbed (moles/g)	Manganese Released H_2O/Birnessite (moles/g)	Manganese Released Co^{2+}/Birnessite (moles/g)
4	1.7×10^{-4}	1.6×10^{-4}	1.2×10^{-4}
6	1.6×10^{-4}	9.6×10^{-5}	7.9×10^{-5}
7	4.7×10^{-4}	0	0
8	8.4×10^{-4}	0	0
10	1.0×10^{-3}	0	0

released is not directly proportional to the amount of cobalt adsorbed. Cobalt adsorption increases with pH but manganese release decreases with pH. Manganese released in water was greater than the release in 0.01M Co^{2+}. Thus the simple exchange of Mn(II) in the birnessite lattice by Co(II) is not the mechanism of interaction. This is in contrast to previous studies (77,79) which suggested that Mn^{2+} would be released into solution upon adsorption of Co(II). One of these studies (79) was conducted at pH 4. Manganese release at pH 4 can be attributed to dissolution of birnessite in an acidic environment (166, 167). Zordan and Hepler (167) reported that manganese dioxide reduction in solutions at pH 4 or below is favorable, as shown below:

$$MnO_{2(s)} + 4H^{+}_{(aq)} + 2e^{-} \rightarrow Mn^{2+}_{(aq)} + 2H_2O_{(aq)} \qquad E = 1.23\ V \qquad (60)$$

Thus, the manganese released from birnessite at pH 4 or below can be attributed to this reduction mechanism.

Electrophoresis was used to characterize the birnessite substrate surface charge. The mobility measurements are presented in Figure 33. The isoelectric point (IEP) is the pH at which the electrophoretic mobility is zero. The IEP for birnessite in 0.01M $NaClO_4$ occurs at pH 3.1 ± 0.5. This agrees favorably with the value of pH 3.3 ± 0.5 reported by Gray and Malati (80) for birnessite but is higher than the values reported by Healy et al. (168) pH_{IEP} = 1.5, and Murray (166) pH_{IEP} = 2.25. The differences observed may result from the varying degrees of crystallinity and the nonstoichiometric nature of the

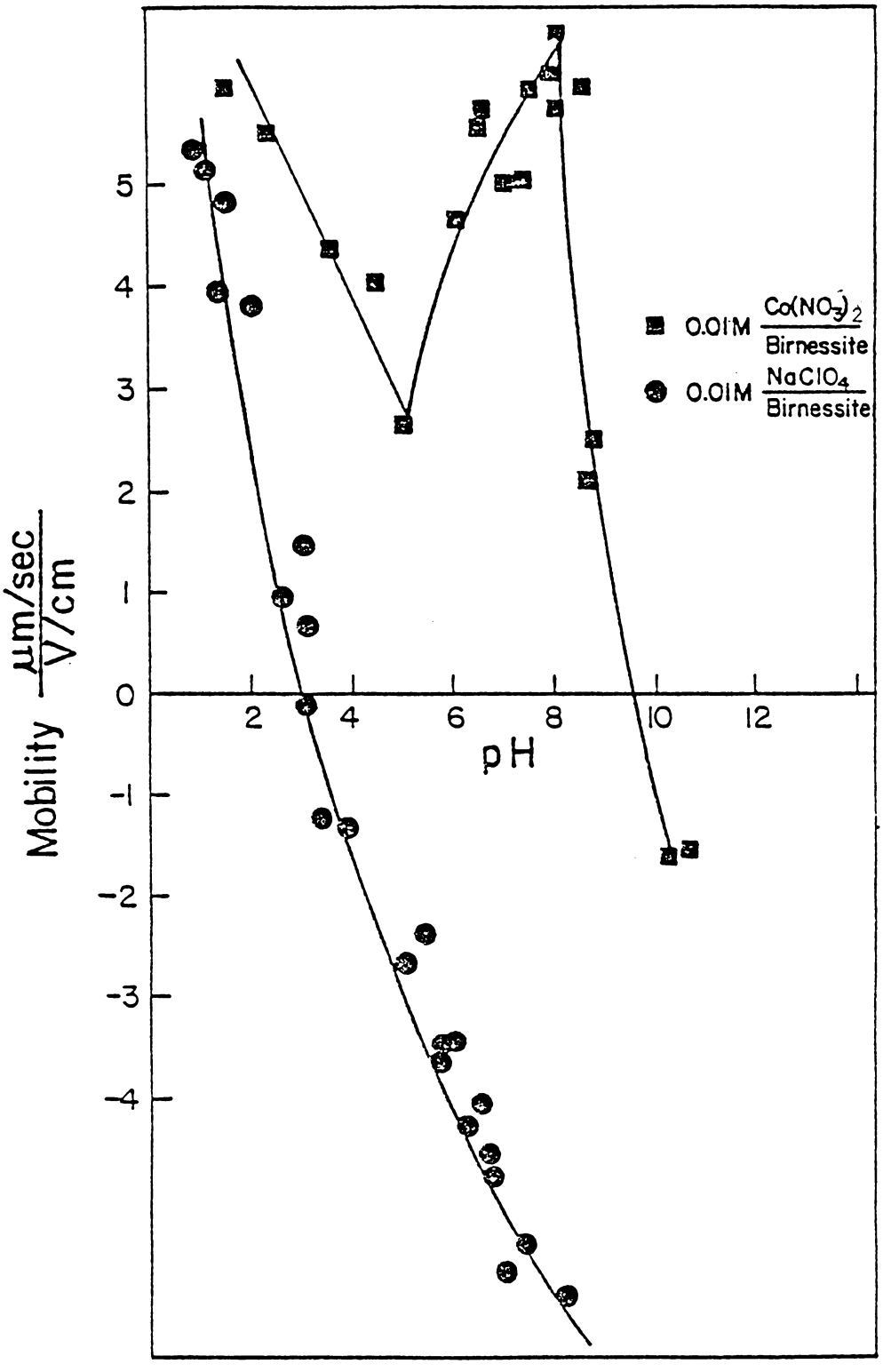

Figure 33. Electrophoretic Mobility of Na^+-Birnessite in 0.01 M $NaClO_4$ and in 0.01 M $Co(NO_3)_2$

manganese dioxide (121).

By comparing the electrophoretic mobility of birnessite in Co^{2+} to that in $NaClO_4$, evidence for specific interactions can be obtained. If changes in the mobility are observed for birnessite in 0.01M $Co(NO_3)_2$ at pH values below 3.1, pH_{IEP} (MnO_2), specific interactions occur because the positive surface does not attract cobalt electrostatically. At pH values above the pH_{IEP}, specific interactions are apparent if the surface charge is more positive in the presence of cobalt.

The electrophoretic mobility of birnessite in 0.01M $Co(NO_3)_2$ changes from 6.0 m.u. at pH 2 to -2.6 m.u. at pH 5 to 6.0 m.u. at pH 7.0. In 0.01 M $NaClO_4$, the mobility of birnessite decreases from 4.0 m.u. at pH 2 to -6 m.u. at pH 7.0. The more positive mobility observed in $Co(NO_3)_2$ versus $NaClO_4$ indicates that the interactions between cobalt and birnessite are not solely due to electrostatic attraction. However, electrophoresis does not reveal the nature of the interaction.

The electrokinetic behavior of birnessite in 0.01M $Co(NO_3)_2$ in the pH 7 to 10 range is similar to that observed for $Co(OH)_2$ in $NaClO_4$ (Figure 8). The pH_{IEP} for Co^{2+} on birnessite is at pH 9.8 ± 0.3 which is approximately the same as that observed for $Co(OH)_2$ in $NaClO_4$, pH 9.9 ± 0.5. These measurements indicate that $Co(OH)_2$ is precipitated on the manganese dioxide surface.

To investigate the chemistry of the specifically adsorbed cobalt, XPS was utilized. XPS binding energies and Co $2p_{1/2}$ - Co $2p_{3/2}$ splitting values for cobalt adsorbed on birnessite at pH 4 to 10 are presented in Table 24. The XPS results show a Co $2p_{1/2}$ - Co $2p_{3/2}$

Table 24

XPS Analysis of Co^{2+}/Birnessite

pH	Co $2p_{3/2}$ Binding Energy (±0.1 eV)	ΔE Co $2p_{1/2}$ - Co $2p_{3/2}$ (±0.2 eV)	ΔE Sat.-Main (±0.2 eV)	$\frac{I_{sat}}{I_{main}}$	Mn $2p_{3/2}$ Binding Energy (±0.2eV)	Mn 3s Splitting (±0.2 eV)
4	780.5	15.1	*ND	*ND	642.1	4.7
6	780.5	15.0	*ND	*ND	642.2	4.8
7	780.5	15.0	*ND	*ND	642.2	4.8
8	781.0	16.0	5.8	0.50	642.2	4.8
10	780.8	16.0	5.7	0.56	642.2	4.7
Co_2O_3(73)	779.2	15.2	*ND	*ND	--	--
CoOOH	780.2	15.1	0.21	0.21	--	--
$Co(OH)_2$	780.9	15.9	0.52	0.52	--	--
Na^+ - Birnessite	--	--	--	--	642.2	4.7
Co^{2+}/Birnessite	780.2	15.1	*ND	*ND	642.2	5.1
MnO	--	--	--	--	640.6(175)	5.8(170)
Mn_2O_3	--	--	--	--	641.9(175), 641.8(175)	5.3(170)

Table 24 (Continued)

XPS Analysis of Co^{2+}/Birnessite

pH	Co $2p_{3/2}$ Binding Energy (±0.1 eV)	ΔE Co $2p_{1/2}$ - Co $2p_{3/2}$ (±0.2 eV)	ΔE Sat-Main (±0.2 eV)	$\frac{I_{sat}}{I_{main}}$	Mn $2p_{3/2}$ Binding Energy (±0.2eV)	Mn 3s Splitting (±0.2 eV)
Mn_3O_4	--	--	--	--	641.4(175)	5.2(170)
MnO_2	--	--	--	--	642.0(175)	4.7(170)

*ND = Not Determined

energy difference of 15.0 eV. A Co 2p spectrum of Co^{2+} adsorbed on birnessite at pH 6 is presented in Figure 34 and is representative of the Co 2p spectra for surface cobalt in the pH 4 to 7 range. No intense satellite features were observed. The dominant surface species on birnessite at pH 4 to 7 is cobalt (III). The presence of Co(III) on birnessite has been reported previously (76), but the chemical nature of Co(III) was not discussed at pH 4 to 7, the binding energy of adsorbed cobalt, 780.5 ± 0.2 eV, indicates that the chemical environment is more like CoOOH, BE = 780.2 eV, than Co_2O_3, BE = 779.2 eV. This agrees with observations by Murray and Dillard (82).

The cobalt XPS results at pH 8 and 10 are unlike the results at pH 4 to 7. A spectrum of Co^{2+} adsorbed on birnessite at pH 8 is presented in Figure 35 and is characteristic also of the spectrum obtained for samples at pH 10. At pH 8 and 10, Co(II) is adsorbed on birnessite as indicated by a Co $2p_{1/2}$ - Co $2p_{3/2}$ splitting of 16.0 eV and the presence of satellite features. The Co $2p_{3/2}$ satellite to main peak separations were 5.8 and 5.7 eV and the Co $2p_{3/2}$ satellite to main peak intensity ratios were 0.50 and 0.56 for pH 8 and 10, respectively. This compares favorably with the values of 5.5 eV and 0.52 for $\Delta E_{sat\text{-}main}$, and I_{sat}/I_{main}, respectively for $Co(OH)_2$. This agreement supports the suggestion that $Co(OH)_2$ is present on the birnessite surface at pH 8 and 10.

Potential oxidizing agents for cobalt on birnessite at pH 7 and below include the manganese dioxide surface (169) or dissolved oxygen (82). To examine the role of dissolved oxygen 0.1M cobalt was adsorbed at pH 6.5 on manganese dioxide in both the presence and in the absence

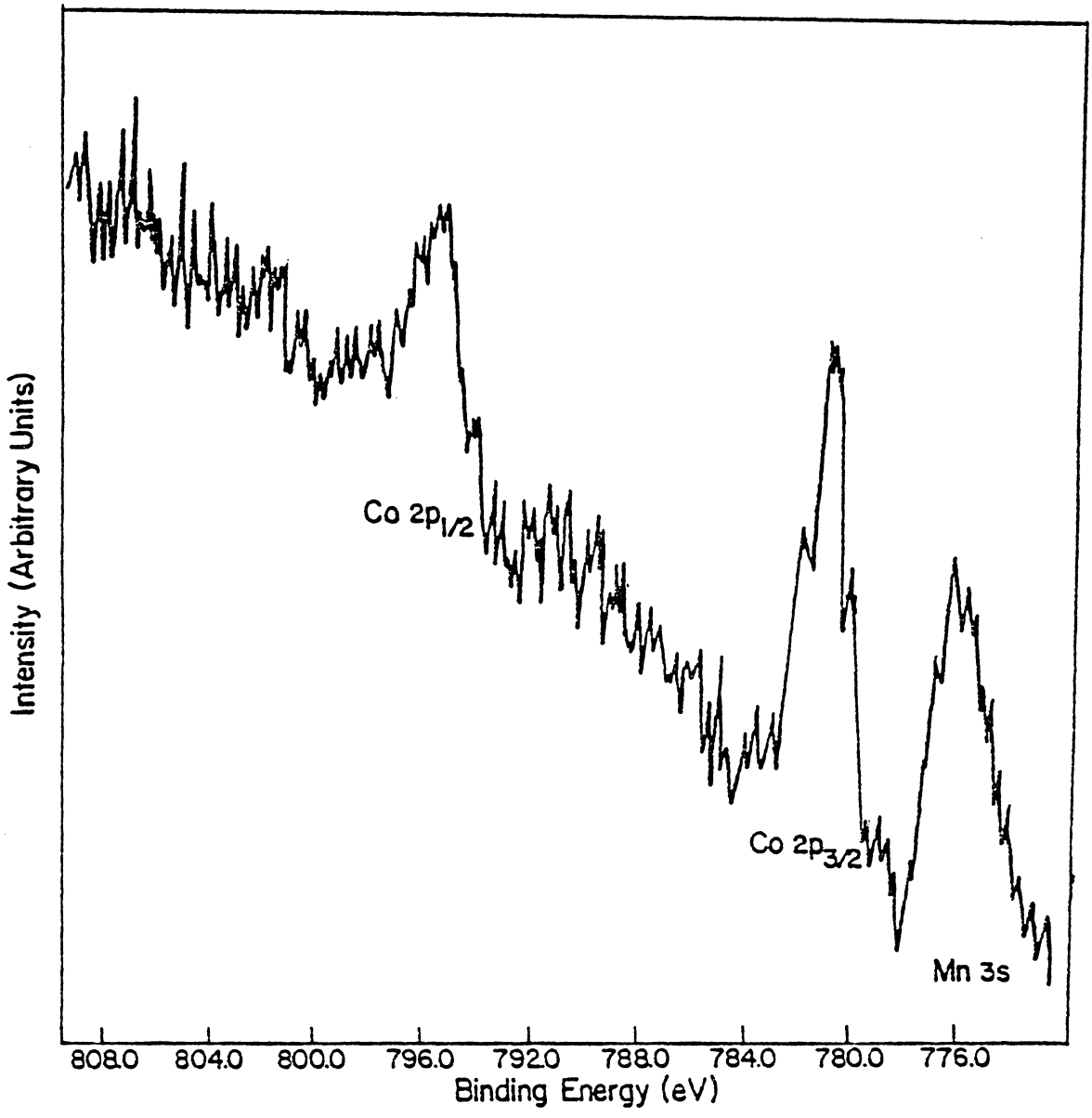

Figure 34. Co^{2+} Treated Birnessite - pH 6

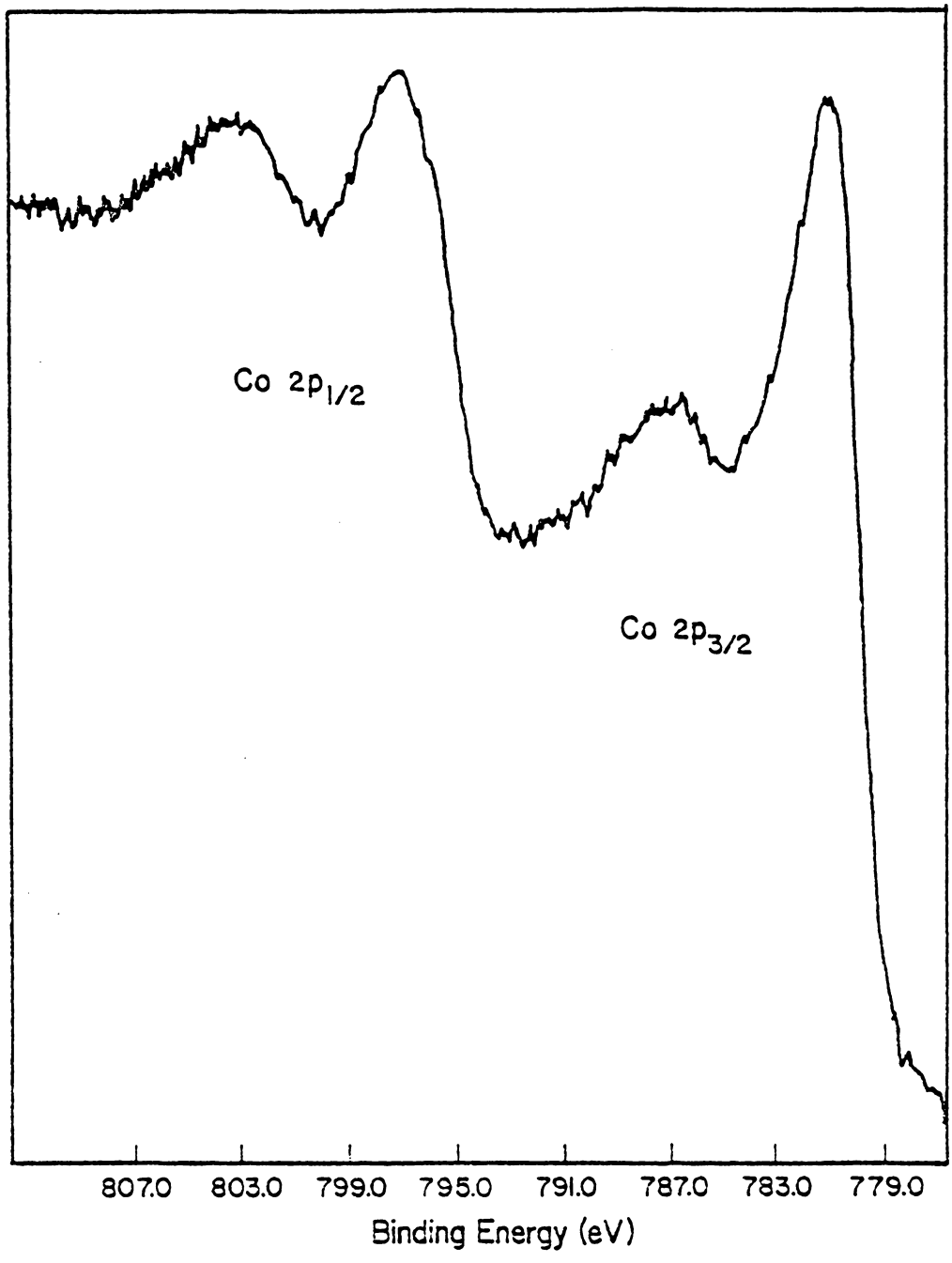

Figure 35. Co^{2+} Treated Birnessite - pH 8

of oxygen. The Co 2p spectra of cobalt adsorbed under both aerobic and anaerobic conditions are presented in Figure 36. The Co $2p_{3/2}$ binding energy and the Co $2p_{1/2}$ -Co $2p_{3/2}$ splitting were 780.5 and 15.0 eV, respectively, for cobalt adsorbed anaerobically. The Co 2p spectral features are the same for cobalt adsorbed under aerobic conditions, indicating that dissolved oxygen is not the oxidizing agent.

To determine whether manganese dioxide was the oxidizing agent, the Mn $2p_{3/2}$ binding energy and the 3s splitting were measured. Measurement of the multiplet splitting of the manganese 3s photopeak is advantageous in distinguishing the chemical environment and oxidation state of manganese (170,171). Multiplet splitting arises when a 3s electron is ejected from a paramagnetic molecule because two final states are possible. The remaining 3s electron couples with the valence 3d electrons, giving rise to a spin parallel or antiparallel to the 3d electrons. Two photopeaks appear when the 3s level is recorded. The higher binding energy peak corresponds to the 3s electron having a spin parallel to the 3d electrons, and the lower binding energy peak corresponds to the 3s electron antiparallel to the unpaired 3d electrons (170,171). A schematic energy level diagram showing these two possible final states is presented in Figure 37 for Mn(IV).

The variation in the Mn 3s splitting is more readily related to the Mn oxidation state than is the Mn $2p_{3/2}$ binding energy. Values for the Mn $2p_{3/2}$ binding energies are 640.6, 641.9, and 642.0 eV for MnO, Mn_2O_3, and MnO_2, respectively. The Mn 3s splittings for these compounds are 5.8, 5.3, and 4.7 for MnO, Mn_2O_3, and MnO_2, respectively

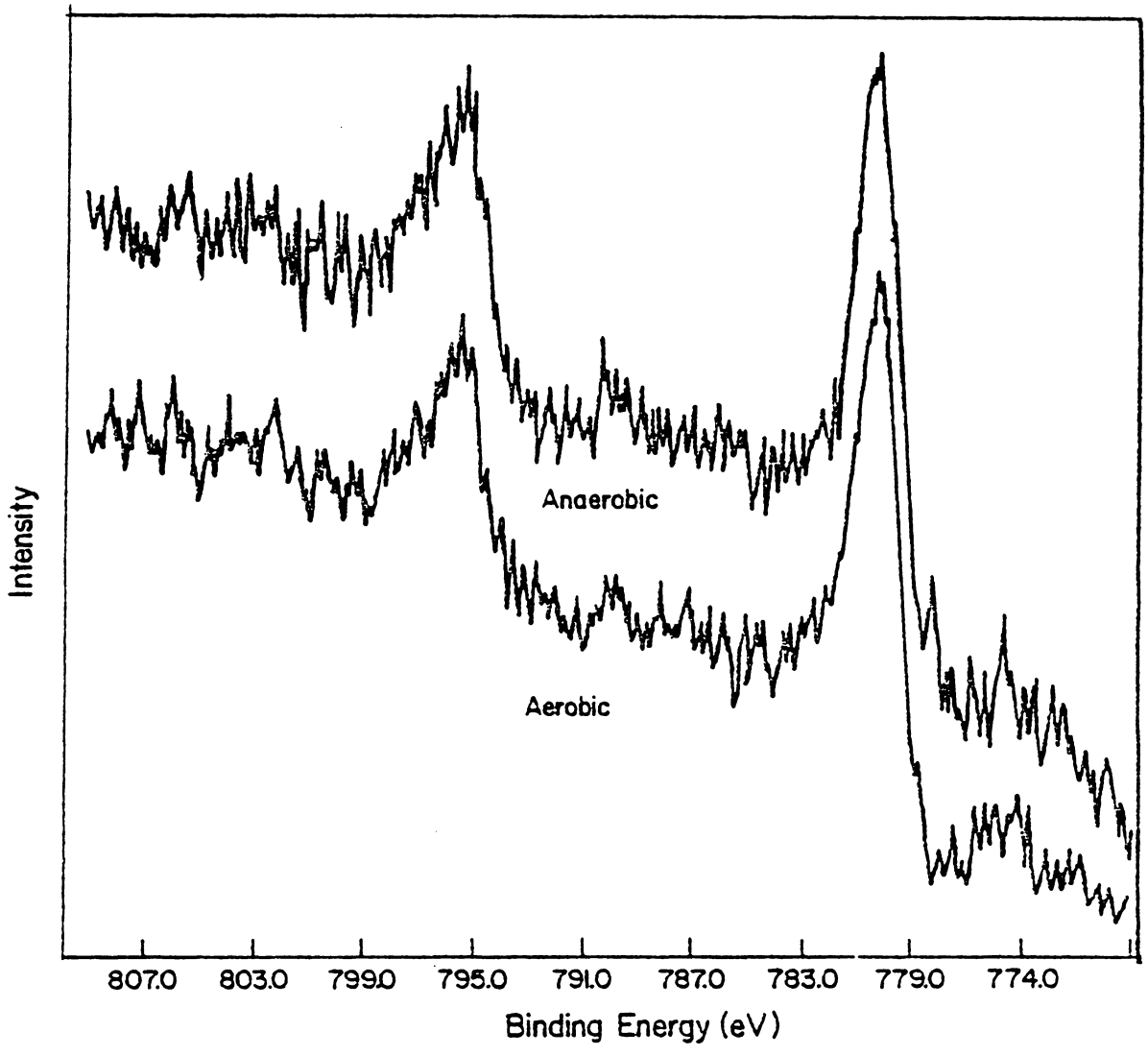

Figure 36. Co^{2+} Treated Birnessite - pH 6.5
Anaerobic and Aerobic

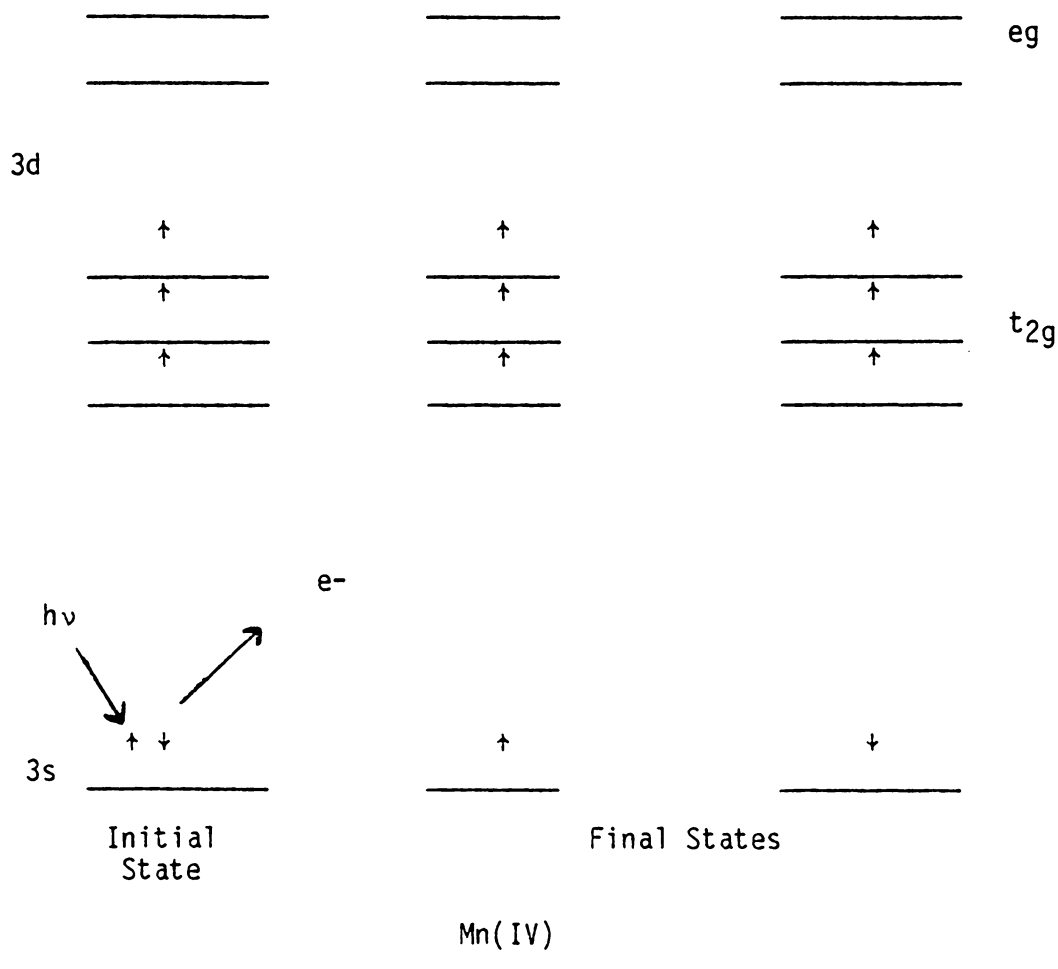

Figure 37. Manganese 3s Multiplet Splitting

(170). Table 24 presents the multiplet splitting results for the manganese 3s photopeaks and the binding energy for the Mn $2p_{3/2}$ level for manganese oxides (170,171).

For the Co^{2+} treated birnessite samples prepared at several pH's (Table 24), the Mn 3s splitting value and the manganese $2p_{3/2}$ binding energies are equal to the value for untreated birnessite. The Mn 3s splittings observed for MnO_2 prepared in Co^{2+} in the pH range 4 to 10 are 4.7 ± 0.2 eV and the Mn $2p_{3/2}$ binding energies are 642.2 ± 0.2 eV. These values correspond to values for the untreated birnessite substrate, 4.7 and 642.2 eV, respectively. Thus neither the Mn 3s splittings nor the Mn $2p_{3/2}$ binding energies provide any indication of manganese reduction of cobalt adsorbed on birnessite. The absence of changes in both the Mn $2p_{3/2}$ binding energies and the Mn 3s splittings could result from the fact that not enough cobalt was adsorbed by birnessite. A sample of birnessite was cobalt saturated aerobically by repeatedly washing the manganese dioxide with 0.1M $Co(NO_3)_2$ at pH 6.5. The Mn 3s splittings for Co^{2+}-saturated and Na^{+}-saturated birnessite are presented in Figure 38. The splitting observed for the Co^{2+}-saturated birnessite was 5.1 eV, which is between that expected for Mn(II) 5.8 eV (170) or Mn(III), 5.3 ± 1.0 eV, (170,171), and the value expected for Mn(IV), 4.7 eV (170). The intermediate Mn 3s splitting value indicates that some reduction of manganese has occurred. No change was observed in the Mn $2p_{3/2}$ binding energy. Thus, Mn_2O_3 (BE = 641.9 eV) plus unreacted MnO_2 (no MnO BE = 640.0 eV) is the final composition for manganese. These observations for cobalt

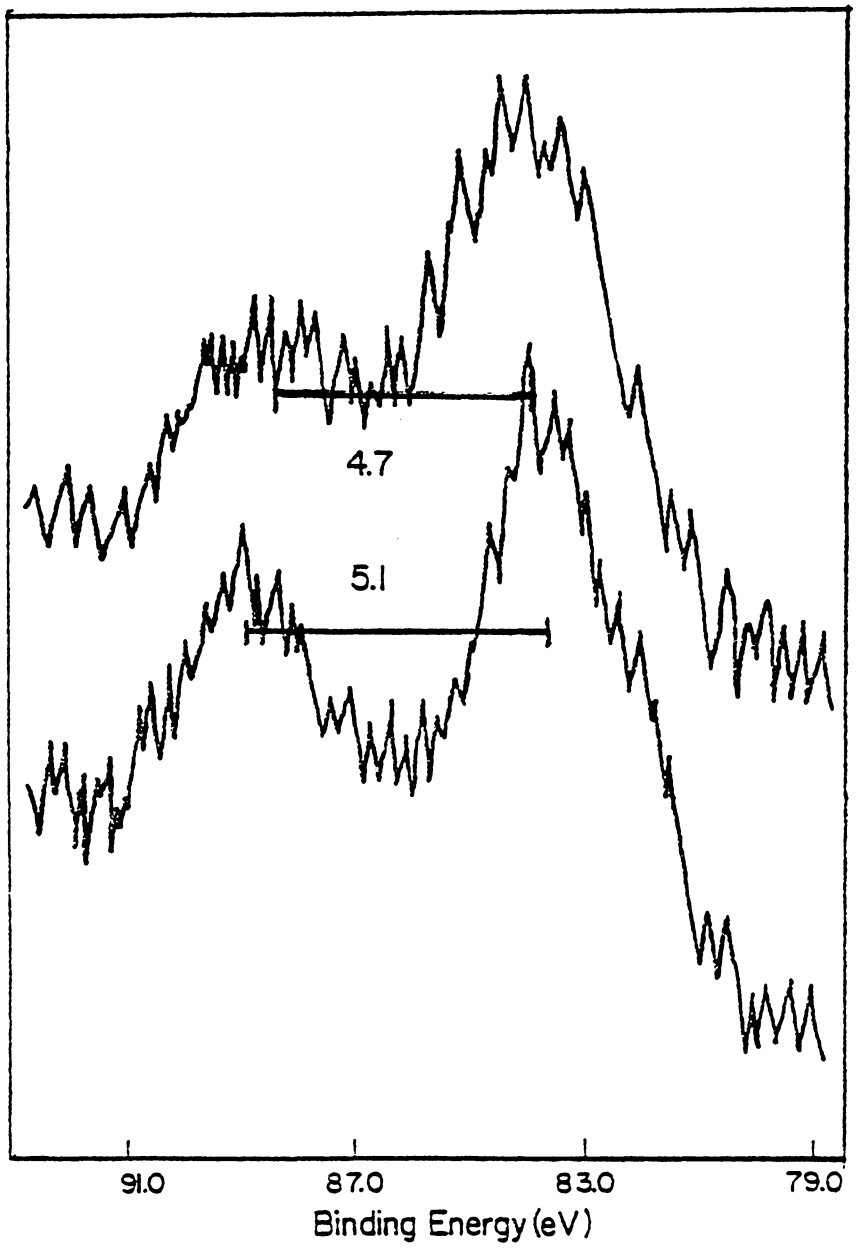

Figure 38. Mn 3s Splitting Na^{+}-Birnessite and Co^{2+}-Birnessite

saturated birnessite support the proposal that Co(II) is oxidized to Co(III) and that Mn(IV) is reduced to Mn(III). A possible reaction is given below:

$$2Co^{2+}_{(aq)} + 5H_2O + 2MnO_{2(g)} \rightarrow 2Co(OH)_{3(g)} + 4H^{+}_{(aq)} + Mn_2O_{3(g)} \quad (61)$$

The free energy for this reaction is:

$$\Delta G = \Delta G_r^\circ + 2.303\ RT\ \log \frac{[H^+]^4}{[Co^{2+}]^2} \quad (62)$$

where ΔG_r° = +93.5 Kjoules/mole. Under the condition of this experiment, 0.5M $Co(NO_3)_2$ and pH = 6.5, the reaction is favorable, ΔG = -238.0 K joules/mole.

E. ADSORPTION OF GLYCINE AND LYSINE ON BIRNESSITE

The purpose of this portion of the study was to investigate the bonding of amino acids to a metal oxide surface and the effect of a transition metal counterion upon adsorption. Glycine and lysine were adsorbed on Na^+-and Co^{2+}-birnessite. No previous studies of the adsorption of amino acids on manganese dioxide have been found in the literature. A study (172) of the adsorption of organic species, dodecylbenzene sulfonate (anionic), nonylphenoxynonyl-ethoxyethanol (nonionic), and p-dodecylbenzyltrimmethylammonium chloride (cationic), concluded that cation exchange was the principal interaction of organics with manganese dioxide. Adsorption of the cationic species occurred but no interaction was observed with the anionic or neutral species (172).

Electrophoretic mobilities of Na^+- and Co^{2+}-birnessite were

measured in 0.01M solutions of glycine and lysine to investigate the effect of the amino acids on the surface charge. If H-lysine, a +2 cation exchanges for Na^+- or Co^{2+}-birnessite, by nonequivalent exchange, the mobility would increase. Nonequivalent exchange is most likely at pH 3 or below, where lysine is present in solution as a +2 cation. Nonequivalent exchange reactions of lysine with Na^+- and Co^{2+}-birnessite are given in Equations 63 and 64, respectively. For the reactions illustrated in this section no indication of the electrostatic or specific nature of the bond is intended by the symbolism used.

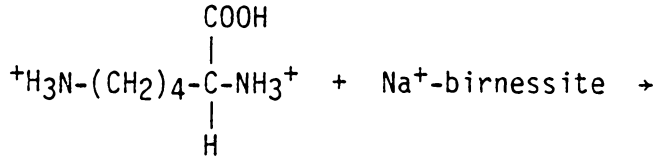

(63)

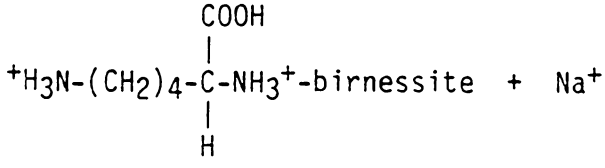

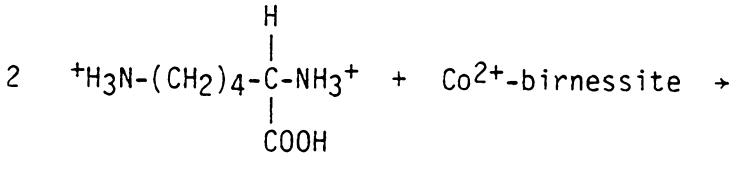

(64)

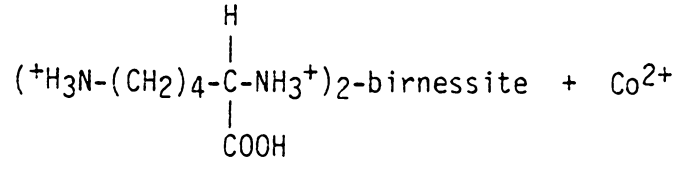

Equivalent exchange can occur between a +2 lysine cation and

either Na^+- or Co^{2+}-birnessite. This reaction would not change the surface charge. The mechanisms of equivalent exchange between a +2 lysine cation for Na^+- and Co^{2+}-birnessite are presented in Equations 65 and 66, respectively.

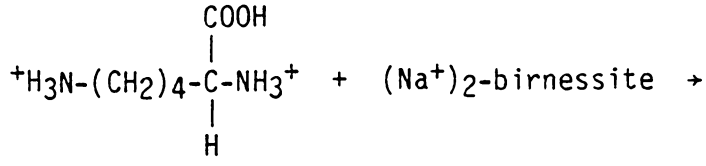

$$^{+}H_3N\text{-}(CH_2)_4\text{-}C(COOH)(H)\text{-}NH_3^{+} + (Na^+)_2\text{-birnessite} \rightarrow$$

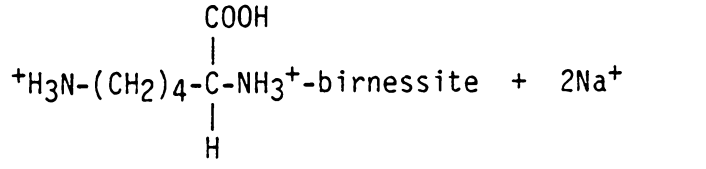

$$^{+}H_3N\text{-}(CH_2)_4\text{-}C(COOH)(H)\text{-}NH_3^{+}\text{-birnessite} + 2Na^+ \quad (65)$$

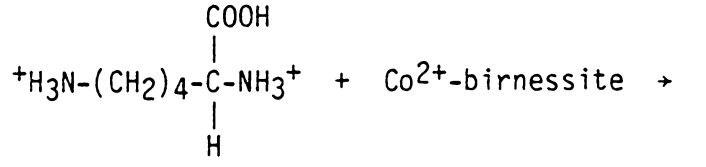

$$^{+}H_3N\text{-}(CH_2)_4\text{-}C(COOH)(H)\text{-}NH_3^{+} + Co^{2+}\text{-birnessite} \rightarrow$$

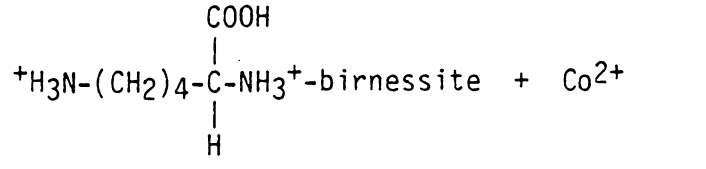

$$^{+}H_3N\text{-}(CH_2)_4\text{-}C(COOH)(H)\text{-}NH_3^{+}\text{-birnessite} + Co^{2+} \quad (66)$$

If glycine or lysine +1 cations exchange with the surface counterions by an equivalent exchange mechanism the mobility would remain the same. Equivalent exchange of glycine with Na^+- and Co^{2+}-birnessite is presented in Equations 67 and 68, respectively.

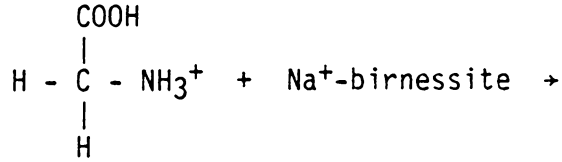

(67)

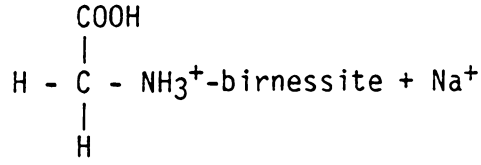

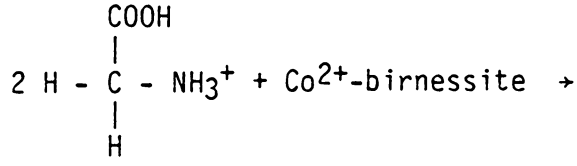

(68)

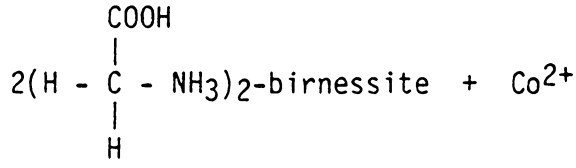

Equivalent exchange of +1 lysine with Na^+- and Co^{2+}-birnessite is presented in Equation 69 and 70, respectively.

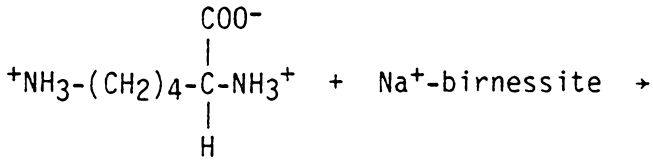

(69)

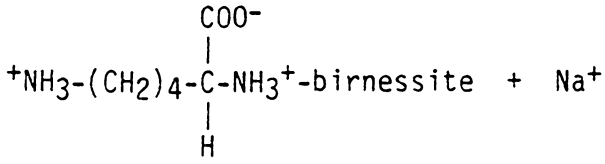

$$2\ {}^{+}NH_3\text{-}(CH_2)_4\text{-}\underset{\displaystyle H}{\overset{\displaystyle COO^-}{\underset{|}{\overset{|}{C}}}}\text{-}NH_3 \ +\ Co^{2+}\text{-birnessite} \rightarrow$$

$$(^{+}NH_3\text{-}(CH_2)_4\text{-}\underset{\displaystyle H}{\overset{\displaystyle COO^-}{\underset{|}{\overset{|}{C}}}}\text{-}NH_3^{+})_2\text{-birnessite} \ +\ Co^{2+} \qquad (70)$$

If glycine or lysine adsorbed as neutral zwitterion, the mobility would either remain the same (Equation 71) or decrease (Equation 72) depending on whether counterions were released. Equations are provided below for the example of the zwitterion adsorption of glycine on Na^+-birnessite.

$$H\text{-}\underset{\displaystyle H}{\overset{\displaystyle COO^-}{\underset{|}{\overset{|}{C}}}}\text{-}NH_3^{+} \ +\ Na^{+}\text{-birnessite} \rightarrow$$

$$H\text{-}\underset{\displaystyle H}{\overset{\displaystyle NH_3^{+}}{\underset{|}{\overset{|}{C}}}}\text{-}COO^- + Na^{+}\text{-birnessite} \qquad (71)$$

$$H\text{-}\underset{\displaystyle H}{\overset{\displaystyle COO^-}{\underset{|}{\overset{|}{C}}}}\text{-}NH_3^{+} \ +\ Na^{+}\text{-birnessite} \rightarrow$$

$$H\text{-}\underset{\displaystyle H}{\overset{\displaystyle COO^-}{\underset{|}{\overset{|}{C}}}}\text{-}NH_3^{+}\text{-birnessite} \ +\ Na^{+} \qquad (72)$$

The electrophoretic mobilities of Na^+- and Co^{2+}-birnessite in 0.01M $NaClO_4$, glycine, and lysine are presented in Figures 39 and 40, respectively. Upon interaction of glycine and lysine with Na^+-birnessite, the electrophoretic mobilities were more positive from pH 2 to 10 than the mobility of Na^+-birnessite in $NaClO_4$. Between pH 2 and 4, it is possible that +2 cations can adsorb by nonequivalent exchange for Na^+ and increase the mobility. Above pH 4 this mechanism is unlikely because the predominant species in solution are +1 lysine cations. Glycine cannot increase the charge by exchange reactions because the highest glycine charge is +1. Because exchange reactions are very unlikely, some alternate possibilities are proposed.

One possible interaction between the amino acids and the birnessite substrate is competition by glycine and lysine with the negative surface oxide sites for coordination to Mn(IV). This adsorption mode would result in a more positive electrophoretic mobility of birnessite in the amino acids compared to that in the $NaClO_4$ as presented below:

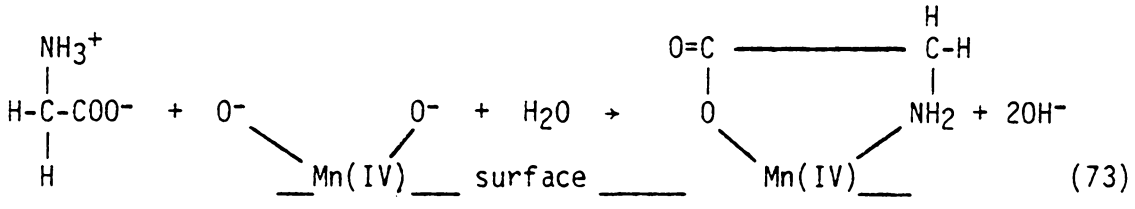

(73)

This is a possible interaction but there are no reports in the literature on the existence of manganese(IV) amino acid complexes (173).

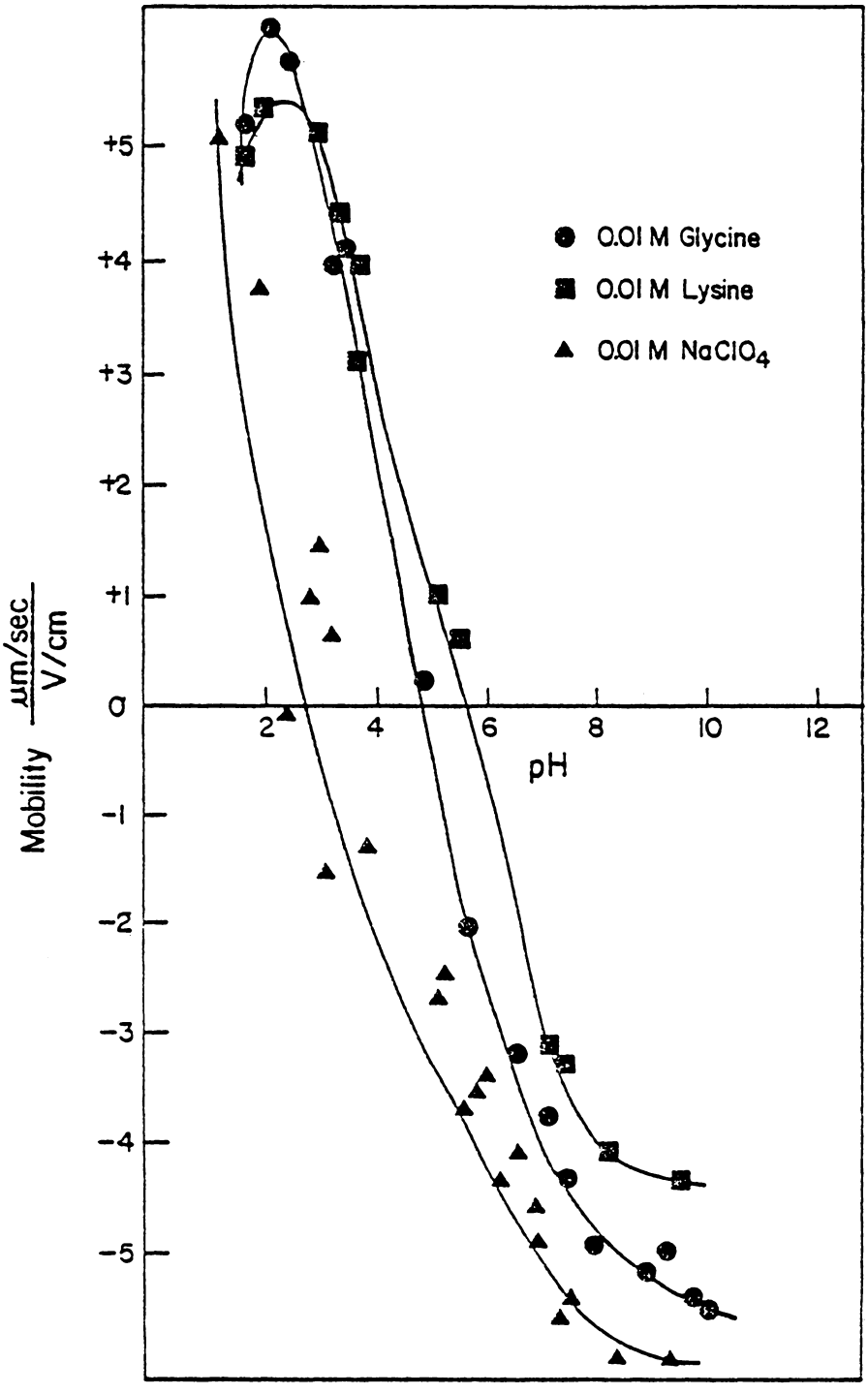

Figure 39. Electrophoretic Mobility of Na^+-Birnessite in 0.01 M Glycine and Lysine

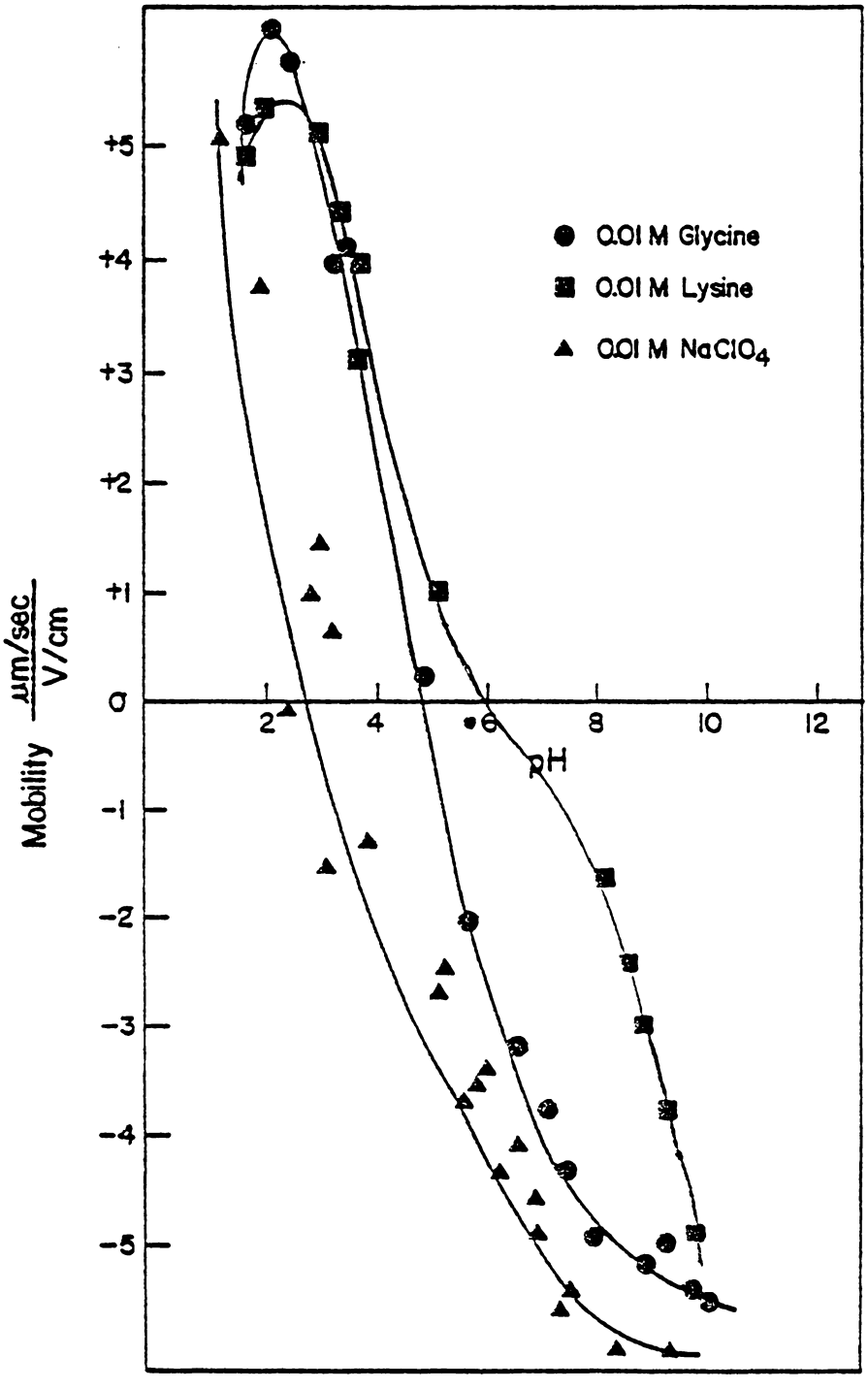

Figure 40. Electrophoretic Mobility of Co^{2+}-Birnessite in 0.01 M Glycine and Lysine

Another possible mechanism for interaction is the oxidation of the amino acids by MnO_2 and reduction of Mn(IV) to Mn(III) or Mn(II). Reports in the literature (174,175) refer to the ability of MnO_2 to oxidize amino acids. Barakat et al. (174) reported that α-amino acids can react with MnO_2 in hot aqueous solution to give the corresponding aldehyde with one carbon less. The example given by Barakat et al. (174) involved the amino acid alanine and is presented below:

$$CH_3 - \underset{\underset{NH_2}{|}}{CH} - COOH \xrightarrow{MnO_2/H_2O} CH_3\overset{\overset{O}{\|}}{C}H + CO_2 + NH_3 \qquad (74)$$

This reaction results both in the oxidation of the α-amine carbon to an aldehyde and in the reduction of Mn(IV) to MnO, $Mn(OH)_2$, or MnOOH. The temperature dependence of this reaction or the exact temperature at which the reaction was conducted was not reported. However, there are reports in the literature that MnO_2 can oxidize amines at room temperature (175). Oxidation of the amino acid would lead to subsequent formation of either Mn(II) or Mn(III) oxides or hydroxides on the birnessite surface. The identification of the manganese product can potentially be determined by electrophoretic mobility measurements. Based on crystal field stabilization energies, Parks (176) predicted that the pH of the IEP for $Mn(OH)_2$ and MnOOH would be 12.4 and 8.1, respectively. Thus $Mn(OH)_2$ and MnOOH have a more positive surface charge than birnessite, IEP = pH 3.1.

The electrophoretic mobilities of glycine and lysine treated Co^{2+}-birnessite are presented in Figure 40. The behavior on the Co^{2+}-birnessite was similar to that observed for Na+-birnessite between pH

2 and 6, which indicates that equivalent interactions occurred in both cases. However, at pH 8 and 10 the mobility was greater for the Co^{2+}-birnessite treated with amino acids than for the amino acid treated Na^{+}-birnessite. This can be due to the presence of Co(III) on the surface or to greater amount of reduced manganese oxides and/or hydroxides that may have resulted.

XPS was used to further investigate the interactions of glycine and lysine with birnessite and to investigate the possibility of oxidation of amino acids by the manganese dioxide surface. The Mn 3s splitting, Mn $2p_{3/2}$ binding energies, N 1s binding energies, N/N^{+} and N/Mn ratios are found in Table 25 for Na^{+}-birnessite and in Table 26 for Co^{2+} -birnessite. The Mn 3s splitting was measured to determine if reduction of the Na^{+}-birnessite surface occurred upon treatment with the amino acids and to gain evidence for an oxidation-reduction mechanism. No significant increase in the Mn 3s splitting was observed in the presence of the 0.01M amino acid on Na^{+}-birnessite.

To effect greater adsorption, Na^{+}-birnessite was saturated by repeatedly washing the substrate with 0.5 M adsorbate solutions. Results showing an increase in the Mn 3s splitting for birnessite saturated with both amino acids are presented in Table 25. Splitting values of 5.1 eV were obtained for both amino acids at 0.5M concentration compared to values of 4.7 eV for Na^{+}-birnessite. The larger energy splitting for the amino acid treated Na^{+}-birnessite verifies that manganese is reduced.

The Mn 3s energy splitting for amino acids on Co^{2+}-saturated

Table 25

XPS Results for Amino Acids Adsorbed on Na^+-Birnessite

pH	N 1s Binding Energy (±0.1 eV)	N/N^+ (±0.1)	N/Mn (±0.002)	Manganese $2p_{3/2}$ Binding Energy (±0.1 eV)	Mn 3s Splitting (±0.1 eV)
Glycine Na^+-Birnessite					
2	400.8, 399.7	2.1	0.029	642.2	4.8
4	400.7, 399.9	2.4	0.022	642.1	4.8
6	- 399.7	one peak	0.025	642.2	4.8
8	- 399.8	one peak	0.021	642.2	4.8
10	- 399.8	one peak	0.016	642.2	4.8
Lysine on Na^+-Birnessite					
2	400.9, 399.7	2.1	0.063	642.1	4.7
4	400.7, 399.6	3.3	0.061	642.1	4.7
6	- 399.7	one peak	0.055	642.1	4.7
8	- 399.6	one peak	0.055	642.1	4.8
10	- 399.6	one peak	0.023	642.2	4.8
Gly-Birnessite (pH 6.5)	- 399.8	one peak	0.030	642.1	5.1
Lys-Birnessite (pH 6.5)	400.8, 399.7	one peak	0.070	642.1	5.1
Glycine	- 399.3	-	-	-	-
(+)-Lysine	400.6, 399.3	0.59	-	-	-
Lysine Monohydrochloride	400.6, -	-	-	-	-

Table 26

XPS Results for Amino Acids Adsorbed on Co^{2+} Birnessite

pH	Nitrogen 1s Binding Energy (±0.1 eV)	N/N^+ (±0.2)	N/Mn (±0.002)	Mn $2p_{3/2}$ Binding Energy (±0.1 eV)	Mn 3s Splitting (±0.1 ev)	Cobalt $2p_{3/2}$ Binding Energy (±0.1 eV)	Co $2p_{1/2}$-Co $2p_{3/2}$ Splitting (±0.1 eV)	Co/Mn Atomic Ratio (±0.002)
Glycine Co^{2+}-Birnessite								
2	400.9, 399.5	3.0	0.031	642.2				
4	400.7, 399.6	3.0	0.023	642.1	5.0	780.4	15.0	0.024
6	- 399.7	one peak	0.048	642.1	5.0	780.5	15.0	0.029
8	- 399.5	one peak	0.051	642.0	5.1	780.4	15.1	0.033
10	- 399.6	one peak	0.051	642.2	5.0	780.4	15.1	0.035
					5.1	780.4	15.0	0.037
Lysine Co^{2+}-Birnessite								
2	400.7, 399.8	2.0	0.068	642.2	5.0	780.4	15.1	0.024
4	400.6, 399.7	4.0	0.067	642.2	5.0	780.5	15.2	0.032
6	- 399.8	one peak	0.057	642.0	5.0	780.4	15.1	0.036
8	- 399.7	one peak	0.082	642.0	5.0	780.4	15.0	0.036
10	- 399.7	one peak	0.117	642.1	5.0	780.5	15.1	0.037
Co^{2+}-Birnessite				642.2	5.1	780.5	15.0	0.040

birnessite was also measured. The energy difference was 5.1 ± 0.1 eV, which is the same as the splitting for the Co^{2+}-birnessite substrate without the amino acid treatment. Thus no increased splitting was observed in the presence of the amino acids to indicate further reduction of manganese on the birnessite surface.

The Mn $2p_{3/2}$ binding energies do not change for amino acid and treated birnessite (BE = 642.1 ± 0.1 eV) compared to Na^+-birnessite (BE = 642.2 eV). This indicates that the oxidation state of the manganese causing the increased splitting is Mn (III) (BE = 641.9 eV) and not Mn(II) (BE = 640.9 eV). Because Mn(III) readily disproportionates into Mn(II) and Mn(IV), it is likely that Mn(II) is also on the surface but was too small a quantity to detect.

XPS analysis indicated that two chemically different forms of nitrogen for glycine and lysine adsorbed on both Na^+- and Co^{2+}-birnessite, at pH 2 and 4. The lower binding energy N is photopeak at 399.7 ± 0.1 eV is characteristic of an $-NH_2$ nitrogen while the higher binding energy N 1s photopeak at 400.8 ± 0.1 eV is indicative of $-NH_3^+$ (155). The protonated amine on the birnessite surface could be the result of exchange with surface sodium or cobalt. Protonated amines on the surface are only observed at low pH where a greater percentage of the amine groups in solution are protonated and exchange is more likely. Posselt et al. (172) observed cation exchange of organic species on the manganese dioxide surface but did not report the pH.

The presence of unprotonated amine groups on birnessite supports the electrophoresis results which indicated that cation exchange was

not the only mechanism of interaction. This is because cation exchange would involve only protonated amine groups. It is unlikely that the amino acids are coordinated to either Mn(IV) or Mn(III) because both Mn(IV) and Mn(III) oxidize amino acids (174,175,177,178). The basic amine groups are probably due to coordination of the amino acids to Mn(II), because only small amounts of amino acid were adsorbed on Na^+ - birnessite (N/Mn atomic ratio ranges from 0.16 to 0.063). It is possible that the amount of Mn(II) on the surface needed to coordinate this amount of amino acid would not be detected in the presence of much larger amounts of Mn(IV) and Mn(III).

The N/N^+ ratios for glycine and lysine on birnessite at pH 2 to 4 indicate that the reaction responsible for the unprotonated amine groups (coordination) was more favorable that for protonated amine groups (cation exchange). Curve resolution of the N 1s photo peaks revealed that two to four times as much unprotonated amine was adsorbed. A representative curve resolved N 1s photopeak for the glycine and lysine adsorbed onto Na^+- and Co^{2+}-birnessite at pH 2 and 4 is presented in Figure 41. The spectrum shown is for glycine adsorbed on Na^+-birnessite at pH 4.

At pH 6, 8, and 10 for glycine and lysine adsorbed onto Na^+-and Co^{2+}-birnessite, XPS N 1s photopeaks are characteristic of unprotonated amine groups. At these pH values, cation exchange is less likely than at pH 2 to 4 because a smaller percentage of the amino acids are protonated (105, 172). Coordination of the amino acids to the manganese surface might occur, because it is the most likely

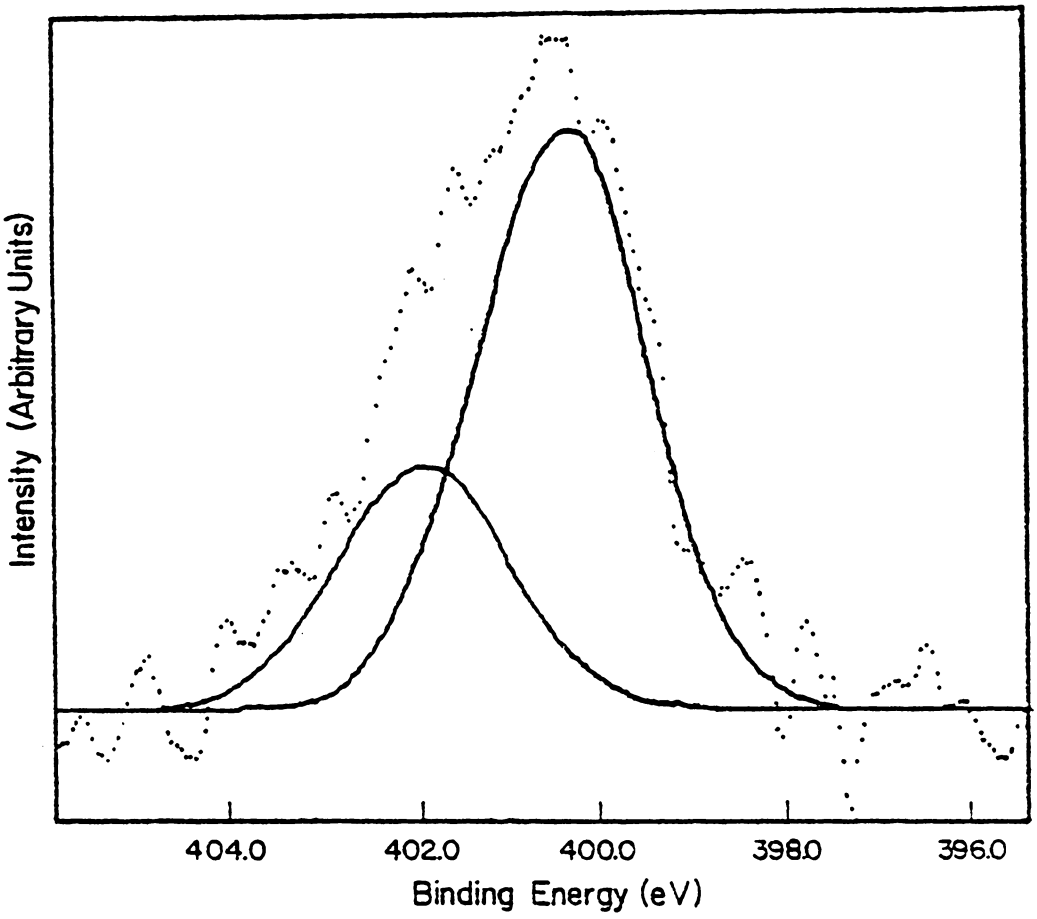

Figure 41. Glycine Treated Na^{+}-Birnessite - pH 4

interaction that would produce unprotonated amine groups under the experimental conditions.

The unprotonated amino acid on the Co^{2+}-saturated manganese dioxide could be bound either to cobalt or to manganese. The N 1s binding energy results do not permit distinguishing these interactions because amines bound to Mn(II) would have the same N 1s binding energy as amines bound to Co(II) or Co(III) (145). No change was observed in the Co $2p_{3/2}$ binding energy of the surface cobalt upon equilibration with glycine or lysine. However, the larger N/Mn XPS ratio demonstrates that greater quantities of amino acid (Tables 25 and 26) are adsorbed on Co^{2+}-birnessite compared to Na^{+}-birnessite. The increase in adsorption is possible due to coordination to cobalt.

In summary, the proposed modes of interaction of amino acids with the birnessite surface are presented below. Mn(III) is suggested as the final oxidation state of manganese as follows:

$$2MnO_2 + H-\underset{\displaystyle H}{\overset{\displaystyle COO^-}{\overset{|}{\underset{|}{C}}}}-NH_3^+ \rightarrow \qquad (75)$$

$$Mn_2O_3 + NH_3 + H-\overset{\displaystyle O}{\overset{\|}{CH}} + CO_2$$

Although oxidation of amino acids was previously observed in hot aqueous solution (174), it appears possible that the reaction occurs on the manganese dioxide surface at room temperature based on electrophoretic mobility measurements and XPS analysis.

Mn(III) disproportionates to form Mn(II) and Mn(IV). It is likely that the amino acids are coordinated to Mn(II) which is an end product of this reaction (Equation 76 and 77).

$$Mn_2O_3 \rightarrow MnO_2 + MnO \qquad (76)$$

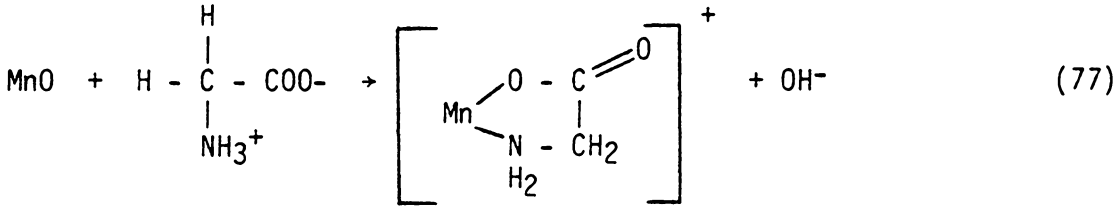

$$MnO + H-\underset{\displaystyle NH_3^+}{\overset{\displaystyle H}{\underset{|}{\overset{|}{C}}}}-COO^- \rightarrow \left[\begin{array}{l} Mn\begin{array}{l}\diagup O-C\overset{\displaystyle O}{\overset{\|}{}}\\ \diagdown N-CH_2\\ \quad H_2\end{array}\end{array}\right]^+ + OH^- \qquad (77)$$

F. COBALT AMINO ACID COMPLEX ADSORPTION ON BIRNESSITE

This portion of the study was carried out to observe the effect of complexation on the nature of the cobalt adsorption reaction. Cobalt amino acid complexes, $Co(gly)_3$, $Co(lys)_3^{3+}$, and $Co(asp)_2^-$ were adsorbed on Na^+-saturated birnessite as a function of pH. Previous discussions in this dissertation showed that oxidation of Co^{2+} occurred on birnessite whereas reduction of the Co(III) in Co(III) complexes was noted on montmorillonite. It was of interest to see how the cobalt amino acid complexes interact with the birnessite substrate.

The pH dependence of cobalt adsorption on birnessite in 0.01M solutions of $Co(gly)_3$ cobalt lysine and cobalt aspartic acid, $Co(asp)_2^-$ is presented in Figure 42. The quantity of cobalt adsorbed increases with increasing pH in the presence of all three complexes. Cobalt adsorbed from $Co(asp)^-$ too shows the most dramatic change with increasing pH and cobalt adsorbed on birnessite in the presence of $Co(gly)_3$ reveals the least pH dependence. The amount of cobalt

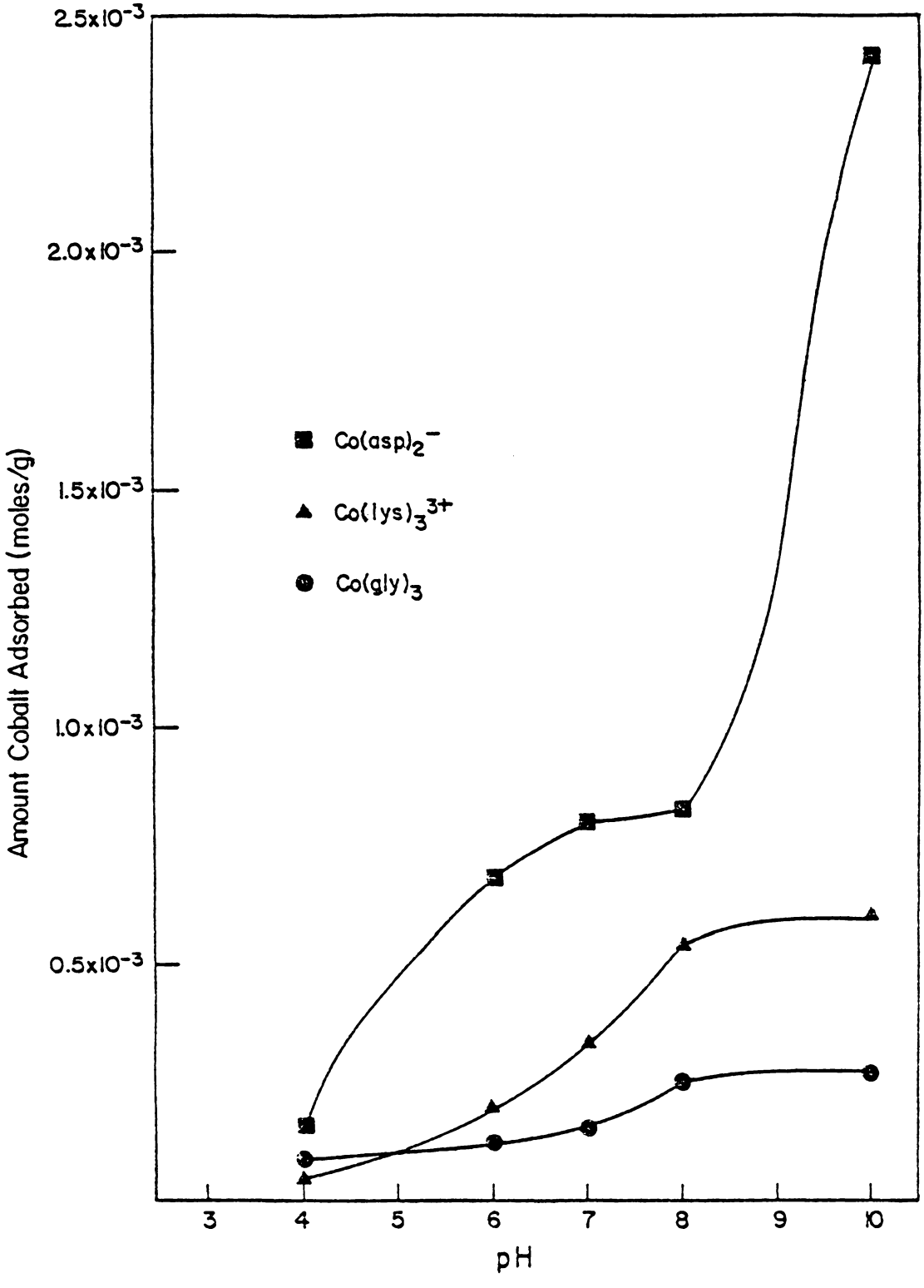

Figure 42. Adsorption of Complexes on Birnessite

adsorbed on birnessite in solutions of 0.01M cobalt amino acid complex decreases in the order:

$$Co(asp)_2^- > Co(lys)_3^{3+} > Co(gly)_3 \quad (78)$$

The interaction of cobalt amino acid complexes with birnessite is not principally due to electrostatic attraction of the complexes to the negatively charged surface. If this were the case the amount of complex adsorbed would vary as:

$$Co(lys)_3^{3+} > Co(gly)_3 > Co(asp)_2^- \quad (79)$$

Adsorption does not depend on steric factors (Table 18) because the cobalt amino acid complexes decrease in size as follows:

$$Co(lys)_3^{3+} > Co(asp)_2^- > Co(gly)_3 \quad (80)$$

However, adsorption does follow the order of susceptibility of the cobalt amino acid complexes to hydrolysis. This is evident upon comparison of the order of complex adsorption (Equation 78) to the order of decreasing hydrolysis rates, as shown below:

$$Co(asp)_2^- > Co(lys)_3^{3+} > Co(gly)_3 \quad (81)$$

Although the acid and base hydrolysis constants have not been reported in the literature, the relative stability of these complexes can be arranged based on steric factors, the basicity of the amino acids and observations of the amount of precipitate at pH 10. The aspartic acid complex is the least stable because the bonding of the terminal acid group to cobalt is strained (185). The relative ease of hydrolysis for

lysine compared to glycine can be determined based on the basicity of the amino acids. The higher the pK of the α-amine and α-carboxylate, the more stable the metal amino acid bond and the lesser the susceptibility of the complex to hydrolysis (178).
Lysine has a pK_a of 8.9 and glycine has a pK_a of 9.6 for the α-amine groups. The pK_a values for the carboxylate groups are about the same, 2.3 for glycine and 2.2 for lysine. The higher value for the alpha amine group of glycine compared to lysine indicates that lysine would be more susceptible to hydrolysis than glycine (178).

This order of decreasing hydrolysis rates (Equation 81) was observed in 0.01M control solutions of the complex at pH 10. As previously discussed, $Co(asp)_2^-$ showed the greatest amount of precipitate (approximately 0.20 precipitate/100 ml control solution) $Co(lys)_3^{3+}$ showed a trace of precipitate and $Co(gly)_3$ showed no precipitate.

Electrophoretic mobility measurements of birnessite in 0.01M cobalt amino acid complex solutions were carried out to determine the the effect of amino acid complexes on the polarity and magnitude of the birnessite surface charge. The mobility for birnessite in 0.01M $Co(gly)_3$, $Co(asp)_2^-$, and $Co(lys)_3^{3+}$ are presented in Figure 43. In 0.01M $Co(gly)_3$, the mobility for birnessite between pH 2 and 10 shows a more positive charge on the surface than in 0.01M $NaClO_4$. If the neutral complex were adsorbed, a mobility equal to or more negative than that of $NaClO_4$ would be observed. The more positive mobilities indicate that positive hydrolysis products of $Co(gly)_3$, such as

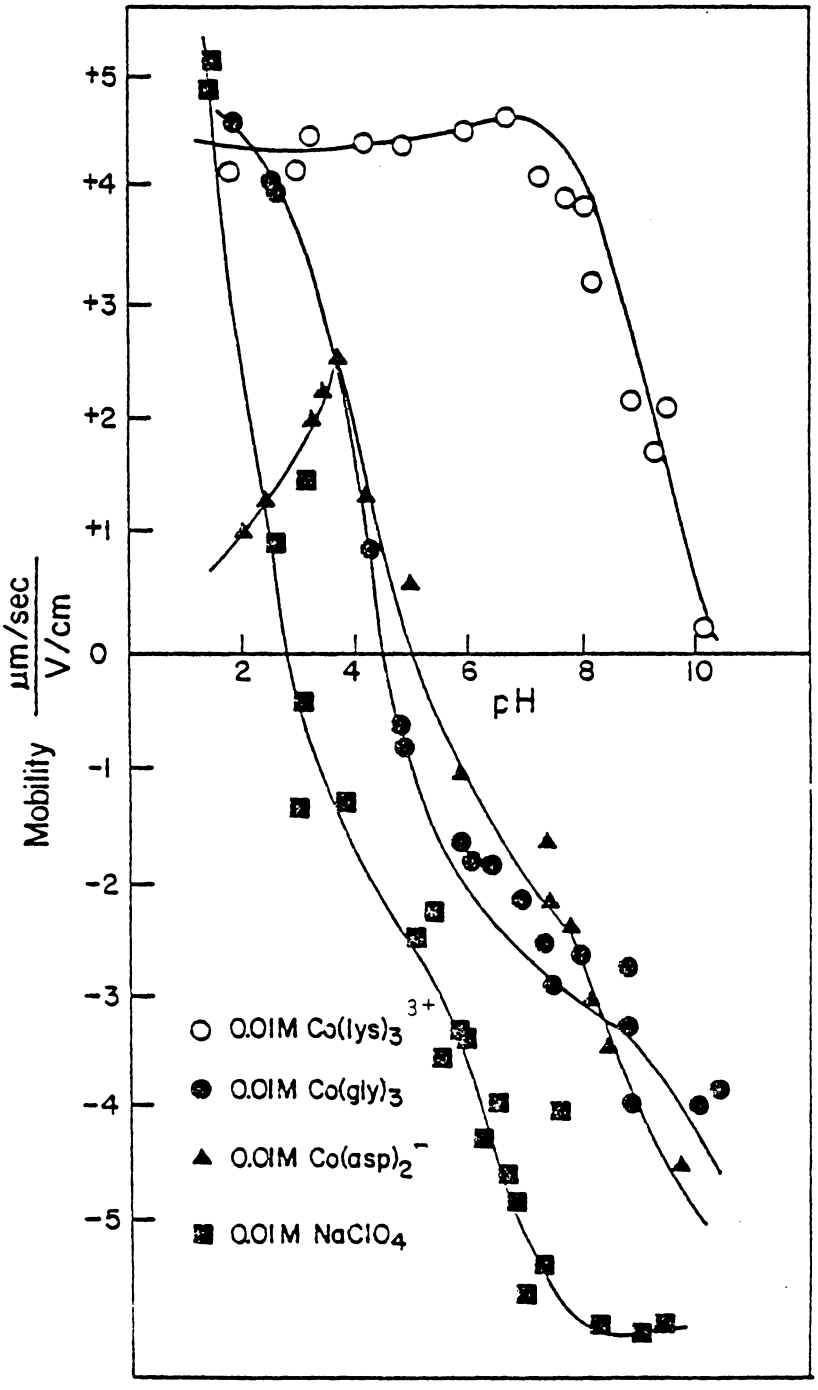

Figure 43. Electrophoretic Mobility of Birnessite in 0.01 M Complexes

$Co(III)(gly)_2^+$, $Co(III)(gly)_2^+$, and Co^{2+}, interact with the surface.

At pH 2 the electrophoretic mobility of Na^+-birnessite in 0.01M $Co(asp)_2^-$, +1 mobility unit (m.u.), is lower than the mobility in 0.01M $NaClO_4$, +4 m.u. This means that the negative complex is adsorbed on the positive birnessite surface. It is reasonable to expect anion adsorption at pH 2 because birnessite has a positive surface charge and would attract the negative aspartic acid complex.

The mobility of birnessite in $Co(asp)_2^-$ is more positive between pH 4 and 10 than the mobility in $NaClO_4$, at the same pH values. The electrophoretic mobility measurements suggest that a positive hydrolysis product of $Co(asp)_2^-$ is adsorbed. Adsorption of the unhydrolyzed negative complex would decrease the mobility, but this behavior was not observed. Interaction of hydrolysis products of $Co(asp)_2^-$, such as $Co(asp)^+$ and $Co(H_2O)_6^{2+}$ would be consistent with the observed results.

The electrophoretic mobility of birnessite in $Co(lys)_3^{3+}$ is positive between pH 2 and 10. At pH 2 the mobility of birnessite is 4.3 m.u. in $Co(lys)_3^{3+}$ compared to 4.1 m.u. in $NaClO_4$. The equality of the mobilities means that little interaction occurs at pH 2 between $Co(lys)_3^{3+}$ and the positive birnessite surface. Between pH 4 and 8, the mobility of birnessite in $Co(lys)_3^{3+}$ has a constant value of 4.5 ± 0.2 m.u., whereas the mobility in $NaClO_4$ decreases from -1.0 m.u. at pH 4 to -6.0 m.u. at pH 8. The positive mobility at pH 4 to 8 means that nonequivalent exchange occurs between $Co(lys)_3^{3+}$ and the birnessite surface (Equation 82).

$Co(lys)_3^{3+}$ + Na^+-birnessite → $Co(lys)_3^{3+}$-birnessite + Na^+ (82)

Nonequivalent exchange between the sodium counterion and hydrolysis products of $Co(lys)_3^{3+}$ such as $Co(lys)_2^{3+}$, $Co(lys)^{3+}$, $Co(lys)^{2+}$ and Co^{2+} could also give the observed mobility. The mobility of birnessite in $Co(lys)_3^{3+}$ decreases from a value of 3.9 m.u. at pH 8 to a value of 0.2 m.u. at pH 10. The observed mobilities are similar to those observed for $Co(OH)_2$ in $NaClO_4$, which had values of 4.2 m.u. and -0.1 m.u. at pH 8 and 10, respectively (Figure 8). It is possible that hydrolysis of $Co(lys)_3^{3+}$ occurs and $Co(OH)_2$ is precipitated onto the surface.

To investigate the chemical nature of the adsorbed complexes, XPS analysis of the adsorbed cobalt amino acid complexes on birnessite was carried out. The N/Co atomic ratios were calculated to derive the maximum ratio of amino acid to cobalt on the surface. The N/N^+ ratios were calculated to determine if the amino acid ligand was bound to the surface or to the cobalt and the Co $2p_{1/2}$ and Co $2p_{3/2}$ photopeaks were measured to investigate the oxidation state and chemical nature of the surface cobalt. Manganese 3s splittings and the Mn $2p_{3/2}$ binding energies were determined to inquire whether reduction of surface manganese occurred. The XPS binding energies for the Co 2p, N 1s and Mn $2p_{3/2}$ photopeaks, Co $2p_{1/2}$ -Co $2p_{3/2}$ splittings, N/N^+ ratio, and N/Co ratios for birnessite treated with cobalt complexes are presented in Table 27.

The XPS Co $2p_{3/2}$ binding energies for $Co(lys)_3^{3+}$ treated

Table 27

Complexes Adsorbed on Birnessite

pH	Co $2p_{3/2}$ Binding Energy (±0.2 eV)	Co $2p_{1/2}$ - Co $2p_{3/2}$ Splitting (±0.1 eV)	N 1s Binding Energy (±0.1 eV)	N/N^+ (±0.1)	N/Co (±0.002)	Mn $2p_{3/2}$ Binding Energy (±0.1 eV)	Mn 3s Splitting (±0.1 eV)	$\frac{I_{sat}}{I_{main}}$	$\Delta E_{sat-main}$ (±0.2 eV)
$Co(lys)_3^{3+}$									
4	780.5	15.2	401.8, 399.4	2.3	0.78				
6	780.4	15.2	401.9, 399.4	2.5	0.37	642.1	5.0	-	-
7	780.6	15.2	- 399.4	-	0.18	642.1	5.0	-	-
8	780.9	15.9	- 399.3	-	0.17	642.6	5.0	-	-
10	780.9	15.9	- 399.3	-	0.04	642.2	4.8	0.48	5.6
						642.2	4.8	0.50	5.4
$Co(lys)_3^{3+}$	781.0	15.1	400.7, 399.3	1 \	6.0	-	-	-	-
$Co(asp)_2^-$									
4	781.0	15.2	- 399.3	-	2.3				
6	780.5	15.1	- 399.3	-	0.53	642.2	4.7	-	-
7	780.5	15.0	- 399.3	-	0.14	642.1	5.0	-	-
8	781.0	15.9	- 399.1	-	0.12	642.1	5.0	-	-
10	780.8	15.8	- 399.3	-	0.07	642.2	4.8	0.47	5.5
						642.1	4.8	0.50	5.4
$Co(asp)_2^-$	781.1	15.1	-	-	2.0	-	-	-	-

Table 27 (Continued)

Complexes Adsorbed on Birnessite

pH	Co $2p_{3/2}$ Binding Energy (±0.1 eV)	Co $2p_{1/2}$ - Co $2p_{3/2}$ Splitting (±0.1 eV)	N 1s Binding Energy (±0.1 eV)	N/N^+ (±0.1)	N/Co (±0.002)	Mn $2p_{3/2}$ Binding Energy (±0.1 eV)	Mn 3s Splitting (±0.1 eV)	$\frac{I_{sat.}}{T_{main}}$	$\Delta E_{sat-main}$ (±0.2 eV)
$Co(gly)_3$									
4	780.4	15.2	399.6	-	0.29				
6	780.5	15.2	399.5	-	0.28	642.2	4.7	-	-
7	780.4	15.2	399.5	-	0.26	642.1	4.7	-	-
8	780.8	15.9	399.5	-	0.12	642.2	4.8	-	-
10	781.0	15.8	399.6	-	0.064	642.2	4.8	0.50	5.3
						642.1	4.7	0.52	5.4
$Co(gly)_3$	781.1	15.1	399.3	-	-	-	-	-	-
$Co(OH)_2$	780.9	15.9		-	-	-	-	0.52	5.6
Na^+ - birnessite		-		-	-	642.2	4.7	-	-

birnessite at pH 4 to 7, 780.5 ± 0.1 eV, and the Co $2p_{1/2}$ - Co $2p_{3/2}$ splitting, 15.1 ± 0.1 eV differ from the values measured for the pure complex, (BE = 781.0, Co $2p_{1/2}$ -Co $2p_{3/2}$ = 15.1 eV). However the binding energies and cobalt splitting values are equal to the values observed for cobalt adsorbed on birnessite at pH 4 to 7. This agreement suggests that a similar cobalt species is adsorbed on the surface in both cases and suggests that hydrolysis of the cobalt amino acid complex occurred.

The N/Co and N/N^+ ratios for $Co(lys)_3^{3+}$ treated birnessite at pH 4 to 7 also support the suggestion that hydrolysis of the complex occurs. The N/Co ratio ranging from 0.78 to pH 4 to 0.18 at pH 7, indicates that less than one lysine ligand is on the surface for each cobalt atom. Both protonated and unprotonated amines were observed on the surface at pH 4 to 6. Protonated amines can be due to exchange of dissociated ligands or protonated terminal amine groups of coordinated lysine. The unprotonated amines can be coordinated to cobalt or dissociated from cobalt and coordinate to surface manganese. The N/N^+ ratios were 2.3 and 2.5 for $Co(lys)_3^{3+}$ on birnessite at pH 4 and 6, respectively. These N/N^+ ratios are much greater than for the pure complex, 1.0 (Table 27). The difference in the N/N^+ ratios for the adsorbed complex compound to the pure complex indicates that some of the adsorbed ligand is dissociated from the complex. This suggestion arises from the observation that the N/N^+ ratio was 3.3 at pH 4 for lysine adsorbed on Na^+-birnessite and that at pH 6 only an unprotonated amine nitrogen peak was recorded for lysine

on Na^+-birnessite. The comparison of N/N^+ ratios for complex and free ligand adsorbed on Na^+-birnessite indicates that dissociated ligands would yield a higher N/N^+ ratio than ligands bound to the complex and that some of the lysine ligands are dissociated from cobalt.

The binding energies and Co $2p_{1/2}$ -Co $2p_{3/2}$ splitting values for $Co(lys)_3^{3+}$ treated birnessite at both pH 8 and 10 are 780.9 and 15.9 eV, respecitvely. The satellite to main peak energy separations are 5.6 and 5.4 eV, and the I_{sat}/I_{main} ratios are 0.48 and 0.50 for pH 8 and 10, respectively. These values agree favorably with the Co $2p_{1/2}$ and Co $2p_{3/2}$ data for $Co(OH)_2$, which has a binding energy of 780.9 eV, Co $2p_{1/2}$ -Co $2p_{3/2}$ splitting of 15.9 eV, $\Delta E_{sat-main}$ of 5.6 eV, and I_{sat}/I_{main} of 0.52. The close agreement found between XPS analysis of $Co(OH)_2$ and $Co(lys)_3^{3+}$ adsorbed at pHs 8 and 10 on birnessite means that hydrolysis, reduction, and precipitation of the complex occurred. Observations discussed earlier concerning the behavior of 0.01M $Co(lys)_3^{3+}$ in solution without birnessite (Table 17) indicate that hydrolysis and precipitation of $Co(OH)_2$ occurs at pH 10 but not at pH 8. The observation of $Co(OH)_2$ on the birnessite surface at pH 8 reveals that birnessite catalyzes the hydrolysis of the complex. $Co(OH)_2$ on the surface at pH 10 can be due to hydrolysis either in solution or on the surface, or a combination of both.

The N/Co atomic ratios for $Co(lys)_3^{3+}$ adsorbed at pH 8 and 10 are 0.17 and 0.04, respectively. These low N/Co ratios provide further evidence of hydrolysis of $Co(lys)_3^{3+}$.

The Co $2p_{3/2}$ binding energy of $Co(asp)_2^-$ on birnessite is 781.0 eV, which is comparable to the value for pure $Co(asp)_2^-$, 781.1 eV. The

Co $2p_{1/2}$ - Co $2p_{3/2}$ splitting value and N/Co ratio for the complex adsorbed at pH 4 are 15.2 eV and 2.3, respectively, and agree with the values for the pure complex, Co $2p_{1/2}$ - Co $2p_{3/2}$ = 15.1 eV and N/Co = 2.0. The XPS Co $2p_{3/2}$ binding energy, Co $2p_{1/2}$ - Co $2p_{3/2}$ splitting, and N/Co ratio for $Co(asp)_2^-$ adsorbed on birnessite at pH 4 indicate that the negative complex is adsorbed.

At pH 6 to 10, the N/Co ratios show that hydrolysis of $Co(asp)_2^-$ occurs. This was indicated by N/Co ratios of less than one, whereas the pure complex has a N/Co ratio of 2.0. The amount of hydrolysis increases with pH, as is indicated by a decreasing N/Co ratio with increasing pH.

The Co $2p_{3/2}$ binding energy was 780.5 eV and the Co $2p_{1/2}$ - Co $2p_{3/2}$ splitting was 15.1 eV for $Co(asp)_2^-$ adsorbed on birnessite at pH 6 and 7. The splitting value indicates that the sorbed cobalt is Co(III) and the binding energy indicates that the pure complex, which as a binding energy of 781.1 eV, is not the sorbed species. These cobalt binding energies and splitting values are the same as those observed for Co^{2+} adsorbed on birnessite at pH 6 and 7. The observation that a similar species adsorbed on birnessite in both the presence of Co^{2+} and $Co(asp)_2^-$, together with the low N/Co ratio, indicates that complex was hydrolyzed.

For $Co(asp)_2^-$ adsorbed on birnessite at both pH 8 and 10, the Co $2p_{3/2}$ binding energy, 780.9 eV, the Co $2p_{1/2}$ - Co $2p_{3/2}$ splitting, 15.9 ± 0.1 eV, the $\Delta E_{sat-main}$, 5.5 ± 0.1 eV, and the I_{sat}/I_{main}, 0.49 ± 0.02 eV, are similar to the corresponding values for $Co(OH)_2$. The close

agreement found between XPS analysis of $Co(OH)_2$ and $Co(asp)_2^-$ treated birnessite means that hydrolysis and reduction of the complex occurred. Earlier discussions indicated that $Co(OH)_2$ did not form in 0.01M solutions of $Co(asp)_2^-$ at pH 8 without birnessite (Table 17). This observation suggests that hydrolysis of $Co(asp)_2^-$ is catalyzed by the birnessite surface. At pH 10 $Co(OH)_2$ does form in solution without birnessite. The $Co(OH)_2$ found on the birnessite can be the result of either solution hydrolysis or hydrolysis by the birnessite surface, or a combination of both.

The adsorption of $Co(gly)_3$ on birnessite shows similarities to the adsorption on the other two complexes. The N/Co ratio decreases with increasing pH indicating that hydrolysis increases with increasing pH. The oxidation state of the surface cobalt was Co(III) at pH 4 to 7. The Co $2p_{3/2}$ binding energy reveals that the surface cobalt is similar to that for Co^{2+} adsorbed on birnessite. At pH 8 and 10, the oxidation state of the cobalt was Co(II). The satellite structure and Co $2p_{3/2}$ binding energy indicated that the surface species was $Co(OH)_2$.

The Mn 3s splitting, 5.0 eV, at pH 4 to 7 for $Co(lys)_3^{3+}$ and at pH 6 and 7 for $Co(asp)_2^-$ adsorbed on birnessite was greater than that observed for untreated birnessite. No increase in the splitting was observed at pH 4 for $Co(asp)_2^-$, where coulombic forces are probably contributing to the adsorption. An increase in the Mn 3s splitting for $Co(gly)_3$ treated birnessite was not observed, probably due to the small amount of adsorbed cobalt. At pH 8 and 10, oxidation of the cobalt did not occur, so as expected Mn 3s splitting is equal to that for pure MnO_2.

Oxidation of Co(II) to Co(III) can account for the reduction of manganese. Reduction of Co(III) to Co(II) must occur and then the cobalt is reoxidized to Co(III) by the manganese dioxide surface.

In summary, for $Co(asp)_2^-$ at pH 4, XPS revealed that adsorption of the negatively charged cobalt amino acid complex by the positively charged birnessite surface occurred. This was indicated by a Co $2p_{3/2}$ binding energy and N/Co ratio equal to that for the pure complex. Additionally, the equivalence of the Mn 3s splitting for treated and untreated MnO_2 supports the notion that the adsorption process is exchange. A suggested mechanism for this interaction is provided below:

$$Co(asp)_2^- + Na^+\text{-birnessite} \rightarrow Co(asp)_2\text{-birnessite} + Na^+ \quad (83)$$

The observations made in this study are : 1) that the amount of cobalt amino acid complex adsorption increases with increasing ease of hydrolysis, 2) that hydrolyzed species are adsorbed, and 3) that reduction of manganese occurs. These facts suggest that the adsorption mechanism involves complex hydrolysis and oxidation of Co(II) to Co(III). It is proposed that the birnessite surface catalyzes hydrolysis of the complexes because the cobalt amino acid complexes are relatively stable to hydrolysis. It is not known whether or not reduction of the hydrolyzed cobalt occurs in solution or on the surface. In either case, water is probably the reducing agent. A possible adsorption mechanism for the interaction of cobalt amino acid complexes with birnessite from pH 4 to 7 for $Co(lys)_3^{3+}$ and $Co(gly)_3$

and at pH 6 and 7 for $Co(asp)_2^-$ is presented below:

$$Co(III)(AA)_3 + \text{birnessite} \rightarrow Co(III)(AA)_2(H_2O)_x\text{-birnessite} + AA \quad (84)$$

$$Co(III)(AA)_2(H_2O)_x\text{-birnessite} \rightarrow Co(III)(AA)\ (H_2O)_x\text{-birnessite} + AA \quad (85)$$

$$Co(III)(AA)(H_2O)_x\text{-birnessite} \rightarrow Co(III)(H_2O)_x^{3+}\text{-birnessite} + AA \quad (86)$$

$$Co(III)(H_2O)_x^{3+}\text{-birnessite} \rightarrow Co(III)(H_2O)_x^{3+} + \text{birnessite} \quad (87)$$

$$Co(III)(H_2O)_x^{3+} + 1/2\ H_2O \rightarrow Co(II)(H_2O)_x^{2+} + 1/4\ O_2 + H^+ \quad (88)$$

$$Co(II)(H_2O)_x^{2+} + \text{birnessite Mn(IV)} \rightarrow Co(III)(H_2O)_x^{3+}\text{-birnessite (Mn(III))} \quad (89)$$

where: AA represents amino acid ligands and x represents the unknown number of coordinated water molecules. This particular scheme suggests that reduction occurs in solution but it is just as possible for reduction to occur on the birnessite surface.

At pH 8 and 10, evidence was presented to indicate the presence of $Co(OH)_2$ on the birnessite surface for each of the three cobalt amino acid complexes. The hydrolysis of the complexes can occur, as presented in Equations 84 to 88, except $Co(OH)_2$ precipitates when Co^{2+} is in solution as shown below:

$$Co^{2+} + 2\ OH^- \rightarrow Co(OH)_2 \quad (90)$$

$$Co(OH)_2 + \text{birnessite} \rightarrow Co(OH)_2\text{/birnessite} \quad (91)$$

It is also feasible that formation of $Co(OH)_2$ occurred on the

birnessite surface. The present experiments were not designed to establish the site of $Co(OH)_2$ formation.

G. XPS ANALYSIS OF MANGANESE NODULES

A study of the chemical nature of metals in selected Pacific Ocean manganese nodules was carried out using x-ray photoelectron spectroscopy. The chemical environment and oxidation state of cobalt in the nodules was the center of this investigation. Comparisons were made between the cobalt that interacted with manganese nodules in the marine environment and the cobalt adsorbed on birnessite in less complicated model conditions. Identification of the oxidation state of manganese, iron, lead, copper, nickel, and titanium was accomplished by examination of the binding energies, 2p satellite features, and/or multiplet splitting.

Identification and location site for the nodules is presented in Table 2. The inside and outside surfaces of the nodule identified as M2P52 were analyzed. This nodule had an inner core that was an orange color and an exterior consisting of a black colored material. This dramatic inhomogeneity was not observed for any of the other eight nodules.

Approximately 1 cm^3 samples were taken from the nodules for analysis and were lightly ground with an agate mortar and pestle to produce a fine uniformly sized powder. The interior and exterior regions were sampled separately for nodule M2P52. Single samples consisting of a split of material from the entire cross section through the nodule were taken for the relatively homogeneous nodules.

The binding energies of manganese and iron, the two principal transition metals in the manganese nodules, are presented in Table 28. The measured manganese 3s multiplet splitting values are also shown in Table 28. The binding energies of manganese in the manganese nodules are in good agreement with the values published for birnessite and determined in this dissertation (74,82). The multiplet splitting value of the nodules, 4.7 ± 0.2 eV, is the same as the multiplet splitting value of Mn(IV) in birnessite. These results indicate that Mn(IV) is the principal oxidation state of manganese in these nodules.

The 2p photoelectron spectrum for iron is similar to the spectra measured for other iron(III) oxides. The measured Fe $2p_{3/2}$ binding energies, 712.0 ± 0.2 eV, are in excellent agreement with the value of 711.9 eV reported for FeOOH by McIntyre and Zetaruk (179), but higher than the value, 711.0 eV, given by Allen et al. (180). The Fe 2p binding energy is greater than those reported for Fe_2O_3, 711.1 eV (173) 710.9 eV (181), and 711.0 eV (179) and for several measurements on FeO (179-181). The Fe 3s splitting value could have aided in establishing the iron oxidation state. However, interference from the Si 2p $K_{\alpha 3,4}$ x-ray satellite peak and the higher binding energy multiplet splitting peak of the Mn 3s level, precluded obtaining an accurate value for the Fe 3s multiplet splitting. Good agreement of the binding energy results with the Fe(III) values for FeOOH supports the notion that the iron oxidation state is Fe(III).

It was important to consider the interference of barium on the cobalt spectrum. The Ba $3d_{3/2}$ and $3d_{5/2}$ photopeaks of barium hydroxide have binding energies of 795.9 eV and 780.8 eV, respectively. They are

Table 28

XPS Analysis Manganese and Iron in Manganese Nodules

Nodule	Binding Energy Mn $2p_{3/2}$ (±0.2 eV)	Multiplet Splitting Mn 3s (±0.2 eV)	Binding Energy Fe $2p_{3/2}$ (±0.2 eV)
Frazer Nodules			
South Tow 4FF A	642.0	4.8	711.5
7 Tow 143 D-C	641.9	4.6	711.5
7 Tow 143 D-E	641.9	4.8	711.8
Geosecs ID	641.9	4.7	711.8
Calvert Nodules			
AMPH 9D	642.0	4.8	712.0
MPH3	641.8	4.7	712.0
DWHD 16	641.8	4.8	712.0
M2P50	642.0	4.7	712.0
M2P52			
inside	641.8	4.8	712.2
outside	642.0	4.6	712.1
Birnessite (MnO_2) (74)	642.3	4.5	---
Birnessite (MnO_2) (82)	641.9	4.7	---
Birnessite (MnO_2)*	642.2	4.7	
α-FeOOH (179)			711.9
α-FeOOH (180)			711.0
α-FeOOH*			711.8

*This work

Table 28

(Continued)

Nodule	Binding Energy Fe $2p_{3/2}$ (±0.2 eV)
Fe_2O_3 (73)	711.1
Fe_2O_3 (179)	710.9
Fe_2O_3 (180)	711.0
FeO (179)	709.2
FeO (180)	710.2

located in the same region as the Co $2p_{1/2}$ and Co $2p_{3/2}$ photopeaks for CoOOH, which appear at 795.2 eV and 780.2 eV, respectively. The XPS 3d spectrum of $Ba(OH)_2$ and the Co 2p spectrum of CoOOH are presented in Figure 44. Barium and cobalt can be distinguished by examining the intensity ratio ^{I}Co $2p_{3/2}$ / ^{I}Co $2p_{1/2}$ and the ^{I}Ba $3d_{5/2}$ / ^{I}Ba $3d_{3/2}$. The peak ratios for barium and cobalt can be evaluated from the photoionization cross section (130) and are presented in Table 29 along with the experimentally measured values for selected barium and cobalt compounds. The peak ratios in the 800 to 780 eV region for manganese nodules are given in Table 29. The photopeak intensity ratios for the nodule samples agree closely with both the theoretical and the experimental values for authentic Co(III) compounds.

XPS is approximately twice as sensitive to barium than cobalt based on photoionization cross section values (130). Interference by barium in measurement of the Co 2p photopeaks would result if a barium signal one tenth that of cobalt was observed. The barium content in the nodules would have to be about one twentieth that of cobalt to interfere with cobalt analysis by XPS. Lack of barium interference was confirmed by quantitative measurements that showed the barium in the nodules was two orders of magnitude smaller than the cobalt content (Table 30).

The Co $2p_{3/2}$ XPS binding energies, the Co $2p_{1/2}$ - Co $2p_{3/2}$ energy differences, and the Co/Mn atomic ratios are presented in Table 31. The atomic ratios were calculated for integrated peak intensity corrected for photoionization cross section. The Co 2p spectrum for AMPH9D is presented in Figure 45.

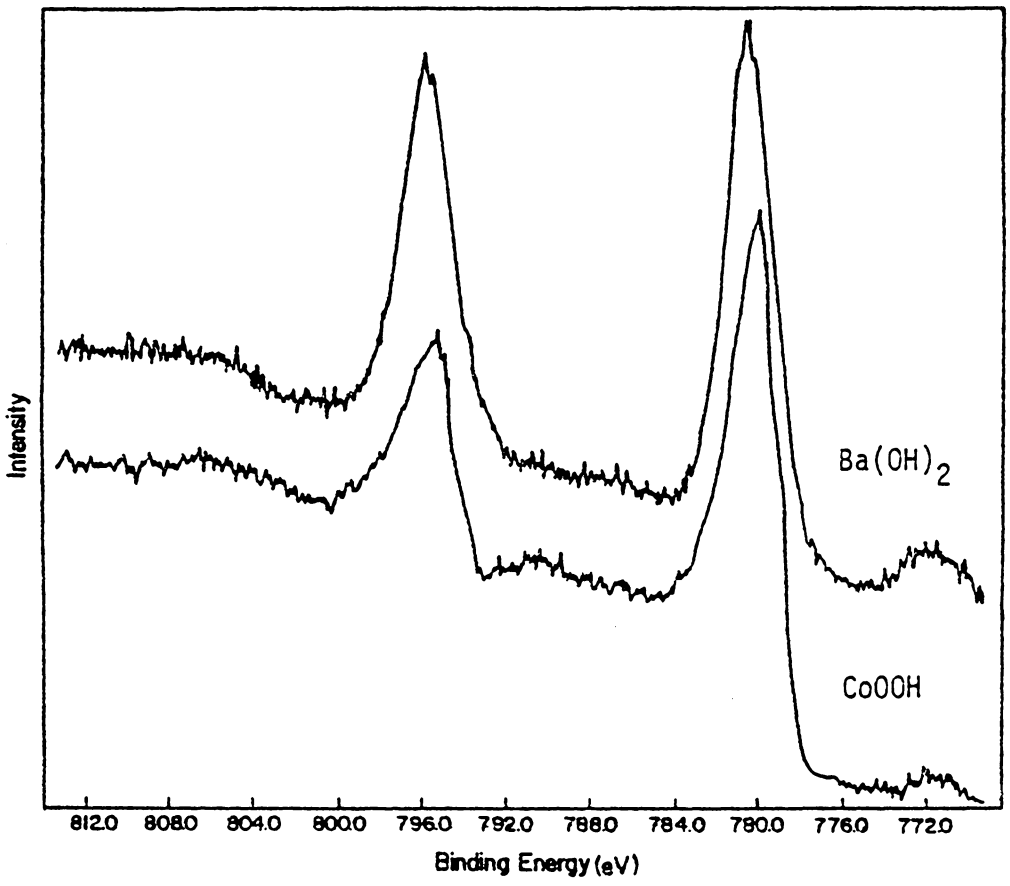

Figure 44. XPS Spectra Ba 3d and Co 2p

Table 29

Experimental and Theoretical Intensity Ratios for Ba 3d and Co 2p Photopeaks

	$\frac{Co\ 2p_{3/2}}{Co\ 2p_{1/2}}$	$\frac{Ba\ 3d_{5/2}}{Ba\ 3d_{3/2}}$
Theoretical (130)	1.94	----
Co_2O_3 (73)	2.01	----
CoOOH	2.00	----
BaO (36)	----	1.43
$Ba(OH)_2$	----	1.44
South Tow 4FFA	2.0	----
7 Tow 143 D-C	2.2	----
7 Tow 143 D-E	1.8	----
Geosecs 1D	2.0	----
AMPH 9D	1.9	----
MP 43	1.9	----
DWHD 16	2.1	----
M2P50	ND*	----
M2P52		
inside	ND	----
outside	ND	----

* Not Detected

Table 30

Barium Content of Nodules

	Weight Percent Cobalt	Weight Percent Barium
South Tow 4FFA	0.66	0.0038
7 Tow 143 D-C	0.78	0.0037
7 Tow 143 D-E	0.9	0.0025
Geosecs 1D	1.0	0.0033

Table 31

Cobalt in Manganese Nodules

Nodule	Co $2p_{3/2}$ Binding Energy (±0.2 eV)	ΔE(Co $2p_{1/2}$-Co $2p_{3/2}$) (±0.2 eV)	XPS Atomic Ratio Co/Mn (±0.05)	Bulk Analysis Atomic Ratio Co/Mn †
Nodules From Frazer				
South Tow 4FFA	780.4	15.0	0.025	0.032
7 Tow 143 D-C	780.4	15.0	0.034	0.038
7 Tow 143 D-E	780.3	15.2	0.050	0.046
Geosecs ID	780.4	14.9	0.062	0.040
Nodules From Calvert				
AMPH 9D	780.3	14.9	0.068	0.076
MP43	780.3	15.1	0.047	0.033
DWHD16	780.4	15.2	0.055	0.048
M2P50	ND*	---	---	0.026
M2P52				
inside	ND*	---	---	0.0060
outside	ND*	---	---	---
Co^{2+}-birnessite pH=6	780.5	15.0	---	---

* Not Determined

† Error not reported by suppliers of nodules

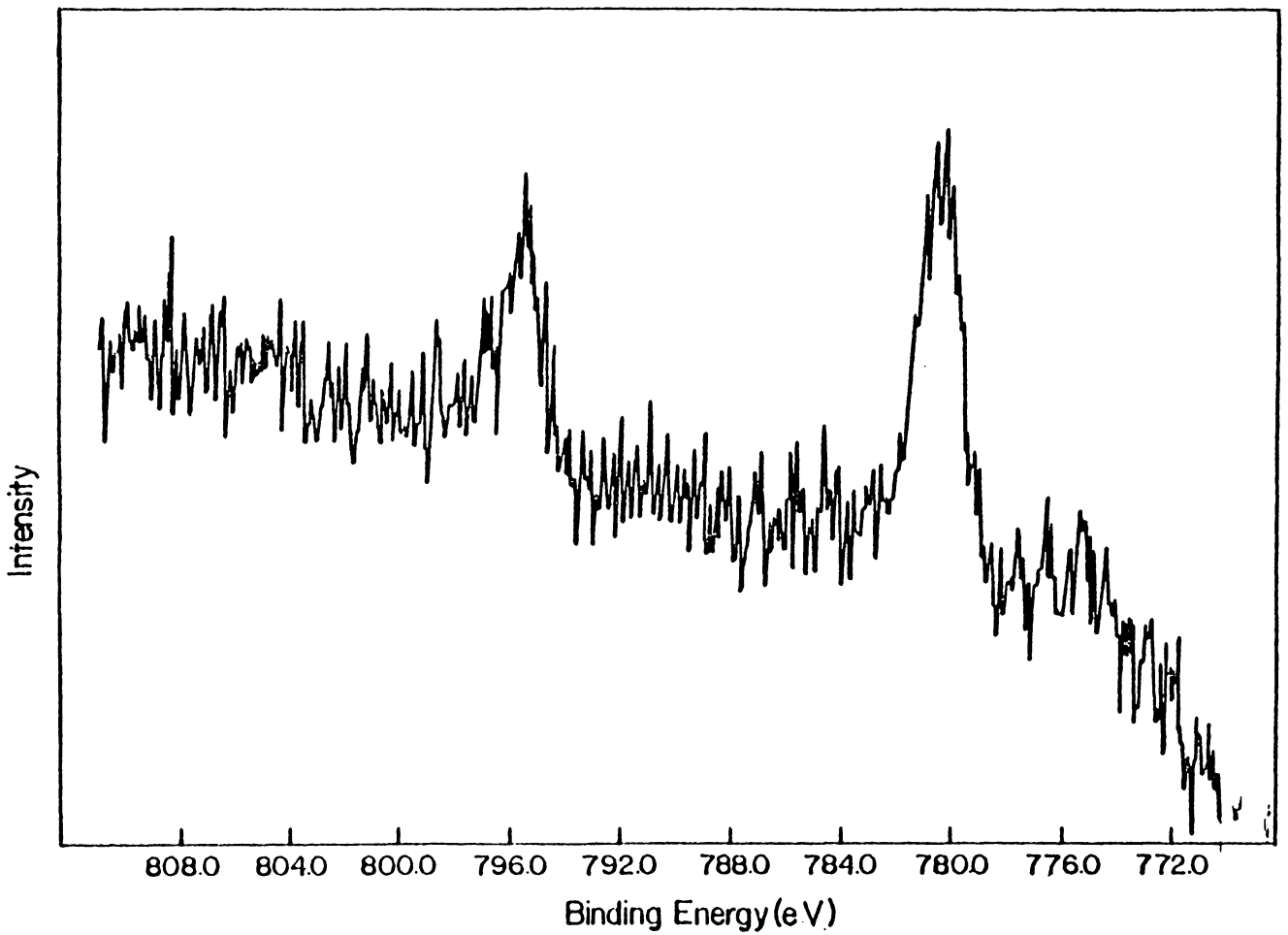

Figure 45. Cobalt in Manganese Nodule AMPH 9D

The XPS Co 2p spectra for the manganese nodules are characteristic of Co(III). The Co $2p_{1/2}$ - Co $2p_{3/2}$ binding energy difference is approximately 15.0 eV and the Co 2p spectra do not exhibit any intense satellite features. Co $2p_{3/2}$ binding energy for the various manganese nodules is approximately the same, which indicates that the chemical nature of the cobalt is equivalent for all nodules. The binding energies are also in agreement with the binding energy for CoOOH, which was noted for cobalt adsorbed on birnessite at pH 6.5 (Table 24). This indicates that the chemical nature of the cobalt adsorbed on birnessite is the same as for cobalt adsorbed on marine manganese nodules.

The Co/Mn ratios determined by XPS and the cobalt to manganese ratios determined from bulk analysis of the nodules are presented in Table 31. As the amount of bulk cobalt increases, the atomic ratio of cobalt on the surface increases. Some of the values for Co/Mn determined by XPS are larger than values determined by bulk analysis and some values are lower. This disagreement in the Co/Mn ratios supports the suggestion that the cobalt is neither concentrated in the particle surfaces nor in the lattice structure, but is homogeneously distributed throughout the nodule.

The binding energies for lead in the manganese nodules and binding energies for PbO, PbO_2, and a lead sample containing a mixture of PbO and PbO_2 are presented in Table 32. No variation in the Pb $4f_{7/2}$ binding energy for the nodules was observed, indicating that lead has the same chemical nature in all of the nodules studied. The Pb $4f_{7/2}$ binding energy for the nodules is 138.0 ± 0.1 eV, in excellent

Table 32

XPS Analysis of Lead in Manganese Nodules

Nodule	Pb $4f_{7/2}$ (±0.1 eV)	XPS Atomic Ratio Pb/Mn (±0.001)	Bulk Analysis Atomic Ratio Pb/Mn (†)
Nodules From Frazer			
South Tow 4FFA	138.1	0.004	-----
7 Tow 143 D-C	138.0	0.003	-----
7 Tow 143 D-E	138.0	0.006	-----
Geosecs ID	138.0	0.004	-----
Nodules From Calvert			
AMPH 9D	137.9	0.005	0.0032
MP43		trace	0.002
DWHD16	138.1	0.004	0.003
M2P50	-----	-----	0.0017
M2P52			
inside	-----	-----	0.0004
outside			
Pb^{2+}-Birnessite (74) (pH=8.0)	137.9	-----	-----
PbO (74)	137.4	-----	-----
PbO_2 (74)	138.4	-----	-----
PbO/PbO_2 (74) (mixed oxide surface)	138.0	-----	-----

† Error not reported by suppliers of nodules.

agreement with the value for lead adsorbed on birnessite, 137.9 eV (74) and for a lead sample containing a mixture of PbO and PbO_2, 138.0 eV (74). In an earlier study of adsorbed lead (74) the Pb 4f photopeaks could be curve resolved to indicate the presence of a mixture of Pb(IV) and Pb(II) on the birnessite surface. In this study no attempt was made to curve resolve the lead photopeaks because of the low Pb $4f_{7/2}$ intensity in the nodules. It can only be speculated that the intermediate Pb $4f_{7/2}$ binding energy may be indicative of a mixture of Pb(II) and Pb(IV) in the nodule.

The Pb/Mn atomic ratio measured by XPS was compared to the bulk Pb/Mn ratio determined by Calvert, and the XPS Pb/Mn ratios determined for the Frazer nodules are presented in Table 32. XPS was unable to detect lead in the Calvert nodules when the bulk Pb/Mn atomic ratio was less than 0.0004. The Pb/Mn atomic ratio determined by XPS was not significantly different than the value determined by Calvert for the two nodules that were compared. This suggests that lead is not concentrated on the particle surfaces of the nodules. However, more nodules with detectable amounts of Pb will have to be analyzed before overall conclusions for lead adsorption can be made.

Copper was detected in one manganese nodule, M2P52. The oxidation of copper can be determined by the binding energy and the presence of shake-up satellites. Frost et al. (182) studied a large number of copper compounds and have found satellite peaks for Cu(II) compounds but not for Cu(I) compounds. The Cu $2p_{3/2}$ spectrum for copper in the M2P52 nodule is presented in Figure 46. Binding energies for selected copper compounds are presented in Table 33. The Cu $2p_{3/2}$ binding

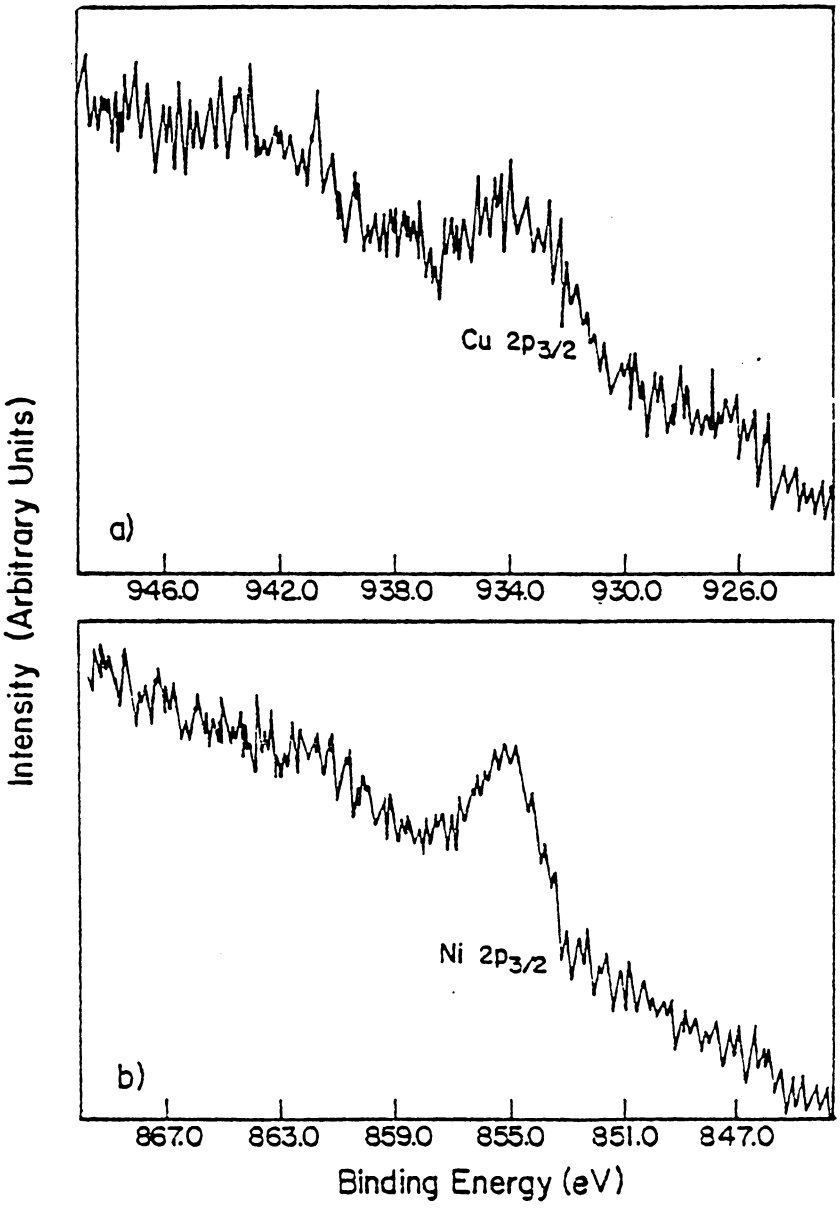

Figure 46. XPS Spectra Copper and Nickel in Manganese Nodules

Table 33

XPS Binding Energies for Copper in Mn Nodules
and for Reference Compounds

Sample	Cu $2p_{3/2}$ Binding Energy (± 0.2 eV)
M2P52	
inside	933.8
outside	933.8
$Cu(OH)_2$ (182)	933.8
CuO (182)	933.2
Cu_2O (182)	932.0
Cu(II) adsorbed on chlorite (9)	935.5
$CuCl_2 \cdot 2H_2O$ (182)	935.6

energies for copper in the core and in the exterior region of nodule M2P52 were equal. Satellite features were observed in the spectra, which indicate that the oxidation state is Cu(II). The binding energy of copper in the manganese nodule, 933.8 + 0.2 eV, is in close agreement with the binding energy for $Cu(OH)_2$ reported by Frost et al. (182), 933.8 eV. It is slightly higher than the binding energy for CuO, 933.2 eV (182), and is approximately 2.0 eV higher than that for Cu(I) in Cu_2O, 932.0 eV (182). The binding energy for copper in the manganese nodule was also less than that for Cu^{2+} on chlorite, 935.5 eV, which was attributed to $CuOH^+$ (9). The lower binding energy found for copper in the manganese nodule compared to copper on chlorite indicates that the electron density is somewhat greater than for $CuOH^+$. It also indicates that the chemical nature of Cu^{2+} on the manganese nodule is different than for Cu^{2+} on clays. From the presence of satellites and comparison of binding energies, it can be concluded that the oxidation state of copper is Cu(II) and that the chemical environment is similar to that of copper in copper hydroxide. However, general conclusions about the oxidation state of copper in manganese nodules cannot be made because only one nodule, M2P52, was analyzed.

Nickel was detected by XPS in manganese nodule M2P52. The nickel binding energies and satellite structure were used to identify the chemical nature of nickel. The Ni $2p_{3/2}$ spectrum detected on the outside of the nodule is presented in Figure 46. Binding energies for nickel in the nodule and reference nickel compounds are presented in Table 34. No significant differences in Ni $2p_{3/2}$ binding energy and satellite features were observed for nickel in the core versus the

Table 34

$Ni\ 2p_{3/2}$ Binding Energies for Nickel in Mn Nodules and for Reference Compounds

Sample	$Ni\ 2p_{3/2}$ Binding Energy (± 0.2 eV)
M2P52	
Inside	854.9
Outside	854.7
$Ni(OH)_2$ (9)	856.0
$Ni(NO_3)_2 \cdot 6H_2O$ (136)	856.9
NiO (184)	854.4
(147)	854.0
Ni_2O_3 (147)	855.7
Ni(II) adsorbed on chlorite (9)	855.6

exterior region of the nodule. The binding energy for nickel in the nodule, 854.8 ± 0.1 eV, was most similar to those reported for NiO, 854.4 eV (184) and 854.0 eV (147), and was less than those reported for $Ni(OH)_2$, 856.0 eV (9), $Ni(NO_3)_2 \cdot 6H_2O$, 856.9 eV (136), Ni_2O_3, 855.7 eV (147), and Ni(II) adsorbed on chlorite, 856.6 eV (9). The satellites occurred at 6.0 eV above the main peak and are consistent with values reported for NiO, 6.2 eV (187) and 6.3 eV (188). The presence not only indicates Ni(II) but also shows that Ni(II) is in an octahedral environment. These results indicate that nickel in the nodule is Ni(II) and has a chemical environment similar to that of NiO.

The measured binding energies for titanium in all nine nodules are presented in Table 35 and are approximately equal, 458.2 ± 0.1 eV. The values are in good agreement with a value determined for TiO_2, 458.3 eV (179). This good comparison provides excellent support for the presence of Ti(IV) in the nodules.

In summary, the binding energy results are consistent with the presence of Mn(IV), Fe(III), Co(III), Pb(II and IV), Cu(II), Ni(II), and Ti(IV) in the manganese nodules. The presence of Co(III) and Pb(IV) in the manganese nodules is consistent with reports in the literature that these metals are oxidized on the manganese dioxide surface. Burns (189) suggested that Fe(III) might also be capable of oxidizing Co(II) to Co(III). An XPS study by Schenck et al. (190) indicated the presence of adsorbed Co(II) on the surface of FeOOH. This suggests that Fe(III) is not principally responsible for the concentration of cobalt into manganese nodules. If this were so, Co(II) or a mixture of Co(II) and Co(III) would be observed by XPS.

Table 35

XPS Analysis Titanium in Manganese Nodules

Nodule	Ti $2p_{3/2}$ Binding Energy (±0.2 eV)
Nodules From Frazer	
South Tow 4FFA	458.3
7 Tow 143 D-C	458.3
7 Tow 143 D-E	458.2
Gaseous 1D	458.1
Nodules From Calvert	
AMPH 9D	458.1
MP43	458.1
DWHD-16	458.2
M2P50	458.3
M2P52	
inside	458.3
outside	458.2
TiO_2 (179)	458.3*
	458.4

* This study

This study indicates that manganese dioxide is responsible for the high concentrations of cobalt in manganese nodules and that Co(II) is oxidized to Co(III).

V. SUMMARY AND CONCLUSIONS

The interactions of cobalt, amino acids, and cobalt amino acid complexes with both montmorillonite and birnessite were studied. X-ray photoelectron spectroscopy (XPS) was used to examine the oxidation state, stoichiometry, and chemical nature of the adsorbed ions. Microelectrophoresis was employed to monitor any change in surface charge that occurred upon adsorption. Together with other analytical methods including infrared and visible spectroscopy, x-ray diffraction, and atomic absorption, insight into the chemical species present on the surface and into the mechanisms of interaction was obtained.

The chemical nature of cobalt adsorption on montmorillonite varied with pH. At pH 4 and 6, the surface species was Co^{2+}, at pH 7 the surface species was $CoOH^{+}$ or a mixture of Co^{2+} and $Co(OH)_2$, and at pH 8 and 10 $Co(OH)_2$ was found on the surface. These surface species were proposed based on changes in the surface charge, XPS Co $2p_{3/2}$ binding energy, Co $2p_{1/2}$ - Co $2p_{3/2}$ energy difference or splitting value, and Co 2p satellite features.

Proposed mechanisms for adsorption of lysine and glycine on Na^{+}-montmorillonite include cation exchange, zwitterion adsorption, and peptide bond formation. These mechanisms were shown to be possible based on infrared spectroscopic analysis of $-NH_3$, COOH, and COO^{-} bands, XPS identification of the N 1s photopeak, and the effect of interaction on the surface charge as revealed by microelectrophoresis. It was found that lysine at pH 2 to 8, and glycine at pH 2 can adsorb by cation exchange. Zwitterion adsorption was postulated at pH 10 for lysine and

at pH 4 and 6 for glycine treated montmorillonite. XRD measurements indicated that these zwitterions were possibly "keyed" into octahedral sites in the clay lattice. It was proposed that peptide formation occurred on the clay surface and was more prevalent for glycine than lysine because of steric factors.

The effect of a transition metal counterion on the clay surface upon amino acid adsorption was also studied. The interactions of lysine and glycine with Co^{2+}-montmorillonite was similar at pH 2 to 6 to the interactions of the amino acids with Na^{+}-montmorillonite. At pH 8 and 10, complexation of cobalt by lysine and glycine was observed. Co(III) amino acid complexes were observed in solution by transmission visible spectroscopy. It was not determined if the complexes formed on the surface and were released into solution or if desorbed cobalt was complexed in solution by the amino acid. Co(III) lysine complexes on the clay surface were observed by visible spectroscopy. In both cases where Co(III) amino acid complexes were observed, in solution and on the clay surface, dissolved oxygen was the proposed oxidizing agent.

Interaction of cobalt(III) amino acid complexes with montmorillonite resulted in hydrolysis and reduction of the complexes. This was indicated by XPS measurement of the Co 2p photopeaks and determination of the N/Co atomic ratio by both XPS and analytical methods. The complex charge was shown to affect the amount of adsorption. Greater amounts of $Co(lys)_3^{3+}$ were adsorbed on the negatively charged clay surface than $Co(gly)_3$ and $Co(asp)_2^{-}$. Visible spectroscopy indicated that complex was adsorbed, electrophoresis showed that the charges on the clay surface reversed, and XRD revealed

that the interlayer spacing was sufficient to accommodate the complex. It was proposed that $Co(lys)_3^{3+}$ could adsorb by nonequivalent exchange.

Previous studies (82) have indicated that Co(II) was oxidized to Co(III) on the manganese dioxide surface. The study of cobalt adsorption on birnessite showed that the MnO_2 surface is the oxidizing agent. Anaerobic experiments revealed that dissolved oxygen was not the oxidizing agent and XPS analysis of the Mn 3s multiplet splitting indicated that surface Mn(IV) was reduced.

Evidence was also obtained for oxidation-reduction reactions on the birnessite surface when treated with amino acids. Electrophoretic mobilities showed that the charge on the birnessite substrate increased in the presence of amino acids. This requires complexation of the amino acids by manganese or reduction of the manganese surface. Mn 3s splitting measurements of glycine and lysine saturated birnessite indicated that the surface was reduced. N 1s photopeaks revealed that the primary interaction was coordination of manganese by the amino acid. No measurements were made to determine if the amino acid was oxidized but the present study showed that the birnessite is reduced in the presence of amino acids and that amino acids can possibly chelate surface manganese.

It was not possible to determine if amino acids adsorbed on Co^{2+}-birnessite were bound to the cobalt or to the manganese of the substrate. Increased adsorption was observed on Co^{2+} vs Na^{+}-birnessite which infers interaction with the cobalt.

Hydrolysis of cobalt amino acid complexes occurred when interacted with birnessite. The chemical environment of cobalt on the surface at a given pH was the same as that observed for Co^{2+}-birnessite at the same pH. N/Co atomic ratios provided further evidence for hydrolysis. Surface catalyzed hydrolysis was the proposed mechanism because cobalt amino acid complexes are relatively stable to hydrolysis. The Mn 3s splitting increased following interaction with $Co(asp)_2^-$ at pH 6 and 7 and for $Co(lys)_3^{3+}$ at pH 4 to 7. These results led to the proposal that the complex is first hydrolyzed, then cobalt(III) is reduced, and finally cobalt(II) is reoxidized by the birnessite surface.

The oxidation state and chemical environment of selected metals in manganese nodules were investigated. It was found by analysis of binding energies, multiplet splittings, and satellite features that Mn(IV), Fe(III), Co(III), Pb(II and IV), Cu(II), Ni(II), and Ti(IV) were present.

This study is unique in that it investigates the adsorption of a metal, amino acids, and a metal amino acid complex related to adsorption on sediment surfaces. Through comparison of the interactions that occurred in the various systems studied, a greater understanding of the coinfluence of metals and organic species upon adsorption was obtained.

REFERENCES

1. McKenzie, R. M., Aust. J. Soil Res. 5, 235 (1967).
2. Farley, R. F. and Draycott, A. D., Plant and Soil 38, 235 (1973).
3. Means, J. L., Crerar, D. A., Borcsik, M. P. and Duguid, J. O., Nature (London) 274, 44 (1978).
4. Means, J. L., Crerar, D. A., Borcsik, M. P. and Duguid, J. O., Geochim. Cosmochim. Acta 42, 1763 (1978).
5. Evans, D. W. and Cutshall, N. H., in "Radioactive Contamination of the Marine Environment", Int. Atomic Energy Agency Vienna, 1973.
6. Davis, J. A. and Leckie, J. O., Env. Sci. Tech. 12, 1309 (1978).
7. Huang, C. P., Elliot, H. A. and Ashmeed, R. M., Jour. Water Poll. Control Fed. 49, 745 (1977).
8. Jenne, E. A., Adv. Chem. Ser. 73, 337 (1968).
9. Koppelman, M. H., Ph.D. Thesis, Virginia Polytechnic Institute and State University, Blacksburg, VA, 1976.
10. Stumm, W. and Brauner, P. A., in "Chemical Oceanography" (J. P. Riley and G. Skirrow, Eds.), Vol. 1, Academic Press, London (1975)
11. Richards, F. A., in "Organic Matter in Natural Waters", (D. W. Hood, Ed.), Institute of Marine Science, College, Alaska, 1970.
12. Slowly, J. F., Jeffrey, L. M. and Hood, D. W., Nature (London) 214, 377 (1967).
13. Saunders, G. W., Bot. Rev. 23, 389 (1957).
14. Yen, T. F. and Tang, J.I.S., in "Chemistry of Marine Sediments" (T. F. Yen, Ed.) Ann Arbor Science Publishers, Inc., Ann Arbor, Mich., 1977.

15. Neihof, R. and Loeb, G., J. Mar. Res. 32, 5 (1974).

16. Schmidt, E. L., Putham, H. D. and Paul, E. A., Soil Sci. Soc. Proc., 88, 107 (1960).

17. Kowalenko, C. G., in "Soil Organic Matter", (M. Schnitzer and S. U. Khan, Eds.), Elsevier Scientific Publishing Co., Amsterdam, 1978.

18. Putham, H. D. and Schmidt, E. L., Soil Sci. 87, 22 (1959).

19. Degens, F. T., in "Organic Matter in Natural Waters" (D. W. Hood, Ed.) Institute of Marine Science, College, Alaska, 1970.

20. Siegel, A. and Degens, E. T., Science 157, 1098 (1966).

21. Khan, S. U., in "Soil Organic Matter", (M. Schnitzer and S. U. Khan, Eds.) Elsevier Publishing Co., Amsterdam, 1978.

22. Miller, S. L. and Orgel, L. E., "The Origins of Life on Earth", Prentice Hall, Inc., Englewood Cliffs, New Jersey, 1974.

23. Bernal, J. D., "The Physical Basis of Life", Routledge and Kegan Paul, London, 1951.

24. Lahav, N. and Chang, S., J. Mol. Evol. 8, 357 (1976).

25. O'Connor, T. P. and Kester, D. R., Geochim. Cosmochim. Acta 39, 1531 (1975).

26. McBride, M. B., Clays Clay Miner. 26, 101 (1978).

27. Singhal, J. P. and Singh, R. P., J. Soil Sci. 24, 271 (1973).

28. Peigneur, P., Maes, A., Cremers, A., Clays Clay Miner. 23, 71 (1975).

29. Farrah, H. and Pickering, W. F., Aust. J. Chem. 29, 1167 (1976).

30. Farrah, H. and Pickering, W. F., Aust. J. Chem. 29, 1177 (1976).

31. Elliott, H. A. and Huang C. P., J. Colloid Interface Sci. 70, 29 (1979).

32. Grim, R. E., "Clay Mineralogy" McGraw-Hill, Inc., New York, 1968.

33. Van Olphen, H., "An Introduction to Clay Colloid Chemistry", John Wiley and Sons, New York (1977).

34. Gray, M. J. and Malati, M. A., J. Chem. Tech. Biotechnol. 29, 129 (1979).

35. Murray, J. W. and Brewer, P. G., in "Marine Manganese Deposits" Elsevier Scientific Publishing Co., Amsterdam, 1977.

36. Dillard, J. G., Crowther, D. L. and Murray, J. W., Geochim. Cosmochim. Acta (in press).

37. Burns, R. G. and Burns, V. M., in "Marine Manganese Deposits", (G. P. Glasby, Ed.), Elsevier Scientific Publishing Co., Amsterdam, 1977.

38. Goldberg, E. D., J. Geol. 62, 249 (1954).

39. Horne, R. A., "Marine Chemistry", Wiley-Interscience, New York, 1969.

40. Cronan, D. S. and Tooms, J. S., Deep-Sea Res. 16, 335 (1969).

41. Healing, R. A., Frazer, J. and Archer, A., in "Manganese Nodules: Dimensions and Perspectives", D. Reidel Publishing Co., Dordrecht, Holland, 1979.

42. Mero, J. L., in "Marine Manganese Deposits" (G. P. Glasby, Ed.), Elsevier Scientific Publishing Co., Amsterdam, 1977.

43. Mero, J. L., "The Mineral Resources of the Sea", Elsevier Publishing Co., Amsterdam, 1965.

44. Tinsley, C. R., Mining Eng. 31 (1975).

45. Li, T. M. and Tinsley, C. R., Mining Eng. 47 (1975).

46. Brooke, J. N. and Prosser, A. P., Trans. Inst. Min. Metall. 78C, 64 (1969).

47. Calvert, S. E. and Price, N. B., Mar. Chem. 5, 43 (1977).

48. Cronan, D. S. and Thoras, R. L., Bull. Geol. Soc. Am. 83, 1493 (1972).

49. Fuerstenau, D. W. and Han, K. N., in "Marine Manganese Deposits", (G. P. Glasby, Ed.), Elsevier Scientific Publishing Co., Amsterdam, 1977.

50. Parks, G. A., in "Chemical Oceanography", (J. P. Riley and G. Skirrow, Eds.), Vol. 1, p. 214, Academic Press, London, 1975.

51. Parks, G. A., Adv. Chem. Ser. 67, 121 (1967).

52. Hohl, H., Sigg, L. and Stumm, W., Adv. Chem. Ser. 189, 1 (1980).

53. Schindler, P. W., Walti, E. and Furst, B., Chimia 30, 107 (1976).

54. Banerjee, D. K., Bray, R. H. and Melsted, S. W., Soil Sci. 75, 421 (1953).

55. Hodgson, J. F., Soil Sci. Amer. Proc. 24, 165 (1960).

56. Tiller, K. G. and Hodgson, J. F., Clays Clay Miner. 9, 393 (1960).

57. Hodgson, J. F. and Tiller, K. G., Clays Clay Miner. 9, 404 (1960).

58. Spencer, W. F. and Gieseking, J. E., Soil Sci. 78, 267 (1954).

59. Chester, R., Nature (London) 206, 884 (1965).

60. DeMumbum, L. E. and Jackson, M. J., Soil Sci. Soc. Amer. Proc. 21, 662 (1957).

61. Hodgson, J. F., Tiller, K. G. and Fellows, M., Soil Sci. Amer. Proc. 28, 42 (1964).

62. Tewari, P. H., Campbell, A. B. and Lee, W., Can J. Chem. 50, 1642 (1972).

63. Healy, T. H., James, R. O. and Cooper, F., Adv. Chem. Ser. 79, 62 (1968).

64. James, R. O. and Healy, T. W., J. Colloid Interface Sci. 40, 42 (1972).

65. James, R. O. and Healy, T. W., J. Colloid Interface Sci. 40, 53 (1972).

66. James, R. O. and Healy, T. W., J. Colloid Interface Sci. 40, 65 (1972).

67. Koppelman, M. H. and Dillard, J. G., A.C.S. Symp. Ser. 18, 186 (1975).

68. Koppelman, M. H. and Dillard, J. G., Clays Clay Miner. 25, 457 (1977).

69. Bancroft, G. M., Brown, J. R. and Fyfe, W. S., Chem. Geol. 19, 131 (1977).

70. Counts, M. E., Jen, J.S.C. and Wightman, J. P., J. Phys. Chem. 77, 1924 (1973).

71. Tewari, P. H. and Lee, W., J. Colloid Interface Sci. 52, 77 (1975).

72. Tewari, P. H. and McIntyre, N. S., J. Colloid Interface Sci. 59, 195 (1977).

73. Koppelman, M. H. and Dillard, J. G., J. Colloid Interface Sci. 66, 345 (1978).

74. Dillard, J. G., Koppelman, M. H., Crowther, D. L., Schenck, C. V., Murray, J. W. and Balistrieri, L., in "Adsorption from Aqueous Solutions (P. H. Tewari, Ed.), Plenum Press, New York (1981).

75. McKenzie, R. M., Aust. J. Soil Res. 13, 177 (1975).

76. Murray, D. J., Healy, T. W. and Fuerstenau, D. W., Adv. Chem. Ser. 79, 74 (1968).

77. McKenzie, R. M., Aust. J. Soil Res. 8, 97 (1970).

78. Basak, B., Malati, M. A. and Gray, M. J., J. Radioanal. Chem. 42, 35 (1978).

79. Loganathan, P. and Burau, R. G., Geochim. Cosmochim. Acta 37, 1277 (1973).

80. Gray, M. J. and Malati, M. A., J. Chem. Technol. Biotechnol. 29, 135 (1979).

81. Burns, R. G., Geochim. Cosmochim. Acta 40, 95 (1976).

82. Murray, J. W. and Dillard, J. G., Geochim. Cosmochim. Acta 43, 781 (1979).

83. Mureinik, R. J., Feltham, A. M. and Spiro, M., J. Chem. Soc., Dalton 1981 (1972).

84. Dalang, F. and Stumm, W., in "Colloid and Interface Science", (M. Kerker, Ed.), Vol. 4, Academic Press, Inc., New York, N.Y.

85. Fripiat, J. J. and Helsen, J., Clays Clay Miner. 14, 63 (1966).

86. Tomita, A. and Tamai, Y., J. Phys. Chem. 75, 649 (1971).

87. Chaussidon, J., Calvet, R., Helsen, J. and Fripiat, J. J., Nature (London) 196, 201 (1962).

88. Bodenheimer, W., Kirson, B. and Yariv, Jh., Israel J. Chem. 1, 69 (1963).

89. Knudson, M. I. and McAtee, J. L., Clays Clay Miner. 21, 19 (1973).

90. Burba, J. L. and McAtee, J. L., Clays Clay Miner. 25, 113 (1977).

91. Schoonheydt, R. A., Velghe, F. and Uytterhoeven, J. B., Inorg. Chem. 18, 1842 (1979).

92. Schoonheydt, R. A., Velghe, F., Baerts, R. and Uytterhoeven, J. B., Clays Clay Miner. 27, 269 (1974).

93. Swartzen-Allen, S. L. and Matijevic, E., J. Colloid Interface Sci. 50, 143 (1975).

94. Berkheiser, V. E. and Mortland, M. M., Clays Clay Miner. 25, 105 (1977).

95. Schoonheydt, R. A., Pelgrims, J., Heroes, Y. and Uytterhoeven, J. B., Clay Miner. 13, 435 (1978).

96. Hathaway, B. J. and Lewis, C. E., J. Chem. Soc. (A) 1183 (1969).

97. Gillard, R. D. and Williams, P. A., Clays Clay Miner. 26, 178 (1978).

98. Hipps, K. W. and Mazur, V., Inorg. Chem. 20, 1391 (1981).

99. Talibudeen, O., Trans. Faraday Soc. 51, 582 (1955).

100. Greenland, D. J., Laby, R. H. and Quirk, J. P., Trans. Faraday Soc. 58, 829 (1962).

101. Greenland, D. J., Laby, R. H. and Quirk, J. P., Trans. Faraday Soc. 61, 2013 (1964).

102. Cloos, J., Calicis, B., Fripiat, J. J. and MaKay, K., in "Proc. Int. Clay Conf.", (L. Heller and A. Weiss, Eds.), Vol. 1, p. 233, Israel Program for Scientific Translations, Jerusalem, 1966.

103. Giles, C. H., MacKwan, T. H., Nakhwa, S. N. and Smith, D., J. Chem. Soc. 3973 (1960).

104. Fripiat, J. J., Cloos, P., Calicis, B. and MaKay, K., in "Proc. Int. Clay Conf.", (L. Heller and A. Weiss, Eds.), Vol. 1, p. 223, Israel Program for Scientific Translations, Jerusalem, 1966.

105. Greenland, D. J., Laby, R. H. and Quirk, J. P., Trans. Faraday Soc. 61, 2024 (1964).

106. McLaren, A. D., Peterson, G. H. and Barshad, I., Soil Sci. Am. Proc. 22, 237 (1958).

107. Sieskind, O. and Wey, R., C. R. Acad. Sci. Paris 248, 1652 (1959).

108. Orcharenko, F. D., Vdovenko, N. V., Tchichkun, V. P. and Tarasevich, Y. I., Ukr. Khim. Zh. 35, 123 (1969).

109. Bodenheimer, W. and Heller, L., Clay Miner. 7, 167 (1967).

110. Bodenheimer, W., Heller, L. and Yariv, S., in "Proc. Int. Clay Conf.", (L. Heller and A. Weiss, Eds.), Vol. 1, p. 251, Israel Program for Scientific Translations, Jerusalem, 1966.

111. Jang, S. D. and Condrate, R. A., Sr., Am. Mineralogist 57, 494 (1972).

112. Jang, S. D. and Condrate, R. A., Sr., Appl. Spect. 26, 102 (1972).

113. Jang, S. D. and Condrate, R. A., Sr., Clays Clay Miner. 20, 79 (1972).

114. Cannesson, P., Cruz, M. I. and Van Damme, H., in "Proc. Int. Clay Conf.", 1978, (M. M. Mortland and V. C. Farmer, Eds.), Vol. 1, 217, Elsevier Publishing Co., Amsterdam, 1979.

115. Defosse, C. and Cannesson, P., Reaction Kinetics Catalysis Letters 3, 161 (1975).

116. Jackson, M. L., "Soil Chemical Analysis - Advanced Course", Dept. of Soils, Univ. of Wisconsin, Madison, Wisconsin.

117. Feigl, F. and Angeri, V., "Spot Tests in Inorganic Analysis", p. 367, Elsevier Pub. Co., Amsterdam, 1972.

118. Micromeritics Instrument Corporation Instrum. Manual 2100-D, 1974.

119. Carter, D. L., Heilman, M. P. and Gonzales, C. L., Soil Sci. 100, 365 (1965).

120. Van Olphen, H. and Fripiat, J. J., "Data Handbook for Clay Minerals and Other Nonmetallic Minerals", Pergamon Press, New York, 1979.

121. Giovanoli, R., Burke, P., Gioffredi, M. and Stumm, W., Chimia 29, 512 (1975).

122. Buser, W., Graf, P. and Feitknecht, W., Helv. Chim. Acta 37, 2322 (1954).

123. Giovanoli, R., Chimia 23, 470 (1969).

124. Ley, H. and Winkler, H., Ber. 42, 3894 (1909).

125. Chuang, T. J., Brundle, C. R. and Rice, D. W., Surface Sci. 59, 413 (1976).

126. Grimblot, J., D'Huyser, A., Bonnelle, J. P. and Beaufils, J. P., J. Electron Spectrosc. Relat. Phenom. 6, 71 (1975).

127. Singlleton, J. H., Vac. Symp. Trans. 15, 267 (1963).

128. Troll, W. and Canaan, R. K., J. Biol. Chem. 200, 803 (1953).

129. Burness, J. H., Dillard, J. G. and Taylor, L. T., J. Amer. Chem. Soc. 97, 6080 (1975).

130. Scofield, J. H., J. Electron Spectrosc. Relat. Phenom. 8, 129 (1976).

131. Shaw, D. J., "Electrophoresis", Academic Press, London, 1969.

132. Skiles, J. A., M. S. Thesis, Virginia Polytechnic Institute and State University, Blacksburg, VA, 1976.

133. Baes, C. F. and Mesmer, R. E., "The Hydrolysis of Cations", John Wiley and Sons, New York, 1976.

134. Weast, R. G., "Handbook of Chemistry and Physics", CRC Press, Cleveland, OH, 1975.

135. Briggs, D. and Bosworth, Y. M., J. Colloid Interface Sci. 59, 194 (1977).

136. Haber, J. and Ungier, L., J. Electron Spectrosc. Relat. Phenom. 12, 305 (1977).

137. Frost, D. C., McDowell, C. A. and Woolsey, I. S., Mol. Phys. 27, 1473 (1974).

138. Cotton, A. F. and Wilkinson, G., "Advanced Inorganic Chemistry", John Wiley and Sons, New York, 1980.

139. Frost, D. C., McDowell, C. A. and Woolsey, I. S., Chem. Phys. Lett. 17, 320 (1972).

140. Kowalczyki, S. D., Ley, L., McFeely, F. R. and Shirley, D. A., Phys. Rev. B 11, 1721 (1975).

141. Carlson, T. A., Carver, J. C., Saethre, L. J., Santibanez, F. G. and Vernon, G. A., J. Electron Spectrosc. Relat. Phenom. 5, 247 (1974).

142. Yin, L., Adler, I. and Tsang, T., Chem. Phys. Lett. 24, 81 (1974).

143. Brundle, C. R., Chuang, T. J. and Rice, D. W., Surface Sci. 59, 195 (1977).

144. McIntyre, N. S. and Tewari, P. H., J. Colloid Interface Sci. 59, 195 (1977).

145. Hegde, M. S., Srinivasan, A., Jagannathan, K. and Chaturved, G., Proc. Indian. Acad. Sci. (Chem. Sci.) 89, 145 (1980).

146. Carlson, T. A., "Photoelectron and Auger Spectroscopy", Plenum Press, New York (1975).

147. Kim, K. S. and Davis, R. E., J. Electron Spectrosc. Relat. Phenom. 1, 251 (1972).

148. Borod'ko, Y. G., Vetchinkin, S. I., Zimont, S. L., Ivlera, I. N. and Shulg'a, Yu. M., Chem. Phys. Lett. 42, 264 (1976).

149. Lehninger, A. L., "Biochemistry", Worth Publishers, Inc., New York (1975).

150. Gillard, R. D., Chem. Rev. 67, 69 (1967).

151. Gillard, R. D., Laurie, S. H., Price, D. C., Phipps, D. A., and Wick, C. F., J. Chem. Soc., Dalton 1385, (1974).

152. Nakamoto, Kazuo, "Infrared Spectra of Inorganic and Coordination Compounds", pp. 201-205, John Wiley and Sons, New York, 1963.

153. Kincaid, J. R. and Nakamoto, K., Spectrochim. Acta 32A, 277 (1976).

154. Nakagawa, I. R., Hooper, J. and Walter, J. L., Spectrochim. Acta 21, 1 (1965).

155. Engerholm, G. C. and Rush, R. M., Appl. Spect. 33, 58 (1979).

156. Chow, S. T. and McAuliffe, C. A., Prog. Inorg. Chem. 19, 51 (1975).

157. Theng, B.K.G., "The Chemistry of Clay-Organic Reactions", John Wiley and Sons, New York, 1974.

158. White, D. H. and Erickson, J. C. J. Mol. Evol. 16, 179 (1980).

159. Lawless, J. G. and Levi, N., J. Mol. Evol. 13, 281 (1979).

160. Hearon, J. Z., J. Nat. Cancer Inst. 9, 1 (1948).

161. Hearon, J. Z. and Burk, D., J. Nat. Cancer Inst. 9, 337 (1948).

162. Jung, G., Ottnad, M., Hartman, H. J., Rupp, H. and Weser, U., Z. Anal. Chem. 263, 282 (1973).

163. Purcell, K. F. and Klotz, J. C., "Inorganic Chemistry", W. B. Saunders, Philadelphia.

164. Willard, H. H., Merritt, L. I. and Dean, J. A., "Instrumental Methods of Analysis", D. Van Nostrand Co., New York, 1979.

165. Lotmar, W. and Feitnecht, W., Z. Krist. 93, 368 (1936).

166. Murray, J. W., J. Colloid Interface Sci. 46, 357 (1974).

167. Zordan, T. A. and Hepler, L. G., Chem. Rev. 68, 737 (1968).

168. Healy, T. P., Herring, A. P. and Fuerstenau, D. W., J. Colloid Interface Sci. 21, 435 (1966).

169. Murray, J. W., Geochim. Cosmochim. Acta 39, 635 (1975).

170. Oku, M. and Hirokawa, K., J. Electron Spectrosc. Relat. Phenom. 7, 465 (1975).

171. Carver, J. C., Schweitzer, G. K. and Carlson, T. A., J. Phys. Chem. 57, 973 (1972).

172. Posselt, H. S., Anderson, F. J. and Weber, W. J., Jr., Env. Sci. Tech. 12, 1087 (1968).

173. Fackler, J. P., Jr., Adv. Chem. Ser., 150, 394 (1975).

174. Barakat, M. Z., Abdel-Wahab, M. F. and El-Sadr, M. M., J. Chem. Soc. 4685 (1956).

175. Lee, D. G., in "Techniques and Applications in Organic Synthesis", Vol. 1, (Robert L. Augustine, Ed.), Marcel Dekker, Inc., New York, 1969.

176. Parks, G. A., Chem. Rev. 65, 177 (1965).

177. Gergely, A. and Kiss, T., in "Metal Ions in Biological Systems", Vol. 9, (Helmut Sigel, Ed.), Marcel Dekker, Inc., New York, 1979.

178. Martin, R. B., in "Metal Ions in Biological Systems", Vol. 9, (H. Sigel, Ed.), Marcel Dekker, Inc., New York (1979).

179. McIntyre, N. S. and Zetaruk, D. G., Anal. Chem. 49, 1521 (1977).

180. Allen, G. C., Curlis, M. T., Hooper, A. J. and Tucker, P. M., J. Chem. Soc. Dalton Trans. II, 14, 1525 (1974).

181. Wagner, C. D., Gale, L. H. and Raymond, R. H., Anal. Chem. 51, 466 (1979).

182. Frost, D. C., Ishitani, A. and McDowell, C. A., Mol. Phys. 24, 861 (1972).

183. McIntyre, N. S. and Cook, M. G., Anal. Chem. 47, 2208 (1975).

184. Matienzo, L. J., Swartz, W. E., Jr. and Grim, S. O., Inorg. Nucl. Chem. Lett. 8, 1085 (1972).

185. Matienzo, L. J., Yin, L. I., Grim, S. O. and Swartz, W. E., Jr., Inorg. Chem. 12, 2762 (1973).

186. Tolman, C. A., Riggs, W. M., Linn, W. J., King, C. M. and Wendt, R. C., Inorg. Chem. 12, 2770 (1973).

187. Hirokawa, K., Honda, F. and Oku, M., J. Electron Spectrosc. Relat. Phenom. 6, 333 (1975).

188. Robert, J., Chem. Phys. 8, 123 (1975).

189. Burns, R. G., Geochim. Cosmochim Acta. 40, 95 (1976).

190. Schenck, C. V., Dillard, J. G., and Murray, J. W., to be submitted (1982).

The vita has been removed from the scanned document

THE INTERACTION OF COBALT, AMINO ACIDS, AND COBALT AMINO ACID COMPLEXES WITH SEDIMENT SURFACES

by

Deborah Lynne Crowther Kay

(ABSTRACT)

Organic molecules such as amino acids have long been considered the cause of some anomalous behavior of metals in the marine environment, with respect to concentration in the water and adsorption on the sediment. Many studies have investigated the adsorption of amino acids and amino acid complexes.

This study investigates the adsorption of cobalt, amino acids, and cobalt amino acid complexes on both Na^+-montmorillonite and Na^+-birnessite (MnO_2). Amino acids were also adsorbed on Co^{2+}-saturated montmorillonite and birnessite.

The oxidation state and chemical nature of sorbed cobalt and the chemical nature of the amino acid amine groups were investigated using x-ray photoelectron spectroscopy (XPS). XPS enabled determination of the stoichiometry of the sorbed complexes.

Electrophoresis revealed changes in the surface charge of the substrate upon interaction with cobalt, amino acids, and cobalt amino acid complexes. These changes provided insight into the reaction mechanisms and chemical species involved. Infrared and visible spectroscopy, x-ray diffraction (XRD), and quantitative analysis enabled further

determination of the reactions that occurred between cobalt, amino acids, cobalt amino acid complexes and the sediment surfaces.

Using XPS, it was found at pH values 4 to 7 that Co(II) adsorbed on montmorillonite as Co(II) and on birnessite as Co(III). The birnessite (MnO_2) surface was determined to be the oxidizing agent.

XPS, XRD, and infrared spectroscopy indicated that amino acid adsorbed on montmorillonite by cation exchange, keying into octahedral sites, and by peptide formation. Increased adsorption was observed on Co^{2+}-montmorillonite in solutions of both glycine and lysine and was attributed to coordination reactions. Both $Co(gly)_3$ and $Co(lys)_3^{3+}$ complexes were observed in solution and were either formed on the clay surface and released, or desorbed cobalt was complexed in solutions. $Co(lys)_3^{3+}$ was observed on the clay surface following interaction of Co^{2+}-montmorillonite with lysine. It is proposed that dissolved oxygen oxidizes cobalt in the amino acid complexes.

XPS and electrophoretic mobility measurements indicated that amino acids interact with birnessite by chelation of the surface manganese. Measurement of the Mn 3s splitting for amino acid saturated birnessite samples showed that the surface was reduced. It was inferred that the manganese dioxide surface oxidizes amino acids, but no proof of oxidized amino acids was obtained.

Hydrolysis of complexes was observed on both the manganese dioxide and montmorillonite surfaces. Because these complexes are known to be relatively stable to hydrolysis in solution, it was proposed that the surface catalyzed the hydrolysis.

The oxidation state and chemical nature of selected metals in Pacific manganese nodules were investigated using XPS. Analysis of binding energies, shake-up satellite features, and multiplet splittings revealed that the oxidation states for the metals in the nodules were Mn(IV), Fe(III), Co(III), Pb(II and IV), Cu(II), Ni(II), and Ti(IV).